The Dissertation Committee for Ross Edward Dugas certifies that this is the approved version of the following dissertation:

Carbon Dioxide Absorption, Desorption, and Diffusion in Aqueous Piperazine and Monoethanolamine

Committee:

Gary T. Rochelle, Supervisor

Benny D. Freeman

Douglas R. Lloyd

A. Frank Seibert

Michael E. Webber

Carbon Dioxide Absorption, Desorption, and Diffusion in Aqueous Piperazine and Monoethanolamine

by

Ross Edward Dugas, B.S.: M.S.

Dissertation

Presented to the Faculty of the Graduate School of

The University of Texas at Austin

in Partial Fulfillment

of the Requirements

for the Degree of

Doctor of Philosophy

The University of Texas at Austin

December 2009

Dedication

To my family

Acknowledgements

I would like to thank Dr. Gary Rochelle for all of his guidance throughout my graduate student experience. His insight and expertise in mass transfer processes have been invaluable in guiding my work. Dr. Rochelle truly enjoys teaching and I've tried to take advantage of that opportunity to learn all I can from him. Over the years I've witnessed his view and approach to solving problems and tried to implement those principles in my work. Today, I am a much better chemical engineer due to his influences. I couldn't be any happier with my decision to choose him as my advisor.

I would also like to thank our group secretaries who have provided support during my time as a graduate student. Maeve Cooney, Lane Salgado, and Jody Lester have all been extremely helpful in addressing problems, meeting deadlines, and essentially making things happen. Their behind-the-scenes contributions in organizing reports, conferences, and day-to-day affairs have made my job as a graduate student much easier.

In addition to learning from Dr. Rochelle, I have learned a significant amount from my peers. Three graduate students stand out among the group. Eric Chen provided lots of instruction and help on a variety of subjects when I first arrived at the University of Texas at Austin. We worked side by side on the pilot plant for about three years.

George Goff also provided a lot of instruction in my early years when nothing seemed to make sense. George always knew the answers to my questions and took time to teach me what I didn't understand. I've always been appreciative that he was never too busy to help redirect an often confused, young graduate student. During my latter years as a graduate student, Jason Davis became my main problem solving peer. We discussed numerous problems I couldn't seem to solve alone. A new perspective, thought invoking questions, and discussions solved many of those problems.

I've had the opportunity and privilege to work with many outstanding graduate students during my 6 ½ years at the University of Texas at Austin. Working alongside and conversing with these graduate students has made my experience as a graduate student much more enjoyable. In particular, I've become very good friends with Bob Tsai, Stephanie Freeman, Jason Davis, and Andrew Sexton.

My parents have always encouraged me to do my best in whatever I chose to do. I am and will be eternally grateful for the opportunities and environment they provided me. They taught me never to give up and that I could do anything I put my mind to. There were times as a graduate student where I didn't think I would make it. Their lessons of hard work, persistence, and discipline eventually prevailed. Their encouragement and support helped get me through some of the tougher times. I am extremely lucky and proud to call myself their son. Thanks, Mom and Dad.

This work was made possible by financial contributions by various sponsors: the Luminant Carbon Management Program, the Industrial Associates Program for CO_2 Capture by Aqueous Absorption, and the Separations Research Program at the University of Texas at Austin. Without financial contributions from these organizations, this work and much of my professional development would not have been possible.

Carbon Dioxide Absorption, Desorption, and Diffusion in Aqueous Piperazine and Monoethanolamine

Publication No._____

Ross Edward Dugas, Ph.D.

The University of Texas at Austin, 2009

Supervisor: Gary T. Rochelle

This work includes wetted wall column experiments that measure the CO_2 equilibrium partial pressure and liquid film mass transfer coefficient (k_g') in 7, 9, 11, and 13 m MEA and 2, 5, 8, and 12 m PZ solutions. A 7 m MEA/2 m PZ blend was also examined. Absorption and desorption experiments were performed at 40, 60, 80, and 100˚C over a range of CO_2 loading. Diaphragm diffusion cell experiments were performed with CO_2 loaded MEA and PZ solutions to characterize diffusion behavior. All experimental results have been compared to available literature data and match well.

MEA and PZ spreadsheet models were created to explain observed rate behavior using the wetted wall column rate data and available literature data. The resulting liquid film mass transfer coefficient expressions use termolecular (base catalysis) kinetics and activity-based rate expressions. The k_g' expressions accurately represent rate behavior

over the very wide range of experimental conditions. The models fully explain rate effects with changes in amine concentration, temperature, and CO_2 loading. These models allow for rate behavior to be predicted at any set of conditions as long as the parameters in the k_g' expressions can be accurately estimated.

An Aspen Plus® RateSep™ model for MEA was created to model CO_2 flux in the wetted wall column. The model accurately calculated CO_2 flux over the wide range of experimental conditions but included a systematic error with MEA concentration. The systematic error resulted from an inability to represent the activity coefficient of MEA properly. Due to this limitation, the RateSep™ model will be most accurate when fine-tuned to one specific amine concentration. This Aspen Plus® RateSep™ model allows for scale up to industrial conditions to examine absorber or stripper performance.

Contents

List of Tables

List of Figures

Chapter 1: Introduction

In recent years there has been an increased awareness of climate change, often called "global warming". Although global warming is a more shocking name, climate change is a more inclusive and accurate term for the environmental changes observed. The American public seems poorly informed on the topic due to conflicting reports and predictions from various groups. This results in extremely differing views on the topic. Many of these views are not based on facts and it is important to understand the facts concerning this important environmental subject.

This chapter provides background information about global temperatures, the greenhouse effect, atmospheric CO_2 levels, CO_2 emissions, and a CO_2 reduction technology — post-combustion carbon capture using aqueous amines.

1.1 GLOBAL TEMPERATURES

The U.S. Department of Commerce oversees the National Climatic Data Center which records and reports various environmental data. Figure 1.1 shows the global mean temperature deviation over land and oceans relative to the 20^{th} century average (NCDC 2009).

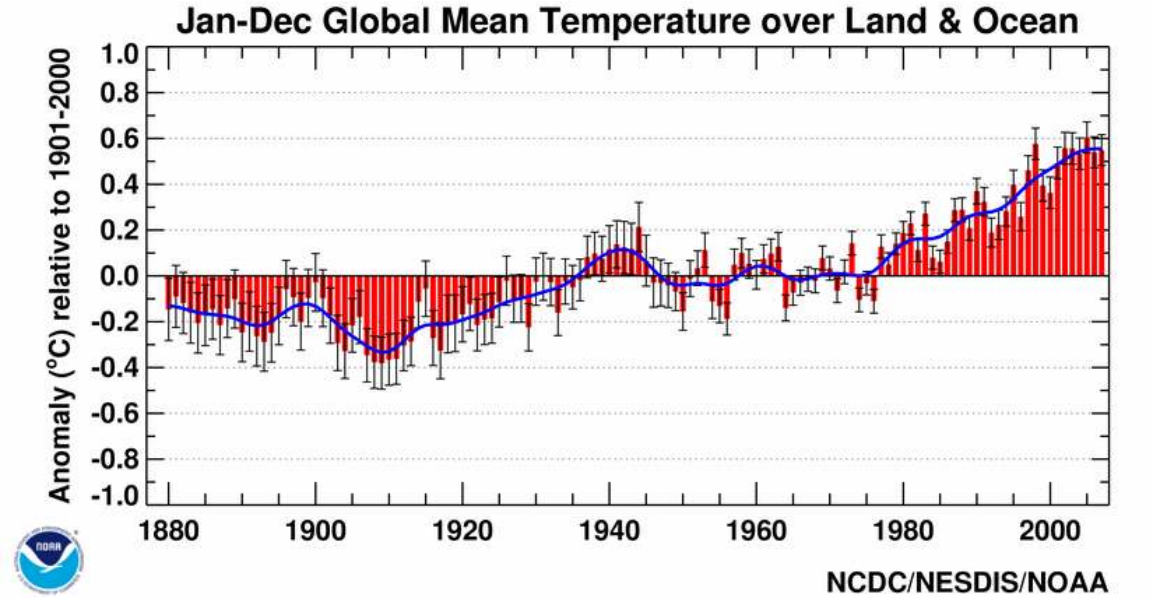

Figure 1.1: Global mean temperature over land and oceans (NCDC 2009)

Temperature data of the National Climatic Data Center was calculated by processing data from thousands of world-wide observation sites on land and sea. Using the collected data, Earth mean temperatures were calculated by interpolating over uninhabited deserts, inaccessible Antarctic mountains, etc. in a manner that takes into account factors such as the decrease in temperature with elevation (NCDC 2009).

1.2 THE GREENHOUSE EFFECT

Increasing global temperatures are often attributed to increasing atmospheric CO_2 levels. CO_2 is a known greenhouse gas that traps heat. Solar radiation from the sun is converted to infrared radiation (heat energy) when it strikes Earth. Greenhouse gases absorb a portion of the reflected infrared radiation and re-emit it to Earth. The heat trapping phenomenon is similar to that of a greenhouse or a car in a parking lot.

Water vapor, ozone (O_3), methane (CH_4), and nitrous oxide (N_2O) are also significant greenhouse gas contributors. According to a report by the National Center for

Atmospheric Research, water vapor is the primary heat trapping gas, accounting for about 60% of the greenhouse effect on a clear day (Kiehl and Trenberth 1997). CO_2, O_3, and the combination of CH_4 and N_2O account for 26, 8, and 6% of the greenhouse effect, respectively.

The concentration of water vapor in the atmosphere cannot be effectively controlled. The next largest greenhouse gas contributor, CO_2, has been shown to be increasing in the atmosphere since the industrial revolution due to the burning of fossil fuels. Therefore, to reduce or mitigate the heat trapping ability of the atmosphere, CO_2 is the most logical greenhouse gas target.

The greenhouse effect is a natural environmental effect which is partially responsible for making the climate on Earth acceptable for humans. Without the greenhouse warming effect, the average global temperature would be around –19˚C rather than 14˚C (IPCC 2007).

1.3 ATMOSPHERIC CO_2 LEVELS

Carbon extracted from deep underground and emitted into our environment leads to increased atmospheric CO_2 concentrations. Figure 1.2 shows the carbon balance on the surface of the Earth (IPCC 2007). The majority of carbon transfer is from natural environmental processes. Anthropogenic, or man-made, CO_2 emissions cause atmospheric CO_2 concentration to rise since they represent an increase of the total carbon in the closed system. Although the ocean is by far the largest carbon sink and much larger than our industrial emissions, the ocean cannot absorb all the anthropogenic CO_2 since there is a natural equilibrium between the carbon in the ocean, the atmosphere, and vegetation. Essentially, carbon put into the ocean will move to the atmosphere while carbon put into the atmosphere will eventually shift to the ocean.

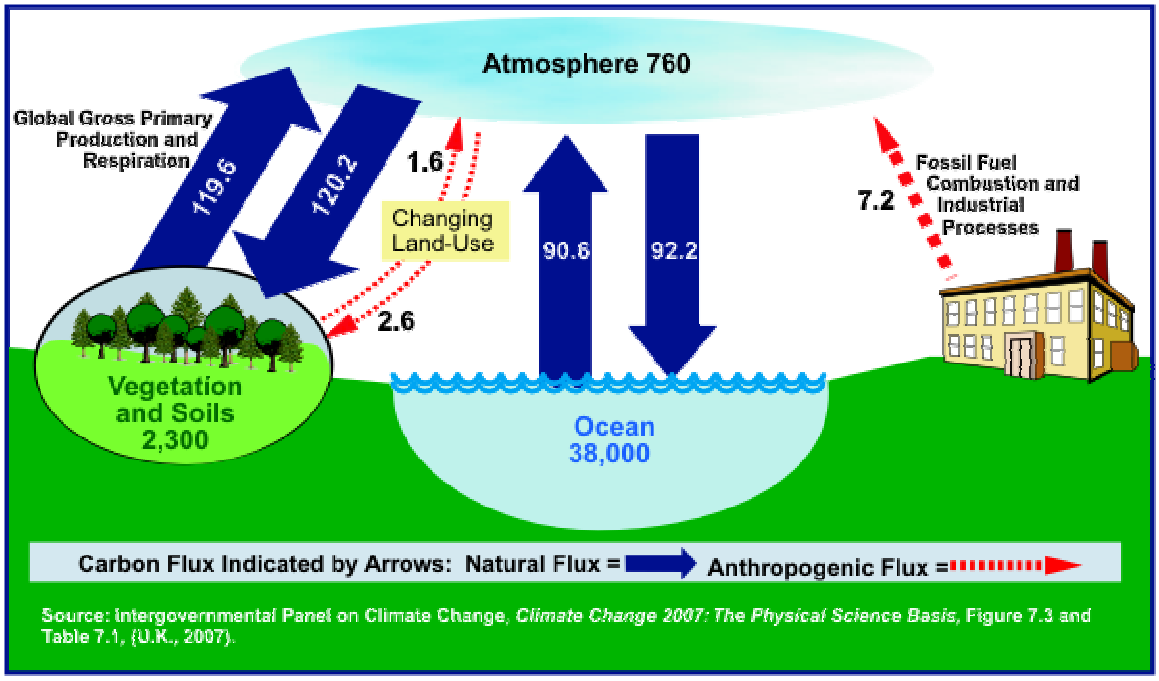

Figure 1.2: Carbon cycle on the surface of the Earth (IPCC 2007)

Figure 1.3 shows that atmospheric CO_2 concentrations have drastically increased over the past hundred years. In fact, Keeling (2005) shows that atmospheric CO_2 concentrations increased about 19% from 1959 to 2004. Recent CO_2 measurements over the last 50 or so years have been obtained via atmospheric testing at various points across the globe. CO_2 concentrations from periods before atmospheric CO_2 testing can be obtained using ice core data. The data in Figure 1.3 from 1744 to 1953 were obtained from the measurement of trapped gases in an ice core drilled at Siple Station in West Antarctica (Neftel, Friedli et al. 1994).

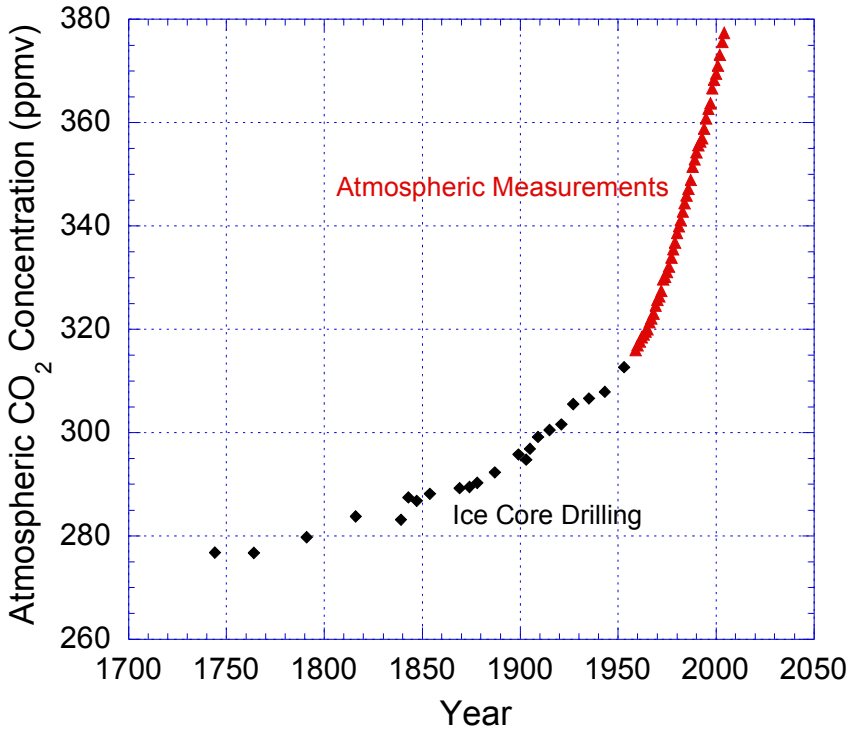

Figure 1.3: Historical atmospheric CO_2 concentrations obtained from Siple Station ice core drilling (Neftel, Friedli et al. 1994) and atmospheric CO_2 measurements (Keeling and Whorf 2005)

Figure 1.3 shows that atmospheric concentrations were relatively stable before and shortly after the industrial revolution which began in the late 1700s. Atmospheric CO_2 concentrations have since increased due to the increasing use of fossil fuels.

Deep ice core drilling at Vostok Station in Eastern Antarctica dates atmospheric CO_2 concentrations back about 417,000 years. Over this much longer period without significant human intervention, atmospheric concentrations were between 180 and 300 ppm, much lower than modern day atmospheric CO_2 levels (Barnola, Raynaud et al. 2003). The large increases in atmospheric CO_2 concentrations are likely due to environmental events such as major volcanic eruptions.

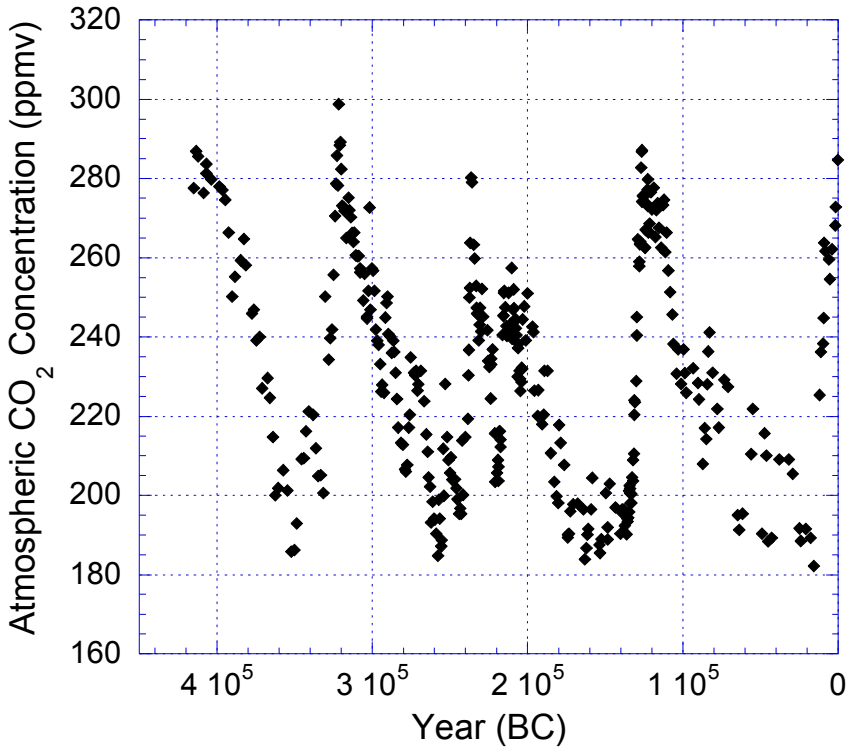

Figure 1.4: Historical CO_2 concentration measured from the Vostok ice core (Barnola, Raynaud et al. 2003)

1.4 CO_2 EMISSIONS

If atmospheric CO_2 concentrations are to be prevented from increasing indefinitely at a fast rate, anthropogenic CO_2 emissions to the atmosphere must be limited. Before addressing the limiting of CO_2 emissions, it is important to understand where the man-made CO_2 emissions originate in order to target a specific source.

The Energy Information Administration maintains the official energy statistics for the U.S. government. Figure 1.5 shows the world CO_2 emissions for petroleum, coal, and natural gas (EIA 2008a).

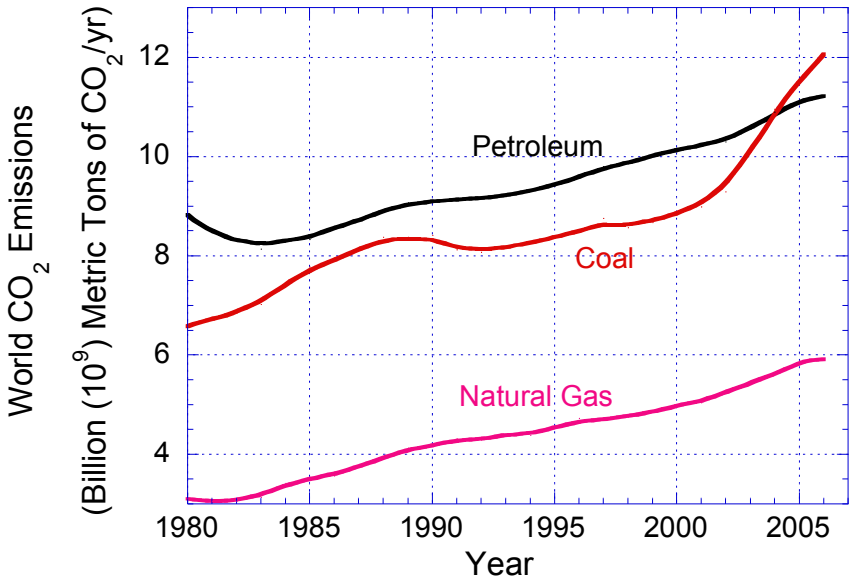

Figure 1.5: World CO_2 emissions from fossil fuels (EIA 2008a)

Coal and petroleum account for the majority of CO_2 emissions. Petroleum is generally used as a transportation fuel for vehicles, which results in a very large number of small emission sources. In the U.S. about 90% of coal is used for electricity generation (EIA 2008b). These large coal-fired power plants represent a significant portion of the total CO_2 emissions and are sufficiently large emission sources to address capturing CO_2.

1.5 AQUEOUS AMINE ABSORPTION/STRIPPING

Aqueous amine absorption/stripping is a mature technology which is capable of capturing CO_2 emissions from a coal-fired power plant. It has the advantage of being a tail-end process which can be added on to an existing power plant. A flowsheet of a typical aqueous amine absorption/stripping system is shown in Figure 1.6.

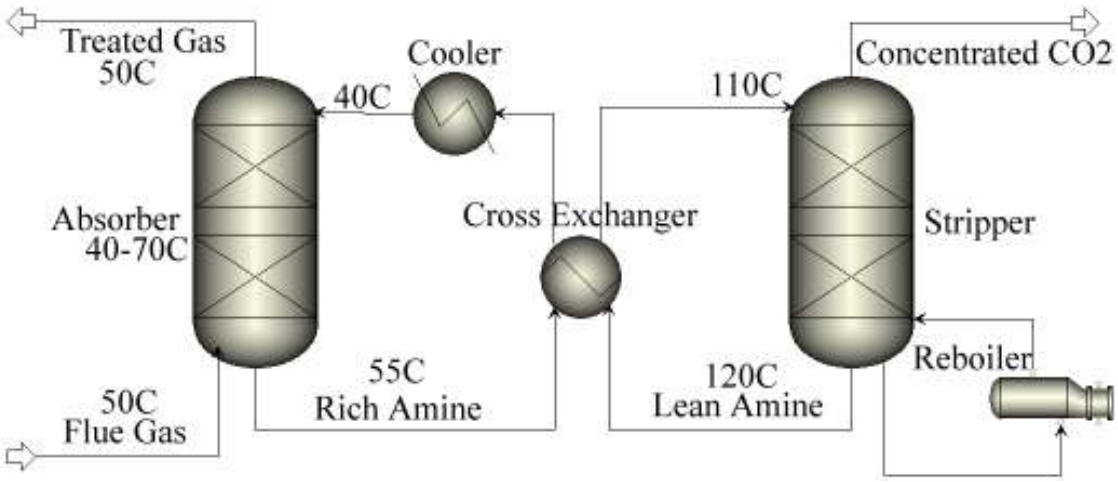

Figure 1.6: Typical absorption/stripping flowsheet for aqueous amine CO_2 capture with temperature estimates

This technology utilizes an aqueous amine solvent which countercurrently contacts the flue gas in a packed absorber. The CO_2 in the flue gas chemically reacts (exothermally) with the amine significantly reducing the CO_2 concentration in the gas stream exiting the absorber. The CO_2-rich amine solution exiting the bottom of the absorber is heated across a cross exchanger and sent to the stripper. The temperature of the stripper is maintained sufficiently high for the amine-CO_2 reaction to reverse itself and liberate CO_2. The CO_2 lean amine leaving the bottom of the stripper is cooled by the cross exchanger and again enters the absorber to remove more CO_2.

The concentrated CO_2 stream exiting the stripper can be compressed into a supercritical form where it can be pumped to its destination. The CO_2 can be used for commercial purposes, enhanced oil recovery, or disposed in abandoned oil and gas wells or saline aquifers.

The primary technological hindrance of implementation to aqueous amine absorption/stripping on power plants is cost. Electricity prices would rise about 80% for

coal-fired power plants that employ CO_2 capture (Rubin, Rao et al. 2004). About 80% of that price increase is associated with the capture and compression of CO_2 while the remaining 20% is attributed to sequestration (Rao and Rubin 2002). In an effort to reduce the cost of carbon capture, alternative amine solvents are being researched. Currently, 30 wt% monoethanolamine (MEA) is considered the baseline solvent for aqueous amine absorption/stripping. Alternative solvents may provide faster rates, higher CO_2 capacities, better degradation or corrosion properties, or better thermodynamic properties, which affect how CO_2 capture systems are operated. New solvents provide the opportunity to obtain significant energy and capital cost savings.

1.6 SCOPE OF WORK

The focus of this work is to compare CO_2 reaction rates of other amine systems to the current standard, MEA. Numerous experimental studies quantifying reaction rates have been performed on MEA and other amines (Versteeg, Van Dijck et al. 1996). However, very little of this work has been performed with concentrated amine solutions which will be required for CO_2 capture from flue gas. Industrial systems will also utilize CO_2 loaded amine solutions since liberating all the CO_2 from the solution is unreasonable due to energy costs. Very little literature data has been compiled for CO_2 loaded amines. Highly concentrated, highly loaded amine systems are non-ideal solutions which provide a completely different ionic environment than dilute, unloaded amine solutions. These dilute, unloaded experimental results do not translate to industrial solutions.

Overall, there is a lack of kinetic data for the CO_2 absorption/desorption rates into highly concentrated, highly CO_2 loaded amine solutions. This work provides the first comprehensive rate study on CO_2 loaded, concentrated piperazine solutions (2–12 m) at both absorber and stripper temperatures. This work also provides a second major rate

study on CO_2 loaded, concentrated monoethanolamine solutions (7–13 m). 7 m MEA/2 m PZ solutions have also been studied in the wetted wall column.

Due to some uncertainty in the viscosity-diffusion coefficient relationship for various amine systems, diaphragm cell diffusion experiments were conducted with MEA and PZ solutions. These systems have also been modeled to explain the observed mass transfer behavior.

Chapter 2: Literature Review

Absorption involves the mass transfer of a substance from the gas phase into the liquid phase. The absorbed substance may be either physically or chemically bound in the solvent. Physical solvents are often used to absorb CO_2 in high pressure environments like natural gas treating. The CO_2 solubility in physical solvents decreases with decreasing pressure and is inadequate for flue gas applications. CO_2 capture from flue gas requires a chemical solvent. Amine solvents react chemically with dissolved CO_2 and store it in a carbamate or bicarbonate form. Amines are organic compounds that contain a basic nitrogen atom.

2.1 General Amine Chemistry

Amines are generally subdivided by structure. Primary amines have nitrogen atoms connected to one carbon atom. Secondary amines have nitrogen atoms connected to two carbon atoms. Both primary and secondary amines provide open structures that allow CO_2 to reach the nitrogen and form carbamates. Tertiary amines have three carbon atoms connected to the nitrogen. This crowded environment around the nitrogen prevents carbamate stability. Tertiary amines produce bicarbonate instead of carbamates. Hindered amines are primary or secondary amines which have bulky groups around the nitrogen. Hindered amines are defined as either a) primary amines in which the nitrogen is attached to a tertiary carbon or b) secondary amines in which the nitrogen is attached to a secondary or tertiary carbon (Satori and Savage 1983). The degree of hindrance will

determine if the hindered amine is capable of producing some carbamate or only bicarbonate. Equations 2.1–2.4 show chemical structures for a primary (monoethanolamine), secondary (diethanolamine), tertiary (triethanolamine), and hindered amine (AMP).

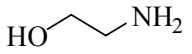

(2.1)

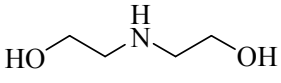

(2.2)

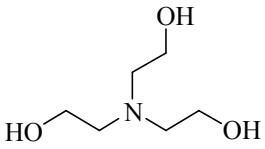

(2.3)

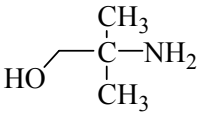

(2.4)

2.1.1 Monoethanolamine and Piperazine

The focus of this work is on monoethanolamine (MEA) and piperazine (PZ) solutions. Piperazine is a secondary amine with two amine groups, providing a large CO_2 capacity. Its cyclic structure exposes the nitrogen groups and results in very fast reaction with CO_2. The ring structure also provides increased resistance against thermal degradation allowing for stripping at higher temperatures (Davis 2009). The structure of piperazine is shown in Equation 2.5.

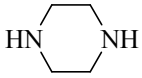

(2.5)

Aqueous monoethanolamine and piperazine solutions will form carbamates and bicarbonate when reacted with CO_2. The MEA carbamate reaction is shown generically in Equation 2.6. The possible piperazine carbamate reactions are listed in Equations 2.7–

2.9. The bicarbonate reaction shown in Equation 2.10 can become significant in both MEA and piperazine systems at high CO_2 loading.

$$MEA + CO_2 + B \leftrightarrow MEACOO^- + BH^+ \quad (2.6)$$

$$PZ + CO_2 + B \leftrightarrow PZCOO^- + BH^+ \quad (2.7)$$

$$PZCOO^- + CO_2 + B \leftrightarrow PZ\left(COO^-\right)_2 + BH^+ \quad (2.8)$$

$$PZH^+ + CO_2 + B \leftrightarrow H^+PZCOO^- + BH^+ \quad (2.9)$$

$$H_2O + CO_2 + B \leftrightarrow HCO_3^- + BH^+ \quad (2.10)$$

Component B can be any base in the system. Bases in MEA and PZ systems include: MEA, PZ, PZH^+, $PZCOO^-$, H_2O, and OH^-. PZH^+ and OH^- are not significant bases in the system since PZH^+ has a very low pK_a and OH^- is not present in significant concentrations. The low pK_a of PZH^+ also suggests via Bronsted theory that the forward rate constant of Equation 2.9 will be several orders of magnitude slower than the forward rate constants of Equations 2.7 and 2.8. Derks et al. (2006) has shown that the reaction in Equation 2.9 is a very small contributor to the CO_2 absorption.

2.1.2 CO_2 Loading

The CO_2 loading is a measurement of the CO_2 concentration in the solution. It is defined as the ratio of CO_2 molecules to alkalinity (active nitrogen) groups. MEA has one alkalinity group per molecule while piperazine has two. For an MEA, PZ, or MEA/PZ system, the definition of CO_2 loading is expressed mathematically in Equation 2.11.

$$CO_2 Loading = \frac{n_{CO2}}{n_{MEA} + 2n_{PZ}} \quad (2.11)$$

2.2 MASS TRANSFER WITH FAST REACTION

2.2.1 Zwitterion Reaction Mechanism

Absorption of CO_2 by amines such as MEA and piperazine is often explained by the zwitterion mechanism, originally proposed by Caplow (1968) and reintroduced by Danckwerts (1979). The zwitterion is an ionic, but neutrally charged intermediate that is formed from the reaction of CO_2 with an amine. The zwitterion mechanism for carbamate formation is a two step process: the CO_2 reacts with the amine to form a zwitterion, followed by the extraction of a proton by a base. In the following example water acts as the base. For simplicity the zwitterion mechanism is shown with the usual convention of irreversible proton extraction.

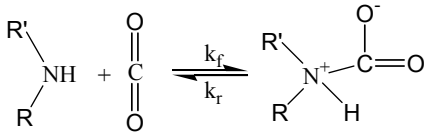

(2.12)

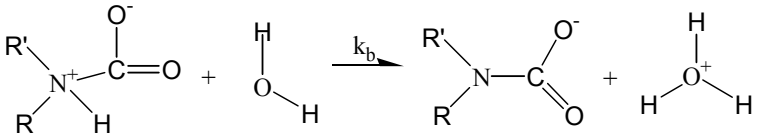

(2.13)

The two step zwitterion mechanism leads to the CO_2 absorption rate shown in Equation 2.14.

$$r_{CO2} = -\frac{[Am][CO_2]}{\frac{1}{k_f} + \frac{k_r}{k_f \sum k_b[B]}} \tag{2.14}$$

Bases can include the amine as well as H_2O and OH^-. In some systems H_2O and OH^- can contribute pronounced effects to the rate of reaction (Blauwhoff, Versteeg et al. 1983). For MEA, the zwitterion is protonated fast in comparison to the reversion rate to MEA and CO_2 (Danckwerts 1979). Since $\sum k_b[B]$ is much greater than k_r for MEA, Equation 2.14 simplifies to Equation 2.15.

$$r_{CO2} = -k_f [MEA][CO_2] \tag{2.15}$$

For many secondary amines, a second order reaction with respect to the amine is observed. This implies that for secondary amines k_r is much greater than $\sum k_b[B]$ yielding Equation 2.16.

$$r_{CO2} = -\frac{k_f}{k_r}[MEA][CO_2]\sum k_b[B] \tag{2.16}$$

The zwitterion mechanism can also be solved with a reversible base protonation step. This causes the reaction in Equation 2.13 to be replaced by Equation 2.17.

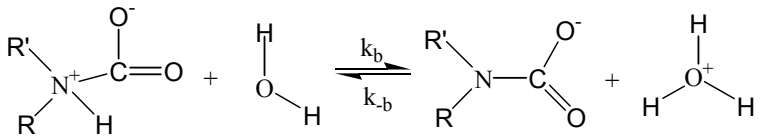

(2.17)

This leads to the following form of the rate equation, which now includes a driving force for the reversion of carbamate to amine and CO_2.

$$r_{CO2} = -\frac{[Am]}{\frac{1}{k_f} + \frac{k_r}{k_f \sum k_b[B]}}\left([CO_2] - \frac{\sum \frac{k_b}{K_{eq,b}}[AmCOO^-][BH^+]}{\sum k_b[Am][B]}\right) \tag{2.18}$$

The $K_{eq,b}$ term in Equation 2.18 is the overall equilibrium constant and is specific to the base pathway. For unloaded solutions, the reverse portion of Equation 2.18 can be ignored to produce the irreversible result of Equation 2.14. If the concentrations of the reactants and products are at equilibrium, the equilibrium constant will reduce the reversible term to $[CO_2]$ which will yield a zero for the rate of CO_2 formation.

2.2.2 Termolecular Reaction Mechanism

Contrary to the zwitterion mechanism, Crooks and Donnellan (1989) presented the termolecular mechanism, which assumes the reaction proceeds via a loosely bound complex. The complex and the reaction mechanism are shown in Equation 2.19.

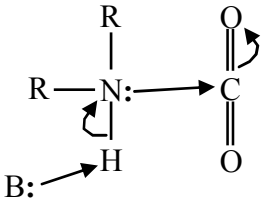

(2.19)

This mechanism coincides with the limiting case for the zwitterion mechanism where k_r is much greater than $k_f \sum k_b [B]$. The rate of CO_2 absorption is identical to the zwitterion result shown in Equation 2.16.

It is theorized that most of the loosely bound complexes break up to produce reagent molecules again while a few react with a second molecule of amine or water to yield ionic products (Crooks and Donnellan 1989). The bond formation and charge separation occur in the second step.

Since both the zwitterion and termolecular reaction mechanisms allow for varying orders of the amine concentration, both can be fitted to experimental data. An equally effective representation of reaction rates should be possible using either mechanism.

2.2.3 Film Theory

Mass transfer of CO_2 from the gas phase into the liquid phase is a film resistance process. Figure 2.1 shows a typical film analysis for CO_2 absorption with fast reaction.

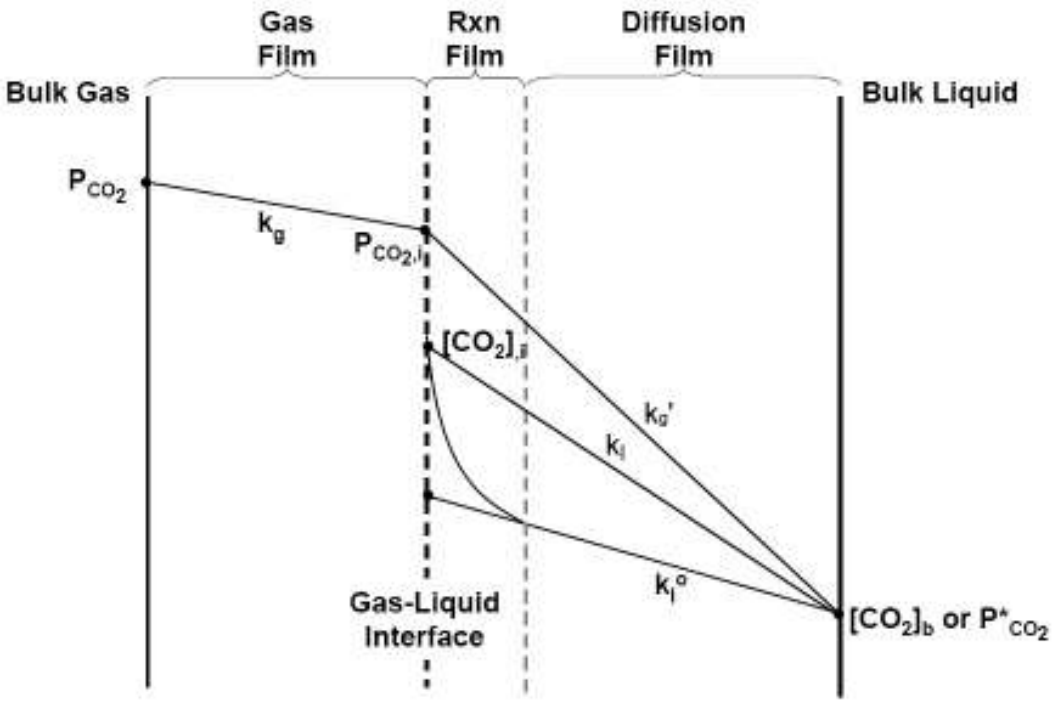

Figure 2.1: Mass transfer of CO_2 into the bulk liquid with fast chemical reaction

Gaseous CO_2 molecules diffuse through the gas film to the gas-liquid interface. At the gas-liquid interface the gaseous CO_2 dissolves according to the Henry's solubility. The dissolved CO_2 is significantly depleted near the interface due to reaction with the amine, while the CO_2 diffuses to the bulk liquid.

The slope of the CO_2 concentration profile defines the mass transfer coefficients. Equations 2.20–2.23 describe the flux equations which can be written using the overall mass transfer coefficient (K_G), gas film mass transfer coefficient (k_g), or a liquid film mass transfer coefficient (k_l or k_g'). k_l is the liquid film mass transfer coefficient. k_g' is the liquid film mass transfer coefficient defined in gas film units. k_g' is convenient to use since partial pressures, not liquid phase concentrations, are experimentally measured. No Henry's constant assumptions are required. k_l^o is the physical liquid film mass transfer coefficient, which does not incorporate reaction.

$$N_{CO2} = K_G (P_{CO2,b} - P^*_{CO2,b}) \tag{2.20}$$

$$N_{CO2} = k_g (P_{CO2,b} - P_{CO2,i}) \tag{2.21}$$

$$N_{CO2} = k_l ([CO_2]_i - [CO_2]_b) \tag{2.22}$$

$$N_{CO2} = k_g^{'} (P_{CO2,i} - P^*_{CO2,b}) \tag{2.23}$$

The flux in Equations 2.20–2.23 is constant, and Equations 2.20, 2.21 and 2.23 can be combined. Combining these three equations yields a series resistance relationship between the mass transfer coefficients.

$$\frac{1}{K_G} = \frac{1}{k_g} + \frac{1}{k_g^{'}} \tag{2.24}$$

Since k_g' encompasses the reaction and the liquid phase diffusion films, it has both a reaction and a diffusion component. These two components can be separated as shown in Equation 2.25. The first term, k_g'', is the pseudo first order term which represents the reaction kinetics of the amine. The second term represents diffusion resistance and depends on the liquid film physical mass transfer coefficient and the slope of the equilibrium line.

$$\frac{1}{K_G} = \frac{1}{k_g} + \frac{1}{k_g^{''}} + \frac{1}{k^o_{l,prod}} \left(\frac{\Delta P^*_{CO2}}{\Delta [CO_2]_T} \right) \tag{2.25}$$

The problem with separating k_g' into these two terms is that these terms are difficult to quantify, particularly the slope of the equilibrium curve, which is extremely steep. Separating k_g' into these two terms generally introduces significant error. Results in the current work are reported as k_g' values.

The third term in Equation 2.25, which includes the slope of the equilibrium line, results from changing a concentration driving force to a partial pressure driving force to

enable a series resistance relationship with K_G, k_g, and k_g''. Equation 2.26 shows the transition using the film schematic shown in Fig 2.1 where RDint denotes the reaction-diffusion interface.

$$N_{CO2} = k_l^o\left([CO_2]_{RD\,\mathrm{int}} - [CO_2]_b\right) = k_l^o\left(\frac{[CO_2]_{RD\,\mathrm{int}} - [CO_2]_b}{P_{CO2,RD\,\mathrm{int}} - P_{CO2,b}}\right)\left(P_{CO2,RD\,\mathrm{int}} - P_{CO2,b}\right) \quad (2.26)$$

As Figure 2.1 shows, there is a gas film resistance, a reaction resistance, and a liquid film diffusion resistance. A system in which the liquid phase diffusion is unimportant leads to the pseudo first order condition. A system in which the reaction resistance is negligible leads to the instantaneous reaction condition. The gas film resistance can be negligible but this case does not require special consideration. It is also possible for two resistances to be negligible.

2.2.4 Pseudo First Order Reaction

The pseudo first order approximation is a simplification to mass transfer with fast reaction in which the liquid reactant and product concentrations are assumed constant throughout the liquid boundary layer. It assumes that the liquid phase diffusion resistance is negligible. This assumption may be justified at high free amine concentrations, low CO_2 fluxes, or at high liquid film physical mass transfer coefficient conditions.

A material balance of a fixed volume requires that the change in flux of dissolved CO_2 must be the result of reaction. A CO_2 material balance for absorption is shown in Equation 2.27.

$$D_{CO2}\frac{\partial^2[CO_2]}{\partial x^2} - k_f[Am][CO_2] = 0 \quad (2.27)$$

The reaction of CO_2 with amines should be considered as a reversible process at appreciable CO_2 loading. The industrial absorption/stripping of CO_2 will occur at appreciable CO_2 loading where the reversibility of the reaction should be considered. Danckwerts (1970) shows that the reversible case can be presented as Equation 2.28 using an equilibrium CO_2 concentration to account for reversibility. That parameter is obtained by using the equilibrium constant with the assumption that both the amine and product concentrations are the same at the interface as in the bulk solution. Essentially this simplification requires the pseudo first order condition for the amine and the product. This simplifies the rate expression form used in Equation 2.18.

$$D_{CO2}\frac{\partial^2[CO_2]}{\partial x^2} - k_f[Am]\left([CO_2] - [CO_2]_e\right) = 0 \qquad (2.28)$$

Equation 2.28 leads to Equation 2.29 using the proper boundary conditions and assuming fast reaction so that physical absorption of CO_2 can be ignored. Here the rate constant is represented as k_2 to conform with convention.

$$N_{CO2} = \frac{\sqrt{D_{CO2}k_2[Am]}}{H_{CO2}}(P_{CO2,i} - P^*_{CO2,b}) \qquad (2.29)$$

The similarity between Equations 2.23 and 2.29 leads to Equation 2.30. The similarity infers that, under pseudo first order conditions, the liquid film mass transfer coefficient can be analytically determined.

$$k_g^{'} = \frac{\sqrt{D_{CO2}k_2[Am]_b}}{H_{CO2}} \qquad (2.30)$$

2.2.5 Instantaneous Reaction

Another special case of mass transfer with chemical reaction occurs when the reaction can be considered instantaneous with respect to diffusion. This case might occur

with very fast reactions or very low reactant concentrations. The diffusion of reactants to the reaction interface and the diffusion of products away from the reaction interface dominate the process. This case can be viewed graphically in Figure 2.2 for a carbamate forming system.

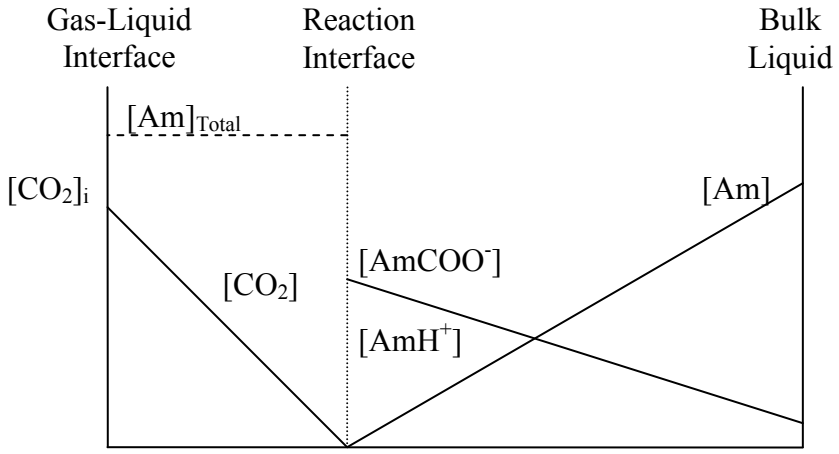

Figure 2.2: Concentration profiles for CO_2 absorption with instantaneous reaction

The instantaneous reaction case is important because it represents a mass transfer extreme and is often seen at stripper conditions. Amine systems for CO_2 capture can also operate between instantaneous and pseudo first order conditions where both reaction kinetics and diffusion properties are significant.

A stripper in a CO_2 capture system can be considered in terms of this instantaneous reaction case. The stripper operates at a higher temperature than the absorber and therefore has much higher CO_2 partial pressure driving forces. Under these very high driving forces, the kinetics become unimportant and mass transfer is limited by diffusion coefficients in the liquid phase.

2.2.6 Bronsted Theory

A significant amount of work on acid-base catalysis was performed by Bronsted (1928). This work provided an important link between equilibrium strength and reaction rates. K_a is the equilibrium constant of the dissociation of an acid which is written with respect to water. A designates the acid and A^- designates the base.

$$A + H_2O \xleftrightarrow{K_a} A^- + H_3O^+ \tag{2.31}$$

K_a is representative of the strength of an acid (or base) and is generally referred in terms of the pK_a defined in Equation 2.32.

$$pK_a = -\log_{10} K_a \tag{2.32}$$

Base catalysis has been widely recognized as a contributing factor in CO_2 reaction rates with amines. Both the zwitterion and termolecular reaction mechanisms can account for acid-base catalysis. Data compiled by Rochelle et al. (2001) show the correlation between rate constants and pK_a for primary, unhindered amines. Similarly, the pK_a of an extracting base can affect CO_2 reaction rates.

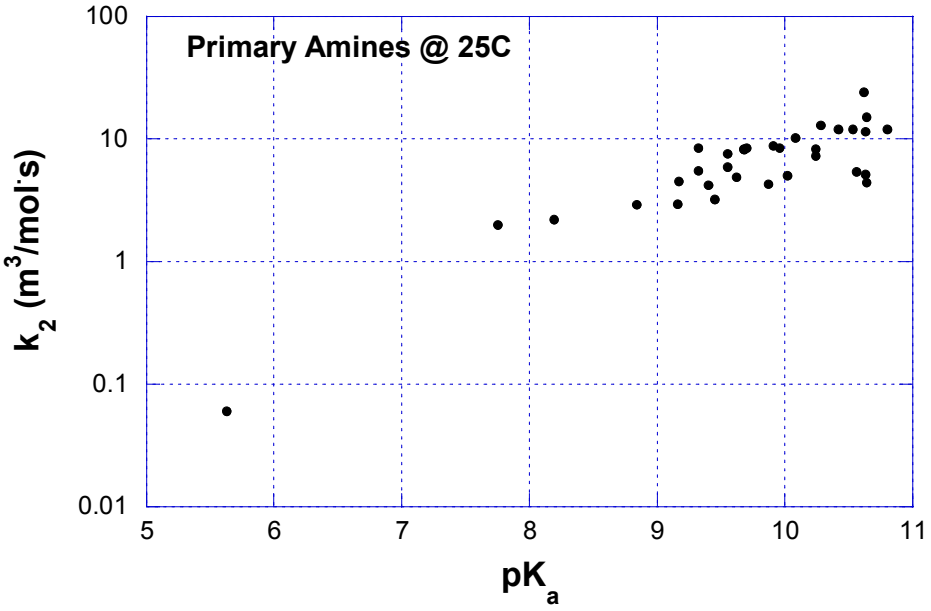

Figure 2.3: Bronsted correlation of CO_2 reaction rates for unhindered, primary amines at 25˚C (Rochelle, Bishnoi et al. 2001)

2.2.7 Mass Transfer Contactors

Various gas-liquid contactors are used to measure absorption or desorption of CO_2 in amine systems. Each contactor has advantages and disadvantages. Three of the more common contactors are briefly introduced here. Each type of contactor may also have multiple versions with unique characteristics but the operating concept for the contactor remains the same.

2.2.7.1 Stirred Cell

The stirred cell is a gas-liquid contactor which operates with a smooth, horizontal gas-liquid interface. This smooth interface is vital in preserving the known contact area for the reaction. The gas and liquid phases can be mixed independently using magnetic stirrers. This allows for both gas and liquid phases to remain homogeneous during CO_2

mass transfer. Gaseous CO_2 can be introduced into the cell at the start of the experiment, pressurizing the cell. The pressure can be measured as a function of time to determine the rate at which the gaseous CO_2 is reacting with the solvent. Derks et al. (2006) is among recent researchers who measure reaction rates using a stirred cell. Figure 2.4 shows a schematic of the stirred cell Derks utilized.

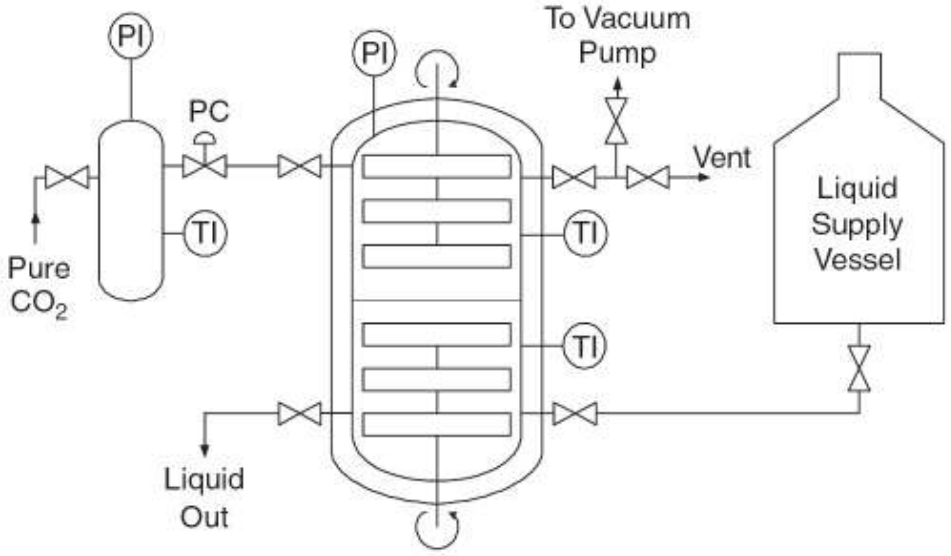

Figure 2.4: Schematic of a stirred cell contactor (Derks, Kleingeld et al. 2006)

The main advantage of the stirred cell is its simplicity. Also, the rate of absorption is measured using a liquid having a single, known composition, assuming k_l^o is sufficiently large.

The disadvantages of the stirred cell include the limitations in k_l^o. A homogenous liquid is required but the solution must not be stirred to the point that the gas-liquid interface is agitated. A fast reaction with large CO_2 fluxes can create possible concentration differences at the gas-liquid interface. The value of k_l^o can also be sensitive to the immersion depth of the liquid phase stirrer (Danckwerts 1970). The volume of liquid in a stirred cell apparatus is much larger than a packed column so any

systems which include significant bulk liquid reactions cannot be modeled using this apparatus. It is also difficult to get large values of k_g so conditions where CO_2 is diluted can be difficult to interpret.

2.2.7.2 Laminar Jet

The laminar jet absorber shoots a jet of liquid through a tiny circular hole. The solvent contacts a CO_2-rich gas phase over a known height before re-entering a slightly larger hole. The jet can be considered a cylindrical rod in uniform motion. Typically the jet is about 1 mm in diameter and a few cm in length. The time of exposure can be determined by the jet height and velocity. The jet is housed in a closed, CO_2 rich environment in which the pressure can be monitored to determine the rate of CO_2 absorption. Aboudheir et al. (2003) is among recent researchers who used a laminar jet absorber. Figure 2.5 shows a schematic of the laminar jet absorber Aboudheir used.

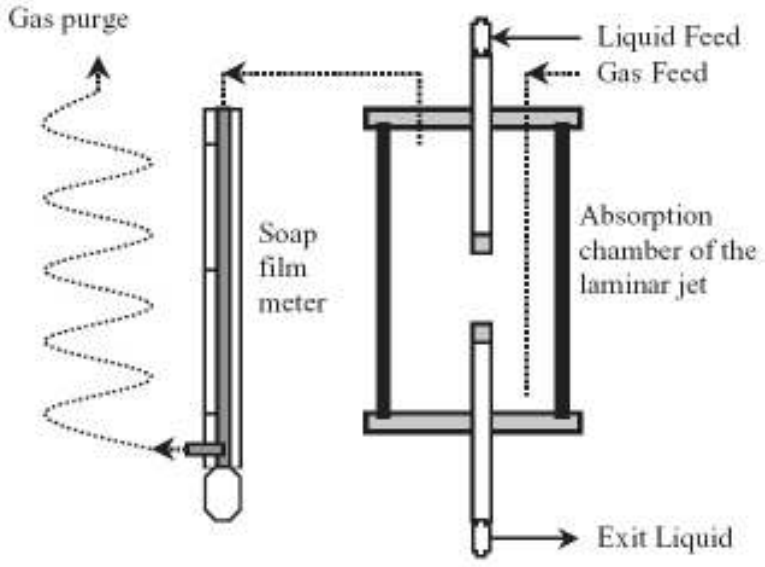

Figure 2.5: Schematic of a laminar jet contactor (Aboudheir, Tontiwachwuthikul et al. 2003)

The laminar jet absorber has the advantage of having very short contact times and therefore very large k_l^o values. At most conditions the free amine at the surface cannot be appreciably depleted from the top to the bottom of the contactor due to the short contact time. Often the contact length of the jet can be adjusted. The laminar jet absorber is well suited to measure absorption rates in fast systems.

The laminar jet requires the selection of a suitable nozzle or orifice to ensure a uniform jet velocity as well as the convergence of the jet at the bottom of the contactor. The laminar jet absorber requires several tens of liters of solution for a comprehensive series of measurements (Danckwerts 1970).

2.2.7.3 Wetted Wall Column

In a wetted wall column the liquid flows in a film, under the influence of gravity, down a surface, usually a tube or rod. The contacting gas flows countercurrent to the liquid and mass transfer occurs over the gas-liquid contact area. The rigid tube or rod has a known surface area which is entirely coated by the thin film of solvent. The length of the rod can be adjustable to vary the contact time and thus vary the liquid film physical mass transfer coefficient. A wetted wall column contactor has been used in this work. The same wetted wall column was used by previous researchers (Bishnoi and Rochelle 2000; Cullinane and Rochelle 2006).

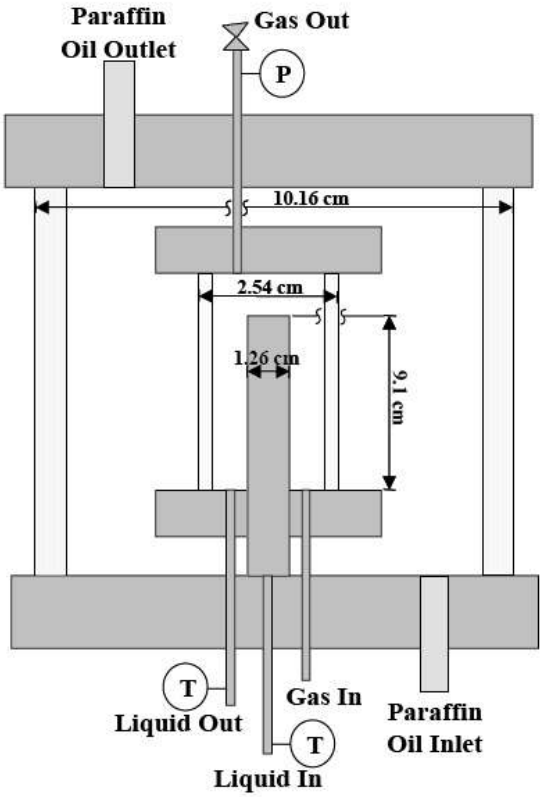

Figure 2.6: Schematic of the wetted wall column contactor used in this work

One major advantage of the wetted wall column is its versatility. It can operate over a wide range of conditions and can absorb or desorb CO_2 equally well. The k_l^o values for the wetted wall column can also be easily compared to packed columns by comparing the flow path lengths. Wetted wall columns have high k_l^o values allowing them to measure fast reacting amines.

Among the concerns of the wetted wall column are the entrance effects. It is important that the solvent is evenly dispersed so that a uniform film coats the entire surface of the rod. Any dry spots on the surface of the rod will not contribute to the flux and will lead to erroneous calculations. It is important to prevent the solution from

rippling as it flows down the side of the contactor. The ripples enhance the liquid film physical mass transfer coefficient, k_l^o, and may affect the rate of absorption.

2.3 RATE STUDIES

2.3.1 Quantifying Reaction Rates

Rate studies for CO_2 absorption rates with amines usually publish rate constants as the culmination of the work. However, rate constants can be misleading. Higher rate constants do not necessarily correspond with faster reaction. Systems that adhere to the pseudo first order assumption have fluxes that can be represented by Equation 2.33.

$$N_{CO2} = \frac{\sqrt{D_{CO2} k_2 [Am]}}{H_{CO2}} (P_{CO2,i} - P^*_{CO2,b}) \qquad (2.33)$$

It is true that increasing the rate constant in Equation 2.33 will lead to a higher flux, but that does not mean that another system with a slower rate constant will have slower fluxes. The important parameter is not the rate constant but the mass transfer coefficient, the group of terms multiplied by the driving force. Therefore, it is important to consider all the aspects of the mass transfer coefficient, not just the rate constant.

Imagine two amine systems with similar rate constants, diffusion coefficients, and free amine concentrations. If one of those systems has a higher CO_2 solubility ($1/H_{CO2}$) in the liquid phase, it will achieve higher CO_2 absorption rates because there are many more reactants present. This concern is ignored analytically by the convention that Henry's constants are usually calculated as the CO_2 solubility in water. That may be an acceptable assumption for much of the kinetic literature data, since dilute, unloaded solutions are typically used. However in industrial application, particularly CO_2 capture from flue gas, concentrated, CO_2 loaded solutions will be used. These highly concentrated, ionic solutions will not have CO_2 activity coefficients of 1.0. Browning

and Weiland (1994) have shown that the effective Henry's constant in 30 wt% MEA varies from 4800 $Pa \cdot m^3/mol$ at 0 CO_2 loading to 7400 $Pa \cdot m^3/mol$ at 0.35 loading. This decreased CO_2 solubility at higher CO_2 loading is significant and should be included in reaction rate considerations. The Henry's constant affects the flux to the first power while the diffusion coefficient, rate constant, and free amine concentration only have a 0.5 power dependence.

There is also a more subtle rate consideration involving partial pressure and speciation. The focus of this work is on CO_2 capture from flue gas, particularly flue gas from coal-fired power plants. In that case, the inlet CO_2 concentration is likely in the 12% or 12,000 Pa partial pressure range at the bottom of the absorber. It is desirable to obtain a CO_2 rich solution which may have a CO_2 partial pressure in the 5,000 Pa range. At a 5 kPa CO_2 partial pressure, different amine solutions will have different CO_2 loadings. If two carbamate producing amines have CO_2 loadings of 0.25 and 0.5 at a 5 kPa CO_2 partial pressure, these solutions will have drastically different free amine concentrations. The amine system at 0.25 loading may have ten times more free amine than the other. Since the free amine concentration is a component of the mass transfer coefficient, it will affect CO_2 mass transfer. The kinetics at rich solution conditions are the most vital for CO_2 capture. The rich solution reacts slowest and therefore the majority of the absorber column must contain relatively rich amine solution. This subtle speciation consideration may warrant consideration for some amine systems.

Both the Henry's constant and speciation concerns can be simply addressed by reporting mass transfer coefficients at conditions typical of industrial processes, in this case CO_2 capture from coal-fired power plant flue gas. In the current work, rate constants are not reported. A liquid phase mass transfer coefficient, k_g', is reported over

a range of applicable CO_2 capture partial pressures. k_g' is defined in Equation 2.34. In the pseudo first order case, k_g' is the grouping of terms including the diffusion coefficient, rate constant, free amine concentration, and Henry's constant.

$$k_g' = \frac{N_{CO2}}{(P_{CO2,i} - P^*_{CO2,b})} \tag{2.34}$$

In summary of this section, when comparing two amine systems a higher rate constant does not necessarily correspond to faster CO_2 mass transfer. A higher k_g' always corresponds to faster CO_2 mass transfer when tested at proper industrial conditions.

Regardless of the weaknesses of rate constants, almost all of the literature data is presented in terms of rate constants. Since k_g' data is generally not available, rate constant data is the best measure available to compare CO_2 reaction rates in various amine systems.

2.3.2 MEA Systems

A significant amount of data is available on rate studies concerning the reaction of CO_2 and MEA. Table 2.1 characterizes the current literature data.

Table 2.1: Literature data on the reaction between CO_2 and aqueous MEA

Reference	Temp (C)	[MEA] (mol/l)
(Jensen, Jorgensen et al. 1954)	18	0.1–0.2
(Astarita 1961)	21.5	0.25–2.0
(Emmert and Pigford 1962)	25	0.1–2.0
(Clarke 1964)	25	1.6–4.8
(Sharma 1965)	25–30	1.0
(Danckwerts and Sharma 1966)	18–35	1.0
(Leder 1971)	80	–
(Sada, Kumazawa et al. 1976a)	25	0.2–1.9
(Hikita, Asai et al. 1977)	5.4–35.2	0.02–0.18
(Alvarez-Fuster, Midoux et al. 1980)	20	0.2–2.0
(Donaldson and Nguyen 1980)	25	0.03–0.08
(Laddha and Danckwerts 1981a)	25	0.49–1.71
(Penny and Ritter 1983)	5–30	0–0.06
(Sada, Kumazawa et al. 1985)	30	0.5–2.0
(Barth, Tondre et al. 1986)	20–25	0.02–0.05
(Crooks and Donnellan 1989)	25	0.02–0.06
(Alper 1990)	5–25	0–0.45
(Littel, Versteeg et al. 1992)	45–60	0–3.2
(Dang and Rochelle 2003)	40–60	2.5–5.0
(Aboudheir, Tontiwachwuthikul et al. 2003)	20–60	3.0–9.1
(Jamal, Meisen et al. 2006)	20–110	0.7–5.0
(Hartono 2009)	25–50	0.5–5.0

Although Table 2.1 includes a large amount of literature data for MEA kinetics, little of it is directly applicable to industrial CO_2 capture systems. Industrial systems would likely operate at absorber temperatures ranging from 40 to 70˚C while the majority of the literature data was collected near ambient conditions. Also, higher temperature data by Leder (1971) and Littel et al. (1992) are likely erroneous due to experimental or calculation inaccuracies (Versteeg, Van Dijck et al. 1996). The only CO_2 loaded, large

data source above 40˚C is Aboudheir et al. (2003). However, laminar jet absorber results from Aboudheir et al. are not easily comparable nor do they seem to coincide with the literature data.

Industrial CO_2 capture systems will operate at high amine concentrations with CO_2 loaded solutions. All of the data with the exception of those by Dang and Rochelle (2003), Aboudheir et al. (2003), and Jamal et al. (2006) were collected using unloaded solutions. Very little of the data besides these three sources was collected at significant MEA concentrations. Industrial operation will likely require at least 4 M MEA to reduce operational costs.

Although data by Jamal et al. include interesting conditions (unloaded absorption experiments up to 50˚C and high temperature desorption experiments of loaded MEA solutions), it is not particularly useful. Jamal does not report rate constants for MEA nor provide raw data on the experimental conditions of the experiments.

Dang et al. provide useful kinetic results but only provide a total of seven data points. Three CO_2 loadings in 2.5 M MEA and four CO_2 loadings in 5 M MEA were examined.

The data collected by Aboudheir are the only valuable, major data source applicable to CO_2 capture systems. As previously mentioned, the extracted kinetics do not seem to agree with other literature data. The difference may be due to the highly concentrated, highly loaded, or highly non-ideal nature of these solutions. The differences for ideal versus non-ideal systems highlight the need to perform rate studies on amine systems similar to those expected for industrial systems. In addition to explaining why the Aboudheir data do not agree with the literature data, the current work

adds to the literature data for highly loaded, highly concentrated MEA solutions using a wetted wall column.

2.3.3 PZ Systems

In contrast to more traditional amines such as MEA, DEA, AMP, and MDEA, there is little data published on aqueous piperazine systems. Table 2.2 summarizes five studies from which kinetic data can be extracted.

Table 2.2: Literature data on the reaction between CO_2 and aqueous piperazine

Reference	Temp	[PZ]
	(C)	(mol/l)
(Bishnoi and Rochelle 2000)	25	0.2–0.6
(Sun, Yong et al. 2005)	30–40	0.23–0.92
(Derks, Kleingeld et al. 2006)	20–40	0.6–1.5
(Cullinane and Rochelle 2006)	25–60	0.43–1.33
(Samanta and Bandyopadhyay 2007)	25–40	0.2–0.8

The main reason for the lack of aqueous piperazine data is that piperazine is historically used in combination with other amines, rather than as a stand-alone solvent. Piperazine has very fast kinetics and is an effective promoter in some systems. Rigorous flux models for aqueous piperazine or piperazine blend systems require piperazine reaction kinetics. Since piperazine is typically used in blended systems, low piperazine concentrations have been examined in past studies. Again, relatively low temperature data have been measured rather than the 40–70˚C conditions more typical of an industrial absorber.

Recent solid solubility data has shown that piperazine can be used in very high concentrations (>50 wt%), possibly making aqueous piperazine feasible for industrial CO_2 capture (Hilliard 2008). Aqueous piperazine systems have also shown high

resistance to thermal degradation which can occur in the stripper and reboiler (Davis 2009).

Only the Bishnoi study in Table 2.2 was conducted with CO_2 loaded amines. The current work explores piperazine rates in loaded systems at higher temperatures and much higher amine concentrations.

2.2.4 MEA/PZ Systems

Piperazine has historically been used as a promoter due to its fast reaction rates and perceived low solubility. Piperazine activated aqueous MDEA, AMP, MEA, and potassium carbonate have all been studied (Bishnoi and Rochelle 2000; Dang and Rochelle 2003; Sun, Yong et al. 2005; Cullinane and Rochelle 2006). Monoethanolamine is the fastest of these four solvents and is being evaluated in the present work. Previous work on MEA/PZ solvents is scarce and is shown in Table 2.3.

Table 2.3: Literature data on the reaction between CO_2 and MEA/PZ blends

Reference	Temp	[MEA]	[PZ]	CO_2 Loading
	(C)	(mol/l)	(mol/l)	(mol/mol_{alk})
(Dang and Rochelle 2003)	40	0.4	0.6	0.06–0.14
	40	1.9	0.6	0.01–0.44
	40–60	3.8	1.2	0.41–0.43
(Okoye 2005)	40–60	4.4	1.2	0.28–0.57

Both literature sources for rate data on MEA/PZ systems study loaded systems. Although Dang and Rochelle (2003) provide data for three different MEA/PZ solvent blends, there is little data at each blend composition. Dang provides a total of seven data points. Rate data by Okoye (2005) is similarly scarce. Okoye provides a total of six data points from his MEA/PZ rate experiments. To complicate matters, data from Okoye does not agree with Dang and seems unreasonable.

The current work seeks to expand the rate data for MEA/PZ blended systems by evaluating 7 m MEA/2 m PZ.

2.4 DIFFUSION COEFFICIENT AND VISCOSITY CONSIDERATIONS

The current work uses a wetted wall column for rate measurements. CO_2 mass transfer in the wetted wall column, utilizing very fast, highly concentrated, highly loaded amines is likely to be dependent on diffusion properties under some conditions. The wetted wall column has a liquid flow path of 9.1 cm. Two-inch industrial packing likely has an average liquid flow path 2–3 cm before remixing. The reduced liquid flow path in packed columns results in a higher liquid film physical mass transfer coefficient, k_l^o. The higher mass transfer coefficient may result in negligible diffusion resistance in packed columns but not in wetted wall column experiments. Therefore, it is very important to understand the diffusion properties to extrapolate reaction rates in industrial columns.

Some researchers have produced viscosity-diffusion coefficient correlations to account for physical property differences (Versteeg and Van Swaaij 1988; Snijder, te Riele et al. 1993). The empirically regressed correlations do not provide first order dependencies as the Wilke-Chang equation may suggest (Equation 2.35). Work by Versteeg and Van Swaaij (1988) has shown that the diffusion of N_2O and CO_2 in aqueous amines generally follows the viscosity dependence in Equation 2.36. Snijder et al. (1993) have shown that alkanolamine diffusion in aqueous alkanolamine solutions follows the viscosity dependence in Equation 2.37.

$$D_{AB} \propto \frac{\sqrt{\psi_B M_B} T}{\mu \cdot V_A^{0.6}} \tag{2.35}$$

$$\left(D_{N2O}\eta^{0.8}\right)_{Amine Solution} = CONSTANT = \left(D_{N2O}\eta^{0.8}\right)_{Water} \tag{2.36}$$

$$\left(D_{Amine}\eta^{0.6}\right)_{Amine Solution} = CONSTANT = \left(D_{Amine}\eta^{0.6}\right)_{Water} \tag{2.37}$$

To make matters more complicated, the N_2O and CO_2 diffusivity relationship in Equation 2.36 was confirmed with MDEA solutions but resulted in less satisfactory results for AMP (Tomcej and Otto 1989; Xu, Otto et al. 1991). If the diffusion relationships are dependent on amines, the relationship in Equation 2.36 may not directly apply to MEA, piperazine, or MEA/PZ systems. The diffusion coefficient must be determined for each system to evaluate rate data where both diffusion and reaction kinetics affect mass transfer. The current work uses a diaphragm cell to measure diffusion coefficients in monoethanolamine and piperazine systems.

Chapter 3: Experimental Methods

This chapter includes information on the experimental methods and apparatus used in this work. A diaphragm cell was used to collect diffusion coefficient data in MEA and PZ solutions. A wetted wall column was used to collect CO_2 partial pressure and CO_2 rate data in MEA, PZ, and MEA/PZ solutions. Supporting equipment and techniques used in the evaluation of data or experimental samples are also discussed.

3.1 DIAPHRAGM CELL

3.1.1 Diaphragm Cell Description

A diaphragm cell was built to measure diffusion coefficients in CO_2 loaded amine solutions. Diaphragm cells are recognized among the best diffusion coefficient measuring devices because they are simple, rugged, and can be very accurate (Cussler 1997). Figure 3.1 shows a picture of the diaphragm cell used in these experiments.

The diaphragm cell consists of a glass tube with a glass frit at the midpoint. The cell body is 13.8 cm tall and 4.1 cm in diameter. The frit is 4 mm thick with a 10–16 μm pore size. The cell holds about 125 ml of solution during an experiment.

Figure 3.1: Diaphragm cell used in the experiments

Teflon end caps fitted with o-rings are used to maintain a closed system. Each end cap also includes a 1/8" Swagelok male connector fitting which is threaded into the end caps. The fitting allows air bubbles to be removed by injecting more solution with a syringe. The male connector fitting can be capped when gas bubbles have been removed from the cell.

Two stainless steel all thread rods are screwed into the inside of each of the Teflon end caps. A stainless steel plate and bored out plastic screw cap are suspended from the all thread rods. A glass rod is suspended through the bored plastic screw cap. The glass rod attaches to a 4-armed glass stirrer which encases a magnet. The stirrer is

positioned a few millimeters from the frit. This ensures the solution composition near the glass frit is the same as the bulk solution in that chamber.

The overall setup of the experiment can be seen in Figure 3.2. The diaphragm cell is suspended vertically in a temperature bath. Two rotating magnets spin around the cell causing the internal glass-encased magnets to mix the solution in each chamber. The stirrer speed was set to 120 rpm. Over time, the solution from the top chamber will diffuse into the bottom chamber and vice versa.

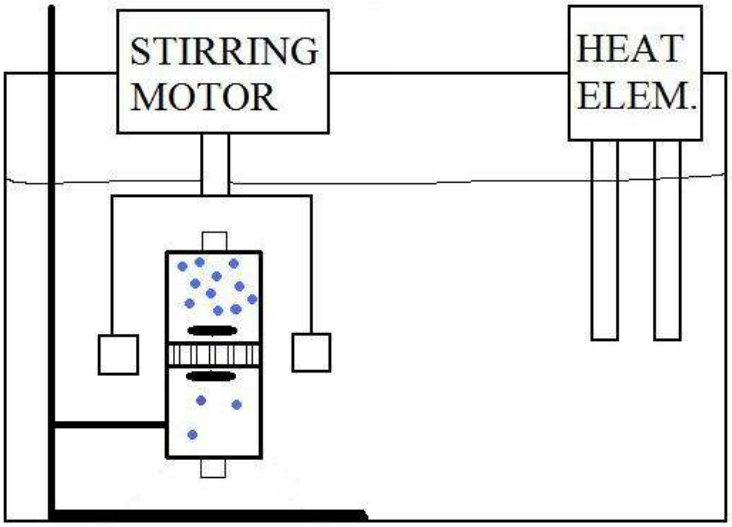

Figure 3.2: Schematic of the diaphragm cell experimental setup

3.1.2 Experimental Design

Diffusion experiments were conducted using 7–13 m MEA and 2–8 m PZ. For each amine concentration a low CO_2 loading and a high CO_2 loading experiment were conducted. In a typical low CO_2 loading experiment for MEA, a solution with a 0.25 loading was placed in the top chamber and a 0.35 CO_2 loading solution was placed in the bottom chamber. In every experiment, the solution with the higher loading was placed in the bottom chamber. Special care was taken to remove all air bubbles. Air bubbles from

the bottom chamber can rise to the glass frit and reduce the effective surface area for diffusion.

Warmer temperatures reduce the length of the experiment since diffusion occurs faster at higher temperatures where viscosities are lower. However, warmer solutions present a thermal expansion concern which can loosen one of the end caps. If the solution expands, pressure instead of diffusion may drive one solution into the other chamber. To reduce the thermal expansion concern, all experiments were conducted at 30˚C. The required experimental time varied substantially depending on the viscosity of the solution. Experiments ranged from 3–17 days. 12 m PZ experiments are not reported because significant CO_2 loading changes were not observed even after very long experimental times.

3.1.3 Data Interpretation

Diaphragm cells require accurate knowledge of the concentration differences, not the concentrations themselves (Cussler 1997). This is advantageous in these experiments because CO_2 loading changes measured via density measurements are more accurate than absolute CO_2 concentrations measured using the inorganic carbon analysis. The density of both MEA and PZ solutions can be treated as linear functions of CO_2 loading (Weiland, Dingman et al. 1998; Rochelle, Dugas et al. 2008).

To calibrate the diaphragm cell, diffusion coefficient values for aqueous potassium chloride concentrations were obtained from the literature (Zaytsev and Asayev 1992). KCl solutions of 8 and 16 wt% were used for calibration since the diffusion coefficient for KCl solutions is nonlinear below 5 wt% KCl.

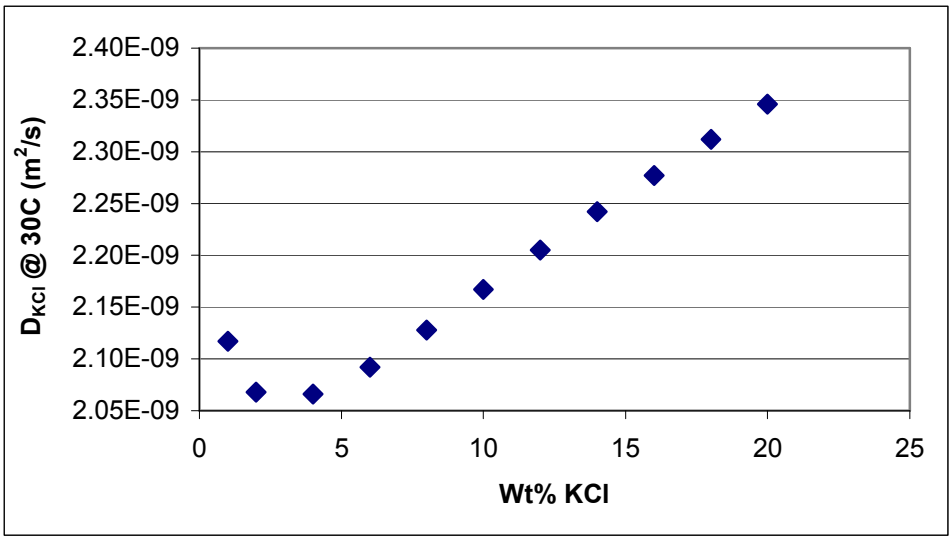

Figure 3.3: Diffusion coefficient values for aqueous potassium chloride at 30˚C (Zaytsev and Asayev 1992)

The diaphragm cell will have an effective diffusion coefficient which is termed the membrane-cell integral diffusion coefficient, $\overline{D}$. It is a complex concentration and time-averaged value which is not easily converted to the fundamental diffusion coefficient (Smith, Flowers et al. 2002). $\overline{D}$ is defined in Equation 3.1.

$$\overline{D} = \frac{C_{b,mean}\overline{D}^{0}(C_{b,mean}) - C_{t,mean}\overline{D}^{0}(C_{t,mean})}{C_{b,mean} - C_{t,mean}} \tag{3.1}$$

$C_{b,mean}$ is the mean of the initial and final bottom chamber concentrations. $\overline{D}^{0}(C_{b,mean})$ is the diffusion coefficient of $C_{b,mean}$. The computation of the membrane-cell integral diffusion coefficient allows for the calculation of the cell constant β.

$$\overline{D} = \frac{1}{\beta t}\ln\left(\frac{C_{b,t=0} - C_{t,t=0}}{C_{b,t=final} - C_{t,t=final}}\right) \tag{3.2}$$

After β is known for the cell, the membrane-cell integral diffusion coefficient can be determined for unknown solutions.

The obtained raw data from each experiment includes the density of the solution in each chamber both before and after diffusion. From these four density measurements and the CO_2 loading measurements on the two original solutions, the change in CO_2 loading for each solution can be determined. The membrane-cell integral diffusion coefficient, $\overline{D}$, of the amine solution can be determined using Equation 3.2.

3.2 WETTED WALL COLUMN

The wetted wall column originally built by Mshewa (1995) has been used by a number of researchers at The University of Texas at Austin under the direction of Dr. Gary Rochelle. These researchers have obtained CO_2 absorption/desorption rate data and CO_2 equilibrium partial pressure data from wetted wall column experiments. Mshewa (1995) studied MDEA, DEA, and MDEA/DEA systems. Pacheco (1998; 2000) studied MDEA, DGA, and MDEA/DGA systems. Bishnoi (2000; 2002a; 2002b) studied PZ and MDEA/PZ systems. Al-Juaied (2004; 2006) studied DGA, MOR, and DGA/MOR systems. Dang (2000; 2003) and Okoye (2005) both briefly examined MEA/PZ systems. Cullinane (2005; 2006) studied PZ and K_2CO_3/PZ systems.

3.2.1 Wetted Wall Column Description

A schematic of the wetted wall column apparatus is shown in Figure 3.4. Figure 3.5 shows a more detailed view of the wetted wall column reaction chamber. Figure 3.6 shows the exact measurements of the inner glass of the chamber.

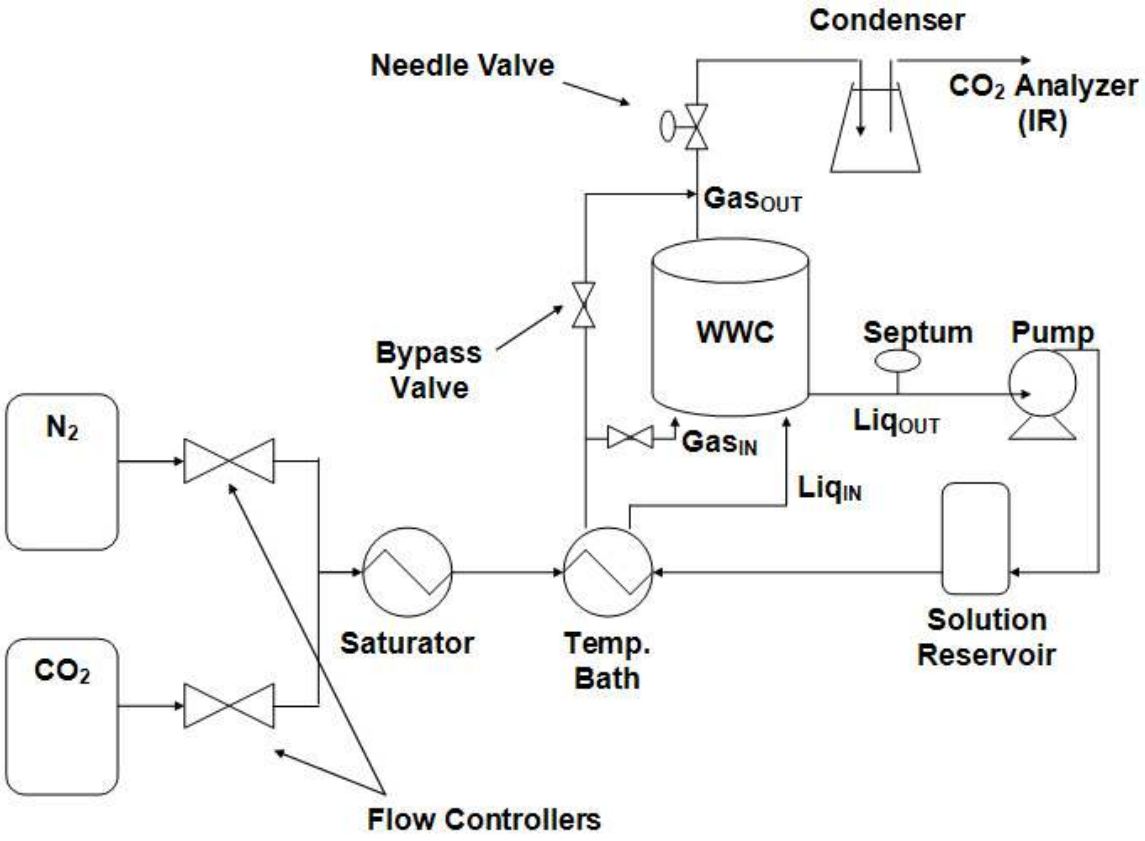

Figure 3.4: Overall schematic of the wetted wall column apparatus

Nitrogen and carbon dioxide are mixed using mass flow controllers to create a simulated flue gas of known concentration. The resultant N_2/CO_2 blend is routed to an oversized saturator which ensures saturation of the gas even at the higher experimental temperatures, 80 and 100˚C. This oversized, jacketed saturator is a new addition to the apparatus and consists of a fritted bubbler with 8–10 inches of water above the frit. Like the rest of the system, the saturator has been designed to operate at pressures up to 100 psig. A picture of the saturator is shown in Figure 3.7.

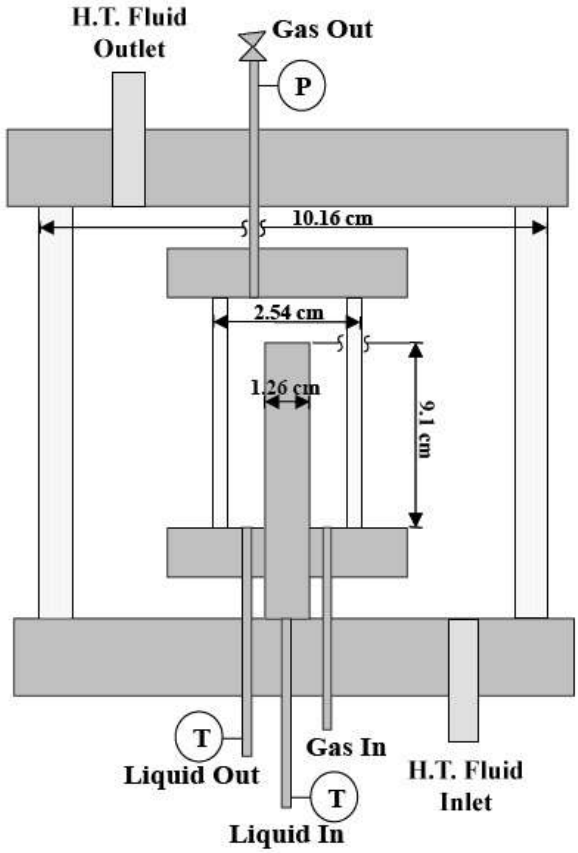

Figure 3.5: Schematic of the wetted wall column reaction chamber

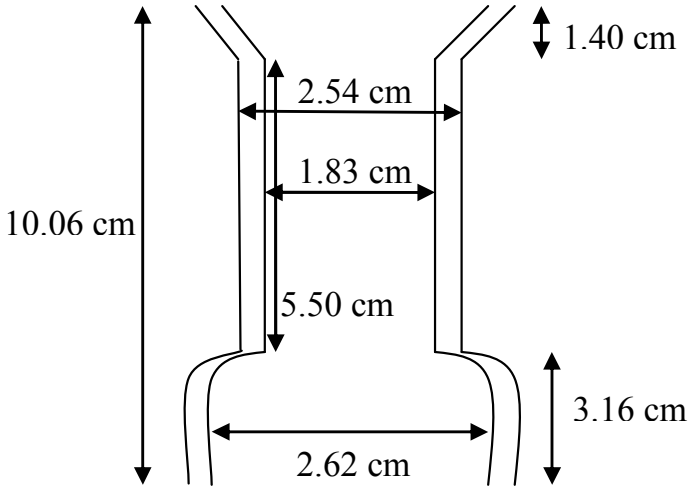

Figure 3.6: Dimensions of the inner glass of the wetted wall column reaction chamber

Figure 3.7: Bubbling saturator used in wetted wall column experiments

Unlike the gas, the solution is recycled though the system. The solution reservoir consists of two 1-liter insulated vessels connected in series. The screw-type positive displacement pump can be controlled to circulate various liquid rates. Solvent flow rates are typically controlled between 2–4 ml/s using a rotameter. The same liquid flow rotameter and calibration as described in Cullinane (2005) was used. A material balance indicates that even at the highest CO_2 flux experimental conditions, the bulk CO_2 concentration in the liquid will remain essentially unchanged.

A Teflon ring around the bottom of the stainless steel rod prevents the liquid and gas from mixing. The ring fits tightly against the inner glass but maintains about 1 mm spacing from the stainless steel rod. The ring is shaped such that the outside perimeter is

higher than the inside so any errant liquid will be funneled to the center and rejoined with the liquid flowing down the stainless steel rod. The Teflon ring has one hole near the midpoint of the inner and outer diameters. The gas enters through this single inlet point. A single gas inlet point, along with the chamber geometry as shown in Figure 3.6, can produce uncertain gas flow profiles. For this reason it is imperative to correlate the gas film mass transfer coefficient over a wide range of operating conditions: temperatures, pressures, and gas flow rates.

Dimethyl silicone fluid (viscosity = 50 cSt) was used as the heat transfer fluid in the wetted wall column, jacketed saturator, and the temperature bath.

3.2.2 Physical Mass Transfer Coefficients

3.2.2.1 Gas film Mass Transfer Coefficient

The gas film mass transfer coefficient, k_g, was determined by Pacheco (1998) for the wetted wall column using unloaded 2 M MEA. The reasoning for selecting MEA was two-fold. First, the kinetics of dilute, unloaded MEA solutions has been studied by various researchers and is well known. Second, the reaction of CO_2 with unloaded 2 M MEA is fast and mass transfer will be dominated by gas film resistance. According to the film resistance relationship, k_g' will be large compared to k_g and any errors in estimating the kinetics will be dwarfed by the dominance of the gas film mass transfer coefficient.

$$N_{CO2} = \frac{(P_{CO2,b} - P^*_{CO2,b})}{\frac{1}{k_g} + \frac{1}{k'_g}} \tag{3.3}$$

Low concentrations of CO_2 were fed to the reactor to prevent depletion of free MEA at the interface. Temperatures ranged from 25–90˚C while the gas flow rate varied from 0.02 to 1.4 l/min (Pacheco 1998). Pressures were generally held at 100 psig.

Pacheco determined the gas side resistance to be between 70 and 95% of the total resistance for these experiments (Pacheco, Kaganoi et al. 2000).

Pacheco followed a form presented by Hobbler (1966) when correlating the gas film mass transfer coefficient. Hobbler used dimensional analysis to correlate gas film mass transfer coefficients in laminar flowing wetted wall columns to the following form.

$$Sh = A \cdot \mathrm{Re}^{B}\, Sc^{C}\left(\frac{d}{h}\right)^{D} \tag{3.4}$$

Equation 3.4 includes the Sherwood, Reynolds, and Schmidt numbers as well as the hydraulic diameter and the height of the contactor. The hydraulic diameter, d, is defined as the outer diameter minus the inner diameter for an annulus. Constants A, B, C, and D can be regressed.

Pacheco (2000) obtained a good fit of the experimental data while simplifying Equation 3.4 to the following form with two regressed parameters. Pacheco's dissertation includes different regressed constants from the paper he published afterwards. The values in the paper (Pacheco, Kaganoi et al. 2000) and shown in Equation 3.5 are correct.

$$Sh = 1.075\left[\mathrm{Re}\, Sc\left(\frac{d}{h}\right)\right]^{0.85} \tag{3.5}$$

As a practical concern it is important to note that the viscosity and density are unimportant since these parameters cancel in the Re and Sc numbers.

The Sherwood number represents the ratio of convective to diffusive mass transport. It can be represented by Equation 3.6 which allows for the determination of the gas film mass transfer coefficient, k_g.

$$Sh = \frac{RTk_g d}{D_{CO2}} \tag{3.6}$$

Bishnoi later retested gas film mass transfer coefficients for the wetted wall column. He used sulfur dioxide absorption into 0.1 M sodium hydroxide, which has much faster kinetics than CO_2 absorption into MEA. Therefore, wetted wall column experiments should be more gas film controlled with the SO_2/NaOH system. Bishnoi also used greater gas flow rates, 5–6 standard l/min. Equation 3.5 matched gas film mass transfer coefficient measurements made by Bishnoi within 10%.

The glass of the wetted wall column containing the reaction chamber was fractured midway through the current experiments during a dismantling. Another piece, which had the same diameters as the original, was substituted. Gas film mass transfer coefficient experiments were performed to ensure compliance with the previous gas film mass transfer coefficient correlation. Experiments were performed using CO_2 absorption into unloaded 2 m PZ. Experimental conditions ranged from 3–5 standard l/min at 40 and 60˚C. Pressures ranged from 15–70 psig. Obtained results were shown to be similar to those predicted by Equation 3.5 (Rochelle, Sexton et al. 2008b). Equation 3.5 was used for the determination of the gas film mass transfer coefficient for all the wetted wall column experiments presented in this work.

It is important to recognize that the gas film mass transfer coefficient is a strong function of geometry and the correlations in this section only pertain to the wetted wall column in this work. Any other wetted wall column would require an independent determination of the gas film mass transfer coefficient.

3.2.2.2 Liquid Film Physical Mass Transfer Coefficient

The liquid film physical mass transfer coefficient was measured in the wetted wall column by Mshewa (1995) using CO_2 desorption from water and various concentrations of aqueous ethylene glycol. Mshewa used a theoretical prediction model for k_l^o based on work from Vivian and Peaceman (1956). Pacheco later added to the data by more thoroughly testing the effect of temperature. Pacheco chose to represent the correlation based on a theoretical model by Pigford (1941) which fit the data within 15% (Pacheco 1998). The Pigford model solves the continuity equation for diffusion into a falling liquid film where convective transport is considered in the direction of the flow while diffusive transport is considered in the direction perpendicular to the gas-liquid interface. The calculations yield the liquid film physical mass transfer coefficient, k_l^o, as a function of the liquid flow rate, the gas-liquid contact area, and a dimensionless driving force, Θ.

$$k_l^o = \frac{Q_{sol}}{A}(1-\Theta) \tag{3.7}$$

The liquid flow rate of the wetted wall column system is calibrated to a rotameter in the system where *x* represents the nominal rotameter reading (Cullinane 2005).

$$Q_{so\ln} = (0.4512x - 0.2901)\sqrt{\frac{7.83-\rho_{Tref}}{(7.83-0.997)\rho_{Tref}}}\sqrt{\frac{7.83-\rho^2}{7.83-\rho_{Tref}^2}} \tag{3.8}$$

The dimensionless driving force, Θ, defined by Equation 3.9, represents the solute driving force. The three terms in Equation 3.9 represent the concentration of the solute at the interface and in the bulk solution at the inlet and outlet of the wetted wall column. Equation 3.9 can be expressed as Equation 3.10 or 3.11 depending on the value of the dimensionless penetration distance, η.

$$\Theta = \frac{[CO_2]_i - [CO_2]_o^{out}}{[CO_2]_i - [CO_2]_o^{in}} \tag{3.9}$$

$$\Theta = 0.7857e^{-5.121\eta} + 0.1001e^{-39.21\eta} + 0.036e^{-105.6\eta} + 0.0181e^{-204.7\eta} \quad for \quad n > 0.01 \tag{3.10}$$

$$\Theta = 1 - 3\sqrt{\frac{\eta}{\pi}} \quad for \quad \eta < 0.01 \tag{3.11}$$

$$\eta = \frac{D_{CO2}\tau}{\delta^2} \tag{3.12}$$

All the wetted wall column experimental conditions produced dimensionless penetration distances, η, less than 0.01 so the simpler form of the dimensionless driving force (Equation 3.11) is applicable.

The film thickness and contact time required for Equation 3.12 are expressed in Equation 3.13 and 3.14. The parameter *W* refers to the circumference of the column

$$\delta = \sqrt[3]{\frac{3\mu Q_{sol}}{\rho g W}} \tag{3.13}$$

$$\tau = \frac{h}{u_s} \tag{3.14}$$

$$u_s = \frac{\rho g \delta^2}{2\mu} \tag{3.15}$$

The complex result of the liquid film physical mass transfer calculation can be simplified greatly by canceling and grouping terms. Equation 3.16 shows the simplified expression for k_l^o. This expression is only valid if η is less than 0.01, which is true for all experimental conditions.

$$k^o_{l,CO_2} = \left(\frac{3^{1/3}2^{1/2}}{\pi^{1/2}}\right)\left(\frac{Q^{1/3}h^{1/2}W^{2/3}}{A}\right)\left(\frac{g\rho}{\mu}\right)^{1/6} D^{1/2}_{CO2} \tag{3.16}$$

3.2.3 Experimental Concerns

The wetted wall column is a complex apparatus and the proper selection of operating conditions is crucial to obtaining high quality data. For a given experiment, the amine concentration(s), CO_2 loading, and temperature are set. These three parameters specify the CO_2 absorption/desorption performance (k_g') of the system. There are four independent operating variables for wetted wall column experiments: liquid flow rate, gas flow rate, total pressure, and CO_2 partial pressure. Proper selection of these four independent operating variables can greatly increase the accuracy of the wetted wall column rate data. There are five data accuracy concerns that are considered in the selection of the four operating variables. The five concerns that can affect data accuracy are: mass flow controller selection, CO_2 analyzer range selection, change in gas phase CO_2 concentration, gas film resistance, and a limiting liquid film physical mass transfer coefficient, k_l^o.

The limiting liquid film physical mass transfer coefficient concern is simply addressed by using a high liquid flow rate, which increases k_l^o. Liquid flow rates were maintained near the maximum reading of the rotameter. If k_l^o is not limiting, the liquid flow rate is unimportant to the experiment. The series resistance relationship is shown below.

$$\frac{1}{K_G} = \frac{1}{k_g} + \frac{1}{k_g^{'}} = \frac{1}{k_g} + \frac{1}{k_g^{''}} + \frac{1}{k^o_{l,prod}}\left(\frac{\Delta P^*_{CO2}}{\Delta[CO_2]_T}\right) \tag{3.17}$$

The gas film resistance concern is addressed by using a high gas flow rate and low total pressure. This increases the gas velocity in the contactor and increases the gas film mass transfer coefficient, making wetted column wall results more dependent on k_g'. k_g was controlled so that the gas film resistance would always be less than 50% of the

total mass transfer resistance. If the gas velocity is too fast the thin liquid film flowing down the contactor can be disturbed and dry spots on the contactor can appear. A fast gas velocity will also decrease the amount of CO_2 reacting in the chamber and reduce the statistical accuracy of the difference in the inlet and outlet gas phase CO_2 concentrations.

The change in gas phase CO_2 is considered in the selection of the gas flow rate, total pressure, and CO_2 partial pressure. The error associated with the change in gas phase CO_2 concentration has been greatly reduced by the use of PicoLog software. This software reads the output of the CO_2 analyzers and helps quantify even small changes in CO_2 concentration. A total of six inlet CO_2 partial pressures were tested for each experiment. This ensures that most of the partial pressures produce statistically significant changes in gas phase CO_2 concentration of the outlet stream.

The mass flow controller selection concern was addressed by adjusting gas flow rates. Mass flow controllers of 20, 15, 2, 0.5, and 0.1 standard l/min were used. Sometimes the six tested CO_2 concentrations were adjusted so that a mass flow controller of a smaller range could be used for the experiment. Using 0–100% of a 0.1 standard l/min controller is more accurate than using 0–20% of a 0.5 standard l/min mass flow controller.

The final data accuracy concern, CO_2 analyzer range selection, is addressed similarly to the mass flow controller concern. To ensure an optimal CO_2 analyzer range setting sometimes the total pressure or CO_2 partial pressures were adjusted.

3.2.4 Experimental Design and Operating Procedure

Each experiment measures the overall mass transfer coefficient, K_G, and the equilibrium P_{CO2} for a solution of known amine and CO_2 concentration at a given

temperature. To do this accurately, the experimental concerns addressed above were taken into account. The associated inaccuracies of each concern were balanced to determine the gas flow rates, liquid flow rate, total pressure, and CO_2 partial pressures for the experiment.

For each experiment six CO_2 partial pressures were tested. The lowest partial pressure was 0 Pa, pure nitrogen. The highest CO_2 partial pressure was double the estimated equilibrium CO_2 partial pressure of the solution. The other four partial pressures were spaced uniformly between the two extremes. This design allows for both absorption and desorption with similar CO_2 fluxes. It also allows for bracketing and determination of the equilibrium CO_2 partial pressure of the solution.

While experimental conditions approach steady state, the wetted wall column operates on bypass mode. The gas is sent around the reaction chamber (Figure 3.4). Once the CO_2 analyzer reading reaches steady state, the value is recorded and the simulated flue gas is redirected through the reaction chamber. When the CO_2 analyzer reading comes to a new steady state, the value is recorded and the gas is again redirected through the bypass. While on bypass mode, gas concentrations are adjusted to test another CO_2 partial pressure. Each of the six partial pressures was tested in this fashion.

The six partial pressures were not tested in increasing or decreasing order. A rotating absorption/desorption experimental design was implemented to avoid systematic error. The shifting absorption/desorption order can help address statistical concerns if some parameters inadvertently increase or decrease throughout the experiment.

3.2.5 Data Interpretation

At each experimental condition 12 CO_2 readings were obtained: six CO_2 partial pressures operating in bypass mode and six in operation mode. The values obtained in bypass mode can be used as a calibration curve since CO_2 concentrations are known via the mass flow controllers. The experimental readings can be fit to the calibration curve. The bypass mode readings are equivalent to the inlet partial pressures. The operation mode readings are the outlet partial pressures. The inlet and outlet partial pressures allow for the calculation of the CO_2 flux for each of the six runs. CO_2 flux can be plotted against the driving force as shown in Figure 3.8.

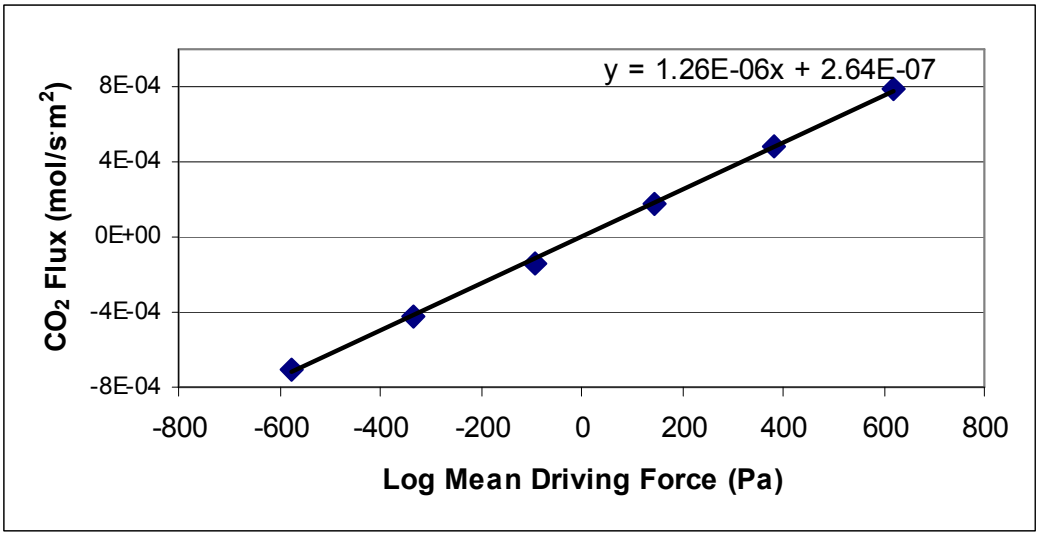

Figure 3.8: Flux against driving force plot for 7 m MEA, 0.351 loading, 60˚C

The log mean driving force is more appropriate than the average of the CO_2 driving forces at the top and bottom of the column. Since the CO_2 profile has a curved or somewhat asymptotic shape, the log mean driving force gives a better weighted average of the driving forces present in the wetted wall column. The log mean driving force can be calculated using Equation 3.18.

$$\Delta P_{CO2,lm} = \frac{\left(P_{CO2,in} - P^*_{CO2}\right) - \left(P_{CO2,out} - P^*_{CO2}\right)}{\ln\left(\frac{P_{CO2,in} - P^*_{CO2}}{P_{CO2,out} - P^*_{CO2}}\right)} \tag{3.18}$$

The equilibrium CO_2 partial pressure, P_{CO2}^*, of the solution is unknown but the solution must have zero flux when it has no driving force. Therefore, the value for the equilibrium partial pressure of the solution can be adjusted until the flux-driving force relationship shown in Figure 3.8 passes through the origin. When the line passes through the origin, the equilibrium CO_2 partial pressure value input into the equation must be correct.

Since the overall mass transfer coefficient, K_G, is defined by the relationship of the flux and driving force, the slope of the line is equal to K_G.

$$N_{CO2} = K_G(P_{CO2,b} - P^*_{CO2,b}) \tag{3.19}$$

Each point in Figure 3.8 could be used independently to determine K_G using the measured flux and driving force. However, this method can produce statistically misleading results. Points near equilibrium (near zero driving force) will have much larger statistical errors than the points far from equilibrium. Table 3.1 demonstrates how representing K_G on a point basis can be misleading. The 550 Pa condition in Table 3.1 shows a K_G of $1.52 \cdot 10^{-6}$ while the curve in Figure 3.8 shows a value of $1.26 \cdot 10^{-6}$. This error is present because the calculation divides by a very small value for the flux.

Table 3.1: Single point K_G determination for 7 m MEA, 0.351 loading, 60˚C

$P_{CO2,in}$	K_G
(Pa)	(mol/s·m^{2}Pa)
0	1.23E-06
275	1.27E-06
550	1.52E-06
825	1.27E-06
1100	1.27E-06
1375	1.27E-06

The K_G obtained from the curve fit method was used in determination of k_g'. k_g' can be determined from K_G using the calculated gas film mass transfer coefficient, k_g, and the series resistance relationships obtained from film theory (Equation 3.17).

3.3 SUPPORTING METHODS AND EQUIPMENT

This section includes information about supporting equipment and methods related to data acquisition from the diaphragm cell and wetted wall column.

3.3.1 CO_2 Loading of Samples

Amine solutions were loaded on a gravimetric basis. Amine solutions of known concentration were poured into a bubbling column equipped with a glass frit. The column was placed on a digital scale while CO_2 was bubbled into the solution. The gas flow rate was limited so that the vast majority of the bubbles absorbed before reaching the surface. This prevented gaseous CO_2 from sweeping away water vapor or amine and changing the solvent concentration. As the CO_2 reacted with the amine and went into the liquid phase, the mass of the CO_2 was registered by the scale. When the desired amount of CO_2 had been added to the solution, the gas flow was stopped. This method seemed to produce CO_2 concentrations accurate within 5%. The actual or reported CO_2 concentration was determined using an inorganic carbon analysis.

3.3.2 Inorganic Carbon Analysis

The inorganic carbon analysis is the definitive method for determining the CO_2 concentration in solution. A CO_2 loaded amine solution is injected into a tube containing 30 wt% phosphoric acid. At the resultant pH all the amine becomes protonated and CO_2 is liberated. The liberated CO_2 is swept away by nitrogen gas bubbling through the acid. The gas is routed through two tubes containing a desiccant (magnesium perchlorate) to dry the gas. The CO_2 concentration of the dry gas is measured by a Horiba PIR-2000 infrared analyzer. The pulse of CO_2 measured by the CO_2 analyzer is recorded by PicoLog, a data recording software. The recorded CO_2 mole fraction can be integrated over the pulse duration to determine the peak area. A calibration of peak area with moles of CO_2 is made using purchased inorganic carbon standards. The standard used in this work is a 1000 ppm carbon standard, which is comprised of a sodium carbonate/sodium bicarbonate mixture. Sodium carbonate and sodium bicarbonate combined in the correct ratios can produce a CO_2 partial pressure similar to that of the atmosphere, thereby increasing shelf life.

3.3.3 PicoLog Software

PicoLog data acquisition software, by Pico Technology Ltd., was used to record data from each of the three CO_2 analyzers used in this work. The software gives a real time customizable graph and spreadsheet of the measurements. To reduce computational intensity but preserve data quality during dynamic changes such as a CO_2 pulse for the inorganic carbon analysis, PicoLog software was set to record and log data once per second.

3.3.4 CO_2 Analyzers

Three CO_2 analyzers were used in this work. A Horiba PIR-2000 infrared analyzer was used to measure CO_2 concentrations from the sweep gas of the inorganic carbon analysis. The PIR-2000 has ranges of 0.05, 0.15, and 0.25 mole%. Generally the 0.05% range was used for inorganic carbon analysis.

Two newer Horiba VIA-510 infrared analyzers were used in the wetted wall column experiments. One analyzer has CO_2 measurement ranges of 0.05, 0.1, 0.5, and 1%. The other analyzer has ranges of 1, 2, 10, and 20% CO_2. Only one analyzer was used at a time. The correct analyzer and range was chosen based on experimental conditions. The wide range of experimental conditions tested in the wetted wall column utilized all the available ranges. Experiments at high CO_2 loading and high temperatures were not performed due to the maximum 20% CO_2 range of the higher range analyzer.

3.3.5 Mass Flow Controllers

During each wetted wall column experiment two mass flow controllers were used to control nitrogen and carbon dioxide flows into the system. 20, 15, 2, 0.5, and 0.1 standard l/min Brooks 5850 mass flow controllers were used. Standard conditions are defined as 0˚C and 1 atmosphere.

Most of the controllers were rated for nitrogen, which presents complications for carbon dioxide flows. Mass flow controllers work by redirecting a small but known fraction of the total gas passing through the controller. The redirected gas receives a known amount of heat and the change in temperature is measured. Based on the temperature change of the present gas and heat capacity of the calibrated gas, the flow rate of the redirected gas and thus total flow rate can be determined. Therefore, if the

experimental gas is different from the calibrated gas then the reported flow rate can be corrected using the ratio of the heat capacity of the two gases.

Since the smallest mass flow controller has a maximum range of 0.1 standard l/min, a diluted CO_2 gas was required for low CO_2 concentration experiments. An approximately 5000 ppm CO_2 in nitrogen blend was purchased and used for experiments which required very low CO_2 concentrations.

The calibration of each mass flow controller was periodically checked to ensure accuracy.

3.3.6 Density Meter

Density measurements to determine the change in CO_2 loading from diaphragm cell samples were performed using a Mettler Toledo DE40 density meter. This density meter is extremely accurate (± 0.0001 g/cm^3) and reproducible. The instrument operates on the oscillating body method which measures the electromagnetically induced oscillation of a U-shaped glass tube. A magnet is fixed to the U-shaped tube and a transmitter induces the oscillation. The period of oscillation of the tube is measured by a sensor. The frequency or period of the oscillation is a function of the mass of the liquid or gas contained in the U-shaped tube.

Chapter 4: Mass Transfer and CO_2 Partial Pressure Results

This chapter includes the experimental results of the diaphragm cell and the wetted wall column. The diaphragm cell measures diffusion coefficients in CO_2 loaded MEA and PZ solutions. The wetted wall column measures CO_2 partial pressure and CO_2 absorption/desorption rates in CO_2 loaded MEA and PZ solutions.

Detailed raw and calculated data for the diaphragm cell and wetted wall column experiments are included in Appendices B and C.

4.1 NECESSITY OF EXPERIMENTS

4.1.1 Need for Diaphragm Cell Experiments

Work by Versteeg and Van Swaaij (1988) has shown that the diffusion of N_2O and CO_2 in aqueous amines generally follows the viscosity dependence in Equation 4.1. Snijder et al. (1993) have shown that alkanolamine diffusion in aqueous alkanolamine solutions follow the viscosity dependence in Equation 4.2.

$$\left(D_{N2O}\eta^{0.8}\right)_{Amine Solution} = CONSTANT = \left(D_{N2O}\eta^{0.8}\right)_{Water} \quad (4.1)$$

$$\left(D_{Amine}\eta^{0.6}\right)_{Amine Solution} = CONSTANT = \left(D_{Amine}\eta^{0.6}\right)_{Water} \quad (4.2)$$

The N_2O and CO_2 diffusivity relationship in Equation 4.1 was confirmed with MDEA solutions but resulted in less satisfactory results for AMP (Tomcej and Otto 1989; Xu, Otto et al. 1991). If the diffusion relationships are dependent on amines, the relationship in Equation 4.1 may not directly apply to MEA, PZ, or MEA/PZ systems.

The current work uses a diaphragm cell to measure diffusion coefficients in MEA and PZ systems.

4.1.2 Need for Wetted Wall Column Experiments

A significant amount of data is available on rate studies concerning the reaction of CO_2 and monoethanolamine. These references are compiled in Table 2.1 of the Literature Review. Almost all of the data was obtained at low MEA concentrations in unloaded solutions. Unfortunately, these data do not allow for the prediction of CO_2 absorption/desorption rates in concentrated, CO_2 loaded MEA solutions, which are non-ideal solutions. These solutions can have significant activity coefficient and ionic strength effects not seen in the present literature data. Therefore, to predict CO_2 absorption/desorption rates at industrial conditions, rate experiments with concentrated, CO_2 loaded MEA solutions must be performed.

Currently, only Aboudheir (2003) has provided a major data source on the CO_2 reaction rates in concentrated, loaded MEA solutions. Dang (2003) provides a few more data points for comparison. This work provides a second major data source of CO_2 reaction rates in concentrated, CO_2 loaded MEA solutions.

As Table 2.2 of the Literature Review summarized, there is little CO_2 rate data in piperazine solutions. Of the five literature sources, none have been tested at industrial conditions. 1.5 m PZ was the most concentrated solution studied. Only Bishnoi (2002a) evaluates CO_2 loaded solutions. The current work measures CO_2 rates at high CO_2 loading in 2, 5, 8, and 12 m PZ. This data should provide a much greater insight into the CO_2 capture performance of industrial systems.

4.2 AMINE CONCENTRATION BASIS – MOLALITY, MOLARITY AND WT%

Wetted wall column rate experiments were conducted on 7, 9, 11, and 13 m MEA, 2, 5, 8, and 12 m PZ, and 7 m MEA/2 m PZ. A molality basis is convenient in experimentation because it does not change with the addition of other components and does not require density measurements. However, many other researchers are accustomed to molarity or amine mass fraction. Table 4.1 shows the experimental amine concentrations on each basis. Molarity and mass fraction are presented on a CO_2-free basis. Calculated molarities use the density at 25˚C. The correlation by Weiland (1998) was used to determine MEA densities. PZ solution densities were obtained by extrapolating density measurements by Freeman back to zero loading (Rochelle, Dugas et al. 2008). A measured density of 1.02 was used for 7 m MEA/2 m PZ.

Table 4.1: Concentration conversions for the wetted wall column experiments

	Molality	Molarity	Mass
	m	M	wt%
MEA	7	5.0	30
	9	5.9	35
	11	6.7	40
	13	7.4	44
PZ	2	1.7	15
	5	3.6	30
	8	4.9	41
	12	6.2	51
MEA/PZ	7 - MEA 2 - PZ	4.5 - MEA 1.3 - PZ	27 - MEA 11 - PZ

Molarity (M) is defined as mol/l solution while molality (m) is defined as mol/kg water. Molarity and molality do not scale linearly.

4.3 DIAPHRAGM CELL RESULTS

Diffusion experiments were carried out in a diaphragm cell for 7, 9, and 13 m MEA and 2, 5, and 8 m PZ. Table 4.2 summarizes results for each experiment.

The membrane-cell integral diffusion coefficient, $\overline{D}$, is a complex concentration and time averaged value which is somewhat different from the fundamental diffusion coefficient, D. The fundamental diffusion coefficient is defined with respect to one species. The membrane-cell integral diffusion coefficient is the effective diffusion coefficient of all of the species in solution. More details are given in Section 3.1.3.

Table 4.2: Diaphragm cell results for monoethanolamine and piperazine solutions

Solution	CO_2 Loading	Temp	Time	Visc	$\overline{D}$	Approach to	Material Balance
	(mol/mol_{alk})	(C)	(h)	(cP)	(m^2/s)	Equilibrium (%)	Error (%)
7 m MEA	0.25-0.35	30	236	2.8	2.2E-10	34	7
	0.45-0.55		261	3.3	4.7E-10	62	4
9 m MEA	0.25-0.35		93	3.8	3.7E-10	19	16
	0.44-0.49		138	4.5	3.2E-10	22	25
13 m MEA	0.16-0.31		261	5.8	3.8E-10	58	7
2 m PZ	0.24-0.32		72	1.7	6.1E-10	24	14
	0.35-0.41		146	1.6	5.8E-10	37	26
5 m PZ	0.25-0.32		166	5.2	2.5E-10	20	32
	0.33-0.39		308	5.4	2.7E-10	48	3
8 m PZ	0.25-0.29		237	14.5	1.2E-10	20	27
	0.34-0.41		409	16.5	8.9E-11	27	4

Table 4.2 includes the viscosity of the average loading of the solutions in the two chambers. For MEA solutions, the viscosity was obtained from correlations produced by Weiland (1998). For PZ solutions, the viscosity was obtained from a regression using viscosity measurements by Freeman (Rochelle, Sexton et al. 2008a). The PZ viscosity equation is similar to the form used by Weiland (1998) for MEA. The equation is shown in Equation 4.3. Ω refers to the mass fraction of PZ on a CO_2-free basis. α refers to the CO_2 loading in mol_{CO2}/mol_{alk}. Temperature is in Kelvin.

$$\eta = \eta_{H2O} \exp\left(\frac{\left[(a\Omega + b)T + (c\Omega + d)\right] \cdot \left[\alpha(e\Omega + fT + g) + 1\right]\Omega}{T^2}\right) \qquad (4.3)$$

The regressed constants from the correlation are shown in Table 4.3. Details on the PZ regression and the quality of the fit are shown in Appendix E.

Table 4.3: Regressed parameters for the PZ viscosity equation

Parameter	a	b	c	d	e	f	g
Value	0.310	5.71	0.417	0.0267	-0.00752	-0.00574	2.51

Table 4.2 also shows an approach to equilibrium and a material balance for each experiment. The material balance was calculated by comparing the change in CO_2 loading of the bottom chamber to the change in CO_2 loading in the top chamber. It does not represent the total amount of CO_2 lost during an experiment. A 25% material balance error could be represented as the top CO_2 loading changing from 0.20 to 0.215 while the bottom chamber CO_2 loading changed from 0.30 to 0.28.

The approach to equilibrium is the change in CO_2 loading in a chamber divided by half the difference in CO_2 loading of the original two solutions. If 0.2 and 0.3 CO_2 loading solutions reach 0.225 and 0.275 CO_2 loadings by the end of the experiment, then the approach would be 50%. A 100% approach would result in both solutions reaching 0.25 CO_2 loading.

12 m PZ was also tested in the diaphragm cell but meaningful results were not obtained. The Mettler Toledo DE40 density meter was not able to analyze the 12 m PZ samples reproducibly. The solutions may be too viscous or may not have been homogeneous. 12 m PZ at 20˚C (the temperature of the density measurement) is about 50–60 cP depending on the CO_2 loading (Rochelle, Sexton et al. 2008a).

Diffusion coefficients are typically a function of viscosity. Figure 4.1 plots the diffusion coefficient and viscosity data in Table 4.2. The diffusion coefficient of 1 m piperazine is shown for comparison (Sun, Yong et al. 2005).

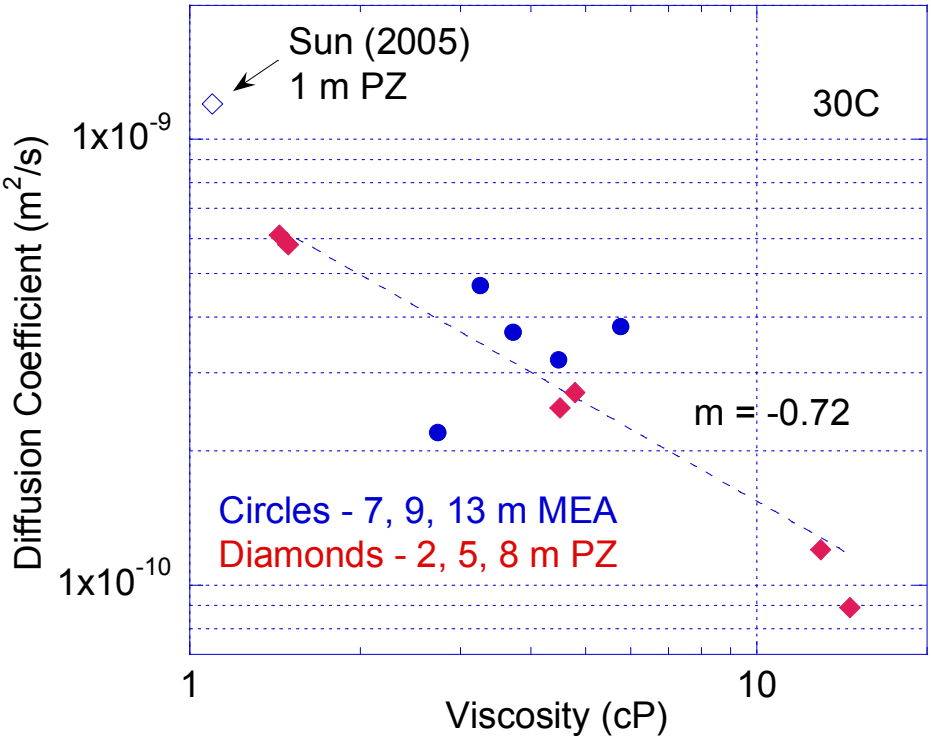

Figure 4.1: Diffusion coefficient-viscosity relationship for MEA and PZ solutions (Sun, Yong et al. 2005)

The data seem to show a slope of –0.72 with a standard error of ±0.12. This 0.72 value can be compared to a 0.8 dependence for N_2O and a 0.6 dependence for amines cited by Versteeg and Van Swaaij (1988). The membrane-cell integral diffusion coefficient cited refers to the carbon dioxide carrying species since CO_2 loading changes were measured. In that case the measured diffusion coefficient would most closely represent the diffusion coefficient of the carbamate species.

The data also compare favorably to the piperazine diffusion coefficient data point measured by Sun (2005). Extrapolating the trend line in Figure 4.1 to the viscosity of the Sun data point would show the trend line slightly underpredicting the diffusion coefficient. However, the diffusion coefficient of PZ carbamate may be slightly lower than PZ due to a larger size and the possibility of more hydrogen bonding with the ionic species.

Overall, the 0.72 dependence the diaphragm cell provides is reasonable and has been used in modeling.

4.4 WETTED WALL COLUMN RESULTS

4.4.1 Tabulated Wetted Wall Column Data

Tables 4.4–4.6 provide tabulated k_g' rate data and equilibrium CO_2 partial pressure data. Section 2.3.1 explains why rate data is presented in terms of k_g' rather than rate constants. k_g' is the liquid film mass transfer coefficient in gas film units, defined by Equation 4.4. Figure 2.1 graphically defines k_g'.

$$k_g' = \frac{N_{CO2}}{(P_{CO2,i} - P^*_{CO2,b})} \tag{4.4}$$

Each row of the following tables represents the results of six experimental inlet CO_2 partial pressures. More detailed data including gas flow rates, pressures, and inlet and outlet CO_2 partial pressures can be found in Appendix C. Appendix C also includes the liquid film physical mass transfer coefficient, k_l^o, and the gas film resistance percentage of each experiment. Experiments were designed to be less than 50% gas film controlled. In some experiments k_l^o may be limiting such that CO_2 mass transfer is restricted by diffusion limitations in the system.

Table 4.4: CO_2 equilibrium partial pressure and rate data obtained from the wetted wall column with aqueous MEA

MEA	Temp	CO_2 Loading	P^*_{CO2}	k_g'
m	C	mol/mol_{alk}	Pa	$mol/s \cdot Pa \cdot m^2$
7	40	0.252	15.7	3.34E-06
		0.351	77	1.40E-06
		0.432	465	7.66E-07
		0.496	4216	3.47E-07
	60	0.252	109	2.92E-06
		0.351	660	1.70E-06
		0.432	3434	9.28E-07
		0.496	16157	3.76E-07
	80	0.271	1053	2.85E-06
		0.366	4443	1.87E-06
	100	0.271	5297	2.98E-06
		0.366	19008	1.40E-06
9	40	0.231	10.4	-
		0.324	34	1.86E-06
		0.382	107	1.40E-06
		0.441	417	8.36E-07
		0.496	5354	3.02E-07
	60	0.231	61	3.80E-06
		0.324	263	2.44E-06
		0.382	892	1.47E-06
		0.441	2862	9.57E-07
		0.496	21249	3.24E-07
	80	0.265	979	3.24E-06
		0.356	4797	1.75E-06
	100	0.265	4940	3.40E-06
		0.356	21534	1.33E-06

MEA	Temp	CO_2 Loading	P^*_{CO2}	k_g'
m	C	mol/mol_{alk}	Pa	$mol/s \cdot Pa \cdot m^2$
11	40	0.261	14.0	3.36E-06
		0.353	67	1.76E-06
		0.428	434	7.14E-07
		0.461	1509	4.34E-07
	60	0.261	96	3.35E-06
		0.353	634	1.80E-06
		0.428	3463	8.71E-07
		0.461	8171	5.02E-07
	80	0.256	860	4.35E-06
		0.359	3923	1.93E-06
	100	0.256	4274	3.72E-06
		0.359	18657	1.56E-06
13	40	0.252	12.3	3.08E-06
		0.372	84	1.28E-06
		0.435	491	6.96E-07
		0.502	8792	1.62E-07
	60	0.252	100	2.98E-06
		0.372	694	1.54E-06
		0.435	3859	7.56E-07
		0.502	29427	1.93E-07
	80	0.254	873	4.21E-06
		0.355	3964	1.85E-06
	100	0.254	3876	3.66E-06
		0.355	18406	1.56E-06

12 m PZ experiments at 40˚C could not be run in the wetted wall column due to the high viscosity of the solution. A thin liquid film on the surface of the stainless steel rod could not be maintained. Also 12 m PZ samples with approximately 0.40 CO_2 loading were not tested due to solubility limitations.

Table 4.5: CO_2 equilibrium partial pressure and rate data obtained from the wetted wall column with aqueous PZ

PZ	Temp	CO_2 Loading	P^*_{CO2}	k_g'
m	C	mol/mol_{alk}	Pa	$mol/s \cdot Pa \cdot m^2$
2	40	0.240	96	3.32E-06
		0.316	499	2.04E-06
		0.352	1305	1.39E-06
		0.411	7127	5.55E-07
	60	0.240	559	3.33E-06
		0.316	2541	2.06E-06
		0.352	5593	1.38E-06
		0.411	25378	3.84E-07
	80	0.239	2492	3.34E-06
		0.324	12260	1.32E-06
	100	0.239	9569	2.40E-06
		0.324	39286	9.12E-07
5	40	0.226	65	4.39E-06
		0.299	346	2.57E-06
		0.354	1120	1.69E-06
		0.402	4563	7.93E-07
	60	0.226	385	4.75E-06
		0.299	1814	2.62E-06
		0.354	5021	1.80E-06
		0.402	17233	6.59E-07
	80	0.238	2192	4.67E-06
		0.321	9699	1.91E-06
	100	0.238	8888	3.52E-06
		0.321	36960	1.02E-06

PZ	Temp	CO_2 Loading	P^*_{CO2}	k_g'
m	C	mol/mol_{alk}	Pa	$mol/s \cdot Pa \cdot m^2$
8	40	0.231	68	4.27E-06
		0.305	530	1.98E-06
		0.360	1409	1.14E-06
		0.404	8153	3.53E-07
	60	0.231	430	4.41E-06
		0.305	2407	2.02E-06
		0.360	7454	9.57E-07
		0.404	30783	3.20E-07
	80	0.253	3255	3.61E-06
		0.289	9406	1.97E-06
	100	0.253	13605	2.18E-06
		0.289	32033	1.20E-06
12	60	0.231	331	4.19E-06
		0.289	1865	1.85E-06
		0.354	6791	7.73E-07
	80	0.222	2115	4.24E-06
		0.290	9141	1.48E-06
	100	0.222	7871	3.78E-06
		0.290	33652	8.30E-07

Table 4.6: CO_2 equilibrium partial pressure and rate data obtained from the wetted wall column with 7 m MEA/2 m PZ

MEA	PZ	Temp	CO_2 Ldg	P^*_{CO2}	k_g'
m	m	C	mol/mol_{alk}	Pa	$mol/s \cdot Pa \cdot m^2$
7	2	40	0.242	27	3.45E-06
			0.333	166	1.96E-06
			0.416	1425	8.76E-07
			0.477	7418	4.32E-07
		60	0.242	178	4.00E-06
			0.333	1256	2.03E-06
			0.416	7122	9.08E-07
			0.477	33704	3.75E-07
		80	0.242	1138	4.29E-06
			0.333	6174	2.12E-06
		100	0.242	4340	4.83E-06
			0.333	26571	1.23E-06

4.4.2 Equilibrium CO_2 Partial Pressure

The figures in the following sections graphically represent the data in Tables 4.4–4.6 along with applicable literature data.

4.4.2.1 Monoethanolamine

Figure 4.2 shows CO_2 equilibrium partial pressure values obtained from the wetted wall column in 7, 9, 11, and 13 m MEA compared to Jou (1995) and Hilliard (2008) values. Hilliard used an equilibrium cell to measure CO_2 partial pressures with an FTIR (Fourier transform infrared spectroscopy) analyzer to quantify the CO_2 concentration. Jou also measured the equilibrium partial pressure with an equilibrium cell.

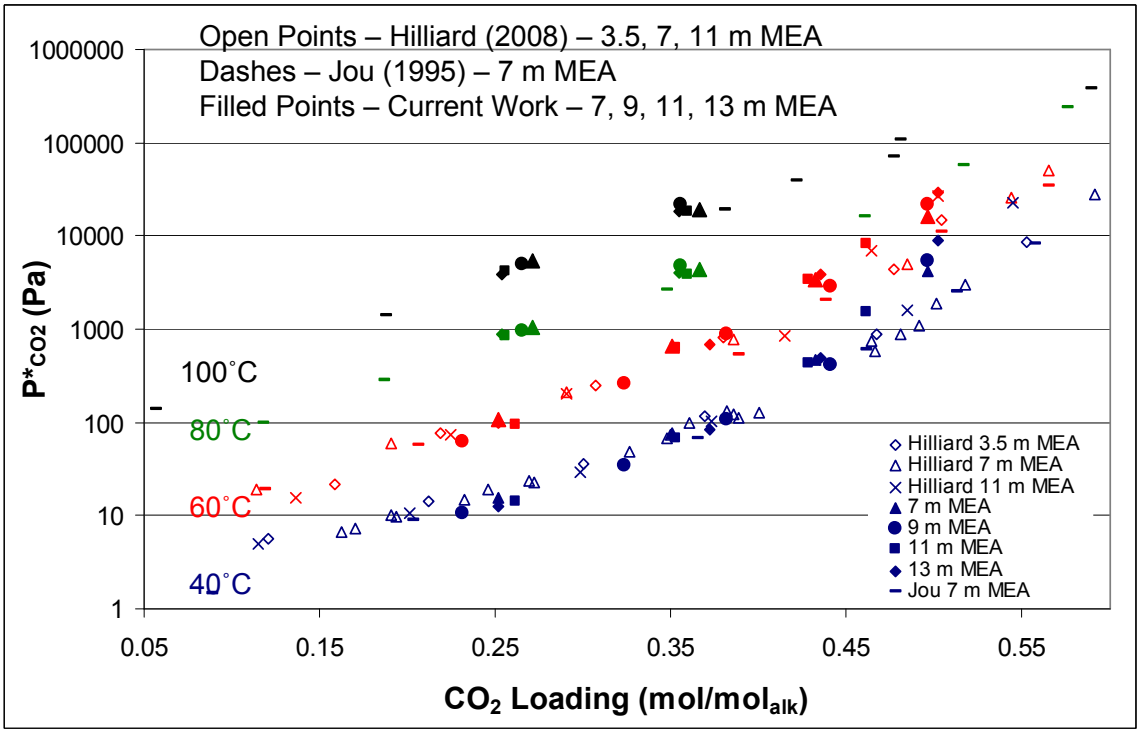

Figure 4.2: Equilibrium CO_2 partial pressure measurements in MEA solutions at 40, 60, 80, and 100˚C (Jou, Mather et al. 1995; Hilliard 2008)

The 3.5, 7, and 11 m MEA data by Hilliard (2008), the 7 m MEA data by Jou (1995) and the current work at 7, 9, 11, and 13 m MEA agree well at each of the four temperatures. The current data represented by the filled data points show minor deviations from the other data near 0.5 loading at 40˚C. The 0.5 loading data at 40 and 60˚C show an amine concentration dependence. At both 40 and 60˚C near 0.5 loading the 13 m data has a higher CO_2 partial pressure than the 11 m MEA data, which is higher than the 7 m MEA data. The 11 m MEA data by Hilliard both at 40 and 60˚C also show a higher CO_2 partial pressure than 7 or 3.5 m MEA data at high CO_2 loading. However, the 7 m MEA, 0.5 loading, 40˚C measurement from the wetted wall column provides a higher CO_2 partial pressure value than the 7 m MEA data by Hilliard (2008) or Jou (1995).

The effect of amine concentration on the CO_2 partial pressure of the MEA system at high loading is expected. Amine concentration should not affect CO_2 equilibrium partial pressures for carbamate-producing systems when compared at equivalent CO_2 loading. However, amine concentration is extremely important in bicarbonate-producing systems. MEA systems begin producing significant bicarbonate concentrations approaching 0.5 loading. This difference is based on the stoichiometry of the carbamate and bicarbonate reactions. The mathematics of the difference are explained in Appendix D.

The increased CO_2 partial pressure of the higher MEA concentrations near 0.5 loading is due to an increased concentration of bicarbonate. At lower CO_2 loading, bicarbonate concentration is insignificant and MEA concentration has no effect on the equilibrium CO_2 partial pressure of the system.

4.4.2.2 Piperazine

Figure 4.3 shows wetted wall column obtained CO_2 equilibrium partial pressure values in 2, 5, 8, and 12 m PZ compared to Ermatchkov (2006a) and Hilliard (2008). Hilliard used an equilibrium cell to measure CO_2 partial pressure with an FTIR (Fourier transform infrared spectroscopy) analyzer to quantify the CO_2 concentration. Ermatchkov measured the equilibrium partial pressure using headspace gas chromatography (2006b).

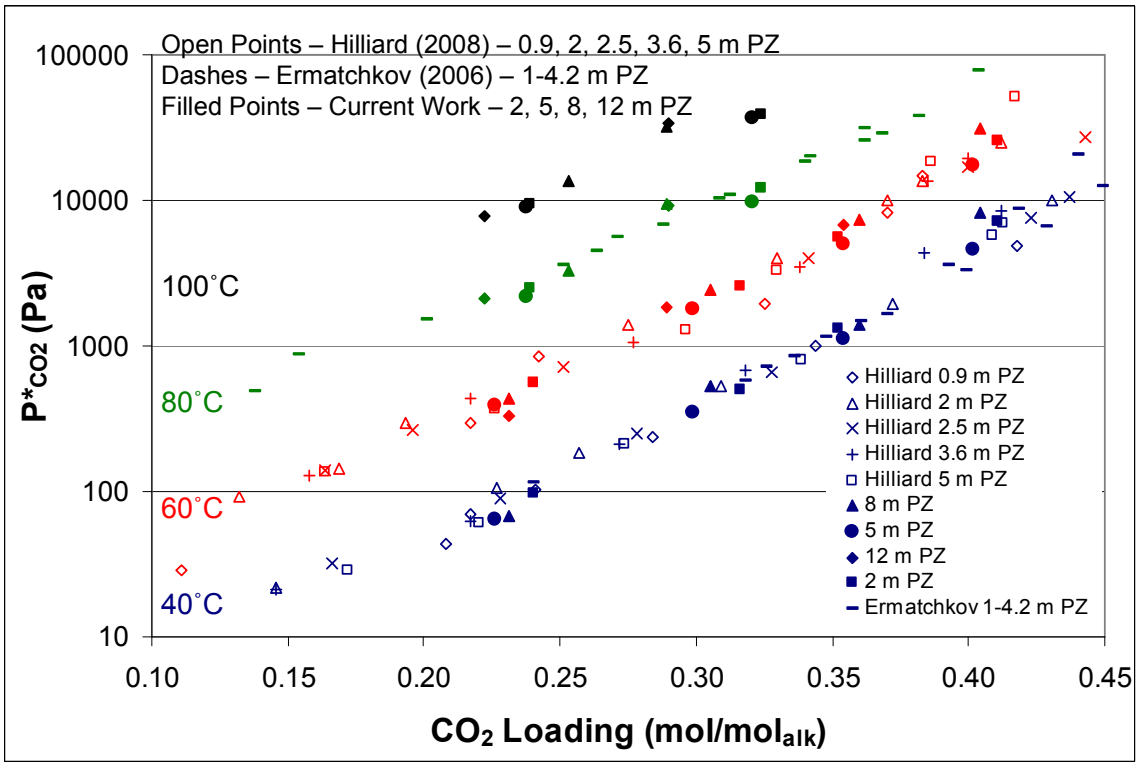

Figure 4.3: Equilibrium CO_2 partial pressure measurements in PZ solutions at 40, 60, 80, and 100˚C (Ermatchkov, Perez-Salado Kamps et al. 2006a; Hilliard 2008)

All the data in Figure 4.3 match very well at 40, 60, and 80˚C. Neither Ermatchkov (2006a) or Hilliard (2008) provide data at 100˚C but the 100˚C data are

reasonable based on the spacing from the 80˚C data and the overlap of the amine concentrations.

Unlike the CO_2 partial pressure measurements in the MEA system, the PZ system does not show a dependence of amine concentration at high loading. This is because the CO_2 loading is not high enough to see appreciable quantities of bicarbonate. Since only carbamates are produced, none of the data show an effect of amine concentration when plotted against CO_2 loading.

4.4.2.3 7 m MEA/2 m PZ

Little data for equilibrium CO_2 partial pressure are available for 7 m MEA/ 2 m PZ. Figure 4.4 includes the current data (filled points) compared against Hilliard (2008) represented as the open points. Hilliard used an equilibrium cell to measure CO_2 partial pressure with an FTIR analyzer to quantify the CO_2 concentration.

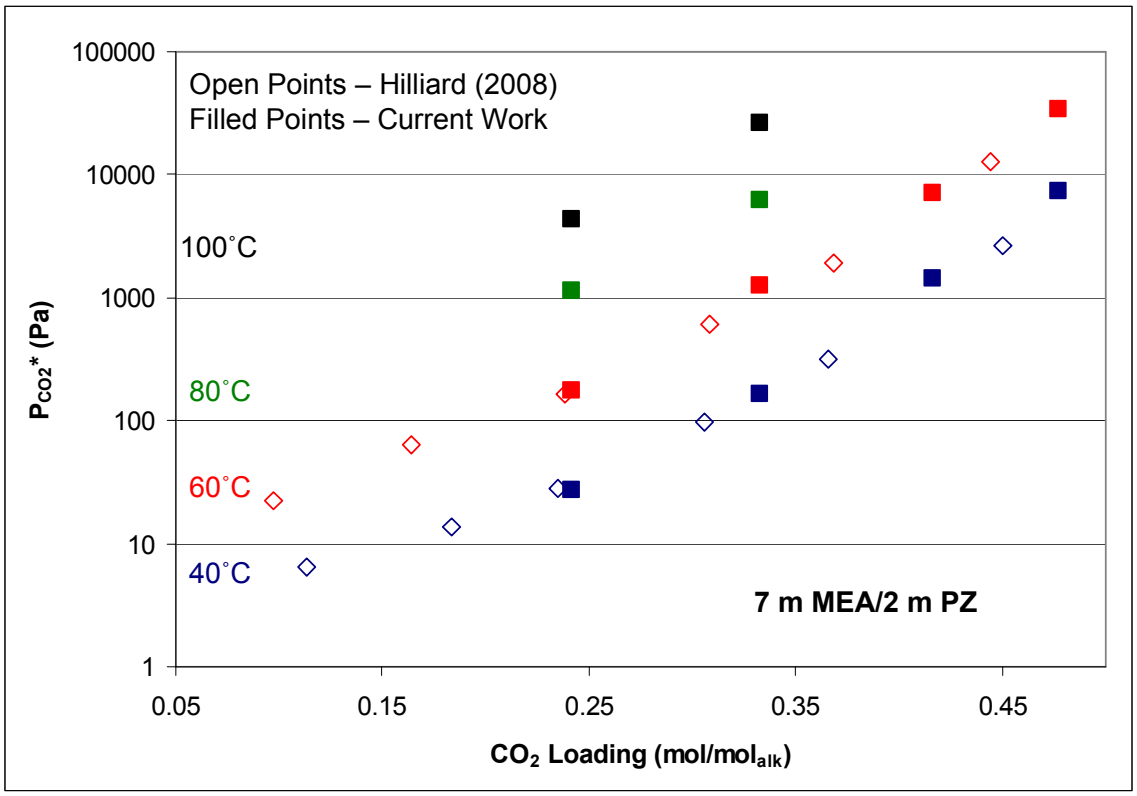

Figure 4.4: Equilibrium CO_2 partial pressure measurements in 7 m MEA/2 m PZ at 40, 60, 80, and 100˚C (Hilliard 2008)

Although there are limited data for 7 m MEA/2 m PZ, the available equilibrium CO_2 partial pressure data show a very good match despite using two different experimental apparatuses.

Other MEA/PZ concentrations were not studied due to concerns about thermal degradation (Davis 2009). Davis found that the more reactive PZ will react preferentially with an oxazolidone intermediate formed by thermally degrading MEA. Essentially, PZ protects MEA from the thermal degradation of the blended system. PZ in the absence of MEA will not thermally degrade significantly because there is no pathway to produce oxazolidone.

4.4.3 CO_2 Capacity

The equilibrium CO_2 partial pressures in Figures 4.2–4.4, allow for the determination of the CO_2 capacity. The CO_2 capacity is defined as the difference in the CO_2 concentration from the rich to the lean amine streams, not the total CO_2 concentration in any particular stream. The CO_2 capacity is the amount of CO_2 that would be removed from the system during one circulation of the amine solution.

The CO_2 capacity is important because of energy tradeoffs of the sensible heat and the heat of absorption. Circulating less solvent reduces the sensible heat duty since the stripper must heat all the solution from the cross-exchanger outlet temperature to the stripper temperature. This temperature difference is the same as the cross-exchanger temperature approach. However, circulating too little solvent to achieve a high CO_2 capacity requires a very low lean loading or CO_2 partial pressure. Stripping to very low CO_2 partial pressures increases the stripping steam required per mole of CO_2 and can cause inefficient operation of the stripper. The optimal operating lean loading and thus CO_2 capacity for a given amine system requires a significant optimization with a complex model. CO_2 reaction rates change drastically with changing CO_2 loading. Since the optimal lean loading and thus CO_2 partial pressure of that lean loading cannot be easily determined, Figure 4.5 is constructed to compare the CO_2 capacity of 8 m PZ and 7 and 13 m MEA at 40˚C for any lean partial pressure. Alternative amine systems allow for an increase in the CO_2 capacity of the system without requiring the system to strip to lower CO_2 partial pressures. Figure 4.5 includes CO_2 loading values next to some of the data points.

Since CO_2 capacity relates to the sensible heat of the solution and the total dissolved CO_2 has a negligible partial heat capacity, CO_2 capacities are calculated on a

mol_{CO2}/kg(water+amine) basis. It is not appropriate to include the CO_2 in the weight of the solution since it has a mostly negligible sensible heat. Essentially, a mole of MEA has almost the same heat capacity as a mole of MEA carbamate (Hilliard 2008). Nguyen has seen the same effect in PZ systems (Rochelle, Chen et al. 2009a).

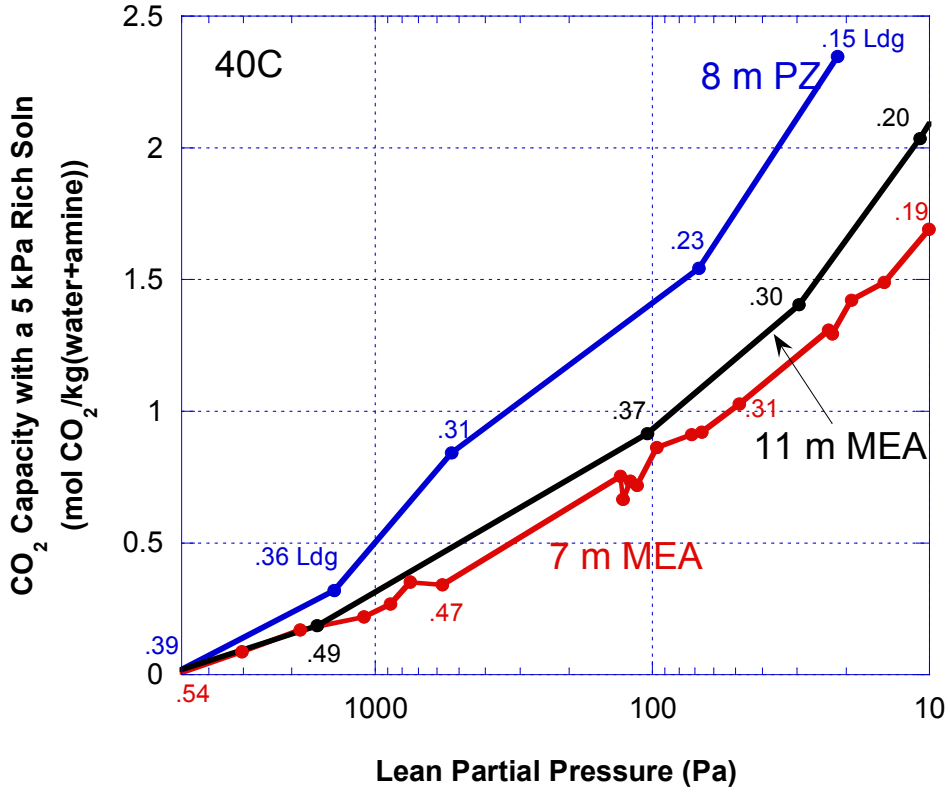

Figure 4.5: Operating CO_2 capacity of 8 m PZ and 7 and 11 m MEA assuming a 5 kPa rich CO_2 partial pressure at 40˚C (7 and 11 m MEA data from Hilliard (2008))

Figure 4.5 assumes a 5 kPa CO_2 partial pressure rich solution. In a coal-fired power plant CO_2 enters the absorber near 12 mole%, or 12 kPa, since it is near atmospheric pressure. Therefore, the assumption of a 5 kPa CO_2 partial pressure rich solution at 40˚C represents a 5/12 or a 42% approach to saturation at the bottom of the absorber if the solution exits at 40˚C.

Under the assumed conditions detailed above, 8 m PZ exhibits about a 70% greater CO_2 capacity than 7 m MEA and about a 50% greater CO_2 capacity than 11 m MEA. The majority of the increased CO_2 capacity is due to the fact that each mole of piperazine has two functional nitrogen groups. This allows PZ to react with CO_2 twice while MEA can only react once. PZ solutions allow for much greater CO_2 capacities than MEA and thereby lower required liquid flow rates and the sensible heat input requirement of the reboiler.

4.4.4 CO_2 Reaction Rates

As explained in Section 2.3.1, CO_2 absorption rates should be reported in terms of k_g'. The definition of k_g' is reiterated in Equation 4.5. k_g' is the liquid film mass transfer coefficient converted to gas phase units.

$$k_g' = \frac{N_{CO2}}{(P_{CO2,i} - P^*_{CO2,b})} \tag{4.5}$$

Obtained k_g' values for each MEA experiment are plotted against the measured equilibrium partial pressure at the temperature of the experiment in Figure 4.6. Figure 4.6 includes 7, 9, 11, and 13 m MEA rate data at 40, 60, 80, and 100˚C.

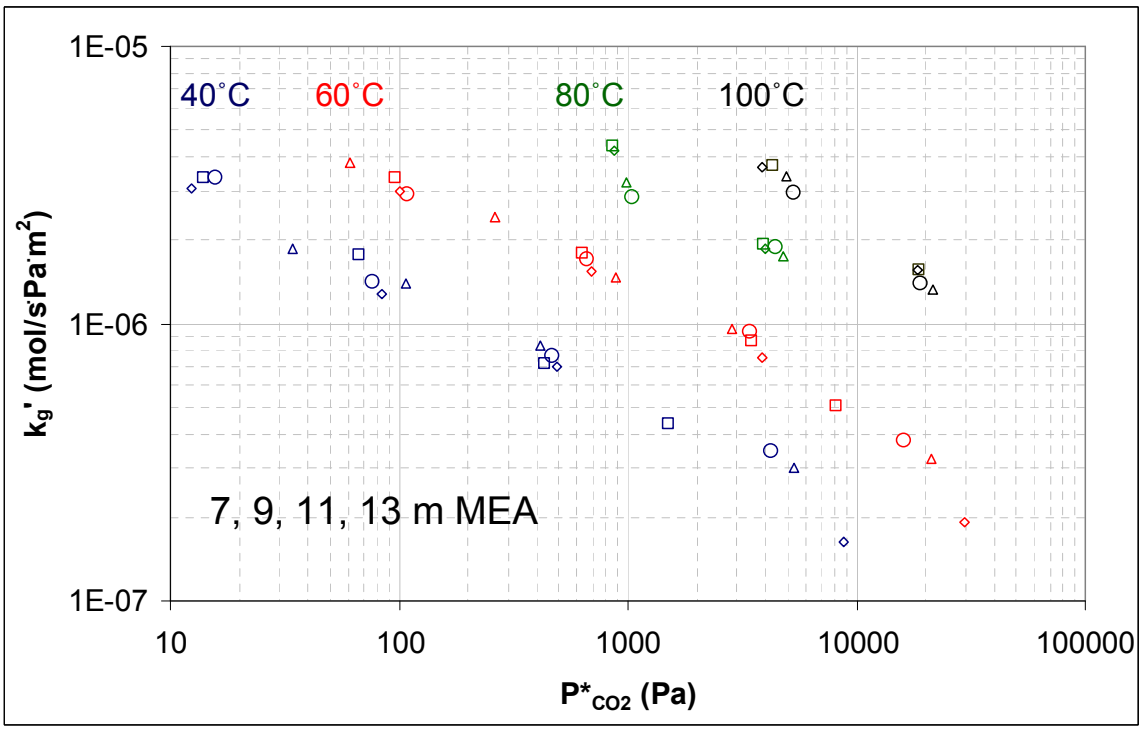

Figure 4.6: CO_2 absorption/desorption rates in MEA solutions at 40, 60, 80, and 100˚C

Each shape in Figure 4.6 represents a different MEA concentration but the MEA concentration does not significantly affect the measured k_g'. This was unexpected considering k_g' is often represented by the pseudo first order approximation result shown in Equation 4.6.

$$k_g' = \frac{\sqrt{D_{CO2} k_2 [Am]_b}}{H_{CO2}} \tag{4.6}$$

Equation 4.6 includes a term for the amine concentration in the numerator. For Equation 4.6 to hold true, other terms in Equation 4.6 must change with concentration to offset the change in the concentration term. The diffusion coefficient and the Henry's constant are both affected by changes in concentration. The Henry's constant shown in Equation 4.6 is not the true thermodynamic Henry's constant, which refers to the

solubility in water. The Henry's constant shown in Equation 4.6 refers to the CO_2 solubility in the solution. It is a function of amine concentration, CO_2 loading, and temperature (Browning and Weiland 1994; Hartono 2009).

The diffusion coefficient of CO_2 will go down slightly with increasing MEA concentration due to the viscosity effect. The CO_2 solubility decreases (H_{CO2} increases) with increasing amine concentration and this change cancels most of the increasing MEA concentration term. Contrary to the data, Equation 4.6 does predict an amine concentration effect on k_g'.

Figure 4.6 seems to imply that k_g' in MEA solutions increases with increasing temperature. However, that assertion is wrong. Rather than each increasing temperature curve having a higher k_g', it has a higher CO_2 equilibrium partial pressure. A close look at Figure 4.6 reveals that k_g' is almost identical with increasing temperature. The 7 m MEA (circles) data point at 40˚C near 15 Pa has a k_g' of approximately $3.3 \cdot 10^{-6}$ mol/s·Pa·m^2. The lowest loading data points for 7 m MEA at 60, 80, and 100˚C each show a k_g' of approximately $3.0 \cdot 10^{-6}$ mol/s·Pa·m^2. Each of these four data points has a similar CO_2 loading and k_g', verified in Table 4.4.

Since temperature has little effect on the measured k_g', the temperature dependent terms in Equation 4.6 must cancel each other. The diffusion coefficient, rate constant, and Henry's constant are all temperature dependent. The diffusion coefficient will decrease with increasing temperature due to viscosity changes. The rate constant will increase with increasing temperature as shown by regressed literature data (Versteeg, Van Dijck et al. 1996). The solubility of CO_2 and N_2O in water decreases with increasing temperature (Versteeg and Van Swaaij 1988). Equation 4.6 does not predict k_g' to be

independent of temperature as the data indicate. Equation 4.6 is not supported by the experimental data.

It would be convenient to show Figure 4.6 in terms of CO_2 loading on the x-axis but the CO_2 loading basis would prohibit the MEA data from being compared to other amines. Different amines can only be compared on a partial pressure basis since the definition of CO_2 loading is somewhat arbitrary and each amine has a different CO_2 loading operating range. However, we can plot the x-axis in terms of the equilibrium CO_2 partial pressure at a given temperature. This results in two points with the same CO_2 loading being plotted at the same value on the x-axis regardless of temperature. In this respect it is similar to plotting the x-axis on a CO_2 loading basis. However, this basis has the advantage that it also allows a fair comparison of the CO_2 reaction rates with different amines. The equilibrium CO_2 partial pressure at 40˚C can be viewed as a surrogate for CO_2 loading. The MEA rate data is plotted against the equilibrium CO_2 partial pressure at 40˚C in Figure 4.7.

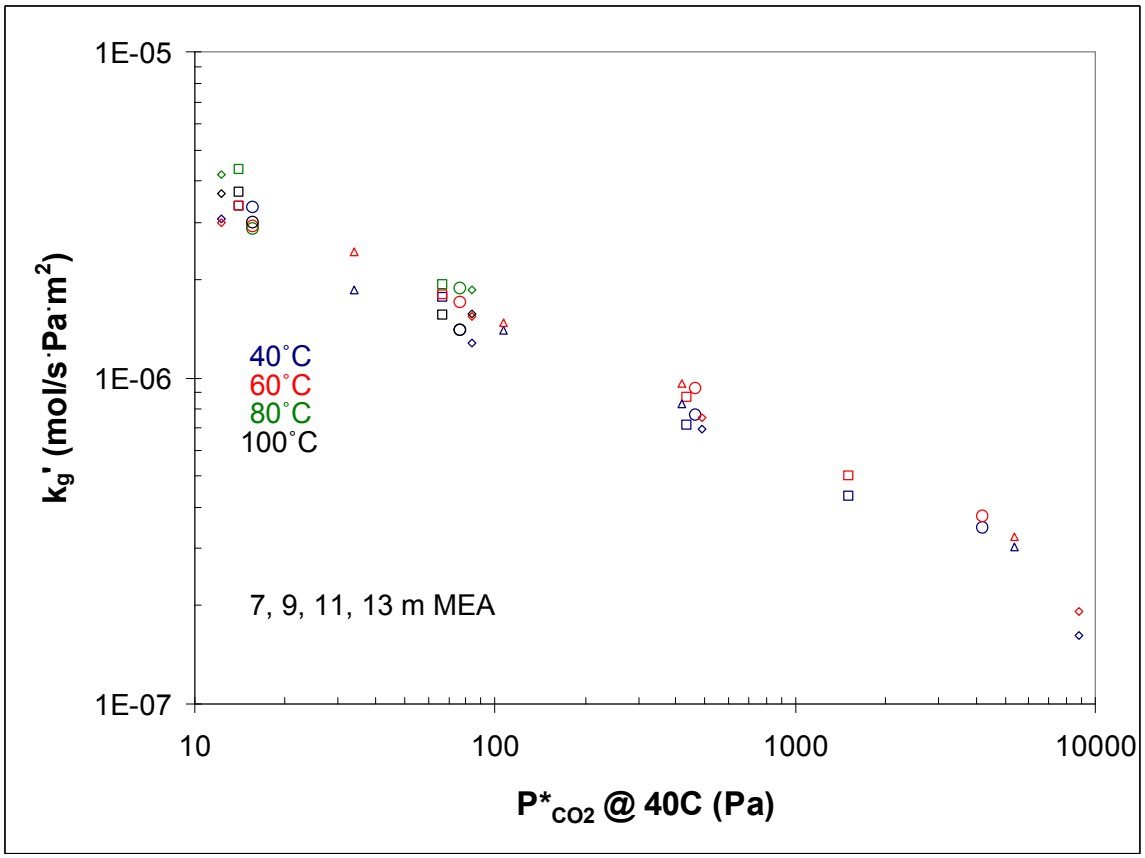

Figure 4.7: CO_2 absorption/desorption rates in MEA solutions at 40, 60, 80 and 100˚C, plotted against the 40˚C equilibrium CO_2 partial pressure

The MEA data clearly show that the amine concentration and temperature do not significantly affect k_g' in aqueous MEA. This makes the determination of k_g' for MEA solutions simple. Measured k_g' values drastically decrease with increasing equilibrium CO_2 partial pressure at 40˚C (CO_2 loading). The 10x drop in k_g' from 0.25 to 0.50 CO_2 loading is primarily due to the reduction of free MEA available for reaction.

PZ rate data at 40, 60, 80, and 100˚C are compared in Figure 4.8. 12 m PZ data is not included in the plot since the equilibrium partial pressures of 12 m PZ at 40˚C could not be determined using the wetted wall column. These solutions were too viscous for wetted wall column operation.

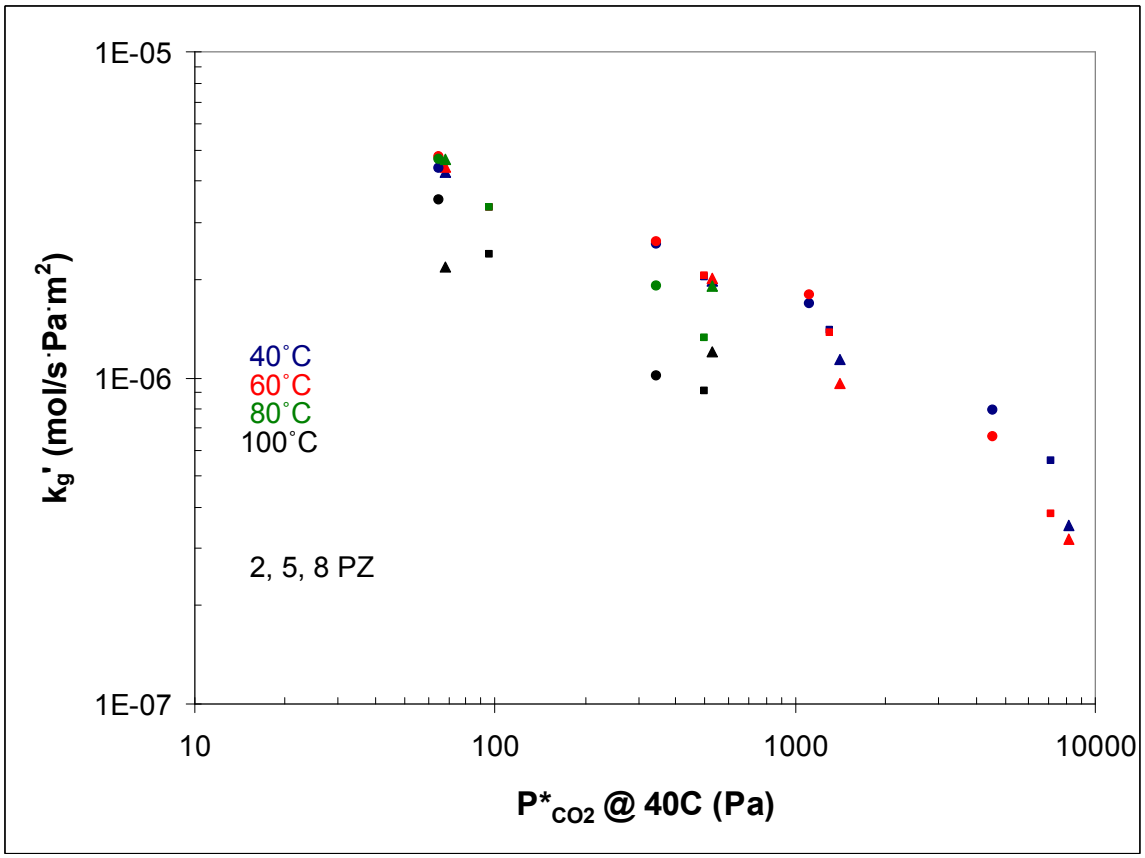

Figure 4.8: CO_2 absorption/desorption rates in PZ solutions at 40, 60, 80 and 100˚C, plotted against the 40˚C equilibrium CO_2 partial pressure

The PZ data do not converge quite as cleanly as the MEA data. Measured k_g' values in aqueous PZ are not dependent on the amine concentration. However, there are some temperature effects. At the lowest CO_2 loading near 70–100 Pa, 100˚C data points drop below the trend of the other data. At the next highest CO_2 loading near 300–500 Pa, 80˚C data points drop from the trend while the 100˚C data points drop far below the trend. At the two highest loadings only 40 and 60˚C data is available but the 60˚C data points routinely fall below the 40˚C data points.

The observed temperature effects in the PZ data suggest that diffusion of products and reactants may be limiting the reaction of the CO_2 with the amine. At the lowest CO_2

loading, there is adequate free amine at the interface and CO_2 fluxes are small at the lower temperatures. Tested CO_2 partial pressures range from 0–2 times the equilibrium partial pressure, not the equilibrium partial pressure at 40˚C. Therefore, fluxes at 100˚C are very high compared to lower temperatures. It is possible that these fluxes combined with fast CO_2 reaction rates are depleting the interface of reactive PZ and PZ carbamate. At the next highest loading, there is less free PZ carbamate at the interface while CO_2 fluxes are higher due to the increased equilibrium partial pressure of the solutions. At this loading, the 80˚C data are now being restrained by diffusion limitations while 100˚C are hampered by the diffusion of reactants and products near the interface. At the higher loadings, the PZ carbamate concentration continues to decrease while CO_2 fluxes continue to increase, thereby possibly slowing the measured mass transfer coefficients at 60˚C.

Although the PZ rate data suggest this diffusion limiting phenomenon, a model is required to verify it. On the other hand, the MEA experiments do not suggest significant mass transfer resistance due to the diffusion of reactants and products.

The proposed diffusion limitation in PZ experiments in the wetted wall column may not be seen in industrial columns. The wetted wall column has a smaller liquid film physical mass transfer coefficient, k_l^o, than a typical industrial column. This is due to the 9.1 cm stainless steel contactor. In a packed industrial column, either structured or random packing, the mean flow path of the solvent is probably closer to 2–3 cm. The more frequent mixing of the solvent will refresh the interface and discourage depletion of the reactants at the gas-liquid interface.

The MEA, PZ, and the MEA/PZ data are compared in Figure 4.9. MEA is represented by the empty points. PZ is represented by the filled data points. 7 m MEA/2 m PZ data are marked with X's.

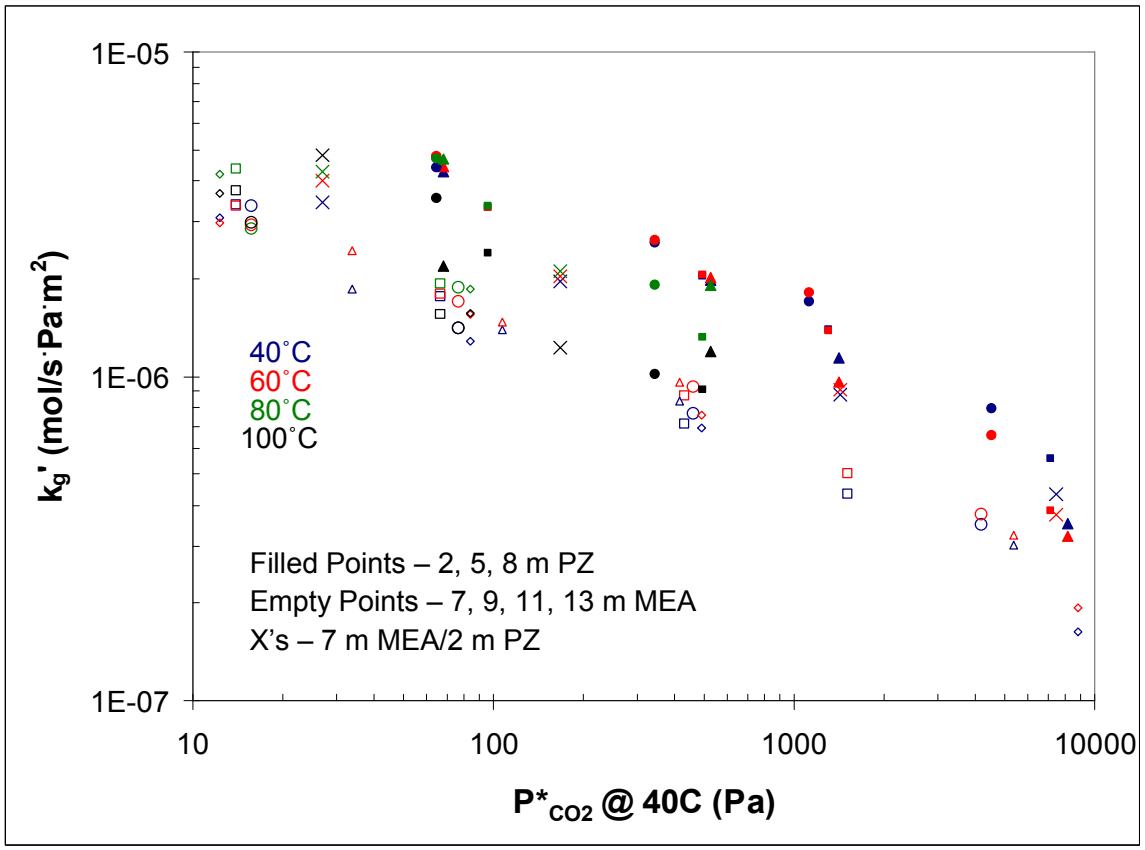

Figure 4.9: CO_2 absorption/desorption rates in MEA, PZ, and MEA/PZ solutions at 40, 60, 80, and 100˚C, plotted against the 40˚C equilibrium CO_2 partial pressure

Most of the PZ data points form a trend line above the MEA data. These data show that k_g' for PZ is 2–3 times faster than MEA. This means PZ reacts with CO_2 2–3 times faster than MEA. To a first approximation 1/2 to 2/3 less packing in the absorber would be required for PZ.

The 7 m MEA/2 m PZ rate data generally fall between the MEA and PZ data. The condition near 200 Pa suggests diffusion limitations at the 100˚C condition.

4.4.4.1 Rate Comparisons with Literature

4.4.4.1.1 Monoethanolamine

Rate data obtained in this work are compared to literature values in this section. As previously stated, there are limited rate data on highly loaded concentrated amines. For a proper comparison on a k_g' basis, some raw data are required.

Figure 4.10 shows a comparison of 7 m MEA rate data at 40 and 60˚C. Aboudheir (2003) provides rate data obtained from a laminar jet absorber. At each condition multiple measurements were made. Figure 4.10 also includes four wetted wall column data points obtained by Dang (2003). Dang used the same wetted wall column used in this work. A single 40˚C data point from Hartono (2009) is included in Figure 4.10.

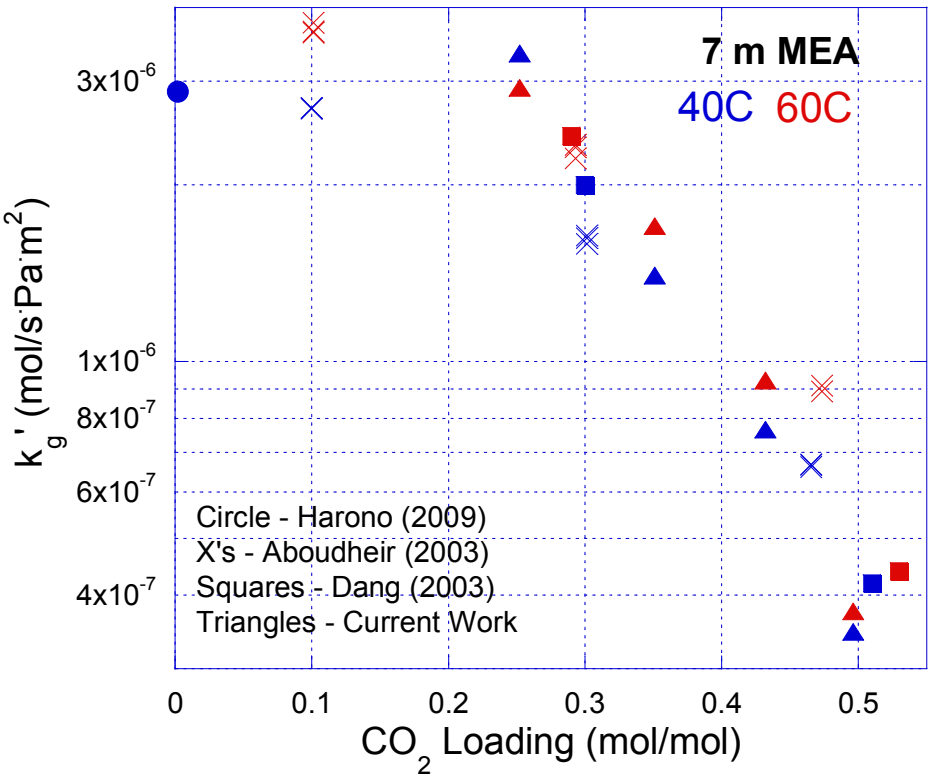

Figure 4.10: CO_2 reaction rate comparison on a k_g' basis for 7 m MEA at 40 and 60˚C (Aboudheir, Tontiwachwuthikul et al. 2003; Dang and Rochelle 2003; Hartono 2009)

The data by Dang coincide with the newly obtained wetted wall column data. The data by Aboudheir also agree at the two higher CO_2 loadings. The data by Aboudheir (2003) near 0.1 loading show a lower k_g' value than an extrapolation of the wetted wall column data would predict. However, the unloaded rate data by Hartono (2009) support these 0.1 CO_2 loading values and suggest that the liquid film mass transfer coefficient, k_g', may not change significantly from 0 to 0.25 CO_2 loading.

No wetted wall column experiments were conducted below 0.2 CO_2 loading. The wetted wall column cannot accurately obtain rate data in MEA solutions at CO_2 loading much lower than 0.25 because the system becomes dominated by the gas film mass

transfer coefficient. The gas film mass transfer coefficient of the column was originally characterized using unloaded MEA (Pacheco 1998).

The data by Aboudheir (2003) show a consistent effect of temperature. In each of the three CO_2 loadings, the 60˚C data points exhibit about 50% higher k_g' values. The wetted wall column data, including Dang (2003) and the current work, do not clearly show a trend. Figure 4.7 more clearly shows that there is no significant temperature effect on the CO_2 absorption/desorption rates in MEA solutions. The wetted wall column apparatus used in the current work and by Dang (2003) is very different from the laminar jet absorber used by Aboudheir (2003).

Unloaded MEA rate data found in the literature could also be compared to the highly loaded, highly concentrated MEA rate data presented here. As the Literature Review detailed, there are numerous sources which report rate data in unloaded, relatively dilute MEA solutions. However, most of these data sources only report obtained rate constants and do not detail values used for the Henry's constant or the diffusion coefficient. Neither do they include fluxes and driving forces which allow for the calculation of k_g'.

Laddha and Danckwerts (1981a) provide calculated rate constants along with the solubility and diffusion parameters that allow for the calculation of the measured flux and K_G. No gas film mass transfer coefficients were given for the stirred cell experiments so k_g' cannot be calculated. The rate constants (expressed in Equation 4.7) for the six tested amine concentrations ranged from 5.49 to 6.28 $m^3/(mol \cdot s)$ at 25˚C (Laddha and Danckwerts 1981a). These rate constants compare favorably with 5.99 $m^3/(mol \cdot s)$ value predicted by a correlation developed from a review of literature data (Versteeg, Van Dijck et al. 1996).

$$-r_{CO2} = k_2[MEA][CO_2] \tag{4.7}$$

Hartono (2009) provides all the important experimental data from his CO_2 absorption into MEA. This allows for the calculation of K_G and then k_g'. The rate experiments performed using a string of discs were determined to be 5–18% gas film controlled. The calculated k_g' from the experiments by Hartono (2009) and the calculated K_G values from Laddha (1981a) are shown in Figure 4.11.

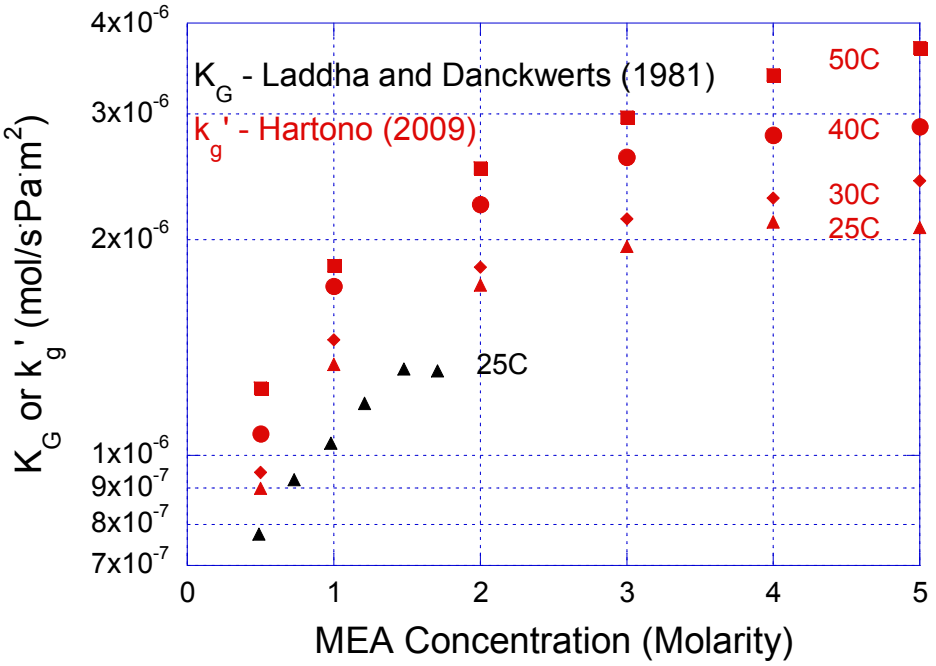

Figure 4.11: CO_2 reaction rates in unloaded MEA solutions (Laddha and Danckwerts 1981a; Hartono 2009)

Figure 4.11 shows the Laddha data at 25˚C below the Hartono data at 25˚C. This is expected since the Laddha data do not remove the gas film resistance from the system. The liquid film mass transfer coefficient, k_g', must be larger than the overall mass transfer coefficient, K_G. In cases where the gas film mass transfer coefficient, k_g, is limiting, K_G can be significantly lower than k_g'. In a stirred cell experiment with

unloaded MEA, it is likely that gas film mass transfer resistance is significant since stirred cells often have this concern. The Laddha data in Figure 4.11 are not as descriptive of CO_2 rates into MEA as the Hartono data. Gas film resistances due to operating conditions and the geometry of the apparatus cannot be extracted from the reported data.

Figure 4.11 shows a dependence of k_g' on the MEA concentration at lower MEA concentrations. At higher MEA concentrations k_g' becomes independent of concentration, although at different amine concentrations for different temperatures. This independence of concentration on k_g' is also seen in the current MEA rate data (Figure 4.7) which was taken at high MEA concentrations.

4.4.4.1.2 Piperazine

Although Table 2.2 of the Literature Review only lists 5 references for CO_2 reaction rates into aqueous PZ solutions, all provide some raw experimental data. Sun (2005), Derks (2006), Cullinane (2006), and Samanta (2007) include unloaded PZ rate data while Bishnoi (2000) provides CO_2 loaded rate data. All five data sources use low piperazine concentrations.

Derks uses a stirred cell and a "semi-continuous" gas phase operation. Numerous CO_2 partial pressures were tested for each amine to determine when the pseudo first order condition applies. At high CO_2 partial pressures, diffusion in the liquid phase limits CO_2 mass transfer. For 1.0 M PZ at 40˚C, approximately 1.5 kPa CO_2 was the threshold for the onset of the pseudo first order condition. Inlet CO_2 partial pressures above 1.5 kPa showed a distinct effect of the partial pressure on the measured K_G. Below the threshold, the overall mass transfer coefficient is independent of the inlet partial pressure.

Sun (2005) and Samanta (2007) each measured the absorption into unloaded PZ solutions using wetted wall columns. Each used very high CO_2 partial pressures, typically about 5 kPa. At these high CO_2 partial pressures and amine concentrations below 1 M, CO_2 fluxes into the liquid phase should be restricted by diffusion. In fact, Sun (2005) tested a few lower CO_2 partial pressures and these data verify that the system is not operating in the pseudo first order regime at the 5 kPa CO_2 pressure experiments, which comprise most of the data. Although we cannot extract a meaningful k_g' value from these raw data, they can still be valuable. These data require a model to account for the diffusion limitations in the system.

Cullinane provides all the required data to calculate k_g'. At each condition, five measurements were made. Obtained k_g' values were shown to range ± 30% from the mean due to the high dependence on the gas film mass transfer coefficient. The 1.2 m PZ experiments were 54–73% gas film controlled. Only 25 and 60˚C experiments were tested. The Cullinane experiments all use very low CO_2 partial pressures (< 250 Pa) so the pseudo first order condition should apply.

Figure 4.12 shows a comparison of the obtained 2 m PZ wetted wall column rate data with some literature obtained values. Figure 4.12 includes an unloaded 1.0 M PZ data point from Derks. This point is actually the obtained overall mass transfer, K_G, not the liquid film mass transfer coefficient, k_g'. Derks does not provide a gas film mass transfer coefficient correlation to quantify if or how much gas phase resistance limits CO_2 absorption into the solution. For purposes of comparison, the K_G obtained from Derks is plotted alongside the k_g' data and the k_g' model prediction from Cullinane (2005).

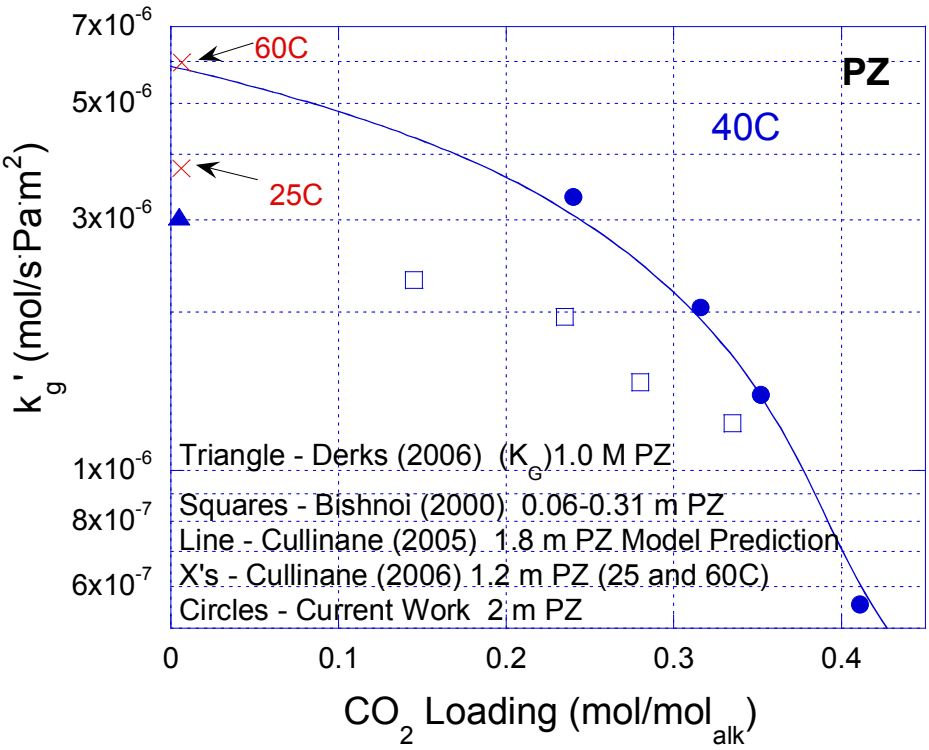

Figure 4.12: CO_2 reaction rate comparison on a k_g' basis for aqueous PZ at 40˚C (Bishnoi and Rochelle 2000; Cullinane 2005; Cullinane and Rochelle 2006; Derks, Kleingeld et al. 2006)

Figure 4.12 shows good agreement of the current 2 m PZ rate data with the 1.8 m PZ model prediction by Cullinane (2005). The loaded Bishnoi data shows mass transfer coefficients below the current data. This is expected due to the very low PZ concentration (0.06–0.31 m PZ) in these experiments. Interestingly, these data show the same trend as the 2 m PZ data. Very low amine concentrations also exhibited a reduced k_g' in MEA solutions (Figure 4.11).

The unloaded data in Figure 4.12 are difficult to analyze. Similar to the MEA data by Hartono (2009), the 25 and 60˚C data points by Cullinane show a significant temperature effect at 0 loading. These 1.2 m PZ data points show an acceptable fit to the

1.8 m 40˚C model prediction. The Derks overall mass transfer coefficient falls significantly below the other unloaded data, which was not unexpected. This suggests that the gas film mass transfer coefficient is likely limiting mass transfer into the PZ solution. The limitation of the gas film mass transfer coefficient is a disadvantage of using stirred cell reactors to measure CO_2 reaction rates of very fast amines.

4.5 DESIGN OF AN ISOTHERMAL ABSORBER

A large amount of rate and equilibrium data has been produced this chapter. This section indicates how the data can be used to design an isothermal absorber.

4.5.1 Design Basis

This example assumes 90% CO_2 removal of a 500 MW power plant with 12% CO_2 in the flue gas. A 500 MW power plant produces approximately 25 kmol/s of flue gas. The solvent is 8 m PZ with lean a rich partial pressures of 0.5 and 5.0 kPa at 40˚C. These partial pressures correspond to 0.31 lean loading and 0.41 rich loading. The isothermal absorber operates at 40˚C. This system is assumed to operate in the pseudo first order regime so the diffusion of reactants and products to and from the reaction interface is unimportant.

4.5.2 Calculations

The first step in the calculations is to determine the CO_2 flux at the top and bottom of the absorber. A log mean average of the two fluxes provides an average flux of the column. Figure 4.8 or Table 4.5 provide values for k_g'.

$$Flux_{CO_2,top} = k'_{g\,8mPZ,0.31ldg,40C}\left(P_{CO_2,top} - P_{CO_2,lean}\right) \tag{4.8}$$

$$Flux_{CO_2,top} = 2\cdot 10^{-6}\frac{mol_{CO_2}}{s\cdot Pa\cdot m^2}\left(1200\ \ Pa - 500\ \ Pa\right) = 1.4\cdot 10^{-3}\frac{mol_{CO_2}}{s\cdot m^2} \tag{4.9}$$

$$Flux_{CO_2,bottom} = k'_{g\,8mPZ,0.41ldg,40C}\left(P_{CO_2,bottom} - P_{CO_2,rich}\right) \tag{4.10}$$

$$Flux_{CO_2,bottom} = 8\cdot10^{-7}\ \frac{mol_{CO_2}}{s\cdot Pa\cdot m^2}\left(12000\ \ Pa - 5000\ \ Pa\right) = 5.6\cdot10^{-3}\ \frac{mol_{CO_2}}{s\cdot m^2} \tag{4.11}$$

$$Flux_{CO_2,lm} = \frac{Flux_{CO_2,top} - Flux_{CO_2,bottom}}{\ln\left(\frac{Flux_{CO_2,top}}{Flux_{CO_2,bottom}}\right)} = \frac{1.4\cdot10^{-3} - 5.6\cdot10^{-3}}{\ln\left(\frac{1.4\cdot10^{-3}}{5.6\cdot10^{-3}}\right)} = 3.0\cdot10^{-3}\ \frac{mol_{CO_2}}{s\cdot m^2} \tag{4.12}$$

A 500 MW power plant generates about 25 kmol/s of flue gas. Assuming 12% CO_2 and 90% removal requires the absorption of 2.7 $kmol_{CO2}$/s. The log mean CO_2 flux can be used to calculate the required area of packing.

$$Packing = \frac{2.7\cdot10^{3}\ \frac{mol_{CO_2}}{s}}{3.0\cdot10^{-3}\ \frac{mol_{CO_2}}{s\cdot m^2}} = 900{,}000\ \ m^2 \tag{4.13}$$

To determine the actual dimensions of the absorber, a gas velocity is required. Gas velocities of 1 m/s or lower are typical to prevent flooding. The total gas flow rate and design flow rate can be used to determine the cross-sectional area of the column. This absorber is operating at 40˚C near atmospheric pressure.

$$Area = \frac{25{,}000\ \ mol}{s}\cdot\frac{s}{1\ \ m}\cdot\frac{8.206\cdot10^{-5}\ \ atm\cdot m^3}{mol\cdot K}\cdot\frac{313.15\ \ K}{1\ \ atm} = 642\ \ m^2 \tag{4.14}$$

A maximum gas velocity of 1 m/s requires a minimum cross sectional area of 642 m^2. This cross sectional area is likely too large for one column but could be divided into multiple absorbers.

The required packing height of the absorber can be determined using the total required packing area and the cross-sectional diameter. The specific area of packings vary but course structured packings often provide surface areas of 250 m^2/m^3. Equation 4.15 determines the required height of packing for this scenario.

$$Height = 900{,}000\ \ m^2 \cdot \frac{m^3}{250\ \ m^2} \cdot \frac{1}{642\ \ m^2} = 5.6\ \ m \quad (4.15)$$

4.5.3 Analysis

This design is not optimal. However, it does show the methodology for sizing an absorber using data presented in this work. This analysis uses only the top and bottom of the absorber to determine the average CO_2 flux. Including intermediate points would greatly increase the accuracy of the analysis.

If CO_2 concentration in the gas phase is assumed to change linearly in the absorber as a function of absorber height, the CO_2 loading must also change linearly to satisfy the CO_2 material balance. A linear change in CO_2 loading produces an exponential change in the equilibrium CO_2 partial pressure of the solution. This exponential change causes the largest CO_2 fluxes to be observed in the interior of an isothermal absorber. Therefore, using just the top and bottom of the absorber to determine the average CO_2 flux is not recommended.

Chapter 5: Modeling

5.1 SPREADSHEET MODELING

As Section 2.2.3 on film theory shows, the liquid film mass transfer coefficient, k_g', results from both reaction and diffusion resistances. These resistances in the liquid film can be separated using a series resistance.

$$\frac{1}{k_g^{'}} = \frac{1}{k_g^{''}} + \frac{1}{k_{l,prod}^{o}}\left(\frac{\Delta P_{CO2}^{*}}{\Delta[CO_2]_T}\right) \tag{5.1}$$

In Equation 5.1, the first term refers to the reaction resistance which is characterized by the pseudo first order condition. The second term represents diffusion resistance and incorporates the slope of the equilibrium line and the physical mass transfer coefficient of the reactants and products.

An analytical expression to calculate k_g' at highly concentrated, highly loaded conditions has previously remained elusive and thus required experimentation to determine CO_2 mass transfer rates. This approach attempts to identify and re-evaluate the assumptions in the typical treatment of calculating k_g'.

The reaction portion of Equation 5.1 requires the reaction rate of CO_2. This can be defined generically by Equation 5.2 in which the order of the reaction with respect to the amine is variable. The value of "x" will be determined by evaluating experimental data.

$$r_{CO2} = -k\gamma_{Am}^{x}[Am]^{x}\gamma_{CO2}([CO_2]-[CO_2]_e) \tag{5.2}$$

Solving the material balance and using the proper boundary conditions with the pseudo first order assumption produces in Equation 5.3, which is more complex than the traditional expression (Equation 2.30).

$$k_g'' = \frac{\sqrt{k\gamma_{Am}^{x}[Am]^{x} D_{CO2}}}{\gamma_{CO2}^{0.5} H_{CO2,H2O}} \tag{5.3}$$

The more complex expression requires an understanding of the rate constant, the activity coefficients of both the amine and CO_2, the order of the amine, and the diffusion coefficient of CO_2. Equation 5.3 can only represent the reaction resistance. Experimental conditions with significant diffusion resistances also require an accurate representation of the slope of the equilibrium line and the mass transfer coefficient of the products and reactants. All of the varying parameters for both monoethanolamine and piperazine are explored in the following sections. Equation 5.4 combines Equations 5.1 and 5.3 to list the generic expression for calculating k_g'.

$$\frac{1}{k_g'} = \frac{\gamma_{CO2}^{0.5} H_{CO2,H2O}}{\sqrt{k\gamma_{Am}^{x}[Am]^{x} D_{CO2}}} + \frac{1}{k_{l,prod}^{o}}\left(\frac{\Delta P_{CO2}^{*}}{\Delta[CO_2]_T}\right) \tag{5.4}$$

Appendix F includes results of the MEA and PZ spreadsheet models.

5.1.1 Monoethanolamine Systems

5.1.1.1 Activity Coefficients

The rate expression is determined by the activity of the reactants, not the concentration of the reactants. It cannot be assumed that activity coefficients are near 1.0 in highly loaded, highly concentrated MEA solutions. These solutions are highly ionic and should be treated thus.

MEA activity coefficients can be obtained from amine volatility experiments. CO_2 activity coefficients can be obtained from Henry's solubility data.

5.1.1.1.1 Monoethanolamine Activity Coefficient

MEA volatility data is scarce but Hilliard (2008) provides 3.5, 7, and 11 m MEA volatility data. These experiments coincide with the CO_2 partial pressure experiments Hilliard conducted in an equilibrium cell. The FTIR analyzer he used simultaneously measured gas phase concentrations of multiple components.

The MEA volatility data was treated via the modified Raoult's Law in Equation 5.5. Reported values of 164 and 666 Pa were used for the equilibrium partial pressure of pure MEA at 40 and 60˚C (DIPPR 1979).

$$y_{MEA}P = P_{MEA} = \gamma_{MEA}x_{MEA}P^*_{MEA} \tag{5.5}$$

The mole fraction of MEA is easy to determine below 0.4 CO_2 loading by assuming each mole of CO_2 reacts with 2 moles of MEA. Above a 0.45 mol_{CO2}/mol_{alk} loading, bicarbonate concentrations can become significant while free MEA concentration becomes very small. At these high CO_2 loadings it is very difficult to determine the free MEA concentration accurately. Due to this uncertainty, no data from Hilliard (2008) above 0.45 CO_2 loading was used in the determination of MEA activity coefficients. Figure 5.1 shows the calculated MEA activity coefficients using the modified Raoult's law.

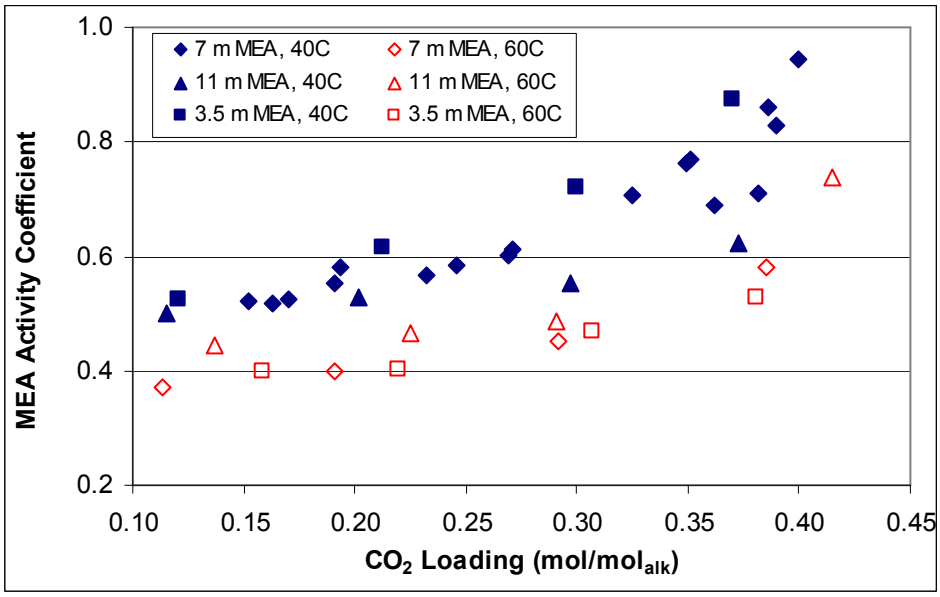

Figure 5.1: Calculated MEA activity coefficients for 3.5, 7, and 11 m MEA at 40 and 60˚C (Hilliard 2008).

The Hilliard data show an increasing MEA activity coefficient with increased CO_2 loading. The MEA activity coefficient is also a function of temperature, with higher temperatures having lower activity coefficients. Amine concentration is not major factor in the determination of the activity coefficient. The 3.5, 7, and 11 m MEA data sets tend to overlap.

The data in Figure 5.1 were regressed to produce an expression for the MEA activity coefficient. The expression in Equation 5.6 is plotted as lines in Figure 5.2 to show regressed values at 40, 60, 80, and 100˚C. Equation 5.6 expresses CO_2 loading in terms of mol/mol$_{alk}$ and temperature in Kelvin.

$$\ln \gamma_{MEA} = -5.71 + 1.74\left(CO_2 Loading\right) + \frac{1503}{T} \qquad (5.6)$$

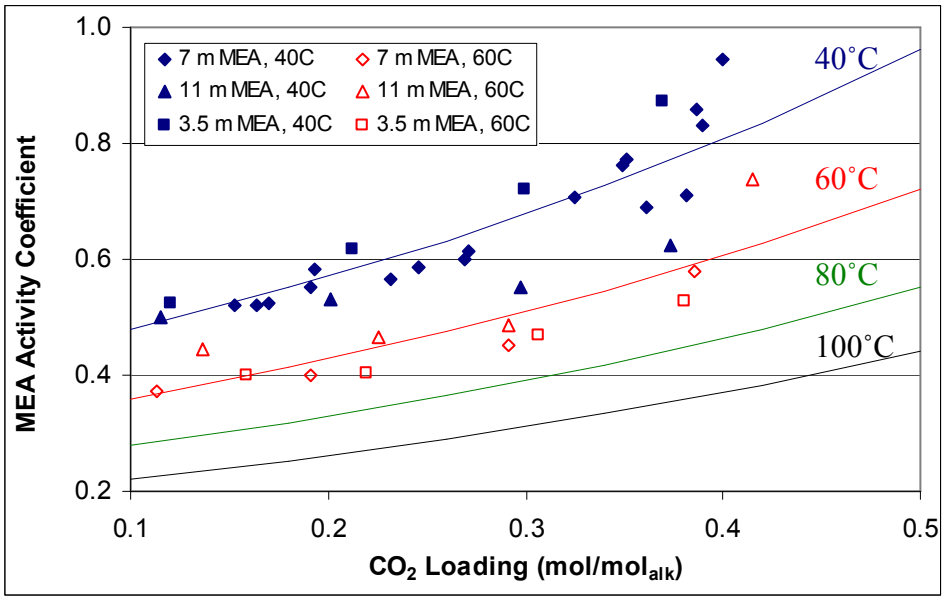

Figure 5.2: Calculated MEA activity coefficients for 3.5, 7, and 11 m MEA at 40 and 60˚C (Hilliard 2008) with regressed lines at 40, 60, 80, and 100˚C.

5.1.1.1.2 Carbon Dioxide Activity Coefficient

The activity of CO_2 in loaded MEA solutions can be obtained from Henry's solubility data with N_2O. Unfortunately, very little N_2O solubility data has been reported in concentrated, CO_2 loaded MEA systems. Browning and Weiland (1994) present 12 N_2O solubility data points in 10, 20, and 30 wt% MEA up to 0.4 CO_2 loading at 25˚C. No other N_2O solubility data varying amine concentration and CO_2 loading are available. The N_2O solubility data were regressed to provide Equation 5.7. Equation 5.7 includes the MEA concentration in wt%.

$$\ln H_{N2O,25C} = \begin{pmatrix} 8.3194 + 4.52 \cdot 10^{-3}(MEA) - 4.78 \cdot 10^{-2}(CO_2 Ldg) \\ + 4.56 \cdot 10^{-2}(MEA)(CO_2 Ldg) \end{pmatrix} \quad (5.7)$$

Figure 4.14 shows the N_2O solubility data points from Browning as well as the regressed curves for 10, 20, and 30 wt% MEA.

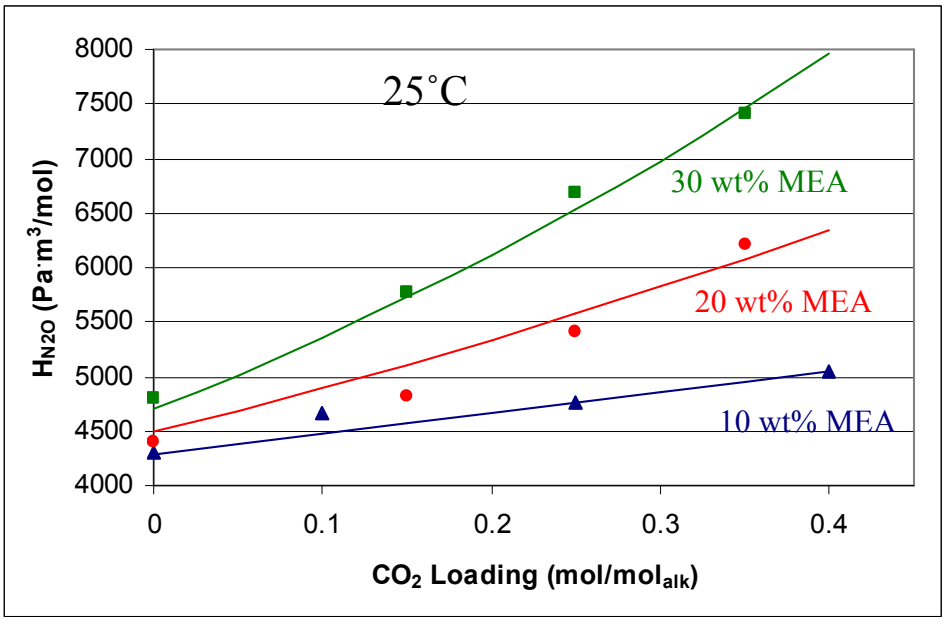

Figure 5.3: N_2O solubility data (Browning and Weiland 1994) and model (lines) in 10, 20, and 30 wt% MEA solutions at 25˚C.

Figure 5.3 shows that Equation 5.7 satisfactorily represents the N_2O solubility as a function of amine concentration and CO_2 loading. Figure 5.3 also illustrates how significantly the N_2O solubility decreases with increased loading and amine concentration. The amine concentration and CO_2 loading must be considered in the estimation of the Henry's constant. Equation 5.7 allows for the calculation of the solubility of CO_2 in MEA solutions via the N_2O analogy, but only at 25˚C. Laddha (1981b) showed that the ratio of N_2O and CO_2 solubilities remained constant for various organic solutions and that the N_2O analogy can be applied to estimate the solubility of CO_2 in aqueous alkanolamine solutions. It is not possible to measure CO_2 solubility in these amine systems directly since CO_2 will react with the amine.

$$\left(\frac{H_{CO2}}{H_{N2O}}\right)_{soln} = \left(\frac{H_{CO2}}{H_{N2O}}\right)_{H2O} \tag{5.8}$$

The CO_2 and N_2O solubility data in water as a function of temperature have been compiled and regressed (Versteeg and Van Swaaij 1988).

$$H_{CO2,H2O} = 2.82 \cdot 10^6 \exp(-2044/T) \;\; Pa \cdot m^3 mol^{-1} \qquad (5.9)$$

$$H_{N2O,H2O} = 8.55 \cdot 10^6 \exp(-2284/T) \;\; Pa \cdot m^3 mol^{-1} \qquad (5.10)$$

Hartono (2009) recently published N_2O solubility data in loaded 30 wt% (7 m) MEA solutions. Hartono measured N_2O solubility from 25–87°C for 0, 0.2, 0.4, and 0.5 CO_2 loading solutions. Figure 5.4 illustrates the N_2O solubility results for each of the 4 CO_2 loadings.

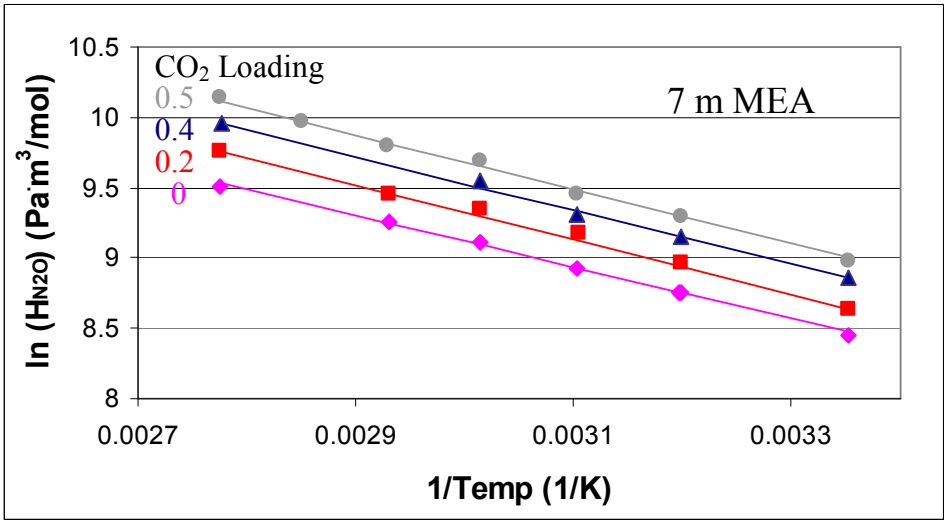

Figure 5.4: N_2O solubility data (points) and trend lines for 0, 0.2, 0.4, and 0.5 CO_2 loaded 7 m MEA (Hartono 2009)

The natural log of the N_2O solubility plotted against inverse temperature yields straight lines for each of the four CO_2 loadings. The slope of the lines corresponds to the temperature behavior of N_2O solubility in 7 m MEA. The slopes of the four lines are approximately equal with an average value of –1905/T. The N_2O solubility temperature effect in loaded MEA solutions can be added to Equation 5.7, which is only valid at

25˚C. Equation 5.11 should be valid from 25 to at least 87˚C, the temperature range of the regressed data.

$$H_{N2O} = \exp\left[\begin{pmatrix} 8.3194 + 4.52\cdot10^{-3}(MEA) - 4.78\cdot10^{-2}(CO_2Ldg) \\ +4.56\cdot10^{-2}(MEA)(CO_2Ldg) \end{pmatrix} - 1905\left(\frac{1}{T} - \frac{1}{298.15}\right)\right] \quad (5.11)$$

Similar to the N_2O solubility from Browning (1994), Hartono shows the N_2O solubility decreasing with increasing CO_2 loading. Unfortunately, the data do not agree completely. Both Hartono and Browning measure N_2O solubility at 25˚C for 7 m MEA. Figure 5.5 shows the disagreement between the two data sets.

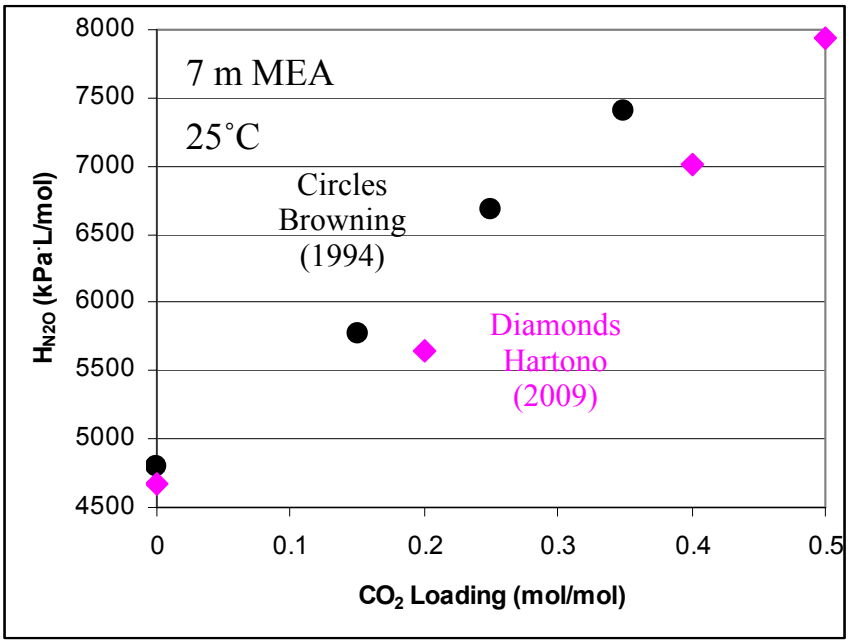

Figure 5.5: N_2O solubility in 7 m MEA at 25˚C (Browning and Weiland 1994; Hartono 2009)

Since these are the only two data sets for N_2O solubility in loaded MEA solutions, it is not possible to tell which data set is erroneous. In this work the Browning (1994) data set has been used to quantify the effects of CO_2 loading and MEA concentration on

N_2O solubility. The Hartono (2009) data set has been used to quantify the effect of temperature on N_2O solubility.

The calculation of the Henry's constant of CO_2 allows for the determination of the activity coefficient of CO_2 using Equation 5.12. The activity coefficient of CO_2 is assumed to be equivalent to the activity coefficient of N_2O.

$$\gamma_{N2O} = \frac{H_{N2O}}{H_{N20,H2O}} = \frac{H_{CO2,}}{H_{CO2,H2O}} = \gamma_{CO2} \tag{5.12}$$

H_{CO2} gives the effective solubility of CO_2 in the solution. $H_{CO2,H2O}$ is the true thermodynamic Henry's constant, which refers to the solubility of CO_2 in pure water. The activity coefficient of CO_2 varies between 1.3 and 3.2 for 7–13 m MEA wetted wall column experiments.

5.1.1.2 Diffusion Coefficient of CO_2

Work by Versteeg and Van Swaaij (1988) has shown that the diffusion of N_2O and CO_2 in aqueous amines generally follows the viscosity dependence in Equation 5.13.

$$\left(D_{N2O}\eta^{0.8}\right)_{sol} = CONSTANT = \left(D_{N2O}\eta^{0.8}\right)_{Water} \tag{5.13}$$

The N_2O and CO_2 diffusivity relationship in Equation 5.13 was confirmed with MDEA solutions but resulted in less reliable results for AMP (Tomcej and Otto 1989; Xu, Otto et al. 1991).

Diaphragm cell experiments in loaded MEA and PZ solutions yield a viscosity dependence of 0.72 with a standard error of 0.12 (Figure 4.1). Although the 0.72 dependence obtained from the diaphragm cell experiments does not necessarily represent CO_2 diffusion, or diffusion of any other specific species, the 0.72 dependence was used for calculation of the diffusion coefficient of CO_2.

$$\left(D_{CO2}\right)_{so\ln} = \frac{\left(D_{CO2}\eta^{0.72}\right)_{Water}}{\left(\eta^{0.72}\right)_{so\ln}} \tag{5.14}$$

The diffusion coefficient of CO_2 in water was calculated using a correlation reported by Versteeg (1988).

$$D_{CO_2} = 2.35\cdot 10^{-6}\exp\left(-2119/T\right) \quad m^2\cdot s^{-1} \tag{5.15}$$

The viscosity of water at the wetted wall column experimental temperatures was obtained from tabulated data by Watson (1986). MEA solution viscosity values were obtained from Weiland (1998). Ω represents the MEA wt% in Equation 5.16. Temperatures are in Kelvin.

$$\eta = \eta_{H2O}\exp\left(\frac{\left[\left(a\Omega+b\right)T+\left(c\Omega+d\right)\right]\cdot\left[\alpha\left(e\Omega+fT+g\right)+1\right]\Omega}{T^2}\right) \tag{5.16}$$

Table 5.1: Parameters for MEA viscosity (Weiland, Dingman et al. 1998)

a	b	c	d	e	f	g
0	0	21.186	2373	0.01015	0.0093	-2.2589

Although the viscosity-diffusion coefficient relationship of 0.72±0.12 includes a large standard error, the power of the viscosity is not very critical in the k_g' expressions developed later. Using values of 0.6 or 0.84 for the power of viscosity introduces less than 1% additional error into the MEA and PZ models after the pre-exponential portion of the rate constant is adjusted appropriately.

5.1.1.3 Free MEA Concentration

The free MEA concentration in molarity, [MEA], was determined using the fraction of the free amine in the Hilliard (2008) model at each wetted wall column condition. The Hilliard model is a sequential regression thermodynamic model capable

of handling systems containing H_2O, CO_2, MEA, PZ, and K^+. Required density data were obtained from the Weiland (1998) density correlation for MEA solutions.

$$\rho = \frac{x_{Am}M_{Am} + x_{H_2O}M_{H_2O} + x_{CO_2}M_{CO_2}}{V} \tag{5.17}$$

$$V = x_{Am}V_{Am} + x_{H_2O}V_{H_2O} + x_{CO_2}V_{CO_2} + x_{Am}x_{H_2O}V^{*} + x_{Am}x_{CO_2}V^{**} \tag{5.18}$$

$$V_{Am} = \frac{M_{Am}}{aT^2 + bT + c} \tag{5.19}$$

$$V^{**} = d + e \cdot x_{Am} \tag{5.20}$$

Table 5.2: Parameters for MEA density (Weiland, Dingman et al. 1998)

a	b	c	d	e	M_{Am}	V_{CO2}	V^*
-5.35162E-07	-4.51417E-04	1.19451	0	0	61.09	0.04747	-1.8218

5.1.1.4 Monoethanolamine Order

With estimations for the activity coefficients of MEA and CO_2, the MEA concentration dependence on k_g' can be examined. The rate data show a second order dependence on the MEA concentration. This second order dependence can be satisfied from either the zwitterion or termolecular mechanism, although the termolecular mechanism is more likely for MEA. The termolecular mechanism allows for the following base catalysis reaction expression.

$$r_{CO2} = -\left(k_{MEA}[MEA] + k_{H2O}[H_2O]\right)\cdot[MEA]\cdot[CO_2] \tag{5.21}$$

For the second order dependence to be observed $k_{MEA}[MEA]$ must be much greater than $k_{H2O}[H_2O]$. Crooks and Donnellan (1989) report k_{MEA} and k_{H2O} values based on 0.02–0.06 M MEA rate data. They report k_{MEA} values about 2200 times larger than k_{H2O}. Bronsted theory, which relates base pKa's to rate constants, would also predict a k_{MEA} value orders of magnitude larger than k_{H2O}. If k_{MEA} is 2200 times larger

than k_{H2O}, more than 99% of the amine in 7 m MEA would have to be reacted before water catalysis becomes significant. In this analysis with high MEA concentrations, water catalysis has been ignored.

Density function theory calculations have also shown that water catalysis of the zwitterion species is thermodynamically implausible due to an increase of energy in the water catalyzed products (Shim, Kim et al. 2009). MEA catalyzed products were shown to have a favorable decrease in energy compared to the zwitterion species.

In order for the second order amine dependence to match the zwitterion mechanism, k_r must be much greater than $\sum k_b[B]$ in Equation 5.22, yielding Equation 5.23. This is not accepted for MEA (Danckwerts 1979) and is even more unlikely at high MEA (base) concentrations tested in the wetted wall column.

$$r_{CO2} = -\frac{[Am][CO_2]}{\frac{1}{k_f} + \frac{k_r}{k_f \sum k_b[B]}} \tag{5.22}$$

$$r_{CO2} = -\frac{k_f}{k_r}[MEA][CO_2]\sum k_b[B] \tag{5.23}$$

The equations of this section have been written with respect to concentration for simplicity. However, the model is activity-based, so activity coefficients can be inputted into all the equations.

The majority of the literature data on MEA rates report kinetics with a first order MEA dependence. These data are generally unloaded and at dilute MEA concentrations using concentration-based kinetics. Concentrated MEA rate experiments evaluated using concentration based kinetics have shown a greater than 1.0 dependence on the MEA concentration (Aboudheir, Tontiwachwuthikul et al. 2003). Therefore, it is not

unrealistic to observe second order MEA kinetics for highly loaded, concentrated MEA using activity-based kinetics.

5.1.1.5 Liquid Phase Mass Transfer Coefficient of Reactants and Products, $k^0_{l,prod}$

The liquid phase mass transfer coefficient of the reactants and products, $k^0_{l,prod}$, was calculated as shown in Section 3.2.2.2. Since the reactants and products are limiting, the diffusion coefficient of the reactants and products must be incorporated.

$$k^o_{l,prod} = \left(\frac{3^{1/3}2^{1/2}}{\pi^{1/2}}\right)\left(\frac{Q^{1/3}h^{1/2}W^{2/3}}{A}\right)\left(\frac{g\rho}{\mu}\right)^{1/6} D^{1/2}_{prod} \qquad (5.24)$$

The diffusion coefficient of the products was obtained utilizing the diaphragm cell diffusion experiments. Equation 5.25 was obtained from a curve fit of Figure 4.1. The diffusion coefficient is represented in m^2/s and viscosity is in cP. Equation 5.25 ratios diffusion coefficients using temperature based on the Wilke-Chang correlation (Equation 2.35). Diffusion experiments were performed at 30˚C, (303.15 K).

$$D_{prod} = 8.2\cdot 10^{-10}\,\mu^{-0.72}\left(\frac{T}{303.15}\right) \qquad (5.25)$$

Viscosity and density parameters required for Equation 5.26 were obtained by the Weiland (1998) correlations for MEA.

5.1.1.6 Slope of the Equilibrium Line

The slope of the equilibrium line in Equation 5.1 results from converting a concentration-based mass transfer coefficient to a partial pressure basis. The slope can be difficult to determine accurately due to the CO_2 partial pressure sensitivity at high loading or temperatures. Partial pressure curves are plotted on a log-based y-axis. The log scale often results in extremely high values for the slope. In cases where diffusion

limits CO_2 mass transfer, poor estimation of the slope of the equilibrium can drastically affect the expected mass transfer.

The equilibrium partial pressure can be uniformly predicted by using an empirical expression developed by Xu (Rochelle, Chen et al. 2009b) using literature data. The empirical relationship in Equation 5.26 is valid for MEA solutions between 40 and 160˚C. Equation 5.26 defines the partial pressure in Pascals with temperature in Kelvin.

$$\ln P_{CO2} = 44.2 + (-116{,}000 J/mol)\cdot\frac{1}{RT} - 29.7\alpha + 11{,}600\frac{\alpha}{T} + 17.3\alpha^2 \quad (5.26)$$

Figure 5.6 shows the fit to CO_2 partial pressure data previously referenced in Figure 4.2.

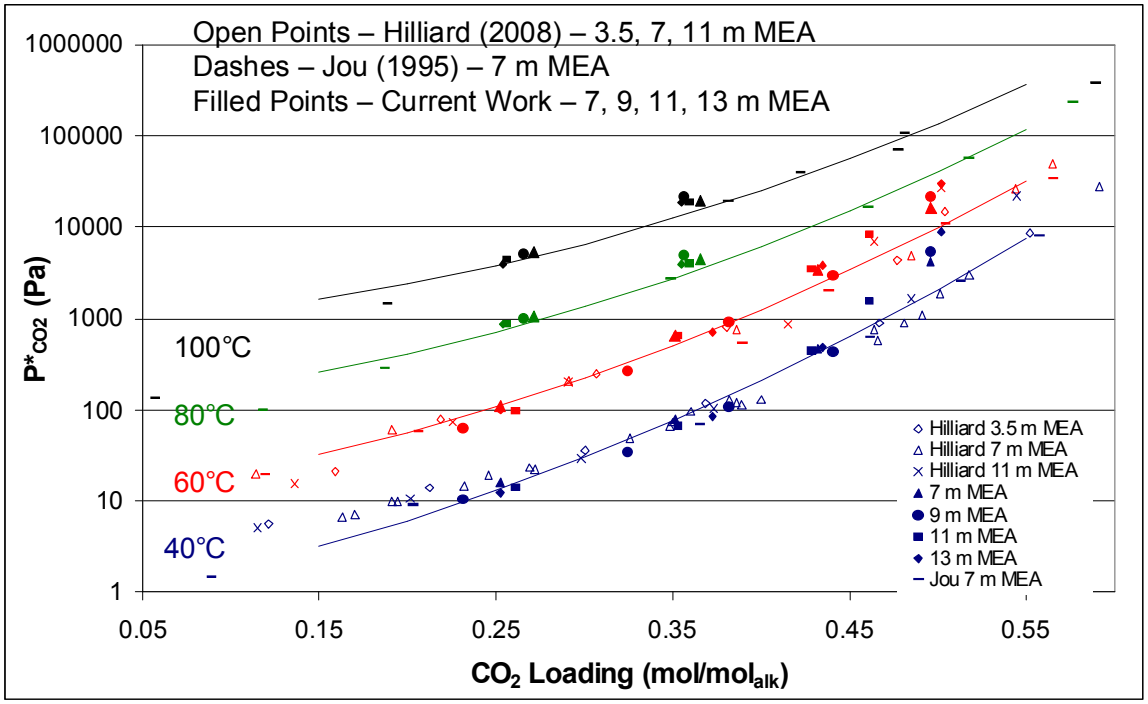

Figure 5.6: Equilibrium CO_2 partial pressure measurements in MEA solutions at 40, 60, 80, and 100˚C (Jou, Mather et al. 1995; Hilliard 2008). Lines – Equation 5.26.

Taking the derivative of Equation 5.26 with respect to CO_2 loading yields a term which can be multiplied by the alkalinity concentration to obtain the slope of the equilibrium line in the required units. This analytical approach provides a consistent representation of the slope of the equilibrium line over a wide range of experimental conditions. The derivative of Equation 5.26 is an extremely long expression and is not reported. This slope estimation method for MEA has a disadvantage in does not incorporate the effect of amine concentration at very high CO_2 loading where bicarbonate concentrations are significant.

5.1.1.7 Rate Constant

The rate constant for MEA has been reported based on a review of the available literature data (Versteeg, Van Dijck et al. 1996).

$$k_{MEA} = 4.4 \cdot 10^8 \exp\left(-\frac{5400}{T}\right) \quad m^3 mol^{-1} s^{-1} \tag{5.27}$$

The temperature dependence of Equation 5.27 has been used in this model although the equation is only valid up to 40˚C. No reliable literature data was available at higher temperatures to verify Equation 5.27 at higher temperatures (Versteeg, Van Dijck et al. 1996). Regardless, this temperature dependence has been extrapolated up to 100˚C for this model.

Equation 5.27 is first order MEA expression using on concentration-based kinetics. Since a second order, activity-based amine concentration dependence was found in the experimental data, the pre-exponential constant required readjustment. The pre-exponential portion of the rate constant was adjusted until the expression in Equation 5.28 was minimized.

$$\sum\left(\frac{k'_{g,calc}-k'_{g,meas}}{k'_{g,meas}}\right)^2 \tag{5.28}$$

The obtained value of k_{MEA} is $2.4\cdot10^6$ $m^6mol^{-2}s^{-1}$ based on the final rate expression shown in Equation 5.29. This rate expression leads to the following expression for k_g' in MEA solutions.

$$r_{CO2} = -k_{MEA}\gamma_{MEA}^2[MEA]^2\gamma_{CO_2}[CO_2] \tag{5.29}$$

$$\frac{1}{k'_g} = \frac{\gamma_{CO2}^{0.5}H_{CO2,H2O}}{\sqrt{k\gamma_{MEA}^2[MEA]^2D_{CO2}}} + \frac{1}{k^o_{l,prod}}\left(\frac{\Delta P^*_{CO2}}{\Delta[CO_2]_T}\right) \tag{5.30}$$

The evaluation of the model is presented in Section 5.2.

5.1.2 Piperazine Systems

5.1.2.1 Activity Coefficients

The rate expression is determined by the activity of the reactants, not the concentration. It cannot be assumed that activity coefficients are near 1.0 in highly loaded, highly concentrated PZ solutions. These solutions are highly ionic and should be treated so.

5.1.2.1.1 Piperazine and Piperazine Carbamate Activity Coefficients

In the MEA analysis, the MEA activity coefficient was obtained via amine volatility data analyzed by the modified Raoult's law. Using the modified Raoult's law for PZ presents a problem since pure PZ is a solid at the experimental temperatures. Piperazine partial pressure data from pure liquid piperazine can be extrapolated to 40˚C, although the PZ correlation is limited to temperatures greater than 106˚C. PZ volatility

data from Hilliard (2008) utilizing the modified Raoult's law approach yields Figure 5.7. The free PZ concentration in Figure 5.7 was obtained from the Hilliard (2008) model.

$$y_{PZ}P = P_{PZ} = \gamma_{PZ} x_{PZ} P^*_{PZ} \tag{5.31}$$

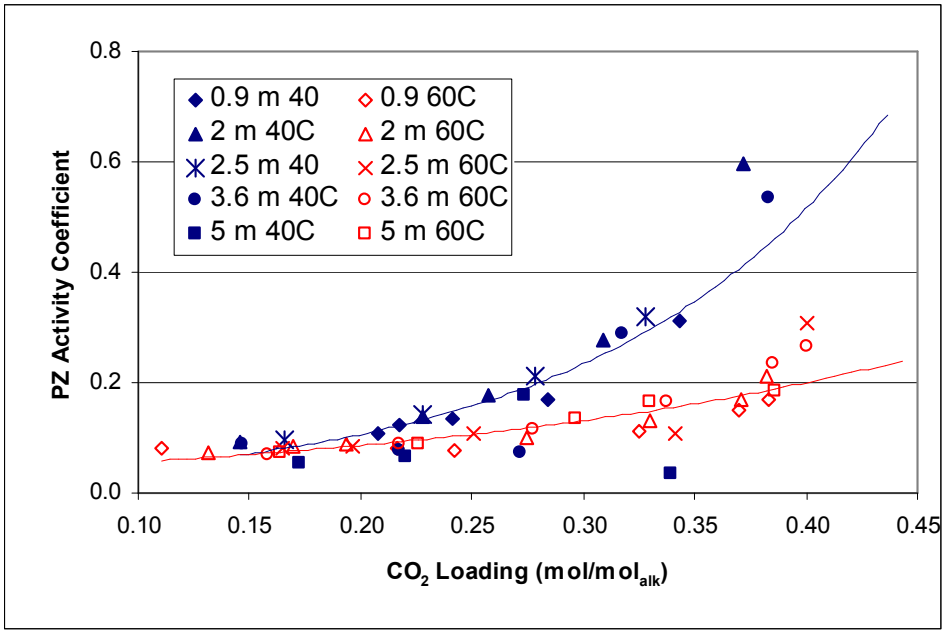

Figure 5.7: PZ volatility data evaluated using the modified Raoult's law with an extrapolated P^*_{PZ}

Results in Figure 5.7 seem unreliable since the activity coefficient of PZ varies a factor of 7 from 0.15 to 0.4 CO_2 loading at 40˚C. Since PZ and PZ carbamate concentrations do not change a factor of 7 over this range, implementing these activity coefficient data would result in a higher PZ activity and a faster CO_2 reaction rate at 0.4 than 0.1 CO_2 loading. Rate experiments have clearly shown that rates are significantly faster at lower CO_2 loading.

This phenomenon results from the modified Raoult's law form which only considers free piperazine. The free piperazine drops significantly at higher CO_2 loading and produces very high PZ activity coefficients. The data generally show a PZ volatility

drop about a factor of 2 from low to high loading. Meanwhile the free piperazine concentration may change a factor of 15.

Since PZ has 2 reactive nitrogen groups, the Raoult's law approach may not be a valid approach to predicting reaction activity coefficients. Considering the case of PZ carbamate where one nitrogen group has reacted with CO_2, the Raoult's law approach for volatility yields no thermodynamic activity due to its ionic nature and inability to enter the vapor phase. The reaction activity is certainly nonzero since the second nitrogen group is known to react very quickly with either CO_2 or a proton.

Since PZ volatility data cannot be used to predict PZ activity coefficients another approach needed to be found. The Hilliard (2008) model was used to predict the PZ and piperazine carbamate activity coefficients at wetted wall column conditions. The Hilliard model is based on the electrolyte non-random two liquid (e-NRTL) model which minimizes the excess Gibbs free energy in determining interaction parameters. Figure 5.8 shows obtained activity coefficients in 5 m PZ at 60˚C.

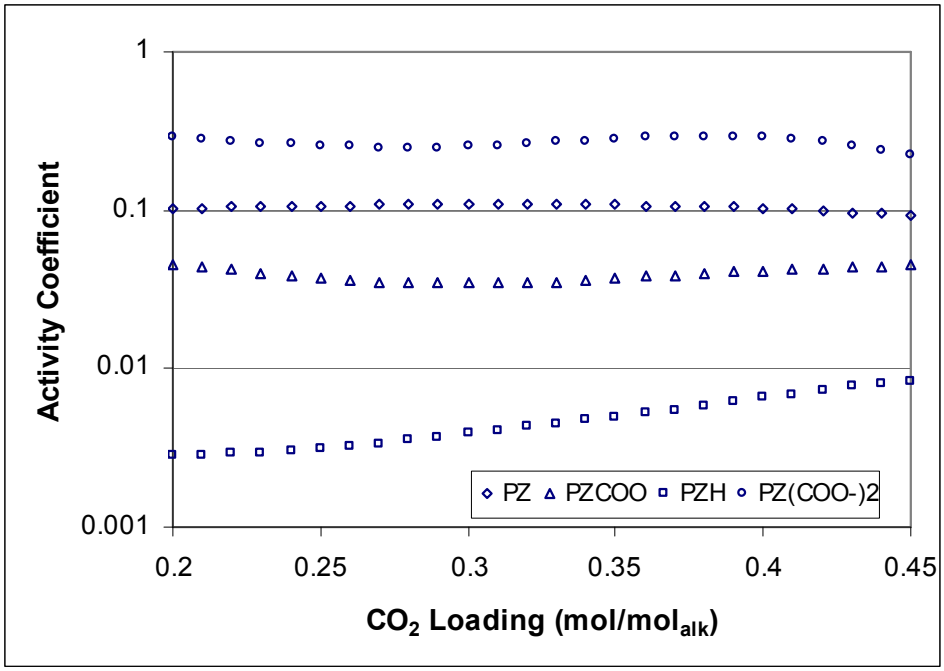

Figure 5.8: Activity coefficient results of the Hilliard (2008) model for 5 m PZ at 60˚C

Table 5.3 shows a summary of the obtained PZ and $PZCOO^-$ activity coefficient values at 2 and 5 m at 40 and 60˚C. The wetted wall column experiments for PZ ranged from 0.22 to 0.41 CO_2 loading. Table 5.3 shows the minimum and maximum values over that loading range.

Table 5.3: PZ and $PZCOO^-$ activity coefficients from the Hilliard (2008) model for 2 and 5 m PZ at 40 and 60˚C between 0.22 and 0.41 CO_2 loading

	PZ		$PZCOO^-$	
	Min	Max	Min	Max
2 m 40C	0.054	0.062	0.033	0.048
2 m 60C	0.075	0.082	0.035	0.042
5 m 40C	0.071	0.077	0.029	0.043
5 m 60C	0.101	0.109	0.034	0.042

It is important to note that the PZ activity coefficients in Table 5.3 are similar to the values in Figure 5.7 at very low loading. Near zero loading, the modified Raoult's

law should accurately represent the activity coefficient of PZ since $PZCOO^-$ is not present.

Both PZ and $PZCOO^-$ are relatively constant with changes in CO_2 loading at each condition. The small variance in γ_{PZ} is not directly correlated with CO_2 loading. However, the PZ activity coefficient increased significantly with increases in amine concentration and temperature. $PZCOO^-$ activity coefficients were relatively constant over the range of experimental conditions.

The Hilliard model contains data from 0.9 to 5 m PZ and is accurate at temperatures up to 60˚C (Hilliard 2008). Above these conditions the model produces some activity coefficients which were not deemed reliable. Rather than extrapolating the model for 8 and 12 m PZ at 80 and 100˚C, data within the reliable range of the model was extrapolated. This was done by regressing the average PZ activity coefficients to Equation 5.32. Equation 5.32 was used to extrapolate to 8, 12 m PZ and 80, 100˚C conditions. Piperazine activity coefficients were regressed on a wt% amine basis with temperature in Kelvin. Since $PZCOO^-$ activity coefficients were relatively constant, an average value was used for all conditions.

$$\ln \gamma_{PZ} = 2.325 + 0.172(PZ) - \frac{1702}{T} \tag{5.32}$$

$$\gamma_{PZCOO^-} = 0.038 \tag{5.33}$$

5.1.2.1.2 Carbon Dioxide Activity Coefficient

No N_2O solubility data in concentrated or CO_2 loaded piperazine solutions are available in the literature. Therefore, the activity coefficient of CO_2 in piperazine solutions cannot be determined via experimental data. The N_2O solubility in CO_2 loaded concentrated piperazine solutions was assumed similar to CO_2 loaded concentrated MEA.

Equation 5.11, obtained from solubility data in MEA was used with one modification. The CO_2 loading in Equation 5.11 was multiplied by 2 since the CO_2 loading is in terms of mol_{CO2}/mol_{alk}. Multiplying the CO_2 loading by 2 allows Equation 5.34 to represent the solubility based on mol_{CO2}/mol_{PZ}. The PZ concentration in Equation 5.34 is represented in wt%. Equation 5.34 was used to determine the Henry's solubility of N_2O in PZ solutions.

$$H_{N2O} = \exp\left[\begin{pmatrix} 8.3194 + 4.52\cdot10^{-3}(PZ) - 4.78\cdot10^{-2}(2\cdot CO_2 Ldg) \\ +\,4.56\cdot10^{-2}(PZ)(2\cdot CO_2 Ldg) \end{pmatrix} - 1905\left(\frac{1}{T} - \frac{1}{298.15}\right)\right] \quad (5.34)$$

Again, the CO_2 and N_2O solubility data in water as a function of temperature have been compiled and regressed (Versteeg and Van Swaaij 1988). These equations were used along with the N_2O analogy to predict the activity coefficient of CO_2 in PZ solutions.

$$H_{CO2,H2O} = 2.82\cdot10^{6}\exp(-2044/T)\ \ Pa\cdot m^3 mol^{-1} \quad (5.35)$$

$$H_{N2O,H2O} = 8.55\cdot10^{6}\exp(-2284/T)\ \ Pa\cdot m^3 mol^{-1} \quad (5.36)$$

$$\gamma_{N2O} = \frac{H_{N2O}}{H_{N20,H2O}} = \frac{H_{CO2,}}{H_{CO2,H2O}} = \gamma_{CO2} \quad (5.37)$$

H_{CO2} gives the effective solubility of CO_2 in the solution. $H_{CO2,H2O}$ is the true thermodynamic Henry's constant, which refers to the solubility of CO_2 in pure water. The activity coefficient of CO_2 varies between 1.1 and 5.6 for the 2–12 m PZ wetted wall column experiments.

5.1.2.2 Diffusion Coefficient of CO_2

The diffusion coefficient of CO_2 in PZ solutions was calculated identically to the diffusion coefficient of CO_2 in MEA solutions.

PZ solution viscosity values were obtained from regressing 5–12 m PZ viscosity measurements at 25, 40, and 60˚C from Freeman (Rochelle, Sexton et al. 2008a). Details of the PZ viscosity regression can be found in the Appendix E.

5.1.2.3 Piperazine and Piperazine Carbamate Concentrations

Piperazine and piperazine carbamate concentrations were estimated using mole fractions from the Hilliard (2008) model at each wetted wall column condition. Required density data were obtained by regressing 2–12 m PZ density measurements at 20, 40, and 60˚C from Freeman (Rochelle, Chen et al. 2009a). Details on the PZ density regression can also be found in Appendix E.

5.1.2.4 Amine Order

With estimations for the activity coefficients of PZ, $PZCOO^-$, and CO_2, the piperazine concentration dependence on k_g' can be examined. A base catalysis reaction expression similar to the expression for the MEA system is written below. Equation 5.38 is written generically.

$$r_{CO2} = -\left(k_{Am}[Am] + k_{H2O}[H_2O]\right)\cdot[Am]\cdot[CO_2] \qquad (5.38)$$

Like the MEA analysis, catalysis by water was ignored. In concentrated piperazine solutions, the water catalysis should be even less significant than in MEA systems because both piperazine and piperazine carbamate have a higher pKa than MEA and more free amine is present at the highest loading conditions.

Ignoring water catalysis but accounting for activity coefficients and both bases in the piperazine system allows Equation 5.38 to be expanded into Equation 5.39. The rate expression can also be written as Equation 5.40 which clearly shows each reaction permutation.

$$r_{CO2} = -\begin{pmatrix} k_{PZ}\gamma_{PZ}[PZ] \\ +k_{PZCOO}\gamma_{PZCOO}[PZCOO^-] \end{pmatrix} \cdot \begin{pmatrix} \gamma_{PZ}[PZ] \\ +\gamma_{PZCOO}[PZCOO^-] \end{pmatrix} \cdot [CO_2] \qquad (5.39)$$

$$r_{CO2} = -\begin{pmatrix} k_{PZ}\gamma_{PZ}^2[PZ]^2 + k_{PZ}\gamma_{PZ}[PZ]\gamma_{PZCOO}[PZCOO^-] \\ +k_{PZCOO}\gamma_{PZCOO}[PZCOO^-]\gamma_{PZ}[PZ] \\ +k_{PZCOO}\gamma_{PZCOO}^2[PZCOO^-]^2 \end{pmatrix} \cdot [CO_2] \qquad (5.40)$$

It is not obvious that this expression is second order with respect to the piperazine activities but the expression is analogous to the MEA expression which results in a second order MEA dependence. Ignoring activity coefficients, Equation 5.40 suggests that doubling PZ and $PZCOO^-$ concentrations would lead to a rate expression four times larger. Although the expression is more complex than the expression for MEA systems, the PZ rate expression is also near second order.

5.1.2.5 Liquid Phase Mass Transfer Coefficient of Reactants and Products, $k^0_{l,prod}$

The liquid phase mass transfer coefficient of the reactants and products, $k^0_{l,prod}$, in aqueous PZ was calculated identically to aqueous MEA.

Density data were obtained from regressing 2–12 m PZ density measurements at 20, 40, and 60˚C from Freeman (Rochelle, Chen et al. 2009a). PZ solution viscosity values were obtained by regressing 5–12 m PZ viscosity measurements at 25, 40, and 60˚C from Freeman (Rochelle, Sexton et al. 2008a). Details on the PZ density and viscosity regressions can be found in Appendix E.

5.1.2.6 Slope of the Equilibrium Line

The slope of the equilibrium line in Equation 5.1 results from converting a concentration-based mass transfer coefficient to a partial pressure basis. The slope can be difficult to determine accurately due to the CO_2 partial pressure sensitivity at high

loading or temperatures. Partial pressure curves are plotted on a log-based y-axis. This produces very high values for the slope. In cases where diffusion limits CO_2 mass transfer, a poor estimation of the slope of the equilibrium can drastically affect the expected mass transfer.

The equilibrium partial pressure can be uniformly predicted by using an empirical expression developed by Xu (Rochelle, Chen et al. 2009b) using literature data. The empirical relationship in Equation 5.41 is valid for PZ solutions between 40 and 190˚C. Equation 5.41 defines the partial pressure in Pascals with the temperature in Kelvin.

$$\ln P_{CO2} = 38.4 + (-102{,}000 J/mol)\cdot\frac{1}{RT} - 20.6\alpha + 13{,}200\frac{\alpha}{T} + 3.23\alpha^2 \quad (5.41)$$

Figure 5.9 shows the fit to previously referenced CO_2 partial pressure data (Figure 4.3).

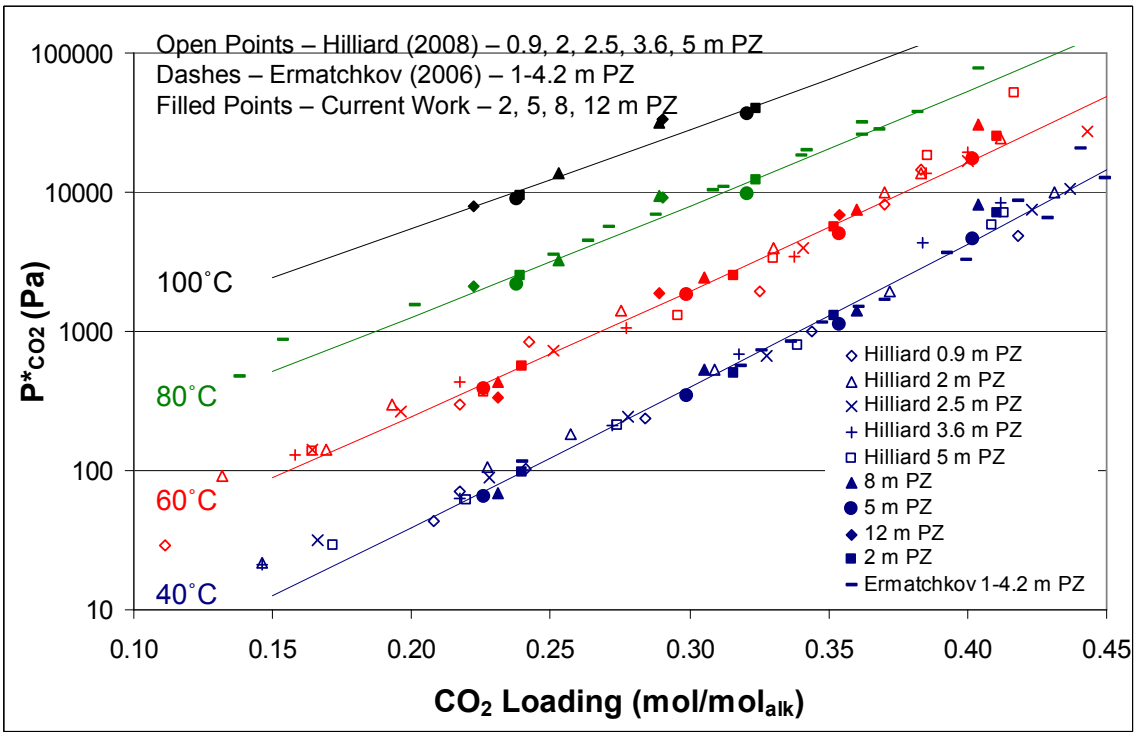

Figure 5.9: Equilibrium CO_2 partial pressure measurements in PZ solutions at 40, 60, 80, and 100˚C (Ermatchkov, Perez-Salado Kamps et al. 2006a; Hilliard 2008). Lines – Equation 5.41.

Taking the derivative of Equation 5.41 with respect to CO_2 loading yields a term that can be multiplied by the alkalinity concentration to obtain the slope of the equilibrium line in the required units. This analytical approach provides a consistent representation of the slope of the equilibrium line over a wide range of experimental conditions. The derivative of Equation 5.41 is an extremely long expression and is not reported.

5.1.2.7 Rate Constants

Literature reported rate constants for PZ are not as straightforward as MEA. Bishnoi (2000) reported a first order PZ rate expression leading to Equation 5.42.

$$k_{PZ} = 4.14 \cdot 10^7 \exp\left(-\frac{33{,}600}{RT}\right) \; m^3 mol^{-1} s^{-1} \tag{5.42}$$

Derks (2006) also reported a first order PZ rate expression. Derks suggests the rate constant expression in Equation 5.43.

$$k_{PZ} = 6.57 \cdot 10^7 \exp\left(-\frac{34{,}100}{RT}\right) \; m^3 mol^{-1} s^{-1} \tag{5.43}$$

Cullinane uses a rigorous kinetic model to interpret rate constants. Cullinane reports a second order piperazine dependence but reports a separate rate constant for each amine-base pairing. The rate expression used by Cullinane is similar to the expression (Equation 5.40) used in this work and is shown below.

$$r_{CO_2} = \sum_B k_{Am-B}[Am][B][CO_2] \tag{5.44}$$

The Cullinane model cannot be compared to the first order models by Derks (2006) and Bishnoi (2000). It is also difficult to compare to the current model because the current model is activity-based while the Cullinane model is concentration-based.

Cullinane reports an activation energy of 35 kJ/mol which is similar to the 33.6 and 34.1 kJ/mol reported by Bishnoi (2000) and Derks (2006). The current model also utilizes an activation energy of 35 kJ/mol.

The rate expression (Equation 5.39 or 5.40) has 2 pre-exponential constants. The value for k_{PZCOO} was assumed to be 70% of k_{PZ}. This 70% value was used by Cullinane for the reported $k_{PZ\text{-}PZ}$, $k_{PZ\text{-}PZCOO}$, $k_{PZCOO\text{-}PZ}$, and $k_{PZCOO\text{-}PZCOO}$ rate constants. The 70% ratio is based on Bronsted theory which relates the pKa of a base to its rate constant. With k_{PZCOO} ratioed to k_{PZ}, the k_{PZ} pre-exponential rate constant was adjusted until the expression in Equation 5.45 was minimized.

$$\sum\left(\frac{k'_{g,calc}-k'_{g,meas}}{k'_{g,meas}}\right)^2 \tag{5.45}$$

The values of k_{PZ} and k_{PZCOO} are $6.9\cdot10^7$ and $4.8\cdot10^7$ $m^6mol^{-2}s^{-1}$, respectively, in the final rate expression shown in Equation 5.46. This rate expression leads to the following expression for k_g' in aqueous PZ.

$$r_{CO2}=-\begin{pmatrix}k_{PZ}\gamma_{PZ}^2[PZ]^2+k_{PZ}\gamma_{PZ}[PZ]\gamma_{PZCOO}[PZCOO^-]\\+k_{PZCOO}\gamma_{PZCOO}[PZCOO^-]\gamma_{PZ}[PZ]\\+k_{PZCOO}\gamma_{PZCOO}^2[PZCOO^-]^2\end{pmatrix}\cdot[CO_2] \tag{5.46}$$

$$\frac{1}{k'_g}=\frac{\gamma_{CO2}^{0.5}H_{CO2,H2O}}{\sqrt{\begin{pmatrix}k_{PZ}\gamma_{PZ}^2[PZ]^2+k_{PZ}\gamma_{PZ}[PZ]\gamma_{PZCOO}[PZCOO^-]\\+k_{PZCOO}\gamma_{PZCOO}[PZCOO^-]\gamma_{PZ}[PZ]\\+k_{PZCOO}\gamma_{PZCOO}^2[PZCOO^-]^2\end{pmatrix}D_{CO2}}}+\frac{1}{k^o_{l,prod}}\left(\frac{\Delta P^*_{CO2}}{\Delta[CO_2]_T}\right) \tag{5.47}$$

5.2 SPREADSHEET MODEL ANALYSES

With the framework for the MEA and PZ spreadsheet models defined, each model can now be analyzed. This section looks at how each parameter in the modified k_g' expression is affected by changes in temperature, amine concentration, and CO_2 loading. Wetted wall column experiments have shown that neither temperature nor amine concentration changes significantly affect k_g' for MEA and often PZ systems (Figures 4.7 and 4.8). This section explains why k_g' is often independent of temperature and amine concentration.

This section also compares model results to applicable literature data and extrapolates the model to explore k_g' at 20˚C. The 20˚C case may be feasible in cold locations such as the North Sea.

The final form of the k_g' expressions can be written as Equation 5.48 and 5.49 for MEA and PZ, respectively. The first term in the k_g' expressions represents the pseudo first order condition. The second term represents the mass transfer resistance due to diffusion of reactants and products near the reaction interface.

$$\frac{1}{k_g^{'}} = \frac{\gamma_{CO2}^{0.5} H_{CO2,H2O}}{\sqrt{k\gamma_{MEA}^2 [MEA]^2 D_{CO2}}} + \frac{1}{k_{l,prod}^{o}} \left(\frac{\Delta P_{CO2}^{*}}{\Delta [CO_2]_T} \right) \tag{5.48}$$

$$\frac{1}{k_g^{'}} = \frac{\gamma_{CO2}^{0.5} H_{CO2,H2O}}{\sqrt{\begin{pmatrix} k_{PZ}\gamma_{PZ}^2 [PZ]^2 + k_{PZ}\gamma_{PZ}[PZ]\gamma_{PZCOO}[PZCOO^-] \\ + k_{PZCOO}\gamma_{PZCOO}[PZCOO^-]\gamma_{PZ}[PZ] \\ + k_{PZCOO}\gamma_{PZCOO}^2 [PZCOO^-]^2 \end{pmatrix} D_{CO2}}} + \frac{1}{k_{l,prod}^{o}} \left(\frac{\Delta P_{CO2}^{*}}{\Delta [CO_2]_T} \right) \tag{5.49}$$

5.2.1 Monoethanolamine

5.2.1.1 Parameter Determination

This section shows how each of the parameters in Equation 5.48 changes with temperature, amine concentration, and CO_2 loading.

The rate constant is independent of amine concentration and CO_2 loading. Figure 5.10 shows the temperature effect on the rate constant.

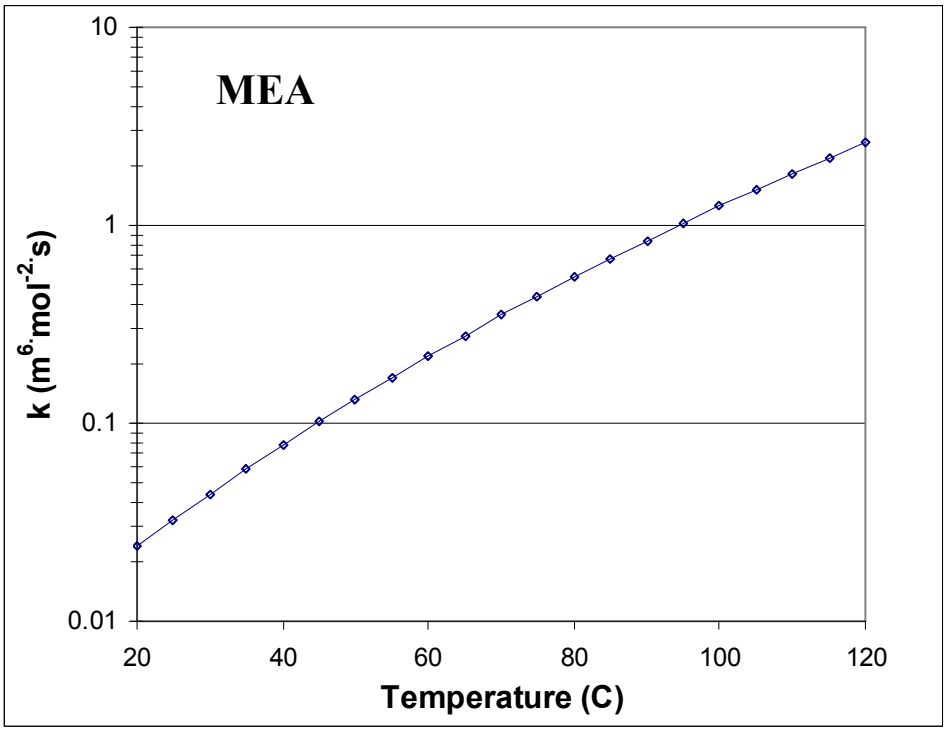

Figure 5.10: Calculated MEA rate constant from 20–120˚C

The MEA rate constant greatly increases with increasing temperature, two orders of magnitude from 20–120˚C. The rate constant has a 0.5 order effect on the pseudo first order term in Equation 5.48.

The MEA activity coefficient is also independent of amine concentration. Figure 5.11 shows how the MEA activity coefficient is affected by changes in temperature and CO_2 loading.

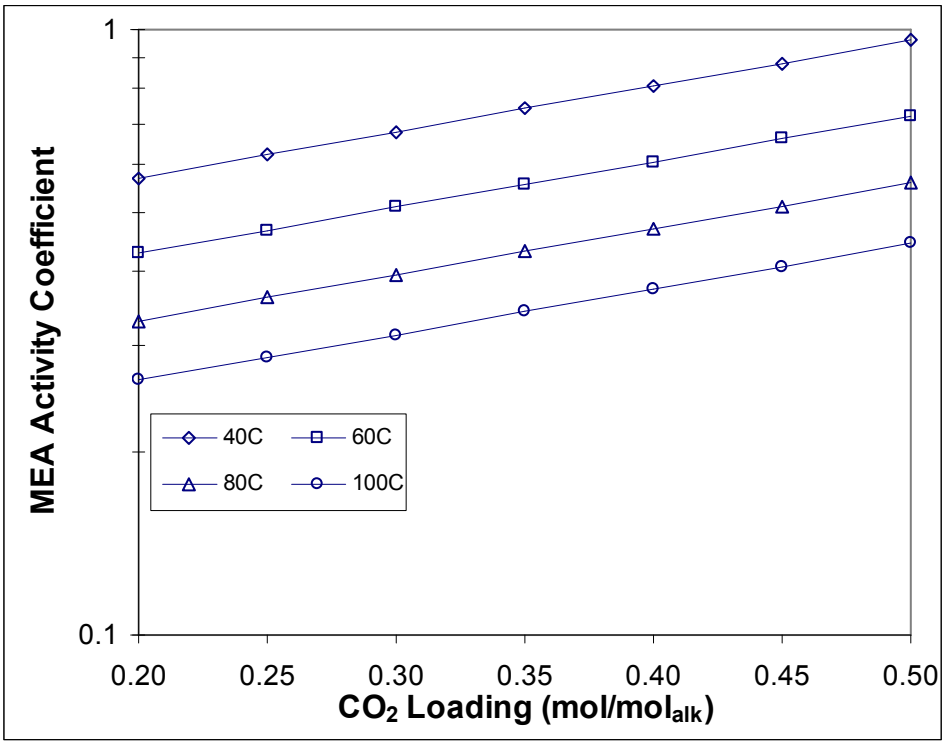

Figure 5.11: Calculated MEA activity coefficients from 40–100˚C at CO_2 loadings from 0.2 to 0.5

The MEA activity coefficient increases with CO_2 loading and decreases with temperature. Values vary about a factor of three over the plotted range. The pseudo first order portion of the k_g' expression has a first order dependence on the MEA activity coefficient.

The CO_2 activity coefficient is a function of CO_2 loading, temperature, and amine concentration. Figure 5.12 plots calculated data for 7 and 13 m MEA.

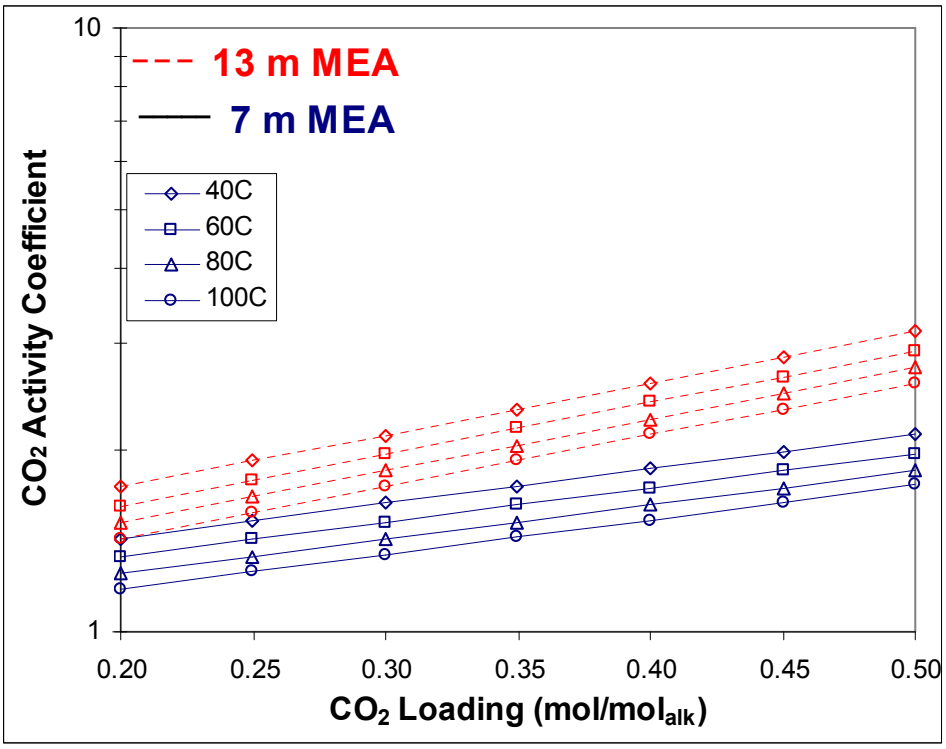

Figure 5.12: Calculated CO_2 activity coefficients from 40–100˚C at CO_2 loadings from 0.2 to 0.5 in 7 and 13 m MEA

The activity coefficient of CO_2 increases with MEA concentration and CO_2 loading and decreases with increasing temperature. CO_2 activity coefficient values vary about a factor of two over the plotted range. The CO_2 activity coefficient has a –0.5 order effect on the pseudo first order k_g' expression.

The free MEA concentration is a strong function of CO_2 loading and amine concentration. It is also a slight function of temperature due to changes in speciation. Figure 5.13 plots the data for 7 and 13 m MEA.

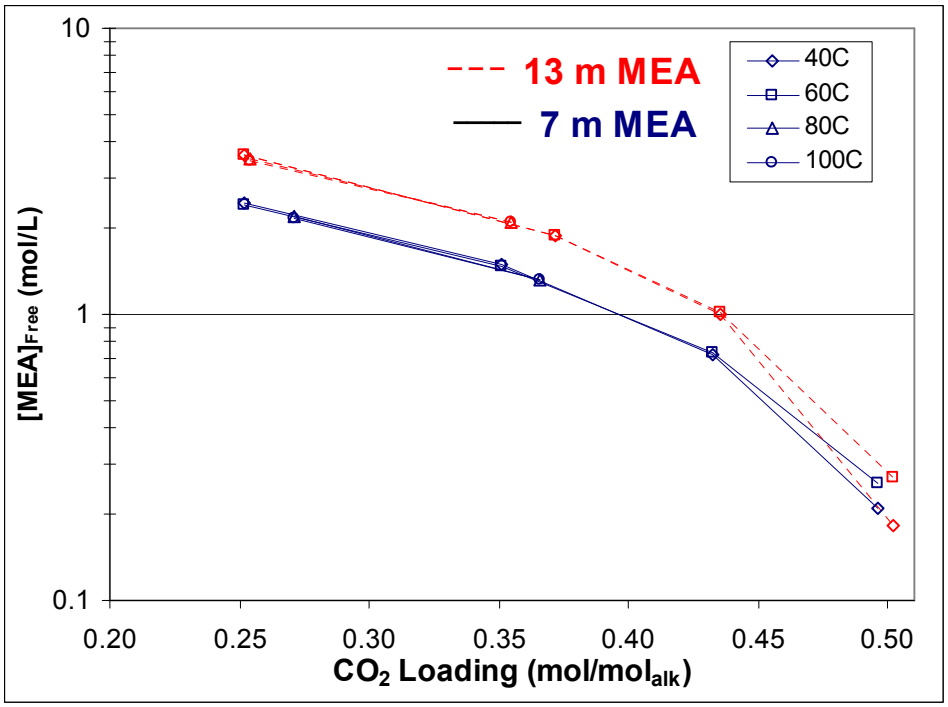

Figure 5.13: Free MEA concentration from 40–100˚C for 7 and 13 m MEA (Hilliard 2008)

Figure 5.13 shows a minor effect of temperature on free MEA. The free amine concentration decreases with both increasing CO_2 loading and decreasing total MEA concentration. The change with CO_2 loading is particularly important since the free MEA concentration can change more than one order of magnitude over the lean to rich CO_2 loading range. The free MEA concentration has a first order effect on the pseudo first order portion of the k_g' expression in Equation 5.48.

The diffusion coefficient of CO_2 is affected by CO_2 loading, temperature, and amine concentration since each of these parameters affects viscosity. Figure 5.14 shows how the calculation of the diffusion coefficient of CO_2 is affected by changes in each of the three parameters.

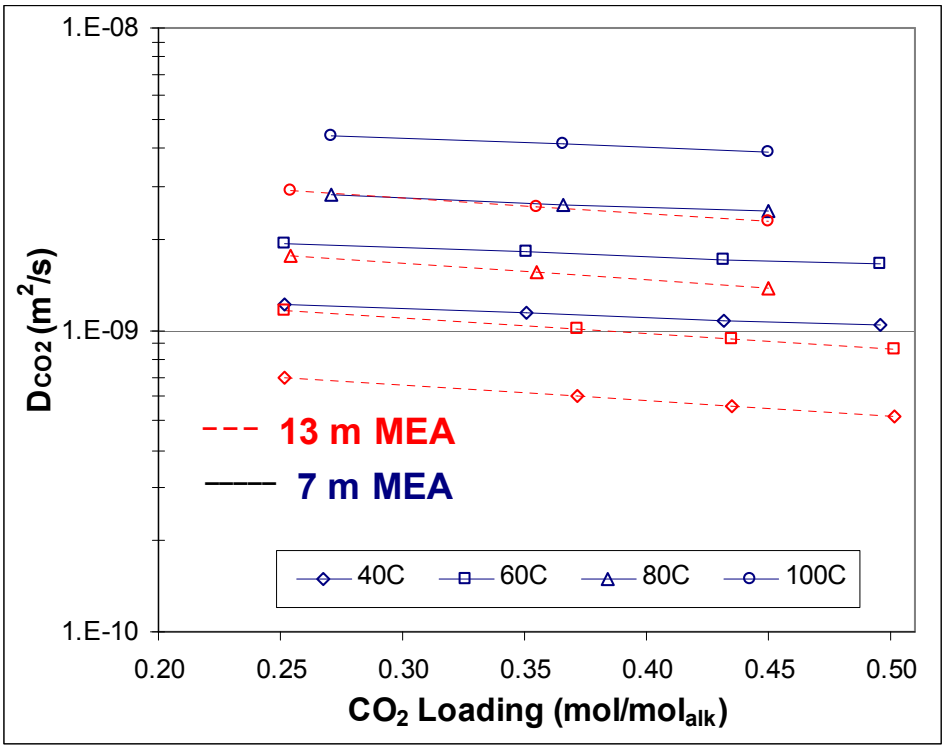

Figure 5.14: Calculated diffusion coefficient of CO_2 for 40–100˚C at 0.2–0.5 CO_2 loadings in 7 and 13 m MEA

CO_2 loading has a minor effect on the diffusion coefficient of CO_2. Both amine concentration and temperature strongly affect the D_{CO2}. The data shown in Figure 5.14 exhibit a full order of magnitude difference between the lowest and highest D_{CO2} values. The pseudo first order portion of the k_g' expression has a 0.5 order dependence on the diffusion coefficient of CO_2

5.2.1.2 Parameter Significance

The previous section has shown how each of the parameters in Equation 5.48 varies with changes in CO_2 loading, temperature, and MEA concentration. However, many of the parameters have different orders in the k_g' expression. This section attempts to compare the significance of each parameter by showing changes in each parameter at

common conditions. The correct order is implemented for each parameter. The order of the parameters is only significant to the pseudo first order portion of Equation 5.48. If diffusion becomes a significant resistance at a given condition, the pseudo first order part of Equation 5.48 becomes less meaningful.

Figures 5.15–5.17 are plotted against CO_2 loading for some extreme conditions: 7 and 13 m MEA. For each parameter the correct order in Equation 5.48 is incorporated. Since Figures 5.15–5.17 each have stated temperatures, only the free MEA concentration, diffusion coefficient of CO_2, and the activity coefficients vary. The values of the rate constant and the Henry's solubility in water would remain constant in each graph.

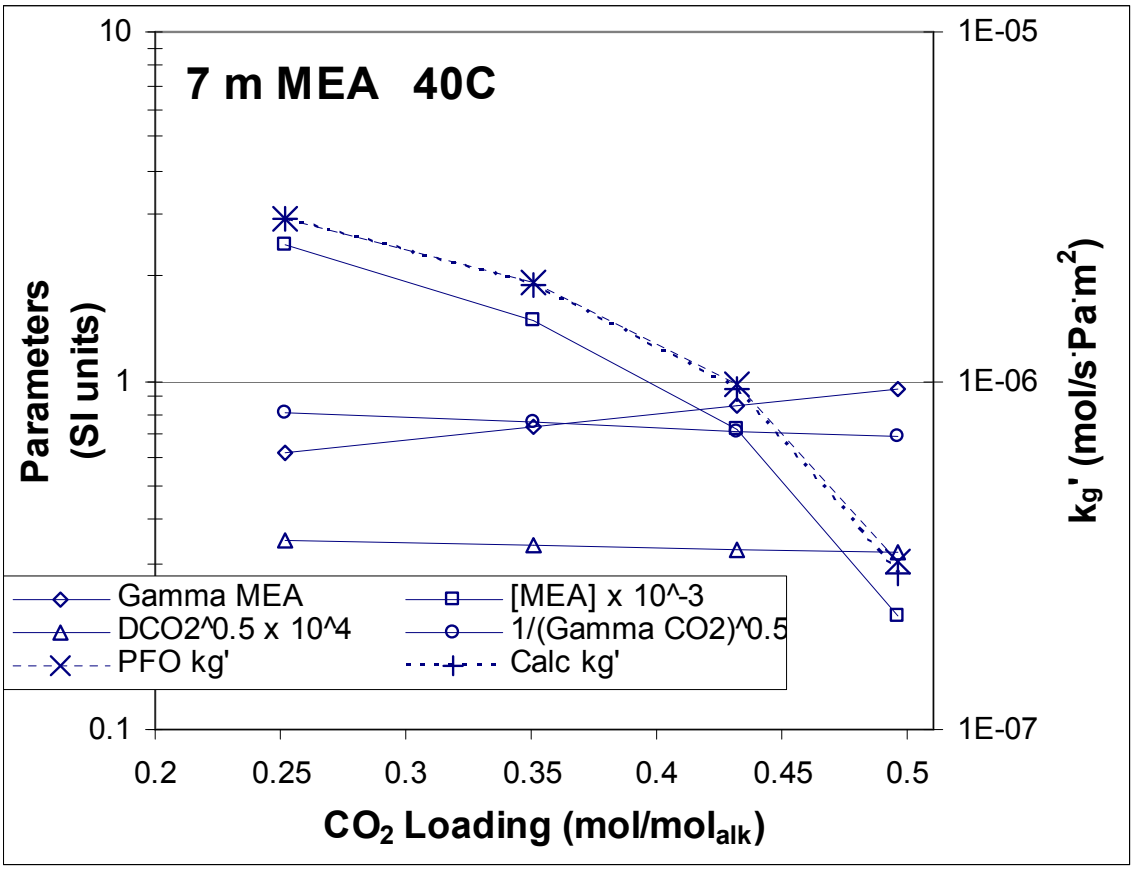

Figure 5.15: Parameter significance against CO_2 loading for 7 m MEA at 40˚C

Figure 5.15 shows that the free MEA concentration curve has nearly the same shape as the calculated k_g' curves. The mass transfer rate is almost completely controlled by the free amine concentration for 7 m MEA at 40˚C. Each of the other parameters is nearly constant over the relevant CO_2 loading range. At 40˚C the pseudo first order k_g' and the calculated k_g' are similar. This is expected because diffusion resistances are small at low temperatures due to the small slope of the equilibrium line.

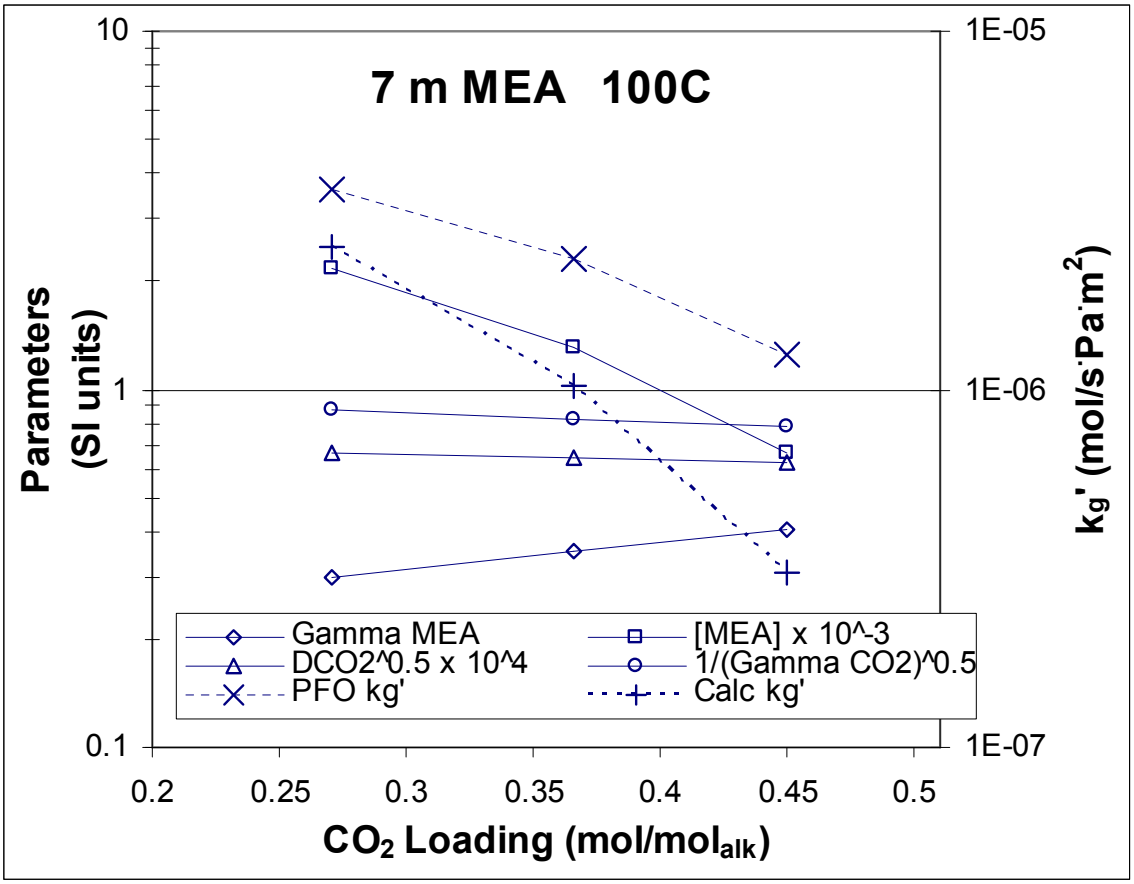

Figure 5.16: Parameter significance against CO_2 loading for 7 m MEA at 100˚C

Figure 5.16 again shows the parameter significances for 7 m MEA but this time at 100˚C. The diffusion coefficient and activity coefficient of CO_2 contributions both decrease slightly with increased CO_2 loading. At 100˚C, the activity coefficient of MEA

has a stronger effect than at 40˚C. Changes in k_g' result primarily from the change in free MEA. The pseudo first order k_g' and the calculated k_g' vary significantly at low loading and even more at higher loading. At 100˚C, MEA solutions encounter significant diffusion resistances that limit CO_2 mass transfer.

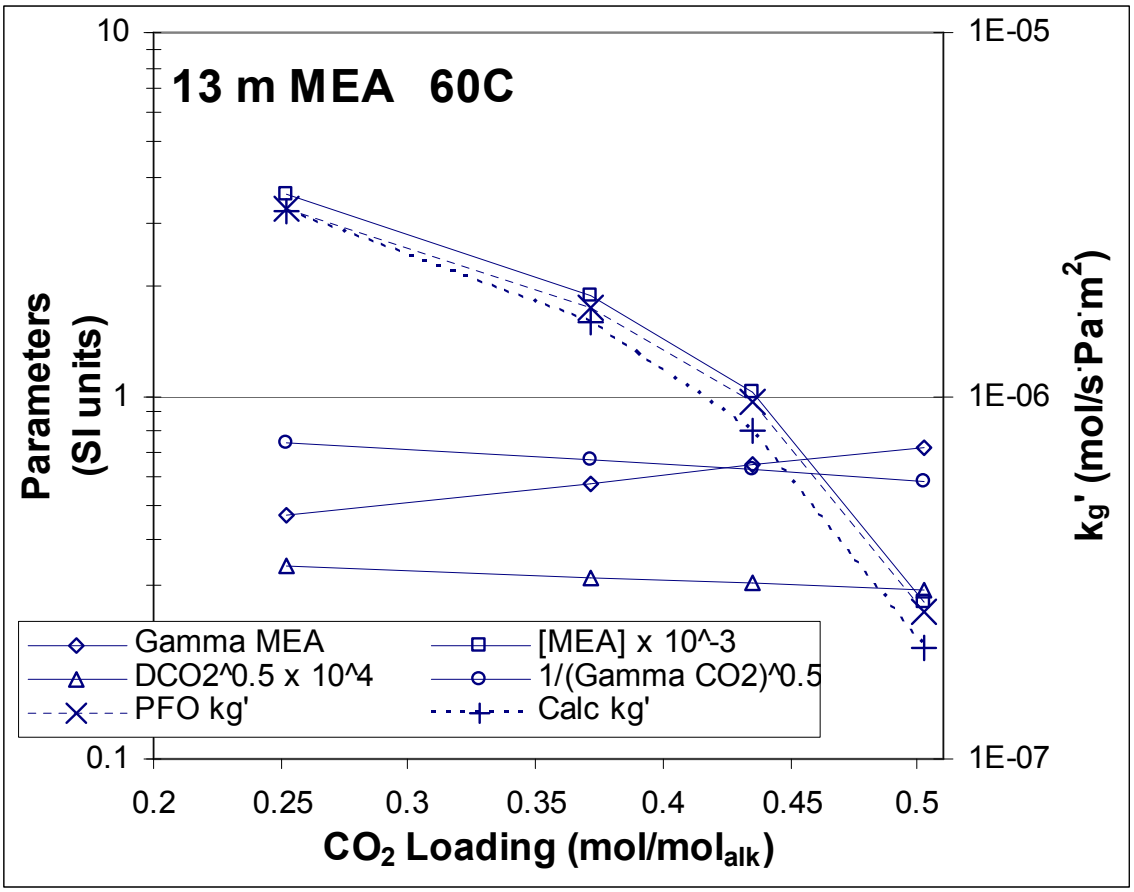

Figure 5.17: Parameter significance against CO_2 loading for 13 m MEA at 60˚C

In 13 m MEA at 60˚C, both the activity and diffusion coefficients of CO_2 show a decrease, essentially canceling the increase of the MEA activity coefficient. Again, changes in the free amine concentration dominate changes in k_g'. At 60˚C, there is a small diffusion resistance in the system. This resistance causes the pseudo first order k_g' and the calculated k_g' to diverge slightly at the higher CO_2 loading conditions.

Figure 5.18 looks directly at the effect of the parameters as a function of temperature. An intermediate condition of 9 m MEA at 0.3 CO_2 loading was selected for this analysis.

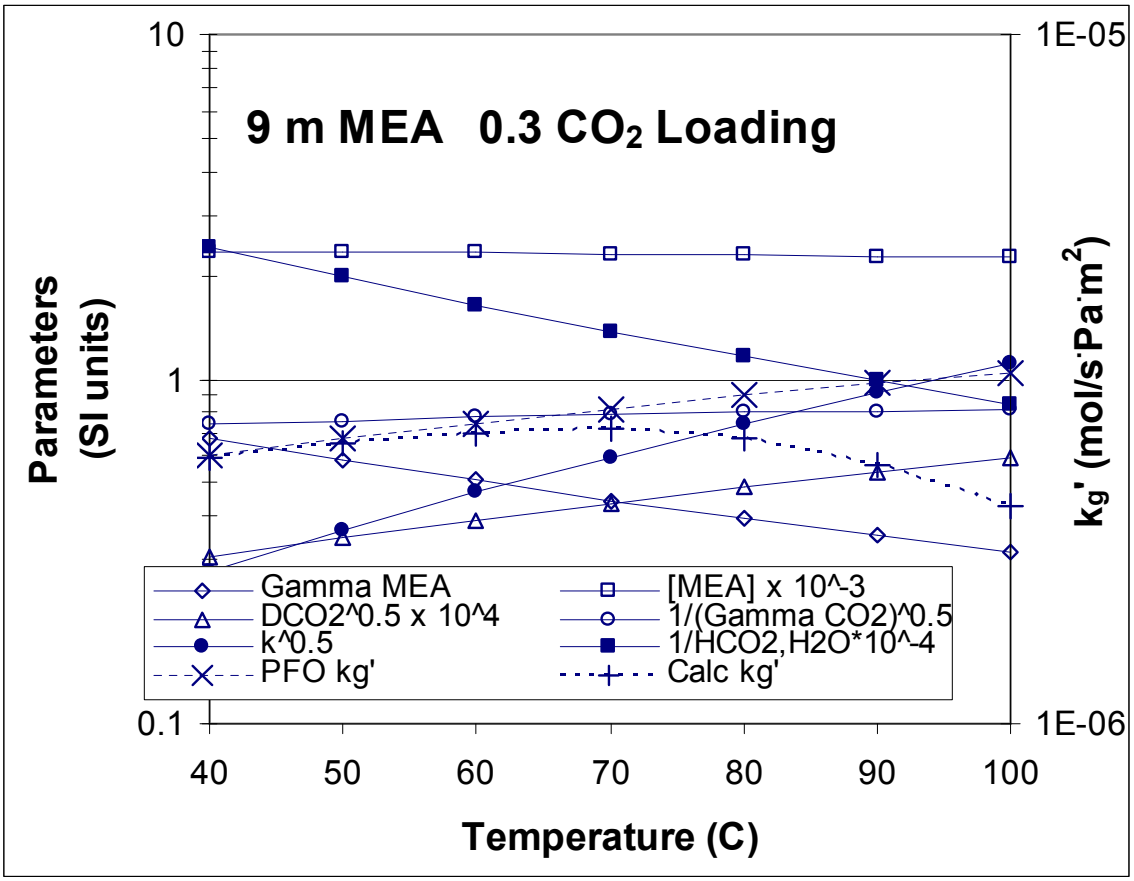

Figure 5.18: Parameter significance against temperature for 9 m MEA at 0.3 CO_2 loading

In agreement with the experimental data, Figure 5.18 shows that k_g' is mostly independent of temperature in MEA solutions. However, the parameters which comprise the k_g' expression have strong temperature dependences. The Henry's solubility in water, the rate constant, the activity coefficient of MEA and the diffusion coefficient of CO_2 are all strongly affected by temperature. However, all these increasing and decreasing effects mostly cancel each other. The pseudo first order k_g' shows about a 50% increase over the

temperature range but that increase is negated by the increased diffusion resistance at higher temperature. The calculated k_g' is relatively but does have a maximum at intermediate temperatures. A critical look at Figure 4.7 shows that this phenomenon was seen for MEA experiments in the wetted wall column.

Figure 5.19 shows the significance of each parameter with changes in amine concentration. 60˚C solutions with a 0.4 CO_2 loading were selected for this analysis.

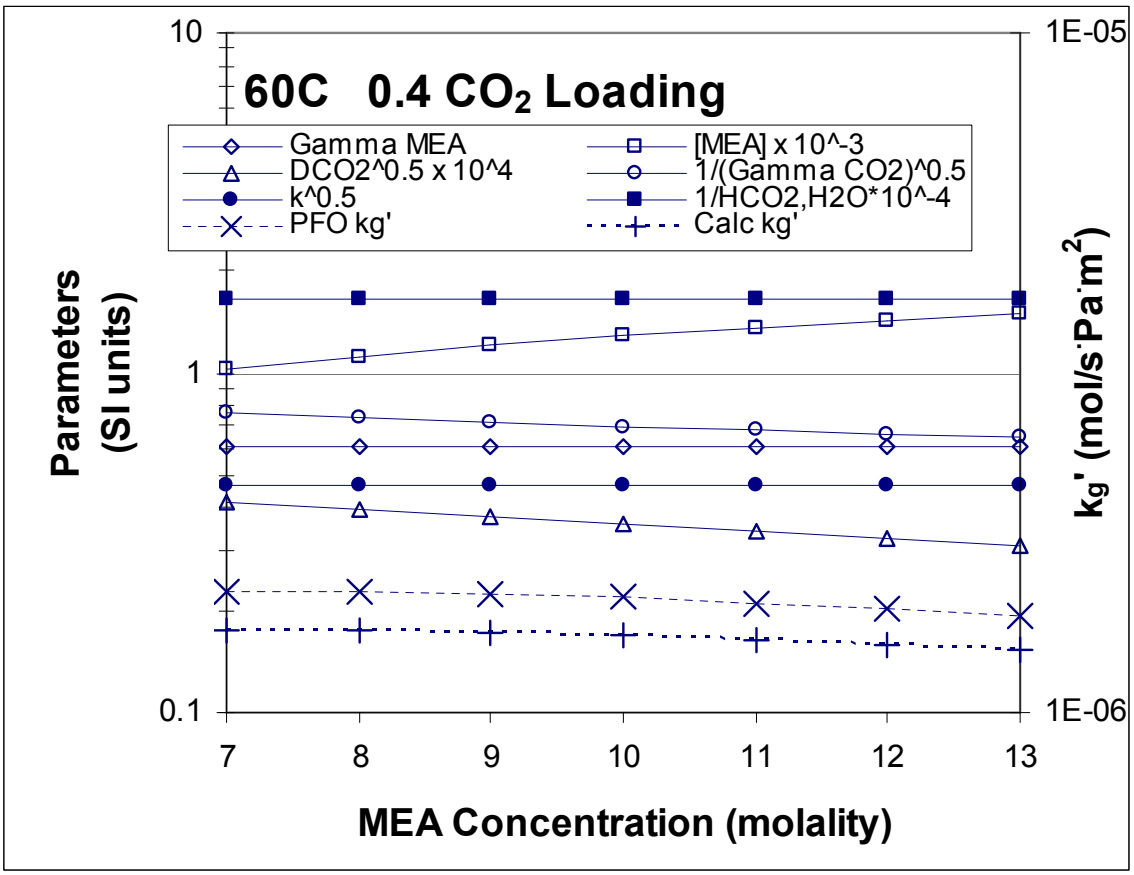

Figure 5.19: Parameter significance against MEA concentration for 60˚C and 0.4 CO_2 loading

Figure 5.19 explains exactly why wetted wall column experiments have shown that k_g' is independent of MEA concentration. With changes in MEA concentration,

most of the parameters are relatively constant in their effect on k_g'. Only the diffusion coefficient of CO_2, the activity coefficient of CO_2, and the free amine concentration vary significantly and those dependences essentially cancel each other. Figure 5.19 also shows an equal spacing between the pseudo first order and calculated k_g' values over the entire MEA concentration range. This suggests that the ratio of the kinetic and diffusion resistances does not change with MEA concentration.

Figure 5.20 shows the importance of the diffusion resistance in 7 and 13 m MEA over the range of experimental temperatures.

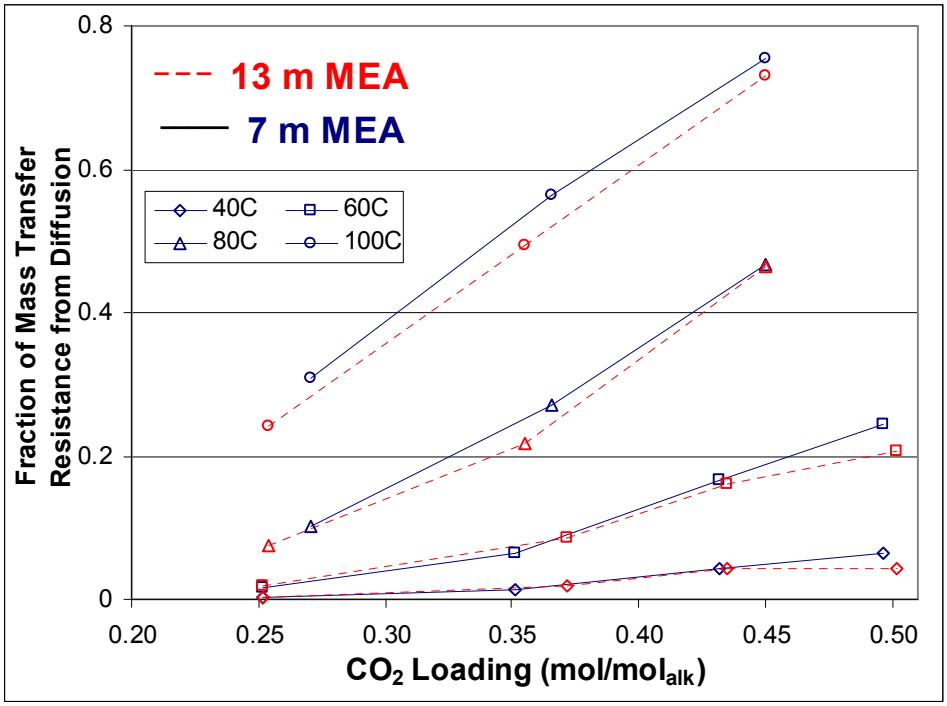

Figure 5.20: Fraction of mass transfer resistance from diffusion for 40–100˚C, 7 and 13 m MEA

Figure 5.20 shows more clearly that the amine concentration does not affect the ratio of the resistances due to kinetics and diffusion in Equation 5.48. Figure 5.19 shows that the pseudo first order k_g' does not change significantly with MEA concentration.

This implies that the value of the diffusion resistance does not change very much either with amine concentration. At higher MEA concentration, the physical liquid film mass transfer coefficient, k_l^o, decreases due to viscosity changes. However, the slope of the equilibrium line also has a concentration term since it must be defined in Pa/(mol/m^3). The increased concentration decreases the slope of the equilibrium line. The diffusion term in Equation 5.48 divides k_l^o by the slope and that term is mostly unchanged with changes in total MEA concentration.

At high temperature, particularly 100˚C, diffusion limits mass transfer even at moderate CO_2 loadings. This is mainly due to a drastic increase in the slope of the equilibrium line in Equation 5.48.

5.2.1.3 Error Analysis

This analysis seeks to show that systematic error has been removed from the model with respect to changing temperature, CO_2 loading, and MEA concentration. The lack of systematic error provides a better confidence in the estimation of the parameters which comprise the k_g' expression, Equation 5.48.

Figure 5.21 shows an overall graph of all the wetted wall column data: 7–13 m MEA, 40–100˚C, 0.23–0.50 CO_2 loading. A parity plot is used to compare measured wetted wall column k_g' values to the calculated k_g' from Equation 5.48.

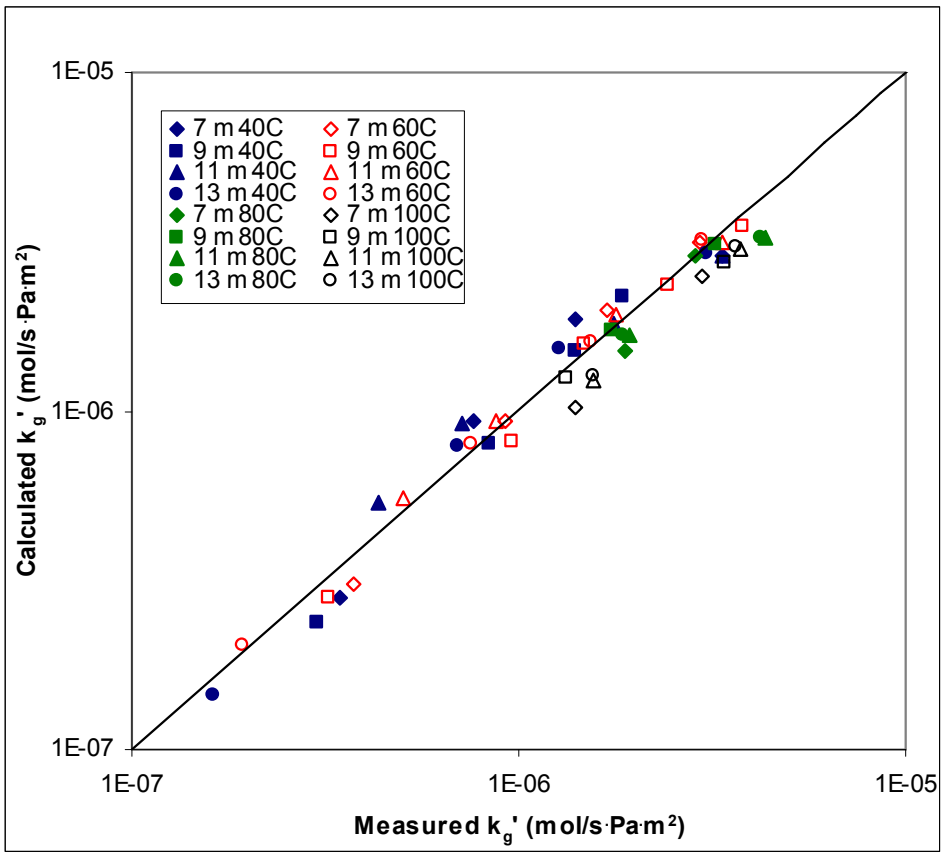

Figure 5.21: Parity plot comparing experimentally measured MEA k_g' values to k_g' values calculated from Equation 5.48

Figure 5.21 shows that k_g' values vary about a factor of 30 from the lowest loading to the highest loading conditions. A brief view shows that all of the points fall relatively close to the parity line. Equation 5.48 represents the measured wetted wall column k_g' in aqueous MEA with an average error of 13%.

Figure 5.22 includes all the data in Figure 5.21 but is plotted differently to show systematic trends with CO_2 loading.

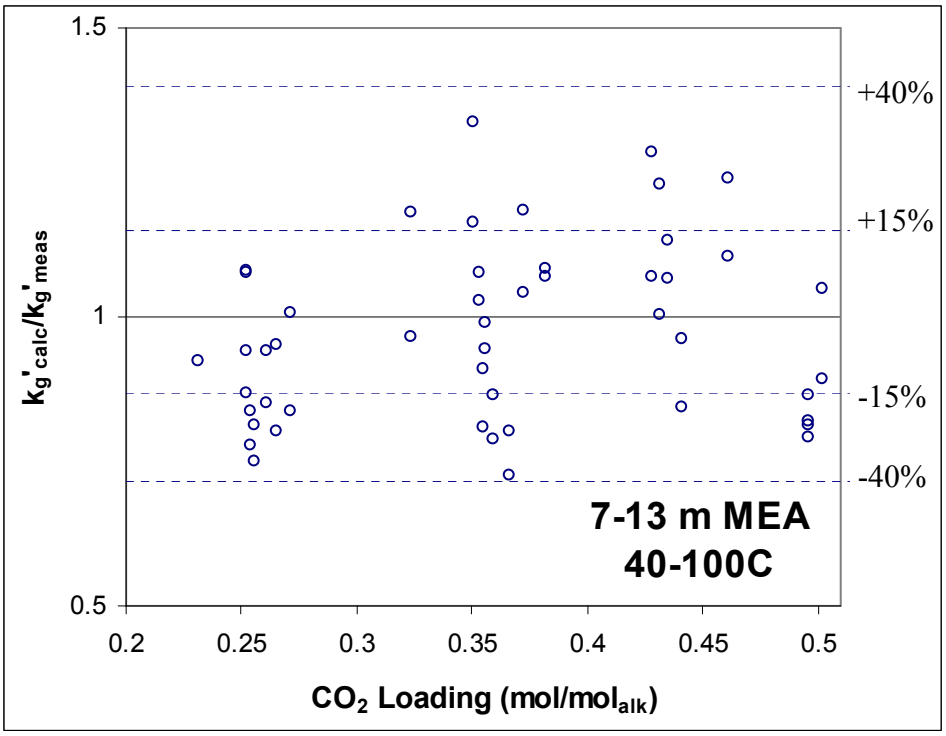

Figure 5.22: Calculated/measured k_g' against CO_2 loading for all MEA wetted wall column conditions

Figure 5.22 has dotted lines to show ±15 and 40% error in the estimation of k_g'. All of the data fall within 40% of the measured k_g' values. This is impressive, since k_g' values vary about a factor of 30. Many of the parameters comprising the k_g' expression change considerably with changes in temperature, MEA concentration, and CO_2 loading. Overall, there does not seem to be a systematic trend with changes in CO_2 loading since the points are centered around the y=1 line.

Figure 5.23 plots all the experimental data against temperature.

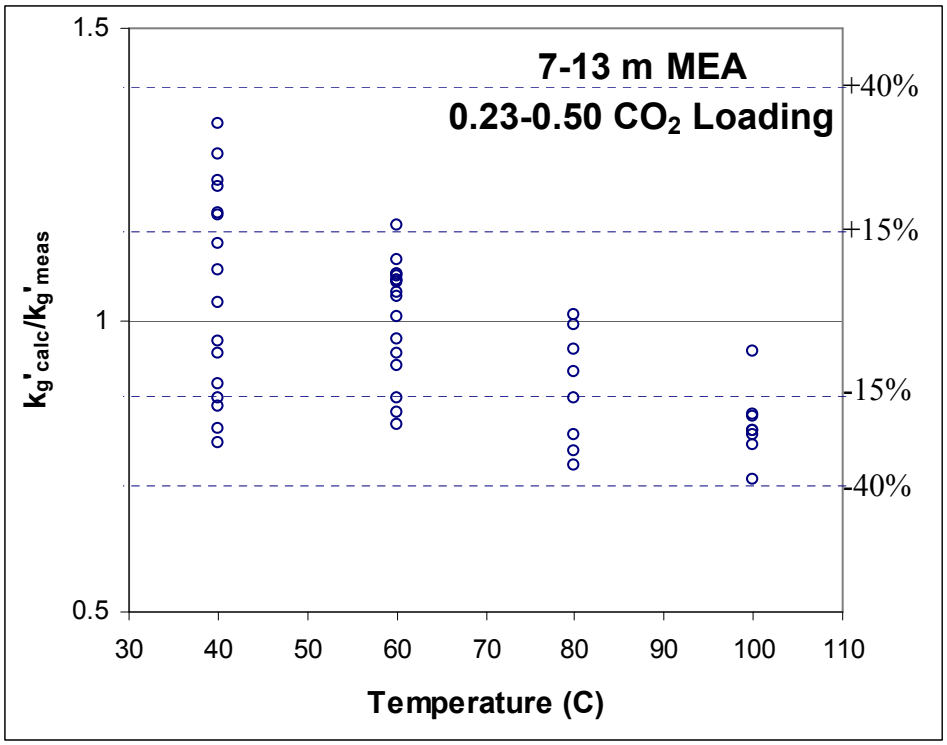

Figure 5.23: Calculated/measured k_g' against temperature for all MEA wetted wall column conditions

Figure 5.23 shows a systematic error with increasing temperature. According to Figure 5.18, many of the parameters comprising k_g' vary considerably with changes in temperature. The slope of the equilibrium line is also extremely sensitive to temperature. Considering how sensitive Equation 5.48 is to changes in temperature, the systematic error shown in Figure 5.23 is relatively small. The systematic temperature error is about 4 kJ/mol. This can be compared to the MEA activation energy of 45 kJ/mol (Equation 5.27). However, the activation energy should not be adjusted to remove the error since the activation energy is known with more certainty than the other temperature dependent terms in the k_g' expression. This systematic error with temperature has not been removed from the model.

Figure 5.24 plots all the experimental data with MEA concentration on the x-axis.

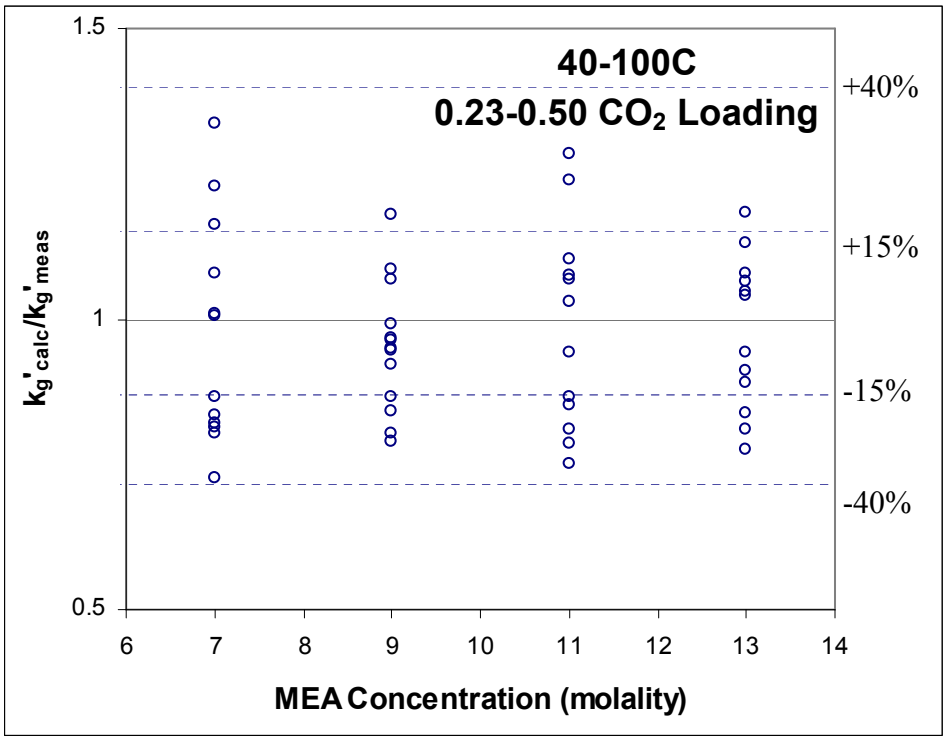

Figure 5.24: Calculated/measured k_g' against MEA concentration for all MEA wetted wall column conditions

Figure 5.24 shows no systematic error in the calculated k_g' values with MEA concentration. Figure 5.19 showed that only a few parameters had mild dependences with changes in amine concentration.

Figures 5.22–5.24 show that systematic error with respect to CO_2 loading, temperature, and MEA concentration has mostly been removed from the model. The absence of significant systematic error increases confidence both in the model and in the determination of each parameter in the k_g' expression.

5.2.2 Piperazine

5.2.2.1 Parameter Determination

This section shows how each of the parameters in Equation 5.49 changes with temperature, PZ concentration, and CO_2 loading.

The PZ and $PZCOO^-$ rate constants are independent of amine concentration, and CO_2 loading. Figure 5.25 shows the temperature effect on the rate constant.

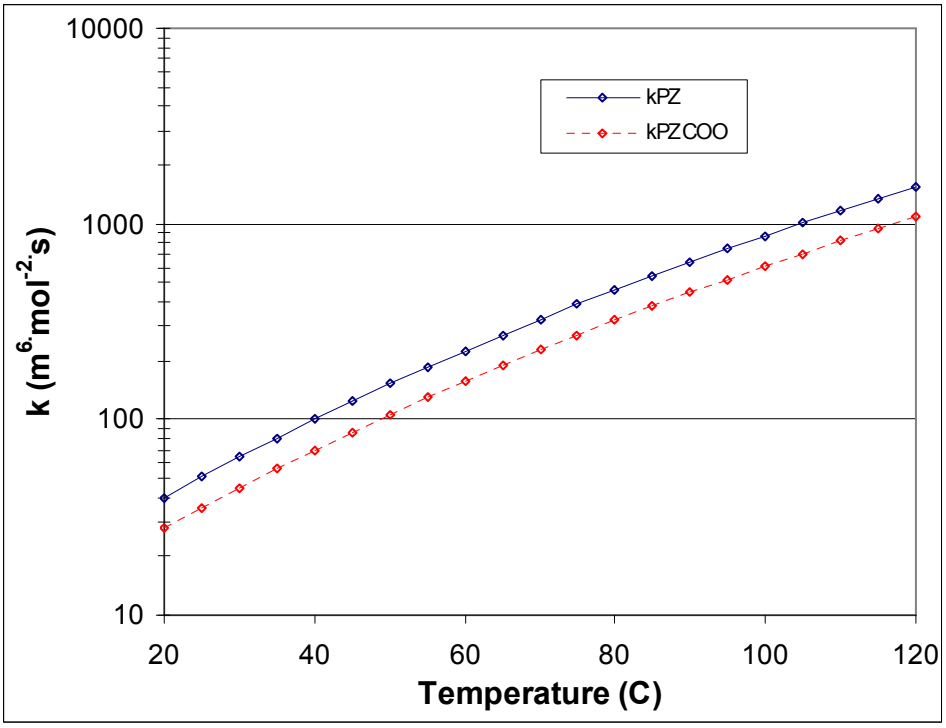

Figure 5.25: Calculated PZ and $PZCOO^-$ rate constants from 20–120˚C

The PZ and $PZCOO^-$ rate constants greatly increase with increasing temperature, about 1.5 orders of magnitude from 20–120˚C. The $PZCOO^-$ rate constant has been set at 70% of the PZ rate constant based on work by Cullinane (2005). The rate constants are approximately to the 0.5 power in the pseudo first order portion of Equation 4.49. Due to

the complexity of the equation, the dependence cannot be explicitly stated since it will change with speciation.

The PZ activity coefficient is independent of CO_2 loading. Figure 5.26 shows how the PZ activity coefficient is affected by changes in temperature and total PZ concentration. The PZ carbamate activity coefficient is essentially independent of temperature, CO_2 loading, and amine concentration. This model defines it as a constant, 0.038. PZ and PZ carbamate activity coefficients were obtained using values from the Hilliard model (2008).

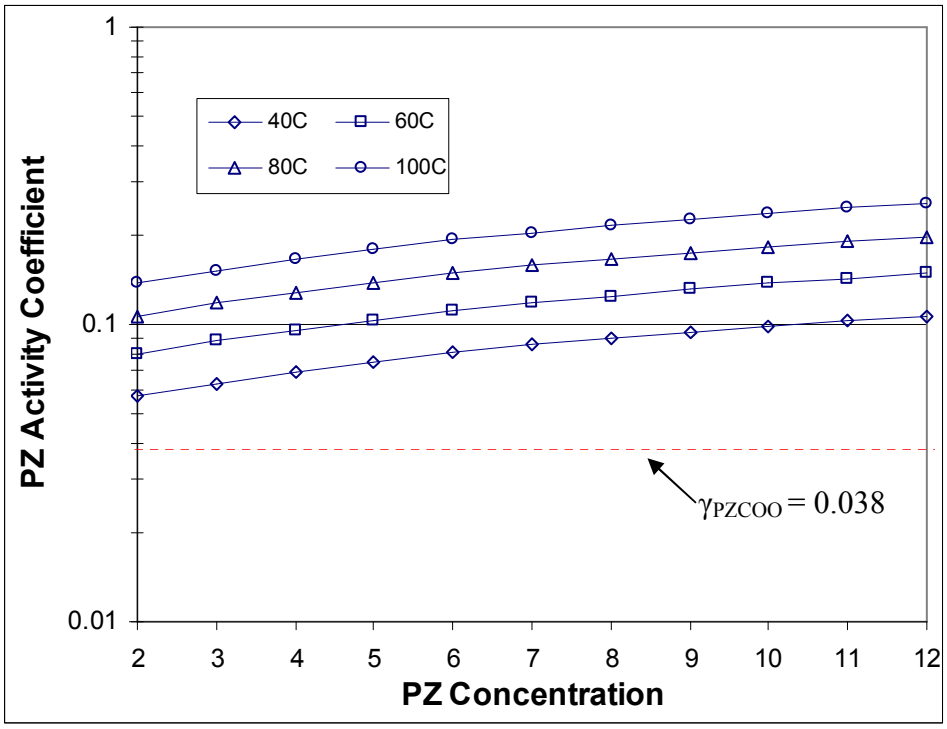

Figure 5.26: PZ activity coefficients for 2–12 m PZ from 40–100˚C (Hilliard 2008)

The PZ activity coefficient increases with total piperazine concentration and temperature. Values vary about a factor of 2 over the plotted range. Like the rate

constants, Equation 5.49 does not define an explicit order for the PZ activity coefficient, but is approximately first order in the pseudo first order expression.

The CO_2 activity coefficient is a function of CO_2 loading, temperature, and amine concentration. Figure 5.27 plots the calculations for 2 and 12 m PZ.

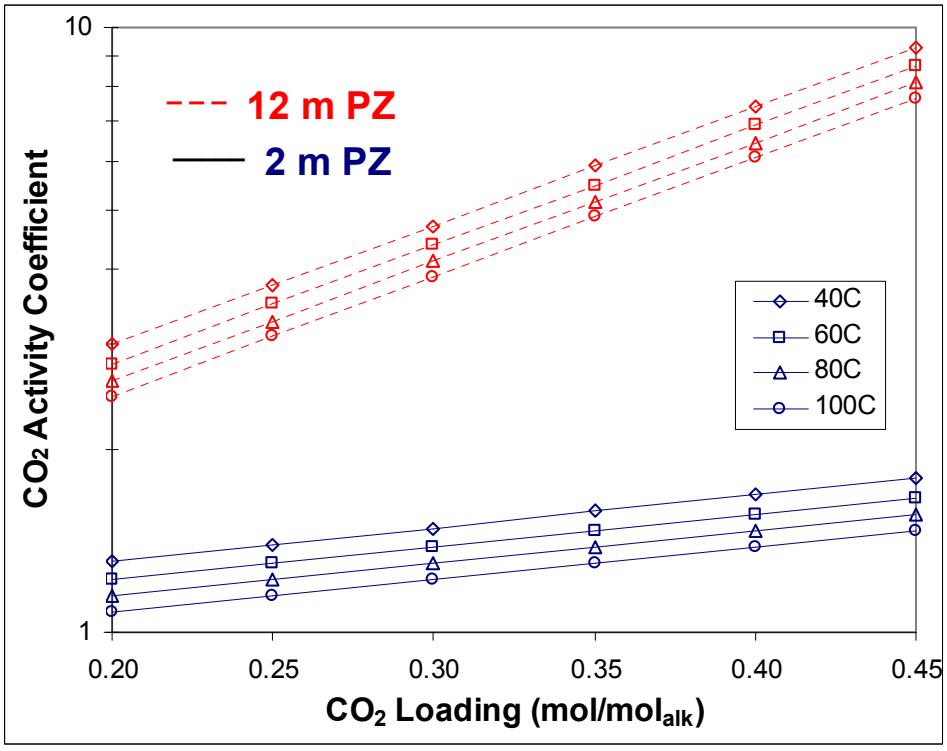

Figure 5.27: Calculated CO_2 activity coefficients at 40–100˚C with 0.2 to 0.45 CO_2 loadings in 2 and 12 m PZ

The activity coefficient of CO_2 increases with PZ concentration and CO_2 loading and decreases with increasing temperature. CO_2 activity coefficient values vary about a factor of 10 over the plotted range. The CO_2 activity coefficient has a –0.5 order effect on the pseudo first order portion of the k_g' expression.

The free PZ and $PZCOO^-$ concentrations are a function of CO_2 loading and amine concentration. They are also a function of temperature since the solution speciation

changes with temperature. Figure 5.28 plots the free PZ concentrations for 2 and 8 m PZ. Figure 5.29 plots the free $PZCOO^-$ concentrations for 2 and 8 m PZ. These values were obtained from the Hilliard model (2008).

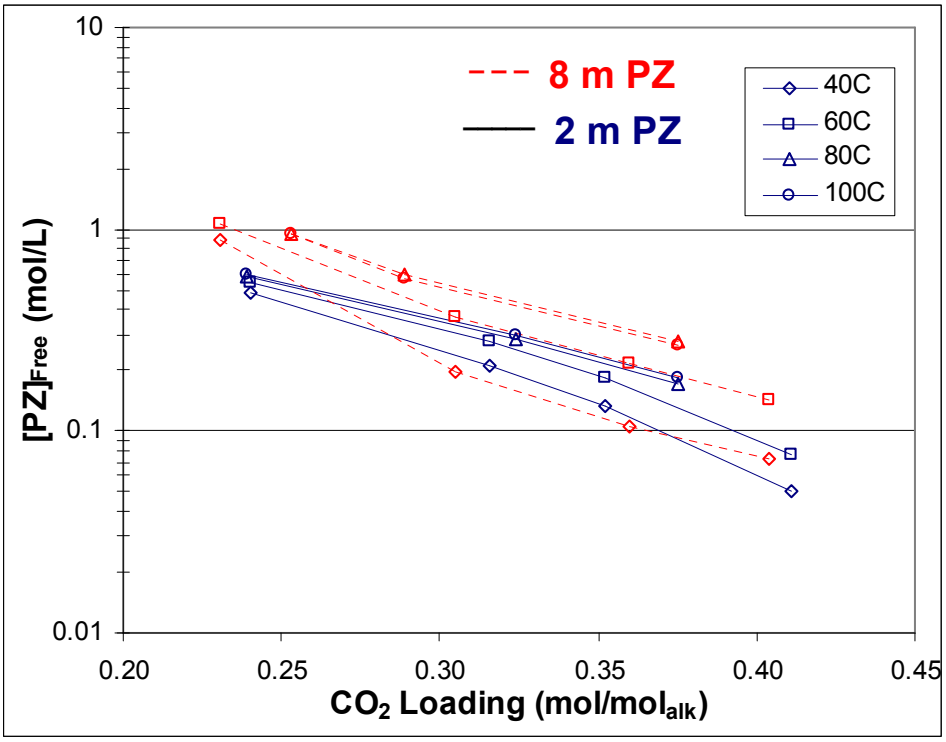

Figure 5.28: Free PZ concentration from 40–100˚C for 2 and 8 m PZ (Hilliard 2008)

Oddly, free piperazine concentrations for 2 m and 8 m PZ are almost equivalent at constant CO_2 loading. This suggests that the total amine concentration plays a large part in the speciation of PZ solutions. Overall, the free PZ concentration varies about a factor of 10 from lean to rich conditions.

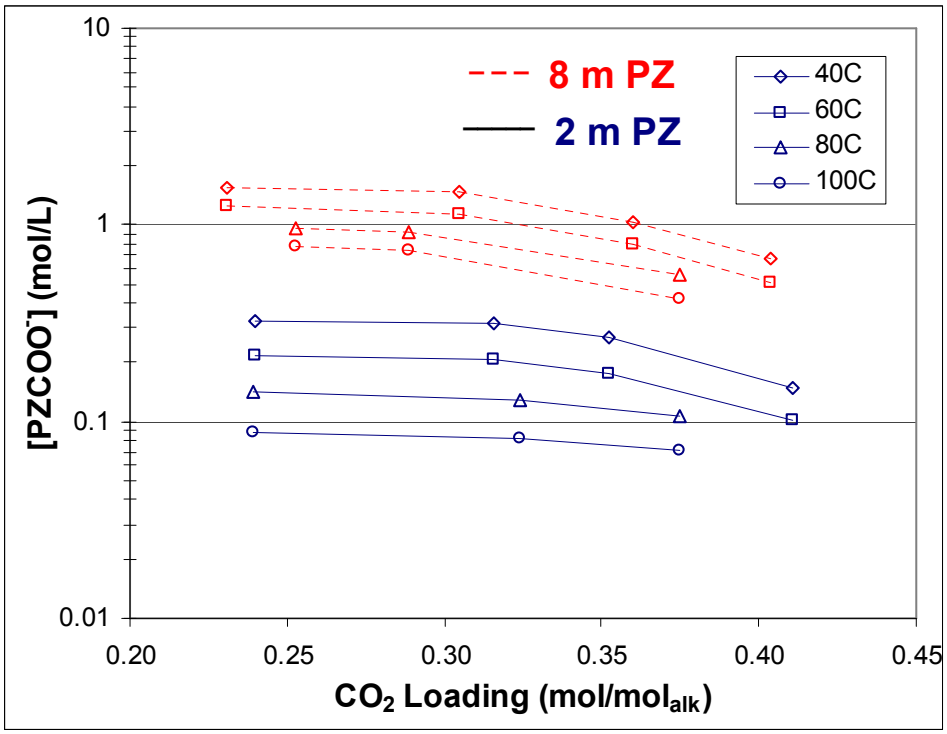

Figure 5.29: $PZCOO^-$ concentration from 40–100˚C for 2 and 8 m PZ (Hilliard 2008)

Figure 5.29 shows a large difference in the $PZCOO^-$ concentrations for 2 and 8 m PZ. This was expected since free PZ concentrations are fairly similar in the Hilliard model. The piperazine material balance must be satisfied. The free PZ concentration is also a significant function of temperature, especially for the 2 m solution. Again, the order of the free PZ and $PZCOO^-$ concentrations in Equation 5.49 is not explicit. They are approximately first order since concentrations are squared under the square root.

Figure 5.30 shows the total free amine concentrations in 2 and 8 m PZ.

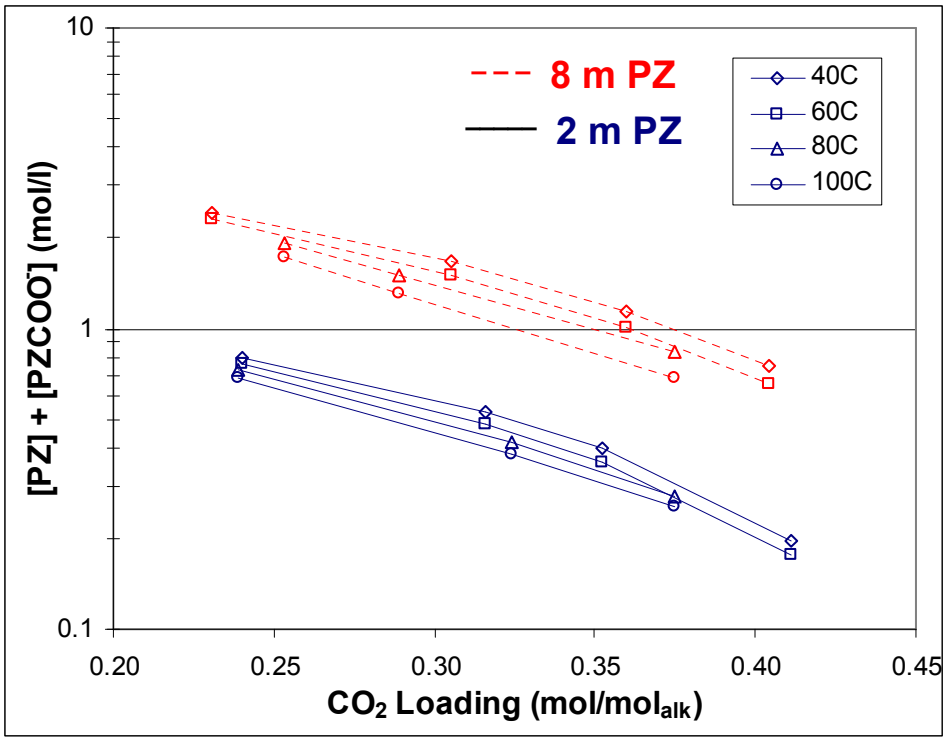

Figure 5.30: Free amine concentrations in 2 and 8 m PZ at 40–100˚C (Hilliard 2008)

The diffusion coefficient of CO_2 is affected by CO_2 loading, temperature, and amine concentration since each of these parameters affects viscosity. Figure 5.31 shows how the calculation of the diffusion coefficient of CO_2 is affected by changes in each of the three parameters.

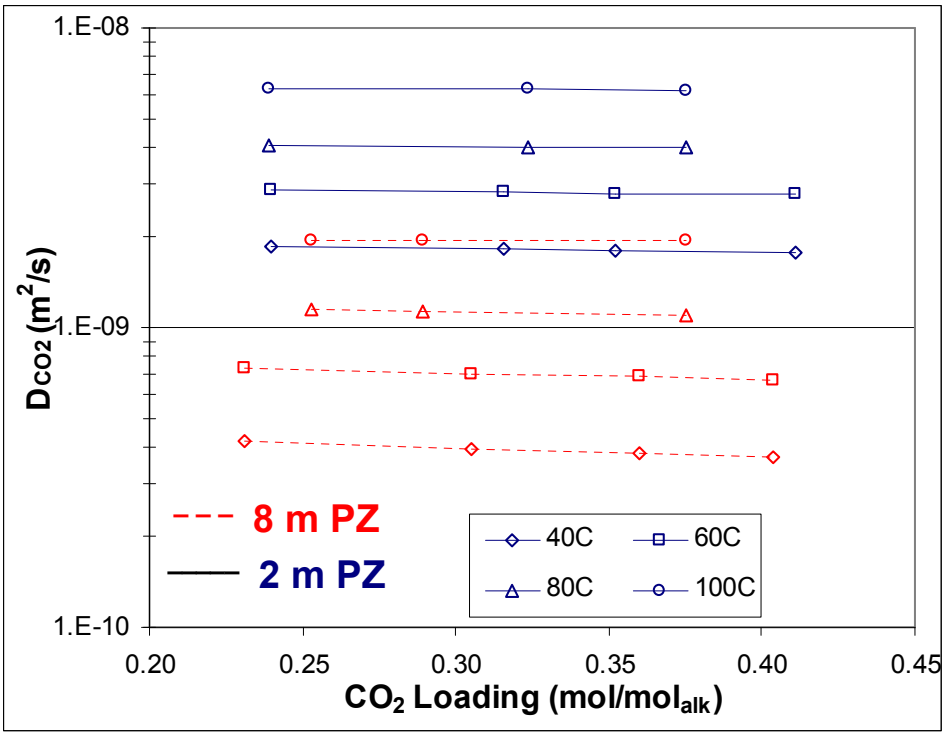

Figure 5.31: Calculated diffusion coefficient of CO_2 from 40–100˚C in 2 and 8 m PZ

CO_2 loading has a fairly minor effect on the diffusion coefficient of CO_2. Both amine concentration and temperature have strong effects on D_{CO2}. Higher amine concentrations and lower temperatures increase viscosity and thus lower diffusion coefficients. The data shown in Figure 5.31 exhibit more than a full order of magnitude difference between the lowest and highest D_{CO2} values. The diffusion coefficient of CO_2 has a 0.5 order effect on the pseudo first order portion of the k_g' expression, Equation 5.49.

5.2.2.2 Parameter Significance

The previous section has shown how each of the parameters in Equation 5.49 vary with changes in CO_2 loading, temperature, and MEA concentration. However, many of the parameters have different powers in the k_g' expression. Some of these powers must

be approximated due to the form of Equation 5.49. This section attempts to compare the significance of each parameter by showing the changes in each parameter at common conditions. Note that the order of the parameters is only significant to the pseudo first order portion of Equation 5.49. If diffusion becomes significant at a given condition, the pseudo first order part of Equation 5.49 becomes less meaningful.

Figures 5.32–5.34 are plotted against CO_2 loading for some extreme conditions: 2 and 12 m PZ. For each parameter the explicit or approximated power in Equation 5.49 is incorporated. Since Figures 5.32–5.34 each have stated temperatures, only the free PZ and $PZCOO^-$ concentrations, diffusion coefficient of CO_2, and the activity coefficient of CO_2 vary. The rate constant and the Henry's solubility in water are constant in each graph.

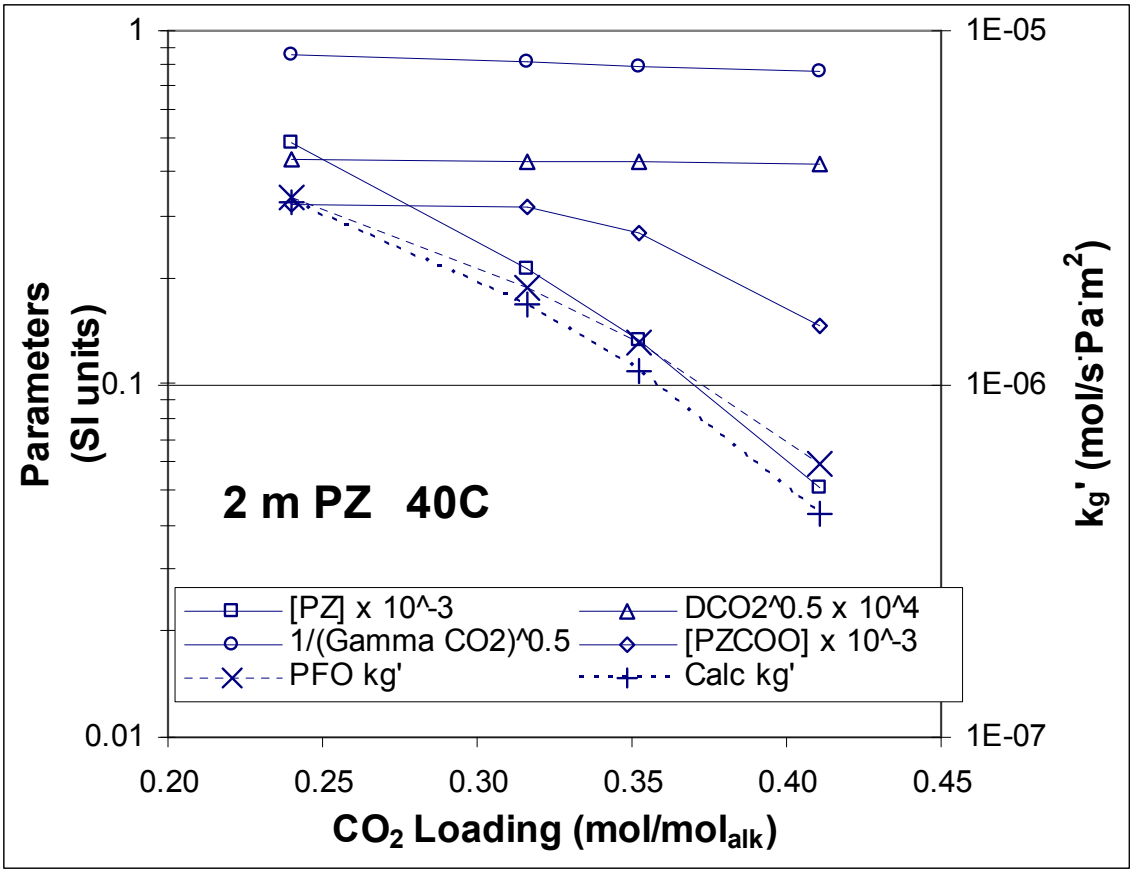

Figure 5.32: Parameter significance against CO_2 loading for 2 m PZ at 40˚C

Figure 5.32 shows that for 2 m PZ at 40˚C, the effects of the activity and diffusion coefficients of CO_2 are minor with CO_2 loading changes. The change in the liquid film mass transfer coefficient, k_g', with increased CO_2 loading is almost completely controlled by the free amine concentrations. The calculated and pseudo first order k_g' calculations are almost identical at this 40˚C condition. This implies that diffusion resistances are negligible. At 40˚C, the slope of the equilibrium line is very small, making the second term in Equation 5.49 of minor significance.

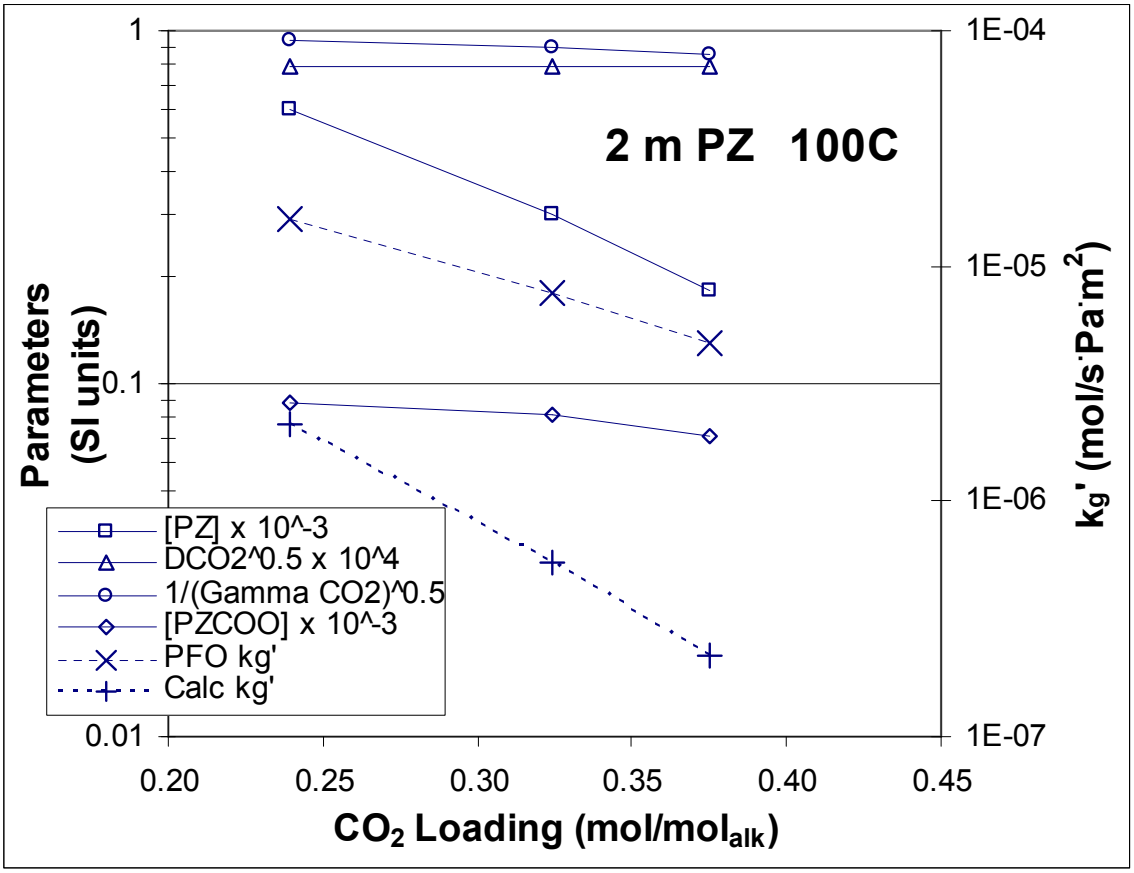

Figure 5.33: Parameter significance against CO_2 loading for 2 m PZ at 100˚C

Figure 5.33 shows the significance of parameters in 2 m PZ at 100˚C. The diffusion and activity coefficients of CO_2 change insignificantly with CO_2 loading. At low loading, $PZCOO^-$ concentration again remains relatively unchanged. The change in the pseudo first order slope is almost completely due to the change in the free PZ concentration. The parameters range two decades in Figure 5.33 while the k_g' scale includes three decades. Since this 100˚C condition is significantly affected by diffusion resistances, the calculated k_g' values fall far below pseudo first order k_g' values. The drop is even greater at the higher loading since less free amine is available. The diffusion of fresh amine to the interface severely limits mass transfer in this case.

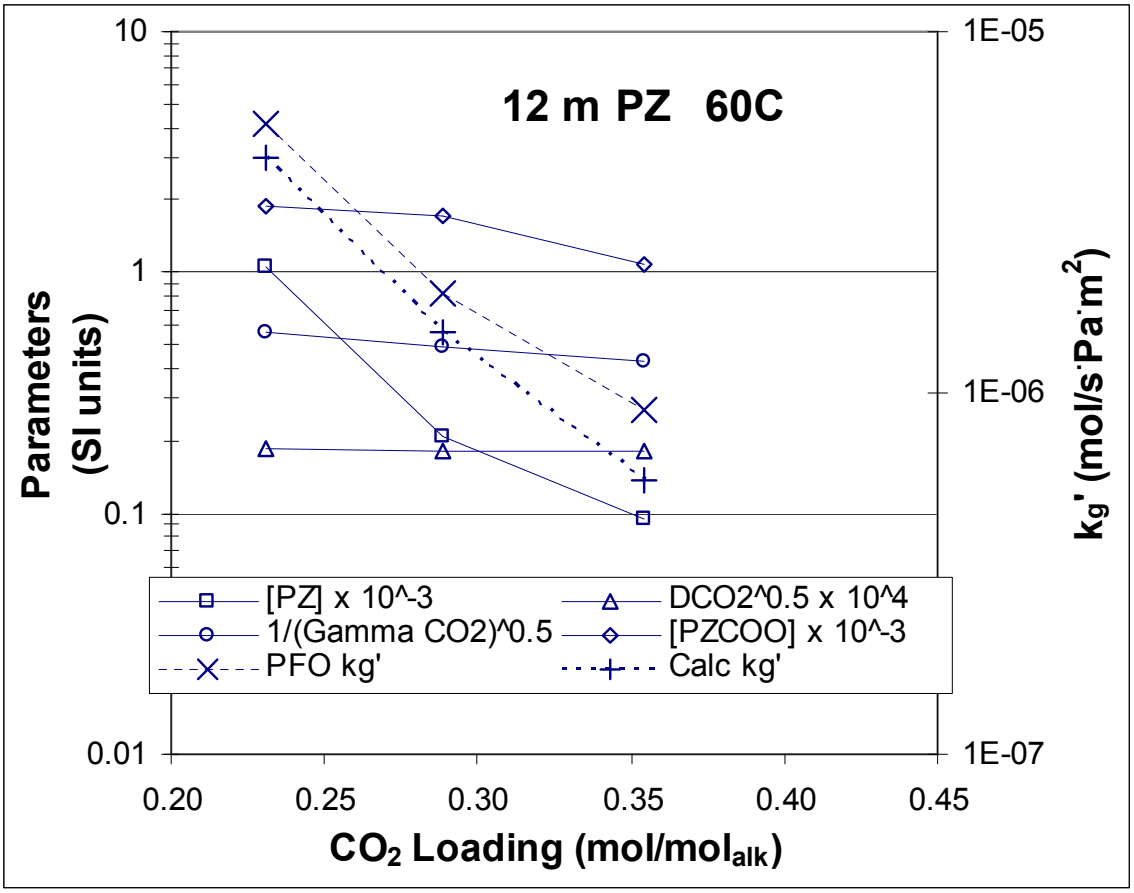

Figure 5.34: Parameter significance against CO_2 loading for 12 m PZ at 60˚C

Figure 5.34 shows the parameter significance as a function of CO_2 loading at 12 m PZ, 60˚C. This condition is not soluble at 0.4 loading so calculations have not been made at that condition. Very similar to the previous two graphs, k_g' is almost completely controlled by the change in the free PZ concentration. The free PZ carbamate concentration begins to contribute to the drop in k_g' near 0.35 loading. Since this solution is at 60˚C, there is a minor diffusion resistance which increases slightly with increasing CO_2 loading.

Figure 5.35 looks at the effect on the parameters as a function of temperature. Intermediate conditions of 5 m PZ at 0.3 CO_2 loading were selected for this analysis.

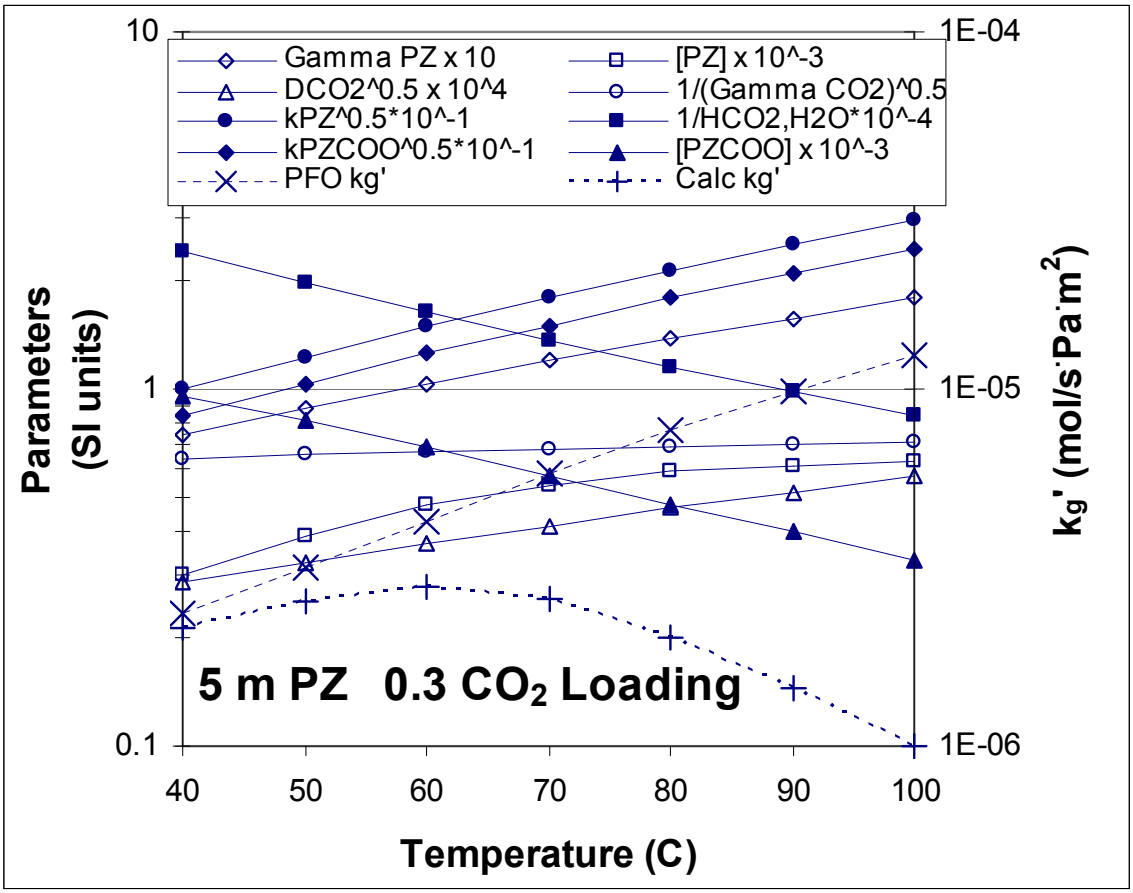

Figure 5.35: Parameter significance against temperature for 5 m PZ at 0.3 CO_2 loading

Figure 5.35 shows that nearly all the parameters in Equation 5.49 are strongly affected by temperature. Only the activity coefficient of CO_2 dependence remains mostly constant with changes in temperature. The contributions of the piperazine activity coefficient, both rate constants, the free piperazine concentration, and the diffusion coefficient of CO_2 each increase significantly with increasing temperature. The thermodynamic Henry's constant ($H_{CO2,H2O}$) and the $PZCOO^-$ concentration dependences each decrease significantly with increasing temperature. Those 8 parameters provide a

significant increase in the pseudo first order rate expression with increasing temperature. However, the higher temperature increases the diffusion resistance. The increased diffusion resistance causes k_g' to remain relatively constant from 40 to 70˚C before it begins to decrease. Overall, the predicted k_g' varies a factor of 2–3 despite seven parameter dependences which vary factors of 2–3. The fact that the PZ model accurately predicts the correct temperature behavior is remarkable considering the wide variance in the parameters.

Figure 5.36 shows the significance of each parameter with changes in total piperazine concentration. Only five parameters are included in Figure 5.36 since the Henry's constant, and rate constants do not change with temperature.

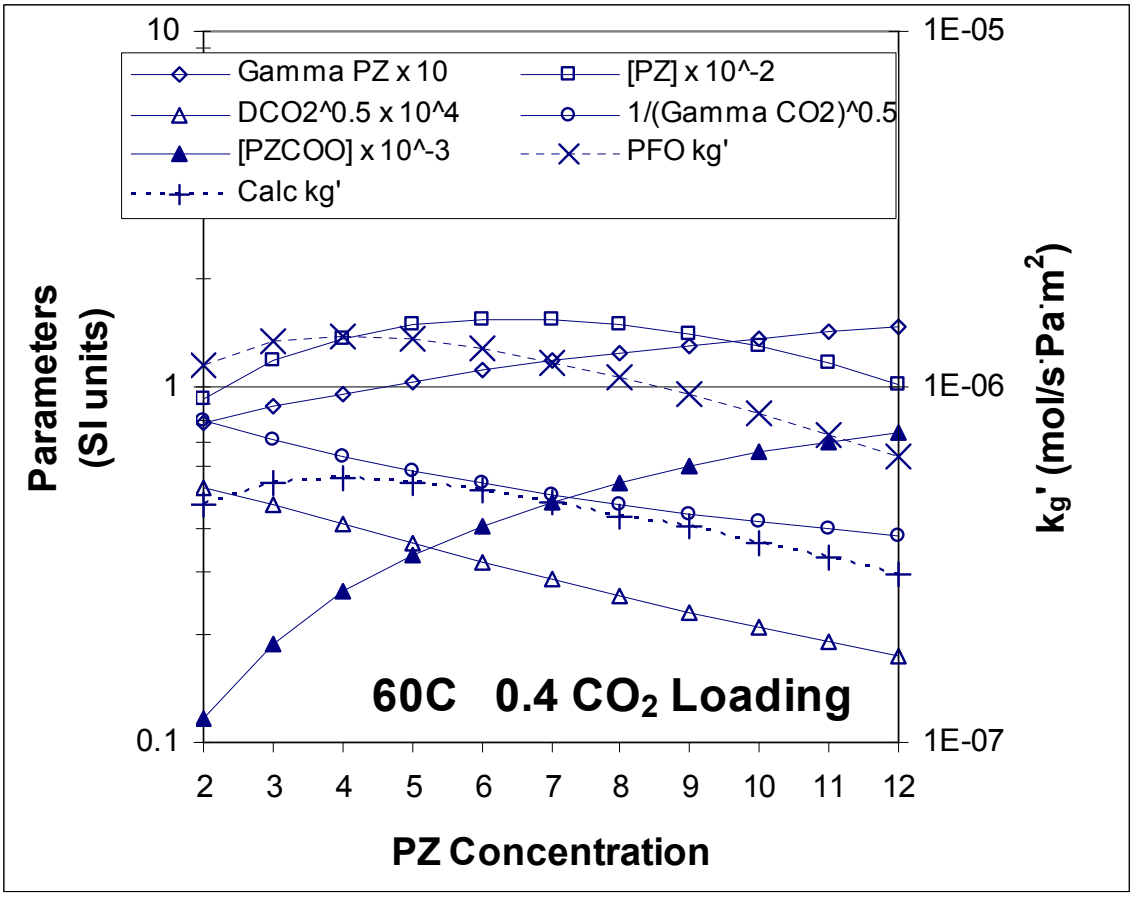

Figure 5.36: Parameter significance against PZ concentration for 60˚C and 0.4 CO_2 loading

Overall, the parameters do not depend on piperazine concentration as much as they depend on temperature. k_g' and k_g'' vary less than a factor of two over the 2–12 m PZ range. An interesting point in Figure 5.36 is that the pseudo first order k_g' and the non-pseudo first order k_g' remain evenly spaced. This implies that PZ concentration does not affect the fraction of the diffusion resistance. Essentially, the ratio of the two terms in Equation 5.49 is unaffected by PZ concentration.

Figure 5.37 explicitly shows the fraction of diffusion resistance for 2 and 8 m PZ.

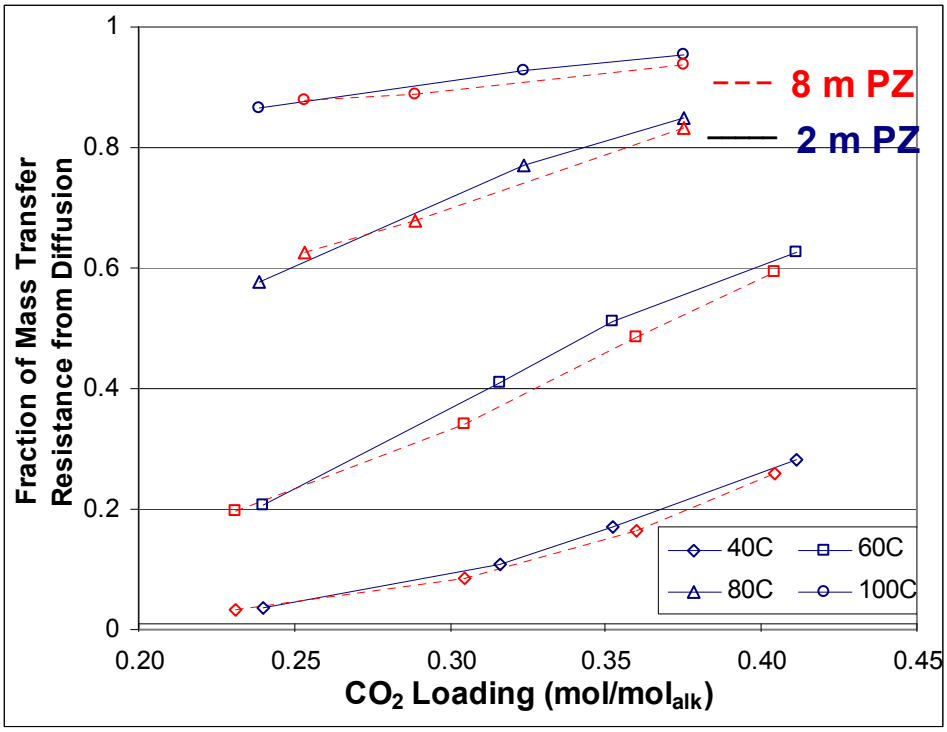

Figure 5.37: Fraction of mass transfer resistance from diffusion for 40–100˚C in 2 and 8 m PZ

As previously stated, the total PZ concentration does not affect the relative importance of the two terms in Equation 5.49. The fraction of resistance due to diffusion remains independent of PZ concentration. At higher concentrations, the physical liquid film mass transfer coefficient, k_l^o, decreases due to viscosity changes. However, the slope of the equilibrium line has a concentration term since it is defined in Pa/(mol/m^3). The increased concentration decreases the slope of the equilibrium line. The diffusion term in Equation 5.49 divides k_l^o by the slope and that term is mostly unchanged with changes in total PZ concentration.

5.2.2.3 Error Analysis

Like the MEA error analysis, this is not a typical error analysis. This analysis seeks to show that most of the systematic error has been removed from the model. The lack of systematic error provides a better confidence in the estimation of the parameters which comprise the k_g' expression, Equation 5.49.

Figure 5.38 shows an overall graph of all the wetted wall column data: 2–12 m PZ, 40–100˚C, 0.22–0.41 CO_2 loading. A parity plot is used to compare measured wetted wall column k_g' values to the calculated k_g' from Equation 5.49.

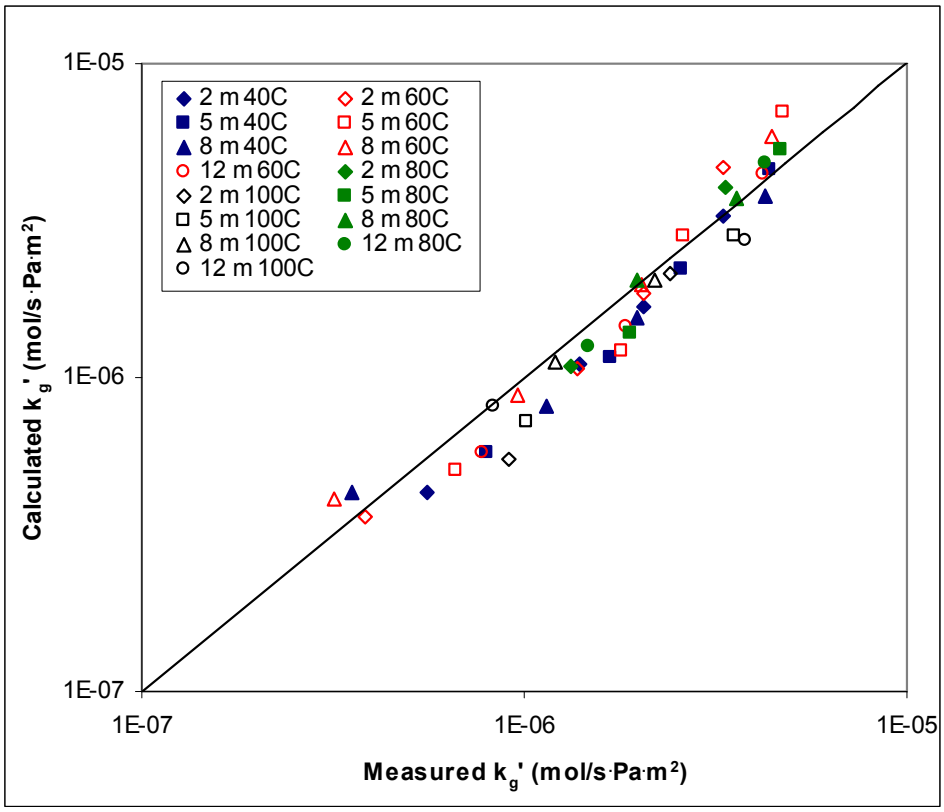

Figure 5.38: Parity plot comparing experimentally measured PZ k_g' values to k_g' values calculated from Equation 5.49.

Figure 5.38 shows that k_g' values vary about a factor of 20 from the lowest loading to the highest loading conditions. A brief view shows that all of the points fall relatively close to the parity line. There are no obvious trends with temperature or amine concentration. However, to analyze and detect the systematic error, a closer look into the data is required. Equation 5.49 represents the measured k_g' in PZ solutions with an average error of 19%.

Figure 5.39 includes all the data in Figure 5.38 but is plotted differently to show systematic trends in CO_2 loading.

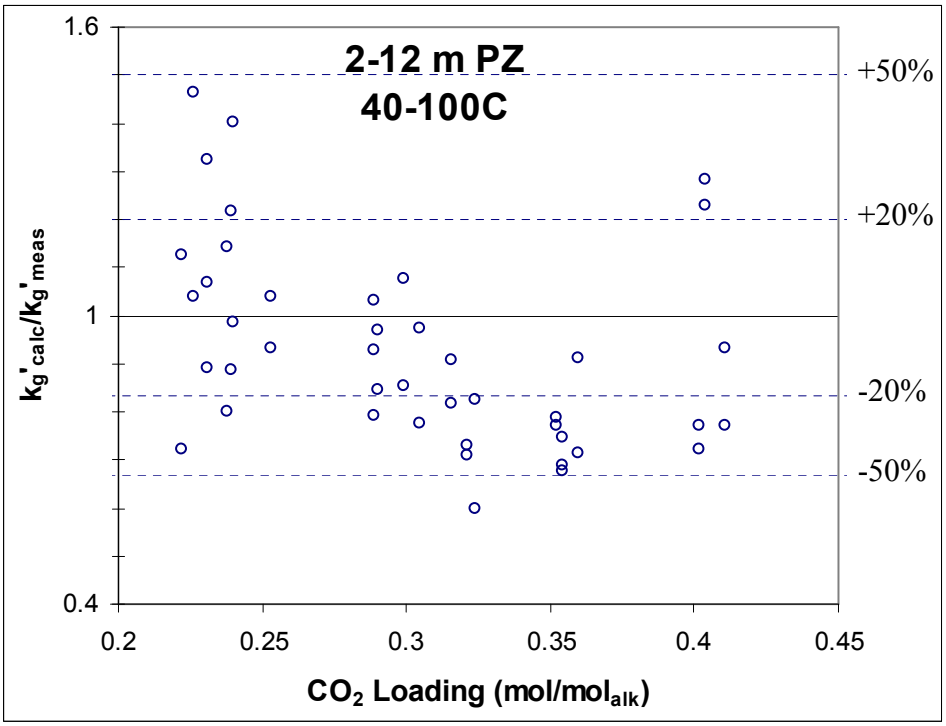

Figure 5.39: Calculated/measured k_g' against CO_2 loading for 2–12 m PZ wetted wall column conditions

Figure 5.39 has dotted lines to show ±20 and 50% error in the estimation of k_g'. All but one of the data points fall within 50% of the measured k_g' values. This is impressive considering the range of conditions. k_g' values vary about a factor of 20.

Many of the parameters comprising the k_g' expression change considerably with changes in temperature, PZ concentration, and loading. Overall, there seems to be a minimal systematic trend with CO_2 loading. Intermediate CO_2 loading conditions slightly underestimate k_g' while low and high loading conditions seem to be relatively evenly spaced around the y=1 line.

Figure 5.40 also shows all the experimental conditions but plots temperature on the x-axis.

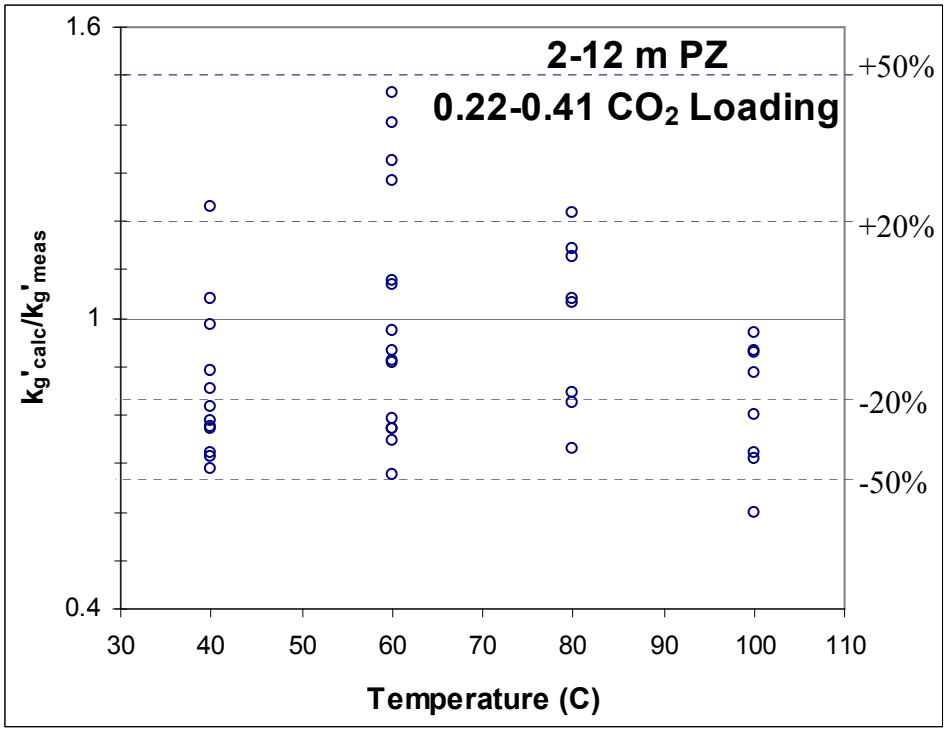

Figure 5.40: Calculated/measured k_g' against temperature for 2–12 m PZ wetted wall column conditions

Figure 5.40 shows no significant systematic error with increasing temperature. According to Figure 5.35, many of the parameters comprising k_g' vary greatly with changes in temperature. The slope of the equilibrium line is also extremely sensitive to

temperature. The lack of systematic temperature error suggests that the temperature dependent terms are being represented accurately.

Figure 5.41 plots all the experimental data with PZ concentration on the x-axis.

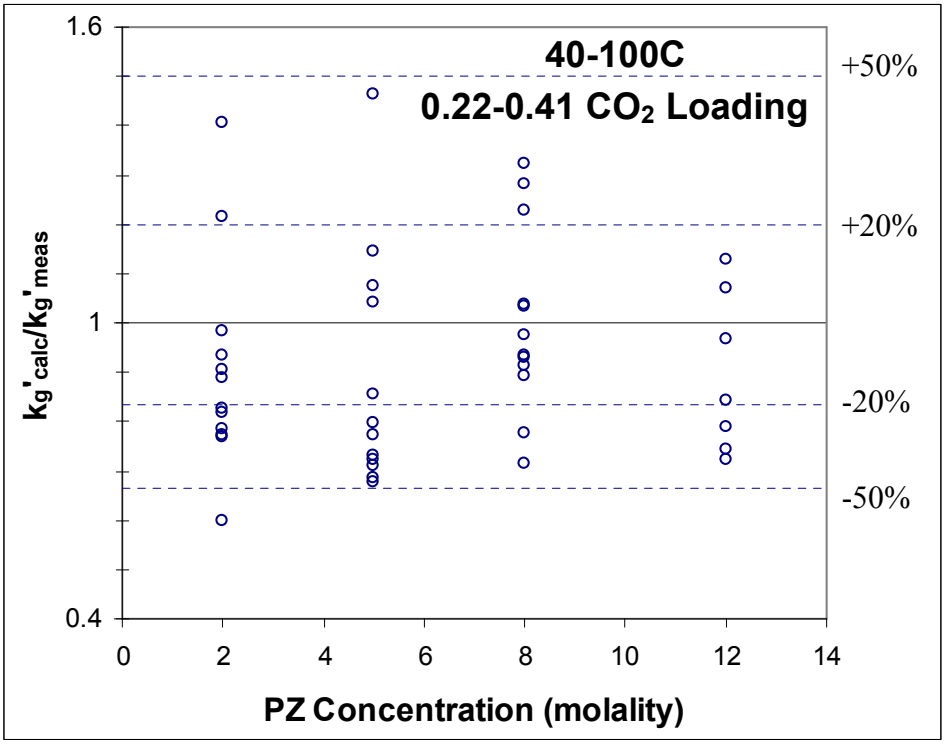

Figure 5.41: Calculated/measured k_g' against PZ concentration for 2–12 m PZ wetted wall column conditions

Figure 5.41 shows no systematic error in the calculated k_g' values with PZ concentration. Figure 5.43 showed that many of the parameters vary significantly with changes in total PZ concentration. Regardless, the concentration dependent terms seem to be properly represented.

Figures 5.39–5.41 show that systematic error with respect to CO_2 loading, temperature, and PZ concentration have essentially been removed from the model. The absence of significant systematic error increases confidence both in the model and in the

determination of each parameter in the k_g' expression. The PZ model has fully explained observed k_g' effects with changing temperature, CO_2 loading, and piperazine concentration.

5.2.3 Model Comparisons to Literature Data

5.2.3.1 MEA Model Comparisons to Literature Data

Figure 5.42 shows a comparison of the model to concentrated MEA rate data by Aboudheir (2003) and Hartono (2009). Aboudheir uses a laminar jet absorber which has a very fast liquid film physical mass transfer coefficient due to short contact times. To compare to this pseudo first order condition, the pseudo first order results of the model are plotted in Figure 5.42. The Hartono data can also be compared to the pseudo first order model results since the diffusion of reactants and products is unimportant at concentrated, unloaded conditions.

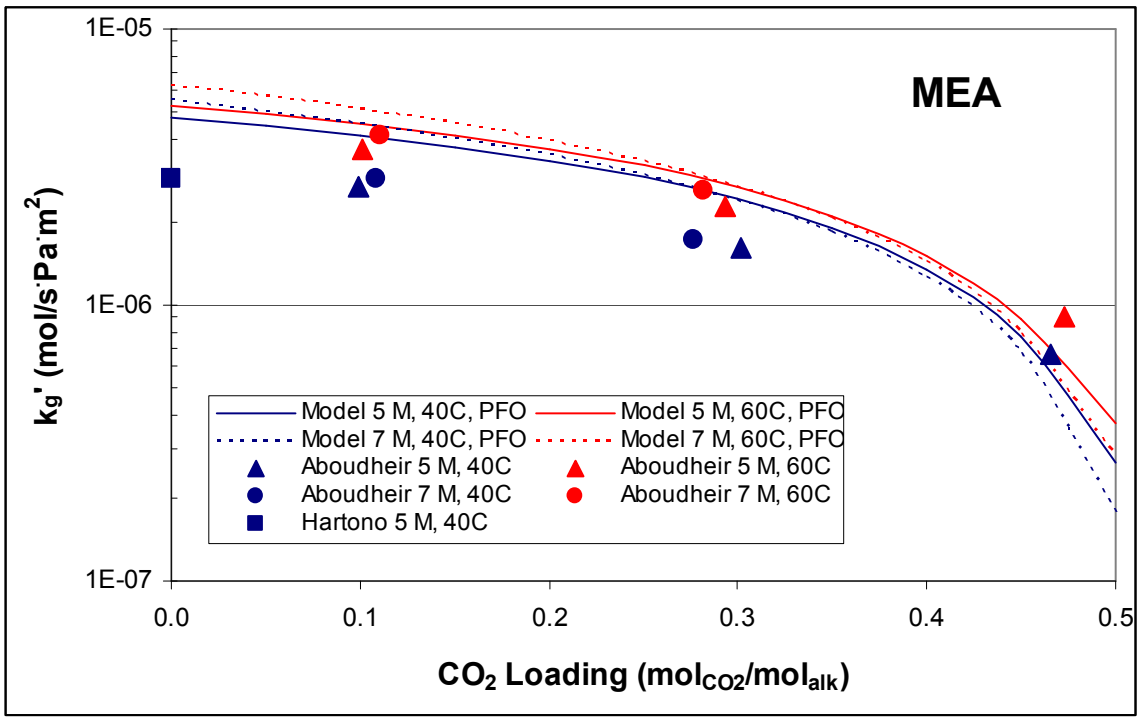

Figure 5.42: Pseudo first order model results compared to 5 and 7 M MEA literature data (Aboudheir, Tontiwachwuthikul et al. 2003; Hartono 2009)

The pseudo first order model results for both 7 and 13 m show temperature trends similar to the Aboudheir data. The model also matches the k_g' values fairly well over the entire CO_2 loading range. The model shows a more drastic change in kg' at higher loading. This was seen in all the experimental data (Figure 4.10). The wetted wall column experimental data could not justify the flattening of the k_g' values at lower CO_2 loading. The model predicts this observed trend.

The model can also be extrapolated to zero loading and more dilute MEA concentrations to evaluate recent data by Hartono (2009).

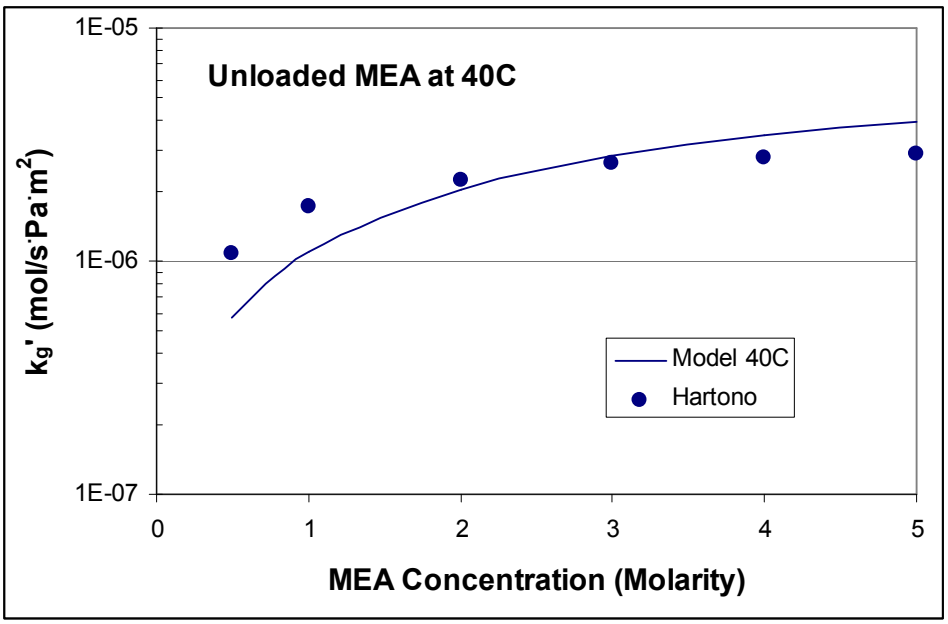

Figure 5.43: MEA model comparison to Hartono (2009) at 40˚C

Overall, the data seem to match the Hartono data adequately. Rates are underpredicted at low MEA concentrations and slightly overpredicted at high MEA concentrations. The model neglects base catalysis by water. This could be a significant contribution to the rates at very low MEA concentrations.

5.2.3.2 Comparison to Cullinane (2006) Piperazine Rate Constants

Figure 4.12 has shown that 1.8 m PZ from the Cullinane model (2005) compares very favorably to 2 m PZ experiments in the wetted wall column. This analysis also seeks to compare the rate expressions.

Due to differences in the form of the Cullinane rate expression and the form of the rate expression used in this work (Equation 5.40), it is difficult to make a straightforward rate constant comparison. An attempt has been made to compare unloaded 1 M PZ.

Cullinane (2006) reports an overall rate constant of 102,000 s^{-1} at 25˚C for unloaded 1 M PZ. This value results from the combination of the k^{o}_{PZ-PZ} and $k^{o}_{PZ-H_2O}$ rate constants multiplied by the piperazine and water molarity, respectively. This model ignores the water catalysis effect. At 1 M PZ this effect can be significant. It is easier to exclude the water catalysis from the Cullinane expression to obtain a 70,100 s^{-1} rate expression only considering PZ catalysis.

The current model can be extrapolated to 1 M but the difference in the form of the rate expressions must be considered. Cullinane utilized a concentration-based model. The CO_2 activity coefficient approaches 1 for unloaded, dilute solutions. The unloaded 25˚C PZ activity coefficient was estimated as 0.0393 by the model. This model predicts the rate constant times the square of the PZ activity coefficient to yield 78,600 s^{-1} at 25˚C. This compares very favorably to the 70,100 s^{-1} value reported by Cullinane (2006).

5.2.3.3 Piperazine Model Comparisons to Literature Data

Figure 5.44 compares the PZ model to work done by Cullinane. Two unloaded, 1.2 M PZ data points are compared. A 1.8 m PZ model developed by Cullinane is also compared. Although Cullinane did not measure rates in CO_2 loaded aqueous PZ, he was able to build the model using unloaded PZ and loaded K_2CO_2/PZ rate data.

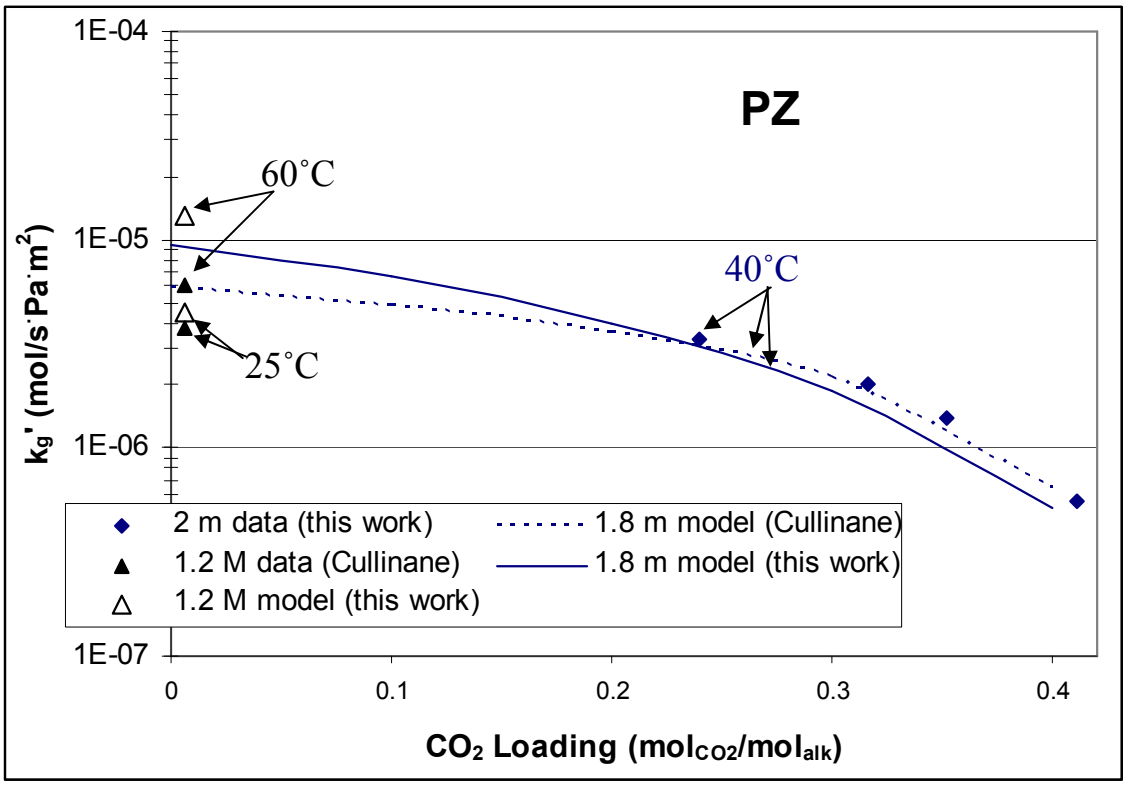

Figure 5.44: PZ model comparison to Cullinane (2005) model and data

Figure 5.44 shows excellent agreement between the two 1.8 m PZ models and the 2 m PZ rate data. The PZ model also adequately predicts k_g' for unloaded PZ solutions. Both 25 and 60˚C experiments by Cullinane are adequately represented by the PZ model. The model did not accurately represent the 0.06–0.30 M PZ data from Bishnoi (2000). The Hilliard (2008) model did not seem to speciate the very dilute PZ solutions correcly. The model predicted almost all the CO_2 being converted to bicarbonate, rather than $PZCOO^-$.

5.2.4 Significant Case: 20˚C Absorber Operation

Experiments included in this work test a large range of amine concentrations. MEA concentrations greater than 13 m and PZ concentration greater than 12 m are

unlikely to be relevant for industrial use. The 40–100˚C temperatures also exhibit a large range of conditions. 120˚C is not a particularly interesting condition because mass transfer in those solutions would be almost completely controlled by diffusion resistances. Special equipment designs, such as using trays instead of packing, could be used to increase the physical liquid film mass transfer coefficient, k_l^o. This model is not very useful in evaluating that condition because k_l^o in this model is based on the wetted wall column. Amine solutions at 20˚C could be analyzed accurately by this model since diffusion resistance would be negligible.

In some locations such as the North Sea it may be feasible to cool amine solutions down to 20˚C. The colder amine solution would allow for a richer solution at the bottom of the absorber. This analysis uses the spreadsheet models to explore the kinetic implications of operating an absorber at 20˚C. The analysis has been carried out with 3 solutions, 7 and 13 m MEA and 8 m PZ.

The bottom of an absorber with flue gas from coal combustion will be approximately 12% CO_2 near atmospheric pressure. This 12 kPa partial pressure must be significantly more than the partial pressure of the amine solution for significant absorption to occur. Due to the reduction of CO_2 driving force and the slower rates at the bottom of the absorber it is unlikely that the amine solution would have a CO_2 loading exhibiting more than a 6 kPa partial pressure. Therefore 20˚C amine solutions are analyzed up to a CO_2 loading which has a 6 kPa CO_2 partial pressure.

None of the 20˚C conditions encounter significant diffusion limitations so no adjustment in k_l^o is required to adjust to an industrial design.

5.2.4.1 7 and 13 m MEA

Using the spreadsheet model, the CO_2 partial pressure and liquid film mass transfer coefficient has been calculated for 0.25–0.6 loading in 7 and 13 m MEA. The results are included in Table 5.4.

Table 5.4: Calculated CO_2 partial pressure and k_g' for 7 and 13 m MEA at 20˚C

MEA	Temp	CO_2 Loading	P^*_{CO2}	k_g'
m	C	mol_{CO2}/mol_{alk}	Pa	$mol/s \cdot Pa \cdot m^2$
7	20	0.25	1.2	2.5E-06
		0.3	3.1	2.1E-06
		0.35	8.8	1.7E-06
		0.4	28	1.2E-06
		0.45	95	6.3E-07
		0.5	353	1.7E-07
		0.55	1433	3.7E-08
		0.6	6345	1.5E-08
13		0.25	1.2	2.5E-06
		0.3	3.1	2.0E-06
		0.35	8.8	1.5E-06
		0.4	28	1.0E-06
		0.45	95	5.3E-07
		0.5	353	8.7E-08
		0.55	1433	1.2E-08
		0.6	6345	5.6E-09

The values in Table 5.4 at 20˚C are compared to 40–100˚C conditions in Figure 5.45. 7 m MEA conditions are denoted by solid lines while 13 m MEA is represented by dashed lines.

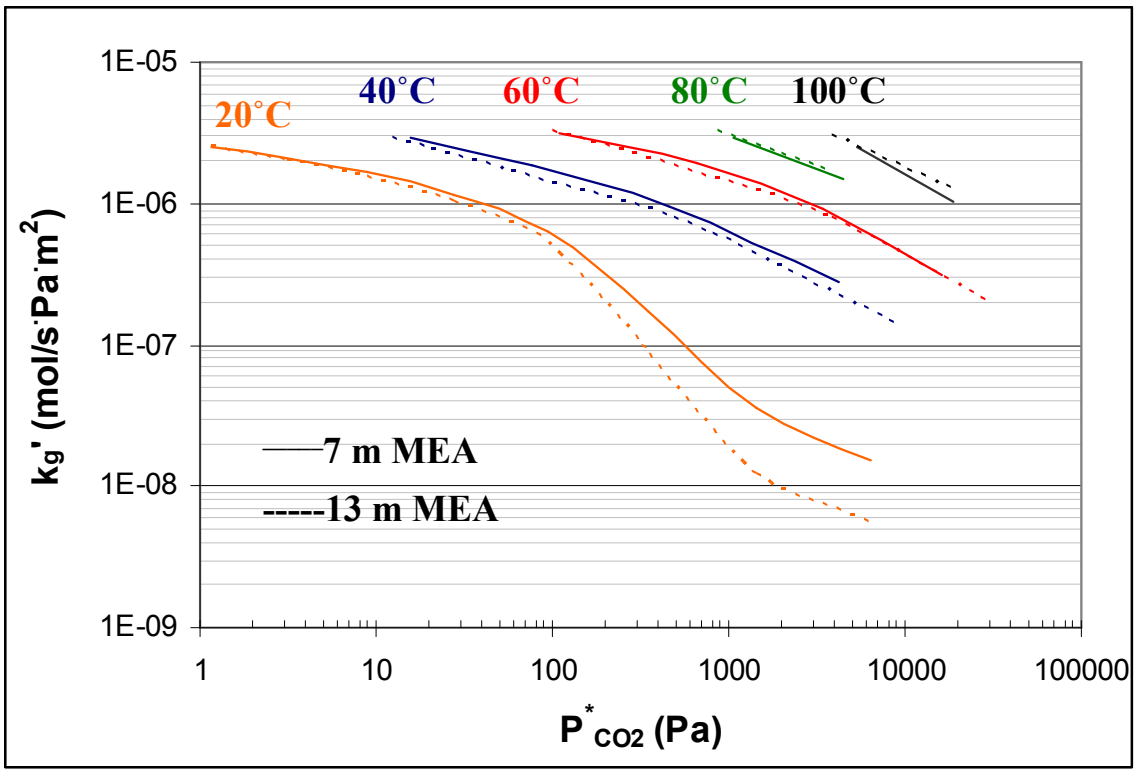

Figure 5.45: Predicted CO_2 absorption/desorption rates in 7 and 13 m MEA at 20–100˚C

Figure 5.45 shows that the 20˚C solutions actually perform similarly to the higher temperature data until near a 100 Pa partial pressure, 0.45 CO_2 loading. Above this loading the free amine concentration is too small to produce significant rates. Rates at the rich end of the absorber in the 2–5 kPa range are 10 times slower than rates at 40˚C.

The 20˚C case is interesting because the colder temperatures allow for the amine solution to achieve higher CO_2 loading at the bottom of the absorber. The higher CO_2 loading leads to a lower energy consumption in the stripper. However, for MEA, CO_2 loadings at 20˚C seem too rich to produce acceptable rates. Operating with a 20˚C rich solution at the bottom of the absorber does not seem to be advantageous for MEA solutions.

5.2.4.2 8 m PZ

Ignoring piperazine solubility issues, 8 m PZ has also been analyzed at 20˚C by the spreadsheet model. Table 5.5 includes the obtained CO_2 partial pressure and k_g' results.

Table 5.5: Calculated CO_2 partial pressure and k_g' for 8 m PZ at 20˚C

PZ	Temp	CO_2 Loading	P^*_{CO2}	k_g'
m	C	mol_{CO2}/mol_{alk}	Pa	$mol/s \cdot Pa \cdot m^2$
8	20	0.2	4.8	1.7E-06
		0.25	17	1.7E-06
		0.3	65	1.1E-06
		0.35	243	6.7E-07
		0.4	932	3.7E-07
		0.45	3627	1.4E-07
		0.5	14344	1.1E-08

The values in Table 5.5 at 20˚C are compared to 40–100˚C conditions in Figure 5.46.

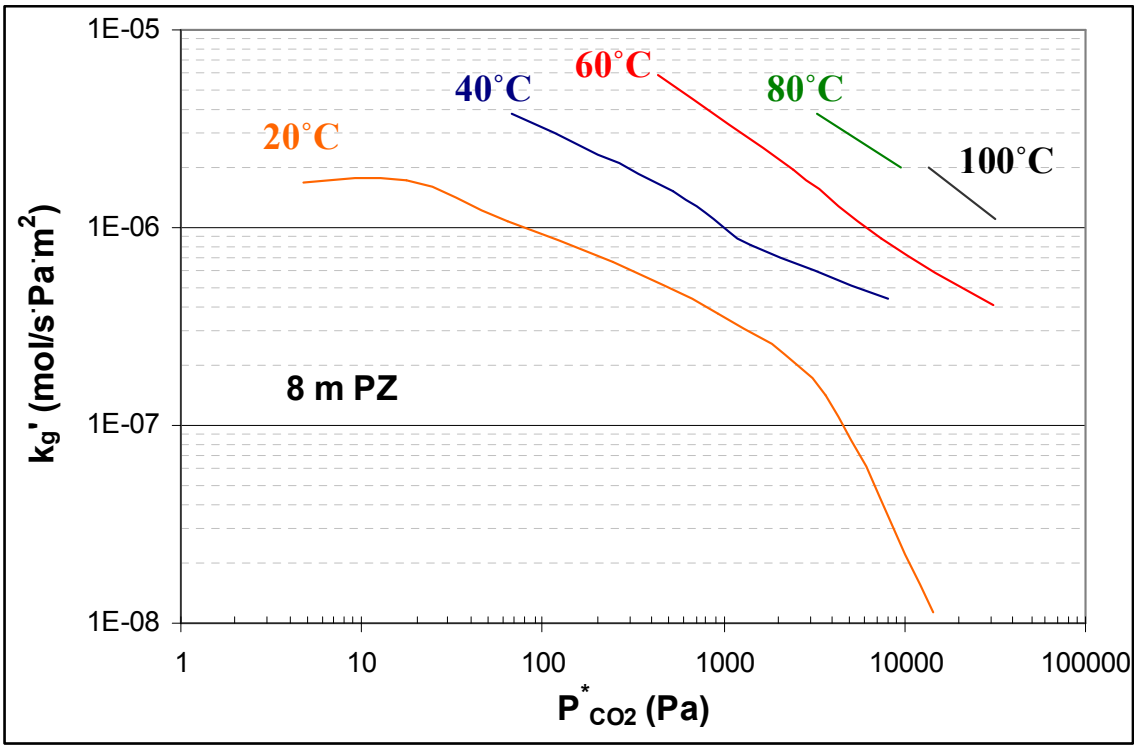

Figure 5.46: Predicted CO_2 absorption/desorption rates in 8 m PZ at 20–100˚C

8 m PZ rates at the rich end of the absorber in the 2–5 kPa range are about 3 times slower than rates at 40˚C. However, the 20˚C case achieves higher CO_2 loadings and a larger CO_2 capacity which may yield enough energy savings to offset the slower rates. A comprehensive absorber/stripper model incorporating both capital and operating costs would be required to quantify if the 20˚C case is more economically favorable than the 40˚C condition. This analysis ignores PZ solubility issues.

5.2.5 MEA and Piperazine Rate Comparison

The MEA and PZ spreadsheet models accurately match experimental data. Experimental measurements have shown PZ to react with CO_2 2–3 times faster than MEA. MEA and PZ reaction rates can also be compared through model results.

Experiments show that k_g' is essentially independent of amine concentration and temperature at lower temperatures. Figure 5.47 shows rate comparisons for 8 m PZ and 7 and 11 m MEA at 40˚C. Rates are compared at 40˚C because this is a likely temperature at the rich end of the absorber column. Rich end kinetics are much more important than lean end kinetics since rates are much slower at higher loading. Rich end kinetics dominate absorber performance.

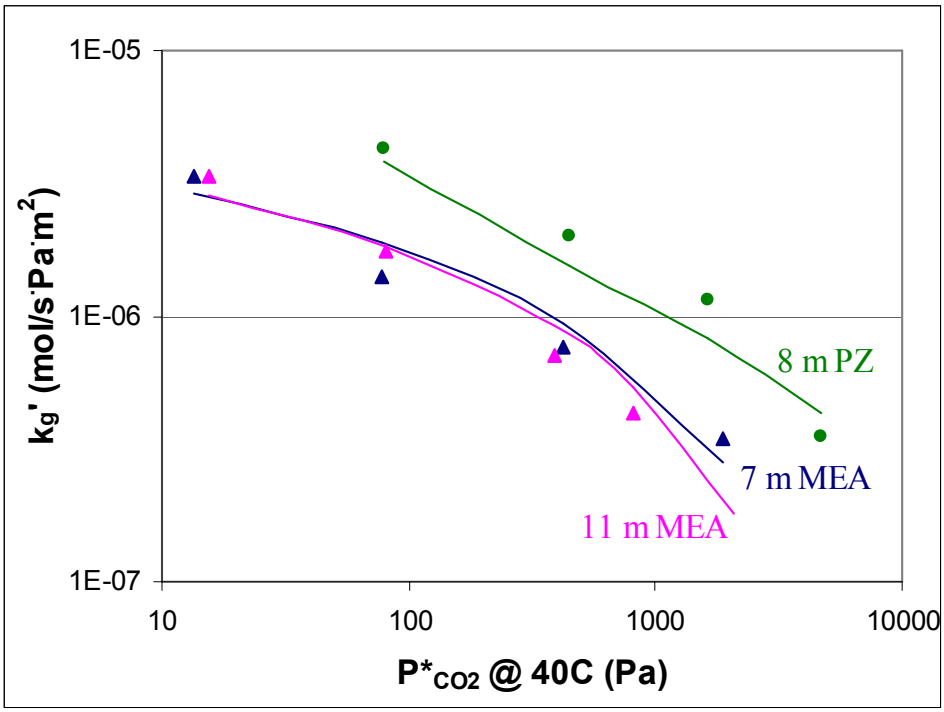

Figure 5.47: 8 m PZ and 7 and 11 m MEA rate comparisons at 40˚C: points – data; lines – model

At rich end conditions (high loading or partial pressure) the model shows a larger rate difference between MEA and PZ than the experimental data. If this trend is accurate, the enhanced absorber performance with PZ will be greater than experimental results suggest. Over the expected CO_2 loading range, the model shows PZ rates 1.5–4 times

faster than MEA. At the rich end of the absorber, which dominates performance, PZ absorbs CO_2 about 3 times faster than MEA.

5.3 ASPEN PLUS® RATESEP™ MODELING

In addition to the spreadsheet models, an Aspen Plus® RateSep™ model was created. Rather than predicting the mass transfer coefficient, k_g', the Aspen Plus® RateSep™ model can predict CO_2 flux. This model can be fitted to wetted wall column data and then scaled up to industrial conditions.

As a starting point the electrolyte NRTL thermodynamic framework of the Hilliard model (2008) was used. However, the Hilliard model is not capable of handling the high amine concentration and high temperature conditions that were tested in the wetted wall column experiments. Hilliard regressed data up to 11 m MEA and 5 m PZ. CO_2 partial pressure estimates are reliable up to 60˚C. Wetted wall column experiments utilized amine concentrations up to 13 m MEA and 12 m PZ at 100˚C. The Hilliard (2008) model did not accurately extrapolate to these higher amine concentrations.

5.3.1 Physical Design

The wetted wall column is modeled as an Aspen Plus® RateSep™ column. The actual wetted wall column has an annulus geometry since the liquid film flows over a rod and the gas flows around it. The Aspen Plus® RateSep™ module cannot mimic this geometry. The column in the model was designed as a typical, cylindrical column. The diameter was adjusted so the column would have the same cross-sectional area for gas flow as the wetted wall column. This results in equivalent gas velocities in the wetted wall column and the model. The design height of the column is the height of the wetted wall column, 9.1 cm.

Mimicking the wetted area of the column requires a similar manipulation. In the wetted wall column, the contact area is the surface area of a metal rod which is coated with a thin film of liquid. The model assumes an arbitrary packing. An interfacial area FORTRAN subroutine was written to ensure that the wetted area of the wetted wall column, 38.52 cm^2, would be duplicated in the model.

The model operates with 3 countercurrent stages. The model does not consider pressure drop.

5.3.2 Primary Monoethanolamine Data Regression

A modified VLE model was created with the same sequential regression approach that Hilliard employed. Hilliard (2008) used heat of absorption, nuclear magnetic resonance, heat capacity, amine partial pressure and CO_2 partial pressure data to regress thermodynamic parameters. This model ignores the heat of absorption data.

The main MEA data regression includes nuclear magnetic resonance, heat capacity, amine partial pressure, and CO_2 partial pressure from Hilliard (2008). Increased importance was placed on the MEA partial pressure data since these data lead to MEA activity coefficients, which are very important to the rate behavior. CO_2 partial pressure data from Jou (1995) and Dugas (Rochelle, Sexton et al. 2009) were also included in the regression. The MEA VLE model includes data ranging from 3.5 m MEA to 13 m MEA with temperatures from 25 to 120˚C. Only data with CO_2 loadings between 0.25–0.6 mol_{CO2}/mol_{MEA} were included in the regression.

In an effort to simplify the regressions and obtain better CO_2 partial pressure predictions, significantly fewer parameters were regressed in this work than that of Hilliard (2008). Some binary interaction parameter pairings were deemed insignificant

and deleted. The complexity of the temperature dependence of the molecule/anion-cation pairings was simplified by deleting some of the temperature dependent terms.

Table 5.6 gives the regressed parameters for the system. Heat of formation, free energy of formation, heat capacity, and molecule/anion-cation binary interaction parameters were regressed. Figures 5.48–5.51 show the CO_2 partial pressure fit of the model against 7, 9, 11, and 13 m MEA. In each figure, the points include various amine concentrations since amine concentration does not affect the CO_2 partial pressure at CO_2 loadings below 0.45.

Table 5.6: Regressed thermodynamic parameters for the MEA/CO_2/H_2O system

Parameter	Component i	Component j	Value (SI units)	Std Dev
DGAQFM/1	MEACOO-		-4.96E+08	1.74E+11
DHAQFM/1	MEACOO-		-6.98E+08	1.74E+11
CPAQ0/1	MEACOO-		1.31E+05	1.74E+11
GMELCC/1	H2O	(MEA+,HCO3-)	14.8	0.642
GMELCD/1	H2O	(MEA+,HCO3-)	-86.2	187
GMELCC/1	(MEA+,HCO3-)	H2O	-5.02	0.139
GMELCC/1	H2O	(MEA+,MEACOO-)	14.5	1.37
GMELCD/1	H2O	(MEA+,MEACOO-)	-297	434
GMELCC/1	(MEA+,MEACOO-)	H2O	-5.29	0.0642
GMELCC/1	MEA	(MEA+,MEACOO-)	60.0	3962
GMELCD/1	MEA	(MEA+,MEACOO-)	1058	1.74E+11
GMELCC/1	(MEA+,MEACOO-)	MEA	4.37	26.2
NRTL/1	H2O	MEA	-127	23.7
NRTL/2	H2O	MEA	4058	1007
NRTL/5	H2O	MEA	20.7	3.93
NRTL/6	H2O	MEA	-0.0243	0.00616
NRTL/1	MEA	H2O	0.585	5.29
NRTL/2	MEA	H2O	775	1776

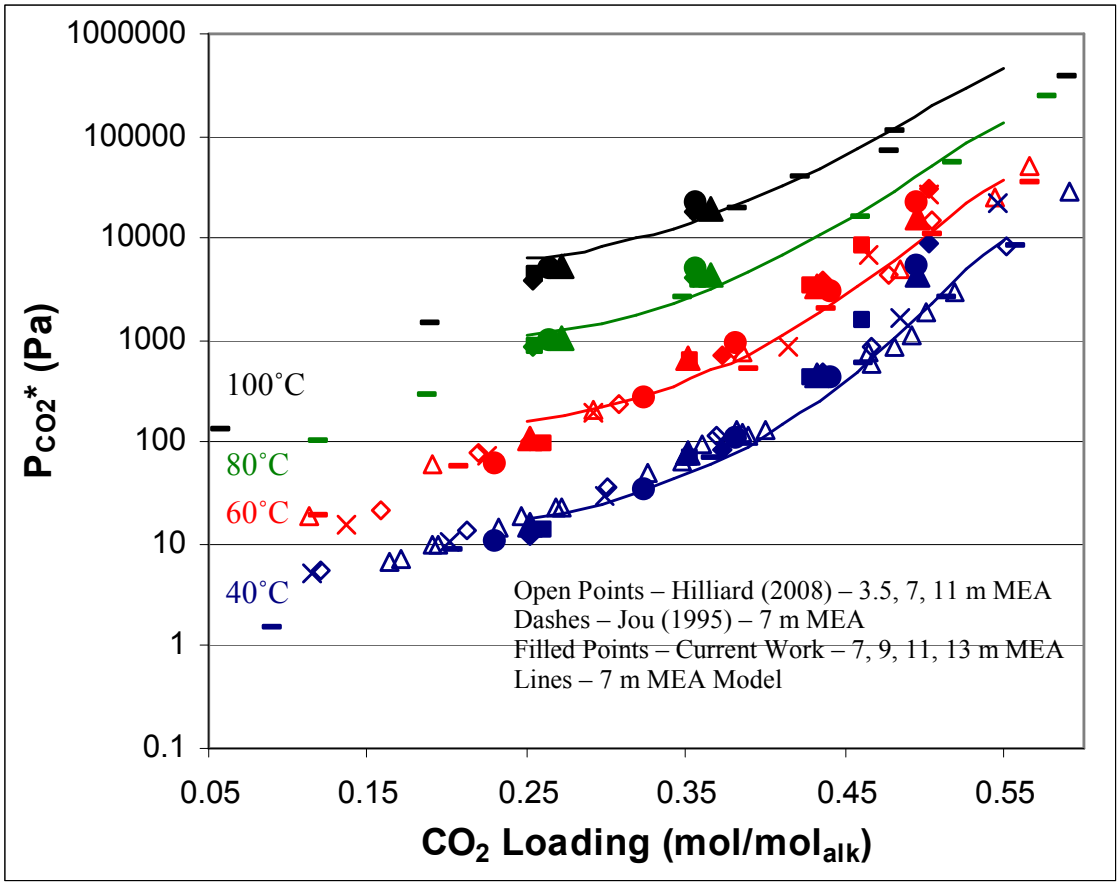

Figure 5.48: CO_2 partial pressure regression results – 7 m MEA

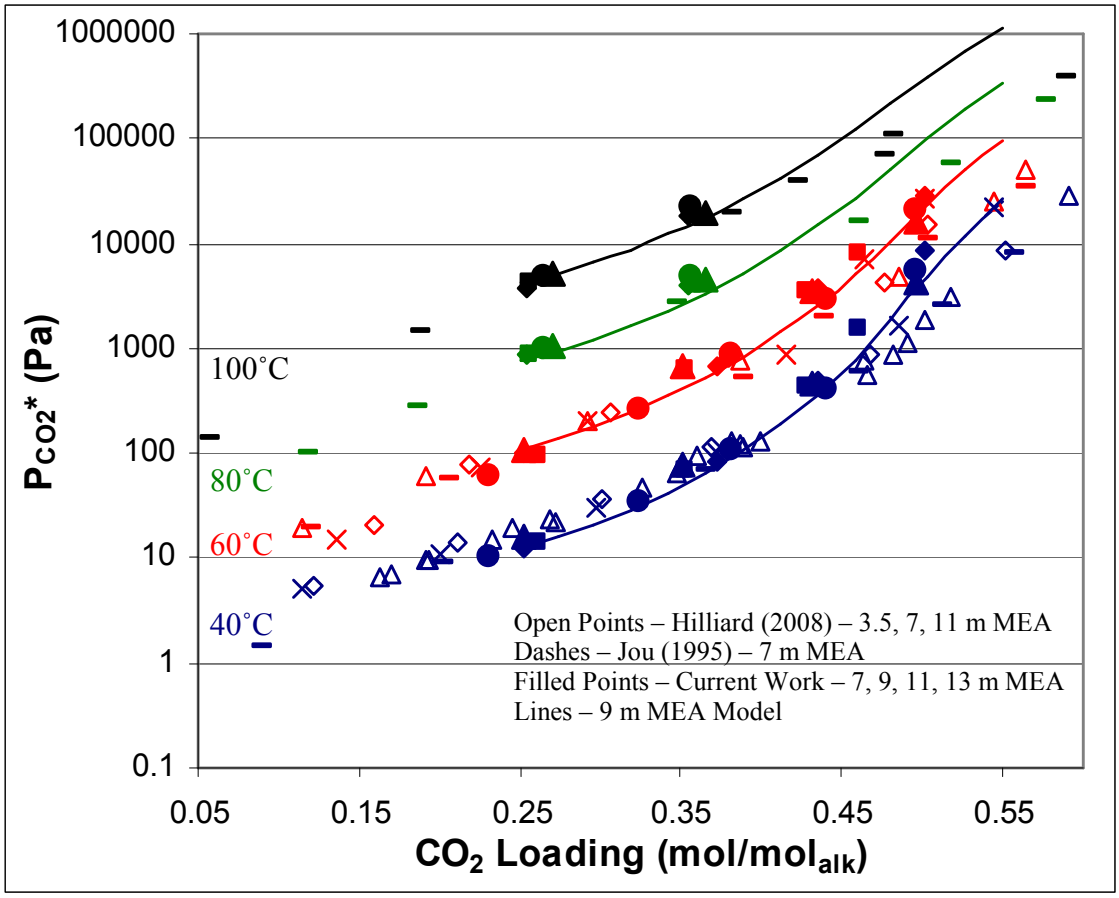

Figure 5.49: CO_2 partial pressure regression results – 9 m MEA

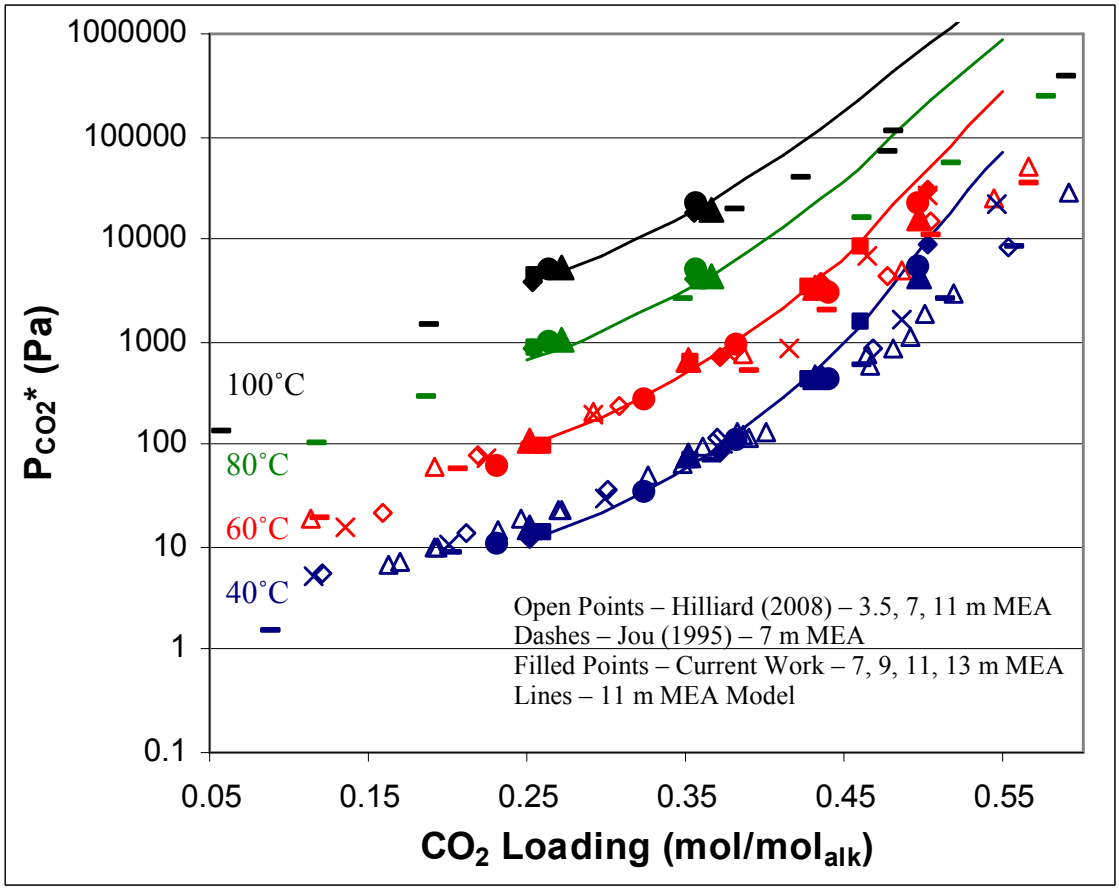

Figure 5.50: CO_2 partial pressure regression results – 11 m MEA

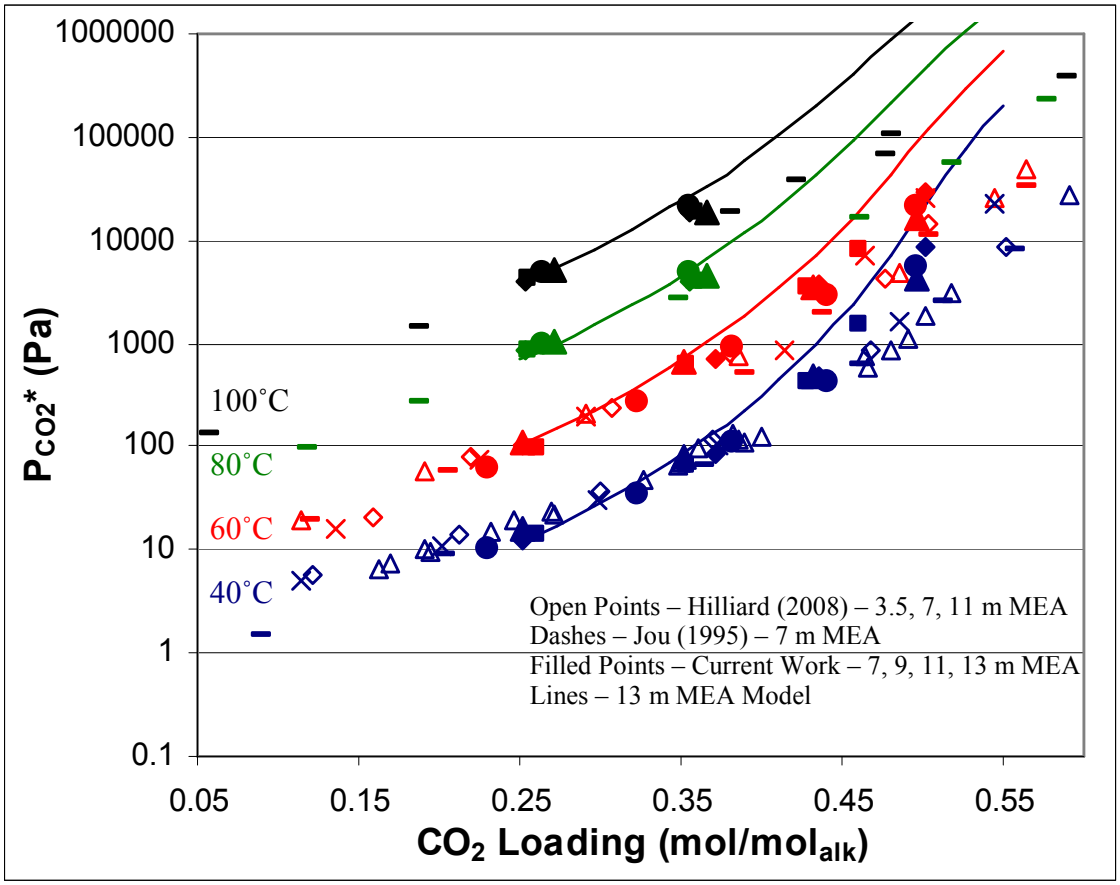

Figure 5.51: CO_2 partial pressure regression results – 13 m MEA

The regression fits the 7 m MEA data at each of the temperatures. At higher amine concentrations the regression accuracy declines, particularly at the rich loadings. The model is least accurate where the bicarbonate concentration is highest: 13 m MEA at high CO_2 loading. Although the regressed CO_2 partial pressure fit is not exceptional, it seems to be the best that can be achieved.

5.3.3 Primary Piperazine Data Regression

A satisfactory regression of the piperazine data was not obtained. PZ and PZ carbamate activity coefficients could not be represented properly. Since the rate model

has a very strong dependence on the activity coefficients, a significant error in the PZ and PZ carbamate activity coefficient representation undermines the integrity of the model. CO_2 activity coefficients in PZ could not be manually adjusted to desired values by adjusting electrolyte pair parameters. An Aspen Plus® RateSep™ model for piperazine solutions was not created.

5.3.4 CO_2 Loading Adjustment

Since the predicted CO_2 partial pressure does not always match the experimental partial pressure, the model has the capability to predict CO_2 absorption when desorption should be occurring. Any conditions operating near the CO_2 equilibrium partial pressure can also produce incorrect CO_2 fluxes. In a model designed to predict flux, this is unacceptable. Therefore, the CO_2 loadings of the amine solutions were adjusted to fit the CO_2 partial pressure exactly. This solves the unacceptable CO_2 driving force issue at the expense of adjusting the free amine concentration. The error introduced into the model by adjusting the free amine concentration is substantially less than not correcting the erroneous CO_2 partial pressure. Table 5.7 gives the MEA wetted wall column conditions and the adjusted model loading that was used to match the measured equilibrium partial pressure.

Table 5.7: Wetted wall column conditions with the adjusted model CO_2 loading to fit CO_2 partial pressure data

MEA	Temp	Experimental CO_2 Loading	Adjusted Aspen CO_2 Loading	P^*_{CO2}
m	C	mol/mol$_{alk}$	mol/mol$_{alk}$	Pa
7	40	0.252	0.218	15.7
		0.351	0.379	77
		0.432	0.456	465
		0.496	0.522	4216
	60	0.252	-	109
		0.351	0.383	660
		0.432	0.460	3434
		0.496	0.516	16157
	80	0.271	0.237	1053
		0.366	0.387	4443
	100	0.271	-	5297
		0.366	0.375	19008
9	40	0.231	0.228	10.4
		0.324	0.329	34
		0.382	0.389	107
		0.441	0.440	417
		0.496	0.507	5354
	60	0.231	-	61
		0.324	0.324	263
		0.382	0.391	892
		0.441	0.438	2862
		0.496	0.501	21249
	80	0.265	0.279	979
		0.356	0.384	4797
	100	0.265	0.268	4940
		0.356	0.376	21534
11	40	0.261	0.268	14.0
		0.353	0.355	67
		0.428	0.426	434
		0.461	0.461	1509
	60	0.261	0.249	96
		0.353	0.361	634
		0.428	0.428	3463
		0.461	0.455	8171
	80	0.256	0.271	860
		0.359	0.359	3923
	100	0.256	0.261	4274
		0.359	0.354	18657
13	40	0.252	0.253	12.3
		0.372	0.349	84
		0.435	0.414	491
		0.502	0.485	8792
	60	0.252	0.248	100
		0.372	0.349	694
		0.435	0.414	3859
		0.502	0.472	29427
	80	0.254	0.264	873
		0.355	0.343	3964
	100	0.254	0.248	3876
		0.355	0.337	18406

In most cases the change in loading is minor. At the highest CO_2 loadings, near 0.5, even relatively small changes in the CO_2 loading can significantly affect the free MEA concentration. This introduces a large error into the Aspen Plus® RateSep™ results at these high CO_2 loading conditions.

Three conditions did not produce model CO_2 loadings that match the partial pressure. These solutions suffer from CO_2 partial pressure curves which flatten at lower CO_2 loading. The CO_2 loading in Aspen Plus® either could not be calculated or was considerably different in these three cases.

5.3.5 CO_2 Activity Coefficients

CO_2 activity coefficients in aqueous MEA were not represented correctly by the main data regressions because no data concerning CO_2 activity coefficients were included in the regression. CO_2 activity coefficients in MEA solutions were characterized outside of Aspen Plus® using experimental data (Browning and Weiland 1994; Hartono 2009). The regressed dependences (Equation 5.11) were implemented into the model by manually adjusting two electrolyte pair interaction parameters. Table 5.8 shows the obtained fit of the Aspen Plus® calculated CO_2 activity coefficient with the calculated CO_2 activity coefficient from Equation 5.11.

Table 5.8: Adjusted electrolyte pair interaction parameters to fit the CO_2 activity coefficient correlation (Equation 5.11)

	Component i	Component j	Value	Default Value
GMELCC	MEA+,MEACOO	CO2	-10.25	-8
GMELCE	MEA+,MEACOO	CO2	175	0

Table 5.9: CO_2 activity coefficient fit in the Aspen Plus® model for MEA solutions

MEA	CO_2 Loading	Temp	Calc γ_{CO2}[1]	Model γ_{CO2}	Calc γ_{CO2}[1]/Model γ_{CO2}
m	mol/mol_{alk}	C			
7	0.25	40	1.54	1.45	0.95
7	0.25	60	1.43	1.16	0.81
7	0.25	80	1.34	1.12	0.83
7	0.25	100	1.26	1.21	0.96
7	0.35	40	1.72	1.68	0.98
7	0.35	60	1.60	1.29	0.81
7	0.35	80	1.50	1.27	0.85
7	0.35	100	1.41	1.44	1.02
7	0.45	40	1.90	1.92	1.01
7	0.45	60	1.76	1.42	0.81
11	0.25	40	1.76	1.90	1.08
11	0.25	60	1.63	1.41	0.86
11	0.25	80	1.53	1.36	0.89
11	0.25	100	1.44	1.53	1.06
11	0.35	40	2.01	2.20	1.10
11	0.35	60	1.87	1.56	0.84
11	0.35	80	1.75	1.54	0.88
11	0.35	100	1.65	1.88	1.14
11	0.45	40	2.26	2.36	1.05
11	0.45	60	2.10	1.62	0.77
13	0.25	40	1.84	2.14	1.16
13	0.25	60	1.71	1.54	0.90
13	0.25	80	1.61	1.48	0.92
13	0.25	100	1.52	1.71	1.12
13	0.35	40	2.12	2.41	1.14
13	0.35	60	1.97	1.66	0.84
13	0.35	80	1.85	1.65	0.89
13	0.35	100	1.75	2.07	1.19
13	0.45	40	2.40	2.48	1.03
13	0.45	60	2.23	1.65	0.74

1 - Calculated from Equation 5.11

Adjusting the two parameters in Table 5.8 does not significantly affect the CO_2 partial pressure. Interaction parameters are implemented on a mole fraction basis and dissolved CO_2 concentrations are extremely small. CO_2 partial pressure is mainly dependent on interaction parameters such as $H_2O/MEA^+,MEACOO^-$ and $MEA/MEA^+,MEACOO^-$ since MEA and H_2O comprise the majority of the solvent mole fraction. Only interaction pairings containing CO_2 will be considered for the calculation of the CO_2 activity coefficient.

5.3.6 Physical Properties

Correctly representing density and viscosity in the model is particularly vital because they affect other parameters. Density values affect the thickness of the liquid film, which is important for the liquid film mass transfer coefficient. The density also affects the viscosity calculation so density parameters must be regressed before viscosity parameters. Viscosity parameters will have a strong effect on the diffusion coefficients of the species in solution. Diffusion coefficients are sometimes strongly tied to mass transfer rates, limiting mass transfer.

5.3.6.1 Density

Monoethanolamine density values were obtained from a correlation produced by Weiland (1998). MEA density values were calculated for 7, 9, 11, and 13 m MEA at loadings ranging from 0.1 to 0.5 at 0.05 increments. Densities were calculated at 40, 60, 80, and 100˚C.

Density values for the nonionic species (MEA, H_2O, CO_2) were determined using the Rackett liquid molar volume model. Density values for ionic species were determined using the Clarke liquid density model, which uses cation-anion pairing parameters. Detailed information and the equations used in these models can be found in the Aspen Plus® help files.

Since the Clarke liquid density model uses apparent electrolyte mole fractions, not every anion-cation species pairing needs to be regressed. Only the species combinations that include two significant species are important to predict density. The regressed density parameters for MEA are shown in Table 5.10.

Table 5.10: Regressed monoethanolamine density parameters

Parameter	Component i	Component j	Value (SI units)	Std Dev
RKTZRA/1	MEA		0.2403	0.0003
VLCLK/1	MEA+	MEACOO-	0.1311	0.0016
VLCLK/2	MEA+	MEACOO-	-0.0628	0.0075
VLCLK/1	MEA+	HCO3-	0.0568	0.0211
VLCLK/2	MEA+	HCO3-	0.1548	0.0977

Figures 5.52 and 5.53 show graphically how well the regressions fit 7 and 13 m MEA. For all cases, the fit is satisfactory.

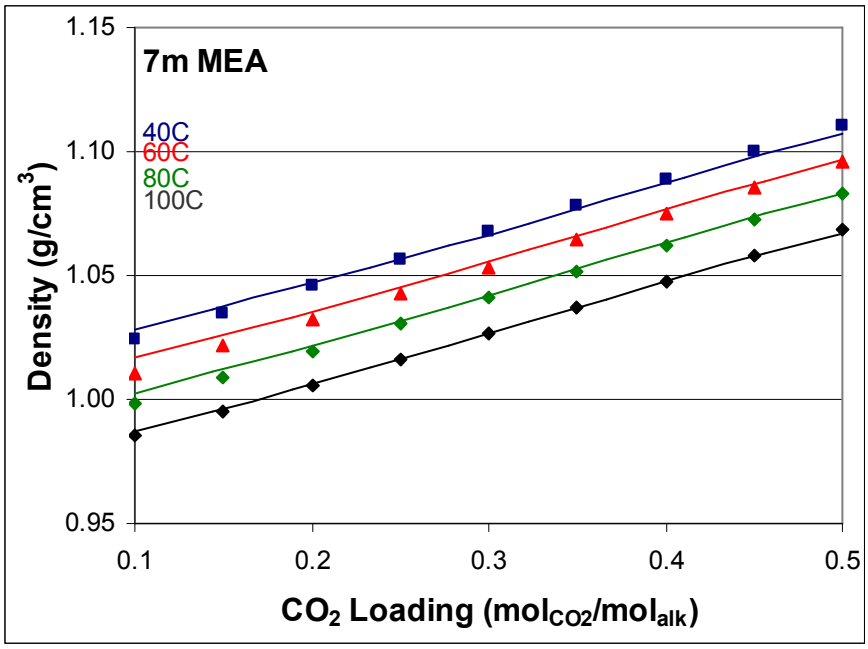

Figure 5.52: 7 m MEA density regression: points – Weiland correlation (1998), lines – Aspen Plus® regression

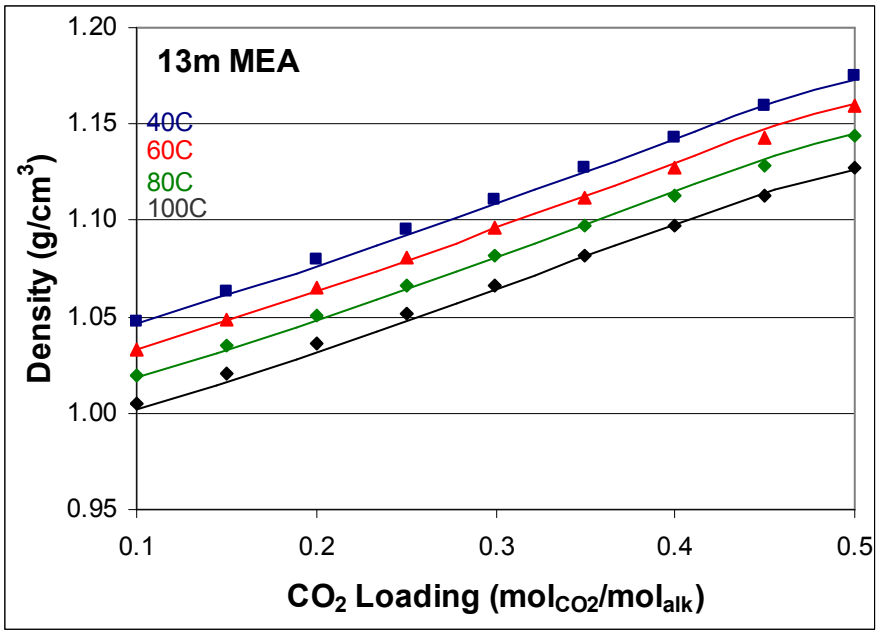

Figure 5.53: 13 m MEA density regression: points – Weiland correlation (1998), lines – Aspen Plus® regression

5.3.6.2 Viscosity

Monoethanolamine viscosity data for the regression were obtained from Weiland (1998) correlations. MEA viscosity values were calculated for 7, 9, 11, and 13 m MEA at 40, 60, 80, and 100˚C with loadings ranging from 0.2 to 0.5 at 0.05 increments.

Viscosity values for nonionic species are determined using the DIPPR liquid viscosity model. The Jones-Dole electrolyte model is used to account for the viscosity contributions of the ionic species. Table 5.11 summarizes the regressed viscosity parameters for the MEA system. Figures 5.54 and 5.55 show how well the regression matched the 7 and 13 m MEA data.

Table 5.11: Regressed monoethanolamine viscosity parameters

Parameter	Component i	Value (SI units)	Std Dev
IONMUB/1	MEA+	-23.57	4.09
IONMUB/1	MEACOO-	24.13	4.09
MULDIP/1	MEA	-43.21	3.38
MULDIP/2	MEA	13411	1087

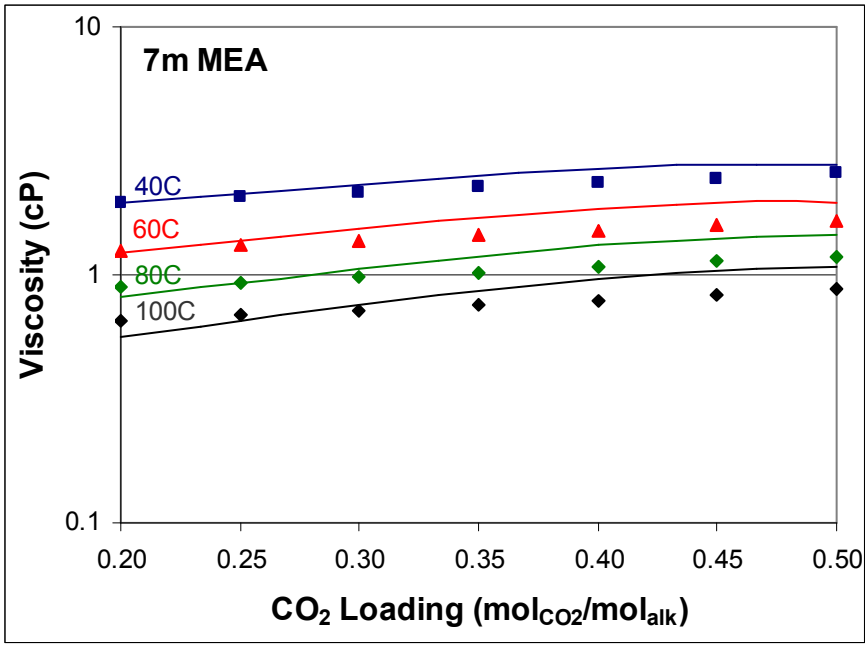

Figure 5.54: 7 m MEA viscosity regression: points – Weiland correlation (1998), lines – Aspen Plus® regression

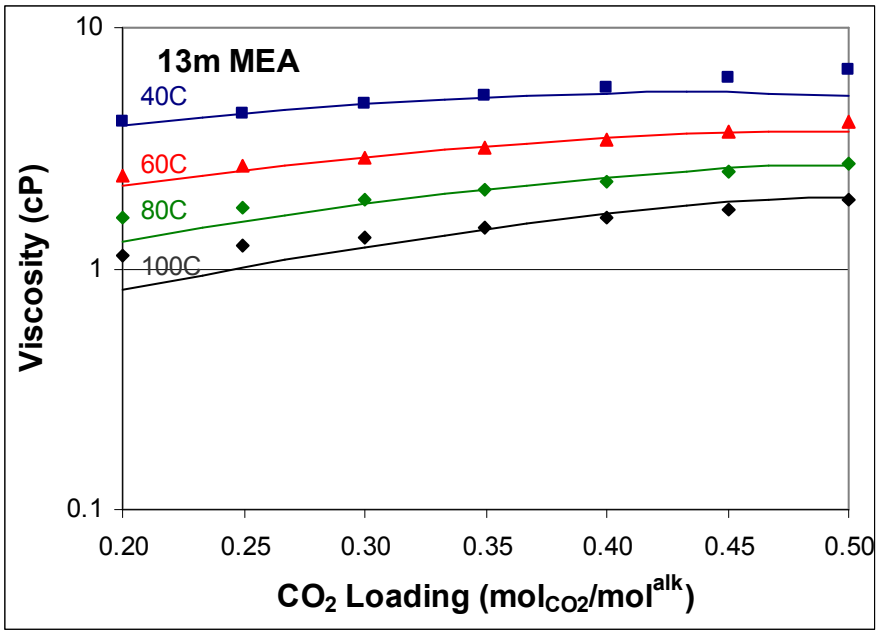

Figure 5.55: 13 m MEA viscosity regression: points – Weiland correlation (1998), lines – Aspen Plus® regression

5.3.7 Mass Transfer Coefficients

The gas and liquid film mass transfer coefficient correlations obtained from the wetted wall column were coded into a FORTRAN subroutine. This forced Aspen Plus® to use the same gas and liquid film mass transfer coefficients as the wetted wall column. k_g and k_l^o correlations are discussed in Section 3.2.2.

5.3.8 Reactions

The reactions for the MEA/CO_2/H_2O system are shown in Table 5.12. Two pairs of forward and reverse kinetic reactions and five equilibrium reactions were used.

Table 5.12: Kinetic and equilibrium reactions of the MEA/CO_2/H_2O system

Rxn No.	Reaction type	Stoichiometry
1	Kinetic	2 MEA + CO2 --> MEACOO- + MEA+
2	Kinetic	MEACOO- + MEA+ --> 2 MEA + CO2
3	Kinetic	MEA + CO2 + H2O --> MEACOO- + H3O+
4	Kinetic	MEACOO- + H3O+ --> MEA + CO2 + H2O
5	Equilibrium	2 H2O <--> H3O+ + OH-
6	Equilibrium	CO2 + 2 H2O <--> H3O+ + HCO3-
7	Equilibrium	HCO3- + H2O <--> H3O+ + CO3--
8	Equilibrium	MEA+ + H2O <--> MEA + H3O+
9	Equilibrium	MEACOO- + H2O <--> MEA + HCO3-

This analysis uses the same rate expression as the spreadsheet model but water catalysis was not ignored. The expression in Equation 5.50 is actually activity-based, not concentration-based. The ratio between k_{MEA} and k_{H2O} was set to 2192, based on termolecular rate constants in MEA solutions (Crooks and Donnellan 1989).

$$r_{CO2} = -\left(k_{MEA}[MEA] + k_{H2O}[H_2O]\right)\cdot[MEA]\cdot[CO_2] \qquad (5.50)$$

K_{eq} can be calculated by the activities of the species in each reaction when the solution is in equilibrium. At equilibrium, the total forward reaction must be equal to the reverse reaction. The K_{eq} is coupled with the activities of the species and the rate constants shown in Equation 5.51.

$$K_{eq} = \frac{k_f}{k_r} = \frac{a_{products}}{a_{reactants}} \qquad (5.51)$$

K_{eq} was calculated at 40, 60, 80, and 100˚C for each forward reaction. The temperature dependence of K_{eq} is shown in Equation 5.52. Calculated K_{eq} values can be fitted to this form accurately.

$$\ln K_{eq} = A + B/T + C\cdot\ln(T),\ T \text{ in (K)} \qquad (5.52)$$

Aspen Plus® uses a power law rate expression, as shown in Equation 5.53, where k is the pre-exponential constant, T is the temperature, T_0 is a reference temperature, E_A is the activation energy, and R is the gas constant.

$$r = k\left(\frac{T}{T_0}\right)^n \exp\left[\frac{-E_a}{R}\left(\frac{1}{T}-\frac{1}{T_0}\right)\right] \tag{5.53}$$

The equilibrium constant form relates to the power law rate expression. The A in the K_{eq} expression can be related to the rate constant while B and C can be related to E_a/R and n, respectively. A simple equation can be implemented inside a design specification in the model to ensure that the reverse rate expression is always thermodynamically consistent with the forward rate expression.

The activation energy was input as 44.9 kJ/mol, based on the value reported by Versteeg (1996). The reference temperature is 298.15 K. Fitting the rate constant to the data produced a value of 6.1×10^6 for the MEA catalysis reaction.

5.3.9 Model Results

Figures 5.56–5.58 show the error in the flux with respect to the MEA concentration, CO_2 loading, and temperature. The final model balances the negative and positive flux errors by adjusting the rate constant until the sum of the squares of the errors was minimized. The final pre-exponential rate constant obtained was $6.1 \cdot 10^6$ based on the form of Equation 5.53.

$$\sum\left(\frac{Flux_{model} - Flux_{meas}}{Flux_{meas}}\right)^2 \tag{5.54}$$

Not all the wetted wall column conditions have been plotted in Figures 5.56–5.58. Some conditions introduce large, expected errors so they were excluded from the analysis. Data points at the highest CO_2 loading, near 0.5, were excluded because the

model cannot accurately predict the correct free amine concentration after the CO_2 loading is adjusted to fit the partial pressure data. The 0.46 CO_2 loading data for 11 m MEA were retained in the analysis. At each experimental condition, six inlet CO_2 partial pressures were tested in the wetted wall column. This analysis only includes highest and lowest of the six inlet CO_2 partial pressures. Any points that had inlet CO_2 partial pressures within 25% of the equilibrium partial pressure were excluded. Also, 7 m MEA, 60˚C at 0.252 loading; 7 m MEA, 100˚C at 0.271 CO_2 loading; and 9 m MEA, 60˚C at 0.231 CO_2 loading were excluded from this analysis. Each of these conditions presented large changes in CO_2 loading when the partial pressure was matched. These errors resulted from a flattening of the CO_2 partial pressure curve at low CO_2 loading. The remaining wetted wall column conditions are examined in Figures 5.56–5.58.

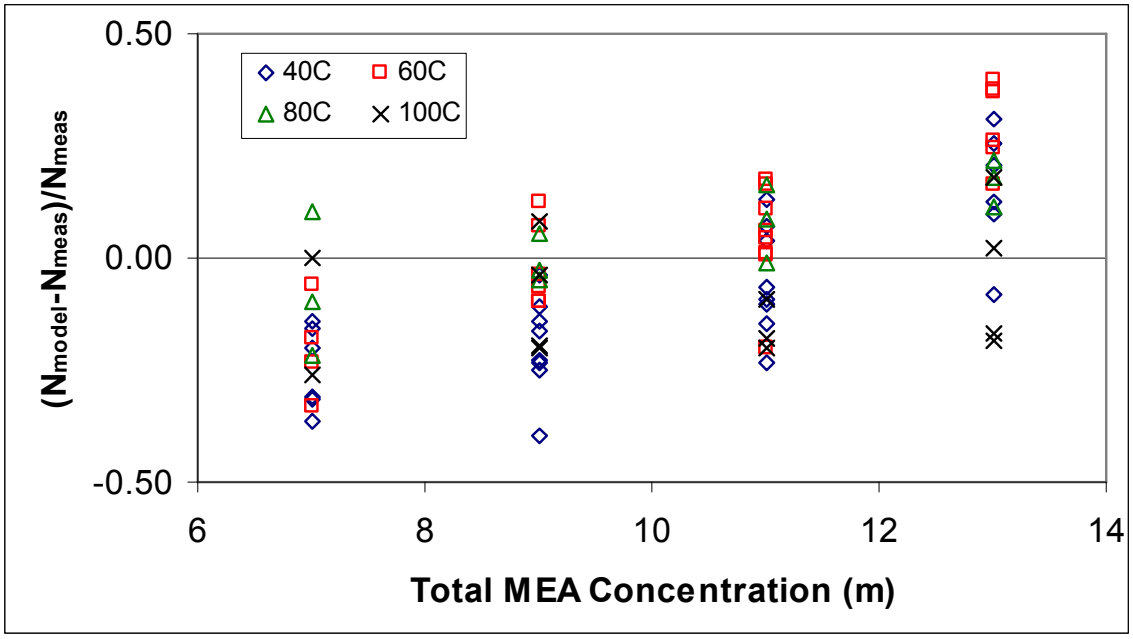

Figure 5.56: Aspen Plus® RateSep™ model error against total MEA concentration for wetted wall column experimental conditions

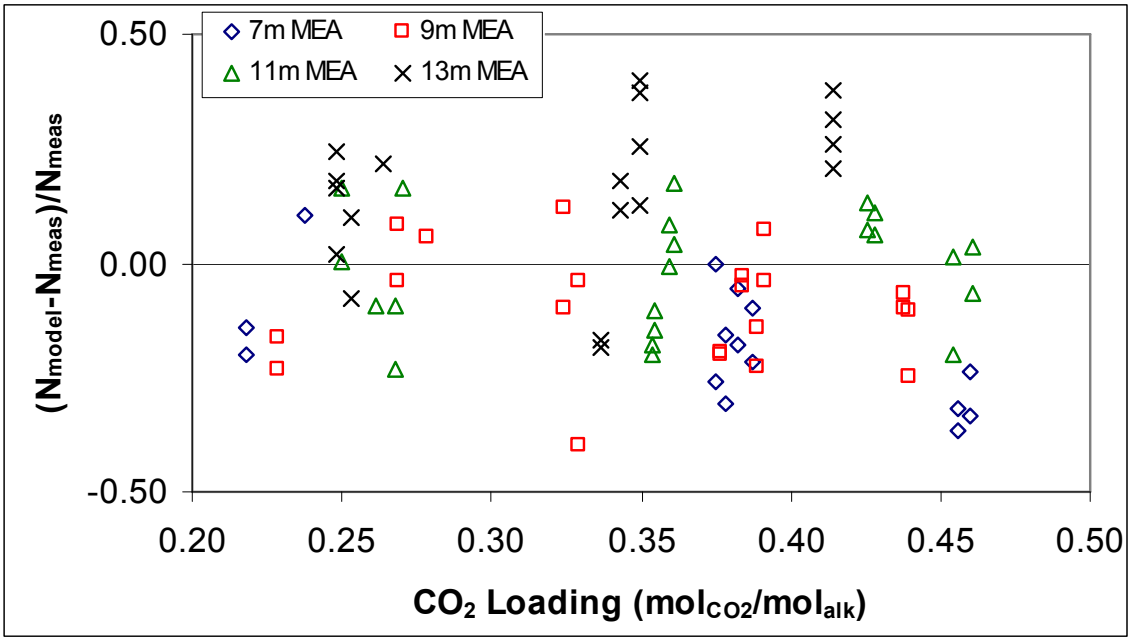

Figure 5.57: Aspen Plus® RateSep™ model error against CO_2 loading for wetted wall column experimental conditions

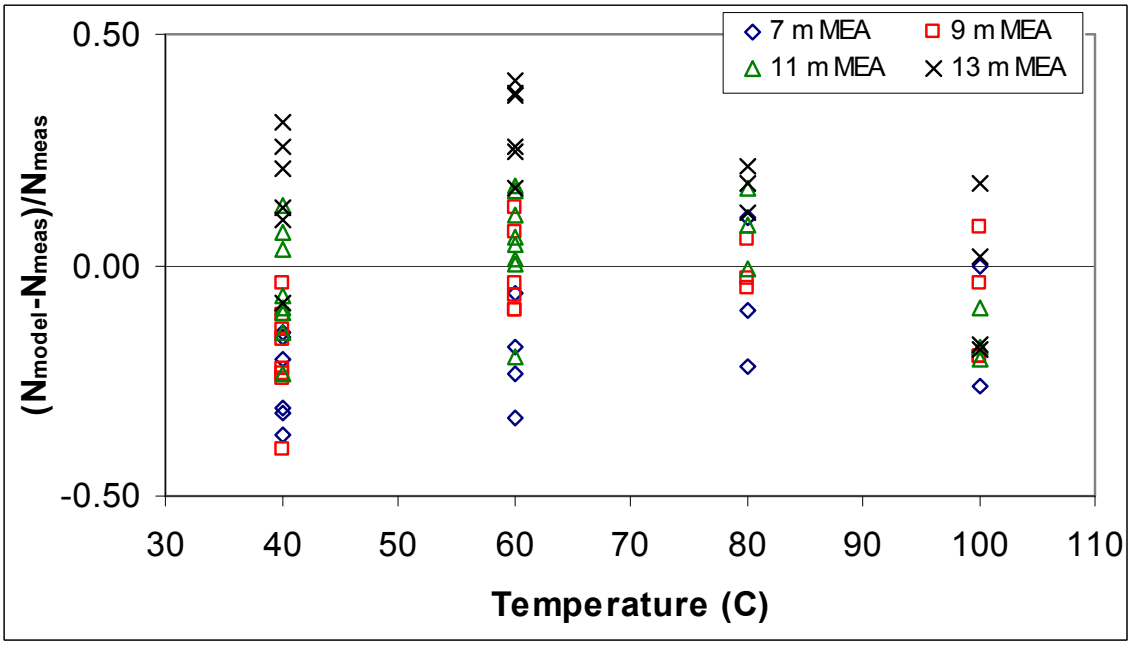

Figure 5.58: Aspen Plus® RateSep™ model error against temperature for wetted wall column experimental conditions

Errors in the flux calculated by the model are always within 50% of the wetted wall column measured fluxes. This is acceptable considering the magnitude of the flux varies about a factor of 100. Absorption and desorption runs are both considered. Model errors seem to spread evenly with changes in CO_2 loading and temperature. There is a significant systematic error in the predicted flux with changes in amine concentration.

The MEA model has a flaw in its ability to predict flux with changing MEA concentration because of an inability to regress MEA activity coefficients accurately. Figure 5.2, utilizing MEA volatility data from Hilliard (2008), showed that the MEA activity coefficient was independent of amine concentration. The spreadsheet model showed no systematic trend with MEA concentration, suggesting that MEA dependent parameters in the k_g' rate expression (Equation 5.48) are correct. Although the MEA volatility data had three times the emphasis of other data in the main MEA regression, the model still showed significant MEA concentration dependences in the MEA activity coefficient. Figure 5.59 includes the same conditions as Figure 5.2 but the activity coefficients are from the model rather than the modified Raoult's law equation.

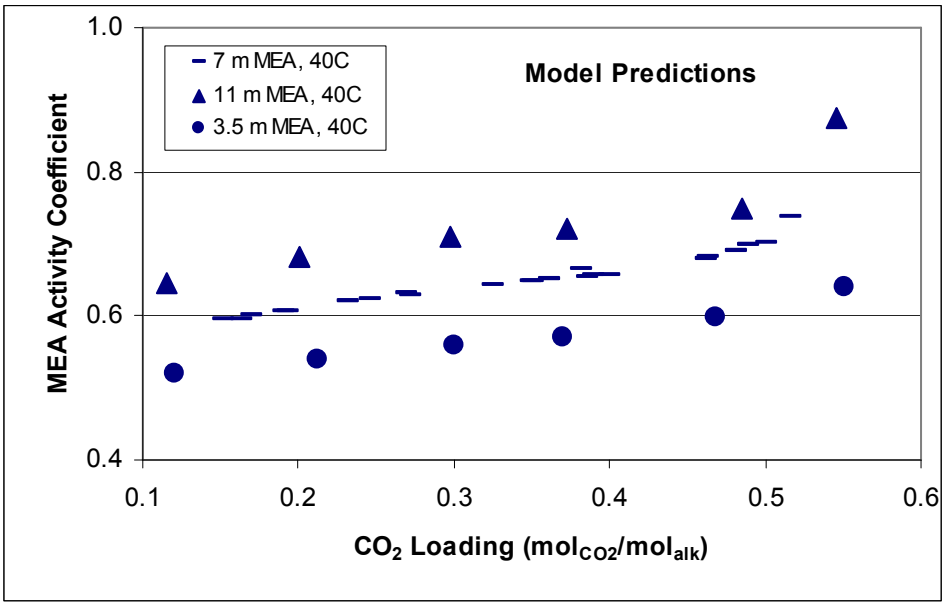

Figure 5.59: Aspen Plus® RateSep™ model prediction of MEA activity coefficients at MEA volatility experiment conditions tested by Hilliard

The increasing activity coefficient with increasing MEA concentration ensures that the model under-predicts rates at low MEA concentrations while overpredicting CO_2 mass transfer rates at the highest MEA concentrations.

Due to the limitation in representing the MEA activity coefficient, the RateSep™ model is most accurate when fine-tuned to one specific amine concentration. The error in the predicted flux seems to be about 25% for each amine concentration.

Chapter 6: Conclusions and Recommendations

This chapter is separated into 3 parts. The scope and methods state the tasks that were performed. The conclusions summarize the results and detail what was learned from this work. The recommendations provide suggestions and recommendations for future work.

6.1 SCOPE AND METHODS

Diffusion experiments were carried out in a diaphragm cell for 7, 9, and 13 m MEA and 2, 5, and 8 m PZ at 30˚C. Each experiment used solutions with a different CO_2 loading on each side of the glass frit. Changes in CO_2 loading were detected using density measurements. Measured changes in density are much more accurate than measured changes in CO_2 loading using the inorganic carbon analyzer. The membrane-cell integral diffusion coefficient, $\overline{D}$, was correlated with the viscosity of the amine solutions.

Wetted wall column experiments were conducted for 7, 9, 11, and 13 m MEA and 2, 5, 8, and 12 m PZ solutions. 7 m MEA/2 m PZ solutions were also tested. Experiments were performed at 40, 60, 80, and 100˚C. Generally, four CO_2 loadings were tested at 40 and 60˚C and two CO_2 loadings were tested at 80 and 100˚C. The wetted wall column can only measure CO_2 equilibrium partial pressures up to about 40 kPa, due to the maximum range of the available CO_2 analyzers. A total of 105 wetted wall column experiments were performed, each testing six inlet CO_2 partial pressures.

Each wetted wall column experiment obtained the equilibrium CO_2 partial pressure of the solution and the liquid film mass transfer coefficient, k_g'. k_g', not the rate constant, is the definitive measure of the reaction rate of an amine solution.

Spreadsheet modeling was performed for both MEA and PZ solutions. A rate expression and an expression for k_g' were developed from the experimental data. Each of the parameters in the k_g' expression was estimated based on literature data. Parameters that lacked literature data were estimated by extrapolating related data. The spreadsheet model was able to detail exactly how parameters in the k_g' expression and k_g' are affected by changes in temperature, CO_2 loading, and amine concentration.

An Aspen Plus® RateSep™ model was created for MEA systems based on the spreadsheet model and wetted wall column data. This model predicts CO_2 flux based on operating conditions. It can be scaled to industrial conditions to predict CO_2 mass transfer characteristics.

6.2 CONCLUSIONS

6.2.1 Diaphragm Cell Experiments

Diffusion coefficients in MEA and PZ vary to the 0.72±0.12 power of viscosity. This value was obtained by measuring diffusion coefficients in 7, 9, and 13 m MEA and 2, 5, and 8 m PZ at 30˚C over a wide range of CO_2 loading. Literature generally reports diffusion coefficients that vary to the 0.8 power of viscosity for N_2O and the 0.6 power for amine solutes (Versteeg and Van Swaaij 1988; Snijder, te Riele et al. 1993). The 0.72 power of viscosity is based on the measured membrane-cell integral diffusion coefficient, $\overline{D}$, which is a complex concentration and time-averaged value, different from the fundamental diffusion coefficient, D.

The diffusion coefficient-viscosity curve for MEA and PZ solutions extrapolates favorably to the reported diffusion coefficient of 1 M PZ (Sun, Yong et al. 2005).

The spreadsheet models implement a 0.72 power of viscosity on the diffusion coefficient.

6.2.2 Wetted Wall Column Experiments

MEA solutions below 0.45 CO_2 loading and all tested PZ solutions (0.21–0.41 CO_2 loading) exhibit equilibrium CO_2 partial pressures independent of amine concentration. The partial pressure is strictly a function of the temperature and CO_2 loading for each system. Wetted wall column experiments and Hilliard (2008) both show an effect of total MEA concentration at very high loading. Aqueous MEA at high CO_2 loading exhibits increasing CO_2 partial pressures with increasing amine concentration. Near 0.5 CO_2 loading, bicarbonate should be present in significant concentrations. Theory suggests that the CO_2 equilibrium partial pressure should be independent of total amine concentration for carbamate production but not for bicarbonate production (Appendix D).

CO_2 equilibrium partial pressures measurement from the wetted wall column in MEA, PZ, and MEA/PZ match literature data very well (Jou, Mather et al. 1995; Ermatchkov, Perez-Salado Kamps et al. 2006a; Hilliard 2008). Only the 40˚C MEA experiments at the highest CO_2 loading seem to deviate from the literature data. Hilliard (2008) shows the same trend, where higher amine concentration solutions have higher CO_2 partial pressures. However, the measured equilibrium partial pressures at 40˚C do not match the magnitude of the Hilliard (2008) and Jou (1995) measurements.

8 m PZ exhibits a 70% greater CO_2 capacity than 7 m MEA and a 50% greater CO_2 capacity than 11 m MEA. The CO_2 capacity is the difference in CO_2 concentrations between lean and rich solutions, the amount of CO_2 removed from the system per unit of solvent. The majority of the increased CO_2 capacity is due to the fact that each mole of piperazine has two functional nitrogen groups. This allows PZ to react twice in the CO_2 reaction, whereas MEA can only react once. Over the 5000–100 Pa operating range at 40˚C, 7 m MEA, 11 m MEA, and 8 m PZ have CO_2 capacities of 0.85, 0.93, and 1.41 mol_{CO2}/kg(water+amine).

The liquid film mass transfer coefficient, k_g', in aqueous MEA is essentially independent of temperature and the total amine concentration in the wetted wall column. The CO_2 loading of the solution dictates k_g'. k_g' varies about a factor of 30 in aqueous MEA with 0.23–0.50 CO_2 loading. The decreased rate is primarily due to the decrease in free amine concentration at higher CO_2 loading.

k_g' in aqueous PZ is independent of temperature and total amine concentration at lower temperatures and constant CO_2 loading in the wetted wall column. 100˚C data points fall below the other k_g' values at low and intermediate CO_2 loadings. At intermediate CO_2 loadings, the drop in the 100˚C rate data is more pronounced. At intermediate CO_2 loading, 80˚C k_g' values also drop below those at lower temperatures. 60˚C k_g' values fall slightly below the 40˚C k_g' values at the highest CO_2 loadings. k_g' ranges about a factor of 20 in aqueous PZ with 0.21–0.41 CO_2 loading.

A drop in k_g' at higher temperature and CO_2 loading is not unexpected, especially for PZ, since it is the faster reacting amine. High temperature and CO_2 loading conditions should encounter more diffusion resistance due to less free amine and a greater slope of the equilibrium line. Diffusion resistances in wetted wall column

experiments with MEA are typically minor. This is not the case for the faster reacting PZ solutions in the wetted wall column. When diffusion resistances become significant, k_g' becomes apparatus dependent. The wetted wall column has a 9.1 cm contactor which produces a 9.1 cm laminar flow path. Amine solutions in either structured or random packed columns will have laminar flow paths significantly shorter than 9.1 cm, yielding larger physical mass transfer coefficients. Industrial columns should not exhibit these drastic drops in k_g' with increasing temperature and CO_2 loading.

Experimental results show that PZ is 2–3 times faster than MEA. This means that to a first approximation 1/2 to 2/3 less column packing would be required for PZ compared to MEA. Both MEA and PZ rate data match well with applicable literature data.

6.2.3 Modeling

6.2.3.1 Spreadsheet Modeling

Wetted wall column experiments show that CO_2 reaction rates in both aqueous MEA and PZ are second order in amine when presented on an activity basis. These activity-based rate expressions were implemented into shell balance equations to produce pseudo first order rate expressions. Implementing diffusion resistances into the pseudo first order rate expressions using film theory provides the following k_g' expressions for MEA and PZ solutions.

$$\frac{1}{k_g^{'}} = \frac{\gamma_{CO2}^{0.5} H_{CO2,H2O}}{\sqrt{k\gamma_{MEA}^{2}[MEA]^{2} D_{CO2}}} + \frac{1}{k_{l,prod}^{o}}\left(\frac{\Delta P_{CO2}^{*}}{\Delta[CO_2]_T}\right) \qquad (6.1)$$

$$\frac{1}{k_g^{'}} = \frac{\gamma_{CO2}^{0.5} H_{CO2,H2O}}{\sqrt{\begin{pmatrix} k_{PZ}\gamma_{PZ}^2[PZ]^2 + k_{PZ}\gamma_{PZ}[PZ]\gamma_{PZCOO}[PZCOO^-] \\ + k_{PZCOO}\gamma_{PZCOO}[PZCOO^-]\gamma_{PZ}[PZ] \\ + k_{PZCOO}\gamma_{PZCOO}^2[PZCOO^-]^2 \end{pmatrix} D_{CO2}}} + \frac{1}{k_{l,prod}^{o}}\left(\frac{\Delta P_{CO2}^{*}}{\Delta[CO_2]_T}\right) \quad (6.2)$$

Each parameter in Equations 6.1 and 6.2 was estimated from literature data. In some cases, literature data could not be used and assumptions were required. The activity coefficient of MEA was obtained from MEA volatility data (Hilliard 2008). The activity coefficients of PZ and $PZCOO^-$ were obtained from the thermodynamic model of Hilliard (2008). Free MEA, PZ, and $PZCOO^-$ concentrations were also obtained from the Hilliard model (2008). The activity coefficient of CO_2 in both MEA and PZ solutions was obtained from N_2O solubility data in MEA (Browning and Weiland 1994; Hartono 2009). In the case of PZ, the CO_2 loading in the CO_2 solubility equation was multiplied by two to make the equation a better indicator of the total CO_2 concentration. The diffusion coefficient of CO_2 was obtained from a D_{CO2} correlation in water (Versteeg, Van Dijck et al. 1996) in conjunction with 0.72 viscosity exponent obtained using diaphragm diffusion cell experiments. The Henry's solubility of CO_2 in water was obtained by correlating literature data (Versteeg and Van Swaaij 1988). The liquid phase mass transfer coefficient of the reactants and products, $k_{l,prod}^{0}$, was calculated using a theoretical model by Pigford (1941). The slope of the equilibrium line was obtained by taking the derivative of the CO_2 partial pressure expressions developed by Xu (Rochelle, Chen et al. 2009b). $PZCOO^-$ rate constants were set to 70% of the value of the PZ rate constant based on work by Cullinane (2006). The temperature dependence of the MEA rate constant was obtained from a review of literature data (Versteeg, Van Dijck et al. 1996). The temperature dependence of the PZ rate constant was obtained from Cullinane (2006). The pre-exponential value in k_{MEA} and k_{PZ} were adjusted to fit the experimental data.

These two pre-exponential rate constants and the assertion of termolecular kinetics are the only parameters that were adjusted to match experimental data. Experimental trends with CO_2 loading, amine concentration, or temperature cannot be fitted by these adjusted parameters. These trends are predicted by the estimated parameters in Equations 6.1 and 6.2.

The literature-based parameter estimations in Equations 6.1 and 6.2 account for the offsetting temperature and amine concentration effects on k_g'. These trends are predicted by the literature data, not fitted by the model.

Equation 6.1 represents the measured k_g' in aqueous MEA with an average error of 13%. Equation 6.2 represents the measured k_g' in aqueous PZ with an average error of 19%. The k_g' representations are excellent considering k_g' can vary up to a factor of 20–30 over the range of experimental conditions. Since the k_g' representations are accurate, the representation of each of the parameters in Equations 6.1 and 6.2 are likely accurate. The determination of k_g' has been fully explained in both MEA and PZ systems using literature data to estimate the parameters in Equation 6.1 and 6.2. Other amine systems can likely be explained similarly.

6.2.3.2 Aspen Plus® RateSep™ Modeling

An Aspen Plus® RateSep™ model was created to model the CO_2 flux for 7-13 m MEA systems. The absorber/stripper model consists of a single column based on the wetted wall column. The model makes use of the sequential regression technique and regressed binary system parameters from Hilliard (2008). Parameters for the tertiary system ($MEA/H_2O/CO_2$) were re-regressed with updated data and fewer regressed parameters.

The main MEA data regression succeeds in accurately predicting CO_2 partial pressure in 7 m MEA. At higher MEA concentrations, the fit get progressively worse. The CO_2 loading of inlet conditions was adjusted to produce an exact match to the wetted wall column measured equilibrium partial pressure. The error introduced by changing the free amine concentration is much smaller than the error introduced by having erroneous driving forces.

Parameters that control the CO_2 activity coefficient in the solution were manually adjusted to produce values that mimic the CO_2 solubility expression (Equation 5.11) based on literature data (Browning and Weiland 1994; Hartono 2009).

The gas and physical liquid film mass transfer coefficient correlations used for the wetted wall column were coded into a FORTRAN subroutine. This causes Aspen Plus® to use the same gas and liquid film mass transfer coefficients as the wetted wall column.

Two pairs of forward and reverse kinetic reactions and five equilibrium reactions were used in the model. The forward rate constants were dynamically linked to each other based on a termolecular evaluation (Crooks and Donnellan 1989). The reverse reaction rates were dynamically linked to the forward rate expressions using design specifications to ensure that the equilibrium constant, K_{eq}, is not violated. The lone independent rate constant was adjusted until the model matched wetted wall column results.

Overall, the model predicts the CO_2 flux within about 40%. The model does not properly account for the MEA activity coefficient with changing amine concentration. This introduces error with changing amine concentration. At each amine concentration the fit can be improved to about ±25%.

6.3 RECOMMENDATIONS

The diaphragm diffusion cell experiments are not as accurate as desired. These experiments also take a significant amount of time, about two weeks each. Experiments at very viscous conditions, such as 12 m PZ, failed and were not reported. Another method to determine diffusion coefficients, such as the Taylor dispersion method used by Hamborg (2008), should prove more accurate and much faster. This technique would allow for the measurement of N_2O over a much wider range of conditions with greater accuracy.

One weakness in the PZ spreadsheet model is the representation of the PZ and $PZCOO^-$ activity coefficients. Results from the Hilliard (2008) model were used. Although the model properly represents the PZ data, more confidence could be placed in amine activity coefficients if these parameters could be directly supported by literature data. Maybe some experiments can be designed to quantify PZ and $PZCOO^-$ activity coefficients.

Another weakness of the PZ spreadsheet model deals with the physical solubility of CO_2 in aqueous PZ. The model assumed a similar behavior to MEA because no data has been published for N_2O solubility in concentrated, CO_2 loaded piperazine solutions. N_2O solubility experiments in PZ and other amine solutions would be useful. Ideally, these experiments would include high amine concentrations at wide temperature ranges and relevant CO_2 loading.

The Aspen Plus® RateSep™ model was unable to produce MEA activity coefficients independent of the total amine concentration. This inability introduces inaccuracies at varying amine concentrations. More flexibility or a workaround in Aspen Plus® to solve this problem would be useful.

From a rate and capacity perspective, PZ is a much better solvent than MEA. A comprehensive study should be performed to see if using concentrated PZ (5–8 molal) would produce significant energy and capital cost savings in a CO_2 capture system.

Appendix A: Nomenclature

This appendix includes all the shorthand nomenclature used throughout the dissertation. The nomenclature is organized alphabetically. Greek symbols are included at the end.

*	equilibrium
A	gas-liquid contact area
alk	alkalinity
Am	amine
$[Am]_b$	concentration of amine in the bulk solution
AMP	2-amino-2-methyl-l-propanol
b	bulk
B	base
C	celsius
cP	centipoise
d	hydraulic diameter (outside diameter minus inside diameter)
$\overline{D}$	membrane-cell integral diffusion coefficient
D_{CO2}	diffusion coefficient of CO_2

DEA	diethanolamine
DGA	diglycolamine
e	equilibrium
FTIR	Fourier transform infrared spectroscopy
g	gravity
h	hour
h	height
H_{CO2}	Henry's constant – CO_2 solubility in solution
$H_{CO2,H2O}$	Henry's constant – CO_2 solubility in water
H_{CO3}^{-}	bicarbonate
i	interface
IR	infrared
k	rate constant
K	Kelvin
K_a	equilibrium constant of acid dissociation with water
k_b	rate constant of the base protonation
k_f	forward rate constant
kg	kilogram
K_G	overall mass transfer coefficient (gas phase units)
k_g	gas film mass transfer coefficient

k_g'	liquid film mass transfer coefficient (gas phase units)
k_g''	pseudo first order liquid film mass transfer coefficient (gas phase units)
k_{H2O}	rate constant of water protonation
k_l	liquid film mass transfer coefficient
k_l^o	liquid film physical mass transfer coefficient
k_{MEA}	rate constant of MEA protonation
kPa	kilopascal
k_r	reverse rate constant
l	liter
Ldg	CO_2 loading
lm	log mean
m	molality (mol/kg water)
m	meter
M	molarity (mol/l solution)
M_b	molecular weight of component b
MDEA	methyldiethanolamine
MEA	monoethanolamine
min	minute
mol	mole

mol_{alk}	moles of alkalinity (moles of functional amine groups, 1 mol MEA = 1 mol_{alk}, 1 mol PZ = 2 mol_{alk})
MOR	morpholine
MW	molecular weight
N_{CO2}	flux of CO_2
OH^-	hydroxide ion
P	pressure
Pa	Pascal
P_{CO2}	partial pressure of CO_2
$P_{CO2,i}$	partial pressure of CO_2 at the gas-liquid interface
$P^*_{CO2,b}$	equilibrium CO_2 partial pressure of the bulk solution
pK_a	$-\log_{10} K_a$
PFO	pseudo first order
prod	products
psig	pounds per square inch gauge
PZ	piperazine
$PZCOO^-$	piperazine carbamate
PZH^+	protonated piperazine
Q	flow rate
R	ideal gas constant

r_{CO2}	rate of CO_2 formation
RDint	reaction-diffusion interface
Re	Reynolds number
s	second
Sc	Schmidt number
Sh	Sherwood number
St	stokes
t	time
T	temperature
T	total
T_{ref}	reference temperature
u	velocity
V_a	molar volume of component A
W	circumference
wt%	weight percent
x	nominal rotameter reading
x_{MEA}	liquid mole fraction of MEA
y_{MEA}	gas mole fraction of MEA

Greek symbols

α	CO_2 loading
β	cell constant
γ	activity coefficient
δ	film thickness
η	viscosity
η	dimensionless penetration distance
Θ	dimensionless driving force
μ	viscosity
ρ	density
Ψ	association parameter in Wilke-Chang equation
ω	mass fraction amine
Ω	mass percentage of the amine

Appendix B: Detailed Diaphragm Cell Data

This appendix includes all the data from the diaphragm cell experiments required to recalculate the membrane-cell integral diffusion coefficient, $\overline{D}$. The initial CO_2 loading and measured density at 20˚C are shown for the solutions in the top and bottom chambers of the cell. The final density was measured at 20˚C after conclusion of the experiment. Assuming a linear density-CO_2 loading relationship, justified by density measurements by Freeman (Rochelle, Dugas et al. 2008), the final CO_2 loading was calculated. Table B.1 also includes the cell constant. Two different diaphragm cells were used in the experiments. Each was calibrated with a KCl solution to determine the cell constant.

Table B.1: Detailed diaphragm cell data

Solution	Initial CO_2 Loading		Initial Density		Final Density		Final CO_2 Loading		T	Time	β	$\overline{D}$
	mol/mol_{alk}		g/cm^3 @ 20˚C		g/cm^3 @ 20˚C		mol/mol_{alk}		˚C	s	$1/m^2$	m^2/s
	Top	Bottom	Top	Bottom	Top	Bottom	Top	Bottom				
7 m MEA	0.246	0.347	1.0656	1.1125	1.0736	1.1039	0.2632	0.3285	30	849300	2306	2.23E-10
	0.448	0.548	1.1012	1.1169	1.1061	1.1118	0.4792	0.5155		940200	2306	4.67E-10
9 m MEA	0.250	0.351	1.0779	1.1002	1.0800	1.0977	0.2595	0.3397		335880	1878	3.66E-10
	0.444	0.488	1.1205	1.1286	1.1214	1.1274	0.4489	0.4815		496188	1878	3.22E-10
13 m MEA	0.159	0.313	1.0623	1.0839	1.0686	1.0780	0.2039	0.2709		939900	2306	3.84E-10
2 m PZ	0.240	0.316	1.0398	1.0499	1.0410	1.0485	0.2490	0.3055		259200	1878	6.11E-10
	0.352	0.411	1.0550	1.0626	1.0564	1.0607	0.3629	0.3963		523800	1878	5.79E-10
5 m PZ	0.252	0.320	1.0826	1.0998	1.0843	1.0973	0.2587	0.3101		596700	1878	2.50E-10
	0.334	0.388	1.1065	1.1193	1.1096	1.1161	0.3471	0.3745		1108200	2306	2.65E-10
8 m PZ	0.253	0.289	1.1170	1.1312	1.1184	1.1301	0.2566	0.2862		853800	1878	1.21E-10
	0.342	0.406	1.1432	1.1619	1.1457	1.1595	0.3506	0.3978		1472700	2306	8.95E-11

Appendix C: Detailed Wetted Wall Column Data

This appendix includes all the relevant data obtained from the wetted wall column experiments. The following tables include amine concentration, CO_2 loading, equilibrium CO_2 partial pressure, temperature, pressure, gas and liquid flow rates, equilibrium inlet and outlet CO_2 partial pressures, and mass transfer coefficients. K_G/k_g represents the fractional gas film resistance of the experiment. Experiments were designed be less than 50% gas film controlled. The following tables also include the solvent flow rate and $k^o_{l,prod}$.

For aqueous MEA, density and viscosity correlations, required to calculate the liquid flow rate and physical liquid film mass transfer coefficient, were obtained from Weiland (1998). The Weiland correlations are valid up to 40 wt% amine, 0.6 CO_2 loading, and 120˚C. 13 m MEA data (44.3 wt%) are extrapolated.

Piperazine density data was obtained by regressing 2–12 m PZ density measurements at 20, 40, and 60˚C from Freeman (Rochelle, Chen et al. 2009a). PZ solution viscosity values were obtained by regressing 5–12 m PZ viscosity measurements at 25, 40, and 60˚C from Freeman (Rochelle, Sexton et al. 2008a). Details on the PZ density and viscosity regressions are included in Appendix E.

MEA/PZ density and viscosity data have not been compiled into density and viscosity regressions. 7 m MEA/2 m PZ solutions were assumed to follow the Weiland (1998) density predictions for 37.5 wt% MEA. 7 m MEA/2 m PZ solutions are 37.5 wt%

amine. No attempt has been made to estimate 7 m MEA/2 m PZ viscosities at wetted wall column experimental conditions. Therefore, $k^{o}_{l,prod}$ has not been calculated.

Table C.1: Detailed wetted wall column data – 7 m MEA

MEA	CO_2 Ldg	P^*_{CO2}	Temp	Pres	Gas_{Dry}	Gas	Liquid	$P_{CO2,in,dry}$	$P_{CO2,in,wet}$	$P_{CO2,out,dry}$	$P_{CO2,out,wet}$	$k^o_{l,prod}$	CO_2 Flux	K_G	k_g	K_G/k_g	k_g'
m	mol/mol_{alk}	Pa	C	psig	Std l/min	Std l/min	ml/s	Pa	Pa	Pa	Pa	m/s	$mol/s \cdot m^2$	$mol/s \cdot Pa \cdot m^2$	$mol/s \cdot Pa \cdot m^2$		$mol/s \cdot Pa \cdot m^2$
7	0.252	15.7	40	20	5.0	5.16	3.2	0	0	6	6	4.6E-05	-2.42E-05	1.93E-06	4.57E-06	0.42	3.34E-06
								10	10	12	12		-9.28E-06				
								20	19	19	19		3.23E-06				
								30	29	24	23		2.42E-05				
								40	39	31	30		3.55E-05				
								50	48	38	37		4.96E-05				
7	0.351	77	40	20	5.0	5.16	3.2	0	0	20	19	4.4E-05	-8.07E-05	1.07E-06	4.57E-06	0.23	1.40E-06
								60	58	65	63		-2.02E-05				
								120	116	109	106		4.44E-05				
								180	174	154	149		1.05E-04				
								240	233	204	198		1.45E-04				
								300	291	252	244		1.94E-04				
7	0.432	465	40	45	5.0	5.09	3.1	0	0	105	103	4.2E-05	-2.46E-04	5.93E-07	2.63E-06	0.23	7.66E-07
								200	196	262	257		-1.45E-04				
								400	393	413	406		-3.05E-05				
								600	589	570	560		7.04E-05				
								800	786	730	717		1.64E-04				
								1000	982	885	869		2.70E-04				
7	0.496	4216	40	60	5.0	5.07	3.1	800	789	1300	1281	4.1E-05	-9.37E-04	2.98E-07	2.09E-06	0.14	3.47E-07
								1600	1577	1995	1966		-7.41E-04				
								2400	2366	2665	2627		-4.97E-04				
								3200	3154	3370	3322		-3.19E-04				
								4000	3943	4025	3967		-4.69E-05				
								5000	4928	4900	4830		1.87E-04				
7	0.252	109	60	20	5.0	5.45	3.2	0	0	43	39	5.9E-05	-1.74E-04	1.82E-06	4.83E-06	0.38	2.92E-06
								60	55	79	72		-7.67E-05				
								120	110	117	107		1.21E-05				
								180	165	158	145		8.88E-05				
								240	220	200	183		1.61E-04				
								300	275	240	220		2.42E-04				
7	0.351	660	60	20	5.0	5.45	3.2	0	0	175	160	5.7E-05	-7.06E-04	1.26E-06	4.83E-06	0.26	1.70E-06
								300	275	405	371		-4.24E-04				
								600	550	635	582		-1.41E-04				
								900	825	855	784		1.82E-04				
								1200	1100	1080	990		4.84E-04				
								1500	1375	1305	1196		7.87E-04				

Table C.2: Detailed wetted wall column data – 7 m MEA

MEA	CO_2 Ldg	P^*_{CO2}	Temp	Pres	Gas_{Dry}	Gas	Liquid	$P_{CO2,in,dry}$	$P_{CO2,in,wet}$	$P_{CO2,out,dry}$	$P_{CO2,out,wet}$	$k^o_{l,prod}$	CO_2 Flux	K_G	k_g	K_G/k_g	k_g'
m	mol/mol_{alk}	Pa	C	psig	Std l/min	Std l/min	ml/s	Pa	Pa	Pa	Pa	m/s	$mol/s \cdot m^2$	$mol/s \cdot Pa \cdot m^2$	$mol/s \cdot Pa \cdot m^2$		$mol/s \cdot Pa \cdot m^2$
7	0.432	3434	60	45	5.0	5.25	3.1	0	0	890	847	5.4E-05	-2.09E-03	6.92E-07	2.72E-06	0.25	9.28E-07
								1250	1189	1820	1732		-1.34E-03				
								2500	2379	2760	2626		-6.10E-04				
								3750	3568	3730	3549		4.69E-05				
								5000	4758	4660	4434		7.98E-04				
								6250	5947	5600	5329		1.52E-03				
7	0.496	16157	60	60	5.0	5.20	3.1	0	0	2500	2403	5.3E-05	-4.69E-03	3.20E-07	2.16E-06	0.15	3.76E-07
								8000	7690	9250	8892		-2.34E-03				
								16000	15381	16250	15621		-4.69E-04				
								24000	23071	23000	22110		1.87E-03				
								32000	30761	29700	28550		4.31E-03				
								40000	38452	36400	34991		6.75E-03				
7	0.271	1053	80	25	5.0	6.05	2.8	0	0	410	339	6.7E-05	-1.45E-03	1.77E-06	4.64E-06	0.38	2.85E-06
								300	248	640	529		-1.20E-03				
								600	496	845	699		-8.64E-04				
								900	744	1040	860		-4.94E-04				
								1200	992	1220	1009		-7.06E-05				
								1500	1240	1410	1166		3.17E-04				
7	0.366	4443	80	30	5.0	5.91	2.7	0	0	1470	1244	6.4E-05	-4.61E-03	1.28E-06	4.04E-06	0.32	1.87E-06
								2000	1692	2970	2513		-3.04E-03				
								4000	3385	4450	3766		-1.41E-03				
								6000	5077	5800	4908		6.27E-04				
								8000	6770	7150	6051		2.66E-03				
								10000	8462	8600	7278		4.39E-03				
7	0.271	5297	100	40	5.0	6.84	2.8	0	0	2700	1974	8.7E-05	-6.91E-03	1.66E-06	3.76E-06	0.44	2.98E-06
								4000	2925	5150	3766		-2.94E-03				
								8000	5850	7750	5667		6.40E-04				
								12000	8775	10450	7642		3.97E-03				
								16000	11700	12600	9214		8.71E-03				
								20000	14625	15100	11042		1.25E-02				
7	0.366	19008	100	55	5.0	6.34	2.8	0	0	7700	6076	8.2E-05	-1.55E-02	9.30E-07	2.77E-06	0.34	1.40E-06
								7500	5918	12100	9548		-9.24E-03				
								15000	11837	17900	14125		-5.83E-03				
								22500	17755	23100	18228		-1.21E-03				
								30000	23673	27900	22016		4.22E-03				
								37500	29591	33600	26514		7.84E-03				

Table C.3: Detailed wetted wall column data – 9 m MEA

MEA	CO_2 Ldg	P^*_{CO2}	Temp	Pres	Gas_{Dry}	Gas	Liquid	$P_{CO2,in,dry}$	$P_{CO2,in,wet}$	$P_{CO2,out,dry}$	$P_{CO2,out,wet}$	$k^o_{l,prod}$	CO_2 Flux	K_G	k_g	K_G/k_g	k_g'
m	mol/mol_{alk}	Pa	C	psig	Std l/min	Std l/min	ml/s	Pa	Pa	Pa	Pa	m/s	$mol/s \cdot m^2$	$mol/s \cdot Pa \cdot m^2$	$mol/s \cdot Pa \cdot m^2$		$mol/s \cdot Pa \cdot m^2$
9	0.231	10.4	40	20	5.0	5.16	3.2	0	0	5	4	4.0E-05	-1.82E-05	2.70E-06	4.57E-06	0.59	-
								10	10	11	10		-3.23E-06				
								20	19	16	16		1.49E-05				
								30	29	21	20		3.79E-05				
								40	39	26	25		5.77E-05				
								50	48	35	33		6.26E-05				
9	0.324	34	40	20	5.0	5.16	3.2	0	0	14	14	3.8E-05	-5.65E-05	1.32E-06	4.57E-06	0.29	1.86E-06
								60	58	54	52		2.42E-05				
								120	116	93	90		1.09E-04				
								180	174	134	130		1.86E-04				
								240	233	186	180		2.18E-04				
								300	291	232	225		2.74E-04				
9	0.382	107	40	20	5.0	5.16	3.1	0	0	26	25	3.7E-05	-1.05E-04	1.07E-06	4.57E-06	0.23	1.40E-06
								60	58	71	69		-4.44E-05				
								120	116	117	113		1.21E-05				
								180	174	164	159		6.46E-05				
								240	233	210	204		1.21E-04				
								300	291	258	250		1.70E-04				
9	0.441	417	40	45	5.0	5.09	3.1	0	0	105	103	3.5E-05	-2.46E-04	6.34E-07	2.63E-06	0.24	8.36E-07
								200	196	260	255		-1.41E-04				
								400	393	390	383		2.35E-05				
								600	589	555	545		1.06E-04				
								800	786	710	697		2.11E-04				
								1000	982	875	859		2.93E-04				
9	0.496	5354	40	45	5.0	5.09	3.1	0	0	600	589	3.4E-05	-1.41E-03	2.71E-07	2.63E-06	0.10	3.02E-07
								1280	1257	1720	1689		-1.03E-03				
								2560	2514	2860	2809		-7.04E-04				
								3840	3771	4000	3928		-3.75E-04				
								5115	5023	5160	5067		-1.06E-04				
								6395	6280	6300	6187		2.23E-04				
9	0.231	61	60	20	5.0	5.45	3.2	0	0	28	26	5.3E-05	-1.13E-04	2.13E-06	4.83E-06	0.44	3.80E-06
								60	55	62	57		-8.07E-06				
								120	110	96	88		9.69E-05				
								180	165	136	125		1.78E-04				
								240	220	172	158		2.74E-04				
								300	275	213	195		3.51E-04				

Table C.4: Detailed wetted wall column data – 9 m MEA

MEA	CO_2 Ldg	P^*_{CO2}	Temp	Pres	Gas_{Dry}	Gas	Liquid	$P_{CO2,in,dry}$	$P_{CO2,in,wet}$	$P_{CO2,out,dry}$	$P_{CO2,out,wet}$	$k^o_{l,prod}$	CO_2 Flux	K_G	k_g	K_G/k_g	k_g'
m	mol/mol_{alk}	Pa	C	psig	Std l/min	Std l/min	ml/s	Pa	Pa	Pa	Pa	m/s	$mol/s \cdot m^2$	$mol/s \cdot Pa \cdot m^2$	$mol/s \cdot Pa \cdot m^2$		$mol/s \cdot Pa \cdot m^2$
9	0.324	263	60	20	5.0	5.45	3.2	0	0	91	83	5.0E-05	-3.67E-04	1.62E-06	4.83E-06	0.34	2.44E-06
								100	92	155	142		-2.22E-04				
								200	183	226	207		-1.05E-04				
								300	275	297	272		1.21E-05				
								400	367	364	334		1.45E-04				
								500	458	436	400		2.58E-04				
9	0.382	892	60	30	5.0	5.35	3.1	0	0	250	234	4.8E-05	-7.83E-04	1.05E-06	3.69E-06	0.29	1.47E-06
								400	374	555	519		-4.86E-04				
								800	748	845	790		-1.41E-04				
								1200	1122	1140	1066		1.88E-04				
								1600	1496	1415	1323		5.80E-04				
								2000	1871	1720	1609		8.77E-04				
9	0.441	2862	60	45	5.0	5.25	3.1	0	0	725	690	4.6E-05	-1.70E-03	7.08E-07	2.72E-06	0.26	9.57E-07
								1250	1189	1700	1618		-1.06E-03				
								2500	2379	2625	2498		-2.93E-04				
								3750	3568	3625	3449		2.93E-04				
								5000	4758	4475	4258		1.23E-03				
								6250	5947	5425	5162		1.94E-03				
9	0.496	21249	60	60	5.0	5.20	3.1	0	0	3000	2884	4.4E-05	-5.62E-03	2.82E-07	2.16E-06	0.13	3.24E-07
								8000	7690	9750	9373		-3.28E-03				
								16000	15381	16800	16150		-1.50E-03				
								24000	23071	23950	23023		9.37E-05				
								32000	30761	30800	29608		2.25E-03				
								40000	38452	37400	35952		4.87E-03				
9	0.265	979	80	25	4.0	4.84	3.2	0	0	440	364	6.3E-05	-1.24E-03	1.76E-06	3.84E-06	0.46	3.24E-06
								300	248	690	571		-1.10E-03				
								600	496	850	703		-7.06E-04				
								900	744	1025	848		-3.53E-04				
								1200	992	1185	980		4.23E-05				
								1500	1240	1360	1125		3.95E-04				
9	0.356	4797	80	30	5.0	5.91	4.0	0	0	1450	1227	6.4E-05	-4.54E-03	1.22E-06	4.04E-06	0.30	1.75E-06
								2000	1692	3100	2623		-3.45E-03				
								4000	3385	4600	3893		-1.88E-03				
								6000	5077	5925	5014		2.35E-04				
								8000	6770	7350	6220		2.04E-03				
								10000	8462	8700	7362		4.07E-03				

Table C.5: Detailed wetted wall column data – 9 m MEA

MEA	CO_2 Ldg	P^*_{CO2}	Temp	Pres	Gas_{Dry}	Gas	Liquid	$P_{CO2,in,dry}$	$P_{CO2,in,wet}$	$P_{CO2,out,dry}$	$P_{CO2,out,wet}$	$k^o_{l,prod}$	CO_2 Flux	K_G	k_g	K_G/k_g	k_g'
m	mol/mol_{alk}	Pa	C	psig	Std l/min	Std l/min	ml/s	Pa	Pa	Pa	Pa	m/s	$mol/s \cdot m^2$	$mol/s \cdot Pa \cdot m^2$	$mol/s \cdot Pa \cdot m^2$		$mol/s \cdot Pa \cdot m^2$
9	0.265	4940	100	40	4.0	5.47	3.0	0	0	2850	2084	7.9E-05	-5.84E-03	1.63E-06	3.11E-06	0.52	3.40E-06
								4000	2925	5300	3876		-2.66E-03				
								8000	5850	7550	5521		9.22E-04				
								12000	8775	9800	7166		4.51E-03				
								15600	11408	11500	8410		8.40E-03				
								20000	14625	14200	10384		1.19E-02				
9	0.356	21534	100	65	4.5	5.52	3.8	0	0	8900	7259	8.1E-05	-1.41E-02	8.21E-07	2.15E-06	0.38	1.33E-06
								10000	8156	15600	12723		-8.86E-03				
								20000	16311	22300	18187		-3.64E-03				
								30000	24467	29200	23815		1.27E-03				
								40000	32623	35600	29034		6.96E-03				
								48000	39147	40000	32623		1.27E-02				

Table C.6: Detailed wetted wall column data – 11 m MEA

MEA	CO_2 Ldg	P^*_{CO2}	Temp	Pres	Gas_{Dry}	Gas	Liquid	$P_{CO2,in,dry}$	$P_{CO2,in,wet}$	$P_{CO2,out,dry}$	$P_{CO2,out,wet}$	$k^o_{l,prod}$	CO_2 Flux	K_G	k_g	K_G/k_g	k_g'
m	mol/mol_{alk}	Pa	C	psig	Std l/min	Std l/min	ml/s	Pa	Pa	Pa	Pa	m/s	$mol/s \cdot m^2$	$mol/s \cdot Pa \cdot m^2$	$mol/s \cdot Pa \cdot m^2$		$mol/s \cdot Pa \cdot m^2$
11	0.261	14	40	20	5.0	5.16	3.2	0	0	6	6	3.5E-05	-2.42E-05	1.94E-06	4.57E-06	0.42	3.36E-06
								10	10	11	11		-5.25E-06				
								30	29	23	23		2.70E-05				
								40	39	31	30		3.75E-05				
								50	48	37	36		5.17E-05				
11	0.353	67	40	20	5.0	5.16	3.1	0	0	19	18	3.2E-05	-7.67E-05	1.27E-06	4.57E-06	0.28	1.76E-06
								60	58	63	61		-1.21E-05				
								120	116	104	101		6.46E-05				
								180	174	151	146		1.17E-04				
								240	233	198	192		1.70E-04				
								300	291	238	231		2.50E-04				
11	0.428	434	40	45	5.0	5.09	3.1	0	0	92	90	3.0E-05	-2.16E-04	5.62E-07	2.63E-06	0.21	7.14E-07
								200	196	258	253		-1.36E-04				
								400	393	401	394		-2.35E-06				
								600	589	566	556		7.98E-05				
								800	786	724	711		1.78E-04				
								1000	982	886	870		2.67E-04				
11	0.461	1509	40	60	5.0	5.07	3.1	0	0	300	296	3.0E-05	-5.62E-04	3.60E-07	2.09E-06	0.17	4.34E-07
								1600	1577	1550	1528		9.37E-05				
								3200	3154	2925	2883		5.16E-04				
								4800	4731	4225	4164		1.08E-03				
								6400	6308	5525	5446		1.64E-03				
								8000	7885	6925	6826		2.02E-03				
11	0.261	96	60	20	5.0	5.45	3.2	0	0	40	37	4.6E-05	-1.61E-04	1.98E-06	4.83E-06	0.41	3.35E-06
								60	55	77	71		-6.86E-05				
								120	110	110	101		4.04E-05				
								180	165	151	138		1.17E-04				
								240	220	193	177		1.90E-04				
								300	275	230	211		2.83E-04				
11	0.353	634	60	20	5.0	5.45	3.1	0	0	180	165	4.2E-05	-7.26E-04	1.31E-06	4.83E-06	0.27	1.80E-06
								300	275	400	367		-4.04E-04				
								600	550	625	573		-1.01E-04				
								900	825	840	770		2.42E-04				
								1200	1100	1070	981		5.25E-04				
								1500	1375	1295	1187		8.27E-04				

Table C.7: Detailed wetted wall column data – 11 m MEA

MEA	CO_2 Ldg	P^*_{CO2}	Temp	Pres	Gas_{Dry}	Gas	Liquid	$P_{CO2,in,dry}$	$P_{CO2,in,wet}$	$P_{CO2,out,dry}$	$P_{CO2,out,wet}$	$k^o_{l,prod}$	CO_2 Flux	K_G	k_g	K_G/k_g	k_g'
m	mol/mol_{alk}	Pa	C	psig	Std l/min	Std l/min	ml/s	Pa	Pa	Pa	Pa	m/s	$mol/s \cdot m^2$	$mol/s \cdot Pa \cdot m^2$	$mol/s \cdot Pa \cdot m^2$		$mol/s \cdot Pa \cdot m^2$
11	0.428	3463	60	45	5.0	5.25	3.1	0	0	825	785	4.0E-05	-1.94E-03	6.60E-07	2.72E-06	0.24	8.71E-07
								1250	1189	1850	1760		-1.41E-03				
								2500	2379	2775	2641		-6.45E-04				
								3750	3568	3700	3521		1.17E-04				
								5000	4758	4700	4472		7.04E-04				
								6250	5947	5625	5353		1.47E-03				
11	0.461	8171	60	60	5.0	5.20	3.1	0	0	1700	1634	3.9E-05	-3.19E-03	4.07E-07	2.16E-06	0.19	5.02E-07
								8000	7690	8000	7690		0.00E+00				
								16000	15381	14500	13939		2.81E-03				
								24000	23071	21000	20187		5.62E-03				
								32000	30761	27500	26435		8.44E-03				
								40000	38452	34200	32876		1.09E-02				
11	0.256	860	80	25	4.0	4.84	4.0	0	0	380	314	6.1E-05	-1.07E-03	2.04E-06	3.84E-06	0.53	4.35E-06
								300	248	630	521		-9.31E-04				
								600	496	800	662		-5.64E-04				
								900	744	965	798		-1.83E-04				
								1200	992	1130	934		1.98E-04				
								1500	1240	1290	1067		5.93E-04				
11	0.359	3923	80	30	5.0	5.91	4.0	0	0	1375	1164	5.6E-05	-4.31E-03	1.31E-06	4.04E-06	0.32	1.93E-06
								2000	1692	2725	2306		-2.27E-03				
								4000	3385	4250	3597		-7.83E-04				
								6000	5077	5650	4781		1.10E-03				
								8000	6770	6950	5881		3.29E-03				
								10000	8462	8400	7108		5.01E-03				
11	0.256	4274	100	40	4.0	5.47	3.8	0	0	2750	2011	7.8E-05	-5.63E-03	1.69E-06	3.11E-06	0.54	3.72E-06
								1690	1236	3550	2596		-3.81E-03				
								3000	2194	4450	3254		-2.97E-03				
								4500	3291	5000	3656		-1.02E-03				
								6000	4388	5825	4260		3.58E-04				
								7500	5485	6850	5009		1.33E-03				
11	0.359	18657	100	65	4.5	5.52	4.0	0	0	8400	6851	7.3E-05	-1.33E-02	9.03E-07	2.15E-06	0.42	1.56E-06
								10000	8156	15000	12234		-7.91E-03				
								20000	16311	20800	16964		-1.27E-03				
								30000	24467	27500	22428		3.95E-03				
								40000	32623	34000	27729		9.49E-03				
								48000	39147	38300	31236		1.53E-02				

Table C.8: Detailed wetted wall column data – 13 m MEA

MEA	CO_2 Ldg	P^*_{CO2}	Temp	Pres	Gas_{Dry}	Gas	Liquid	$P_{CO2,in,dry}$	$P_{CO2,in,wet}$	$P_{CO2,out,dry}$	$P_{CO2,out,wet}$	$k^o_{l,prod}$	CO_2 Flux	K_G	k_g	K_G/k_g	k_g'
m	mol/mol_{alk}	Pa	C	psig	Std l/min	Std l/min	ml/s	Pa	Pa	Pa	Pa	m/s	$mol/s \cdot m^2$	$mol/s \cdot Pa \cdot m^2$	$mol/s \cdot Pa \cdot m^2$		$mol/s \cdot Pa \cdot m^2$
13	0.252	12.3	40	20	5.0	5.16	3.2	0	0	5	5	3.1E-05	-1.94E-05	1.84E-06	4.57E-06	0.40	3.08E-06
								10	10	12	11		-6.86E-06				
								20	19	18	17		1.01E-05				
								30	29	22	21		3.31E-05				
								40	39	30	29		4.04E-05				
								50	48	38	37		4.92E-05				
13	0.372	84	40	20	5.0	5.16	2.7	0	0	20	19	2.6E-05	-8.07E-05	1.00E-06	4.57E-06	0.22	1.28E-06
								60	58	66	64		-2.42E-05				
								120	116	110	107		4.04E-05				
								180	174	160	155		8.07E-05				
								240	233	208	202		1.29E-04				
								300	291	255	247		1.82E-04				
13	0.435	491	40	45	5.0	5.09	3.1	0	0	105	103	2.6E-05	-2.46E-04	5.50E-07	2.63E-06	0.21	6.96E-07
								200	196	265	260		-1.52E-04				
								400	393	415	408		-3.52E-05				
								600	589	575	565		5.86E-05				
								800	786	740	727		1.41E-04				
								1000	982	900	884		2.35E-04				
13	0.502	8792	40	60	5.0	5.07	3.0	0	0	650	641	2.5E-05	-1.22E-03	1.51E-07	2.09E-06	0.07	1.62E-07
								3000	2957	3450	3401		-8.44E-04				
								6000	5914	6275	6185		-5.16E-04				
								9000	8871	8999	8870		1.87E-06				
								12000	11828	11750	11582		4.69E-04				
								15000	14785	14525	14317		8.91E-04				
13	0.252	100	60	20	5.0	5.45	2.7	0	0	38	35	3.9E-05	-1.53E-04	1.84E-06	4.83E-06	0.38	2.98E-06
								60	55	75	69		-6.05E-05				
								120	110	115	105		2.02E-05				
								180	165	158	145		8.88E-05				
								240	220	196	180		1.78E-04				
								300	275	233	214		2.70E-04				
13	0.372	694	60	20	5.0	5.45	2.7	0	0	170	156	3.5E-05	-6.86E-04	1.17E-06	4.83E-06	0.24	1.54E-06
								300	275	410	376		-4.44E-04				
								600	550	640	587		-1.61E-04				
								900	825	875	802		1.01E-04				
								1200	1100	1090	999		4.44E-04				
								1500	1375	1325	1215		7.06E-04				

Table C.9: Detailed wetted wall column data – 13 m MEA

MEA	CO_2 Ldg	P^*_{CO2}	Temp	Pres	Gas_{Dry}	Gas	Liquid	$P_{CO2,in,dry}$	$P_{CO2,in,wet}$	$P_{CO2,out,dry}$	$P_{CO2,out,wet}$	$k^o_{l,prod}$	CO_2 Flux	K_G	k_g	K_G/k_g	k_g'
m	mol/mol_{alk}	Pa	C	psig	Std l/min	Std l/min	ml/s	Pa	Pa	Pa	Pa	m/s	$mol/s \cdot m^2$	$mol/s \cdot Pa \cdot m^2$	$mol/s \cdot Pa \cdot m^2$		$mol/s \cdot Pa \cdot m^2$
13	0.435	3859	60	45	5.0	5.25	3.1	0	0	860	818	3.5E-05	-2.02E-03	5.91E-07	2.72E-06	0.22	7.56E-07
								1250	1189	1840	1751		-1.38E-03				
								2500	2379	2850	2712		-8.21E-04				
								3750	3568	3815	3630		-1.52E-04				
								5000	4758	4800	4568		4.69E-04				
								6250	5947	5775	5495		1.11E-03				
13	0.502	29427	60	70	5.0	5.18	2.8	0	0	2900	2801	3.2E-05	-4.80E-03	1.75E-07	1.89E-06	0.09	1.93E-07
								9000	8693	11100	10721		-3.47E-03				
								18000	17385	19200	18545		-1.98E-03				
								27000	26078	27400	26465		-6.61E-04				
								36000	34771	35600	34385		6.61E-04				
								46500	44912	44800	43271		2.81E-03				
13	0.254	873	80	25	4.0	4.84	4.0	0	0	385	318	5.5E-05	-1.09E-03	2.01E-06	3.84E-06	0.52	4.21E-06
								300	248	635	525		-9.45E-04				
								600	496	795	657		-5.50E-04				
								900	744	985	814		-2.40E-04				
								1200	992	1130	934		1.98E-04				
								1500	1240	1300	1075		5.64E-04				
13	0.355	3964	80	30	5.0	5.91	4.0	0	0	1350	1142	5.0E-05	-4.23E-03	1.27E-06	4.04E-06	0.31	1.85E-06
								2000	1692	2800	2369		-2.51E-03				
								4000	3385	4150	3512		-4.70E-04				
								6000	5077	5700	4824		9.40E-04				
								8000	6770	7000	5924		3.13E-03				
								10000	8462	8450	7151		4.86E-03				
13	0.254	3876	100	30	4.0	5.96	4.0	0	0	2350	1577	7.2E-05	-5.89E-03	1.93E-06	4.10E-06	0.47	3.66E-06
								2500	1678	3800	2550		-3.26E-03				
								5000	3356	5350	3591		-8.77E-04				
								7500	5034	6750	4530		1.88E-03				
								10000	6712	8300	5571		4.26E-03				
								12500	8389	9800	6577		6.77E-03				
13	0.355	18406	100	65	4.5	5.52	4.0	0	0	8600	7014	6.6E-05	-1.36E-02	9.06E-07	2.15E-06	0.42	1.56E-06
								10000	8156	14600	11907		-7.28E-03				
								20000	16311	20700	16882		-1.11E-03				
								30000	24467	27300	22265		4.27E-03				
								40000	32623	33600	27403		1.01E-02				
								48000	39147	38500	31399		1.50E-02				

Table C.10: Detailed wetted wall column data – 2 m PZ

PZ	CO_2 Ldg	P^*_{CO2}	Temp	Pres	Gas_{Dry}	Gas	Liquid	$P_{CO2,in,dry}$	$P_{CO2,in,wet}$	$P_{CO2,out,dry}$	$P_{CO2,out,wet}$	$k^o_{l,prod}$	CO_2 Flux	K_G	k_g	K_G/k_g	k_g'
m	mol/mol_{alk}	Pa	C	psig	Std l/min	Std l/min	ml/s	Pa	Pa	Pa	Pa	m/s	$mol/s \cdot m^2$	$mol/s \cdot Pa \cdot m^2$	$mol/s \cdot Pa \cdot m^2$		$mol/s \cdot Pa \cdot m^2$
2	0.240	96	40	20	5.0	5.16	3.0	0	0	37	36	6.1E-05	-1.49E-04	1.92E-06	4.57E-06	0.42	3.32E-06
								35	34	58	56		-9.28E-05				
								70	68	80	78		-4.04E-05				
								105	102	103	100		8.07E-06				
								140	136	126	122		5.65E-05				
								175	170	146	141		1.17E-04				
2	0.316	499	40	20	5.0	5.16	3.0	0	0	145	141	6.1E-05	-5.85E-04	1.41E-06	4.57E-06	0.31	2.04E-06
								300	291	365	354		-2.62E-04				
								600	581	575	557		1.01E-04				
								900	872	790	766		4.44E-04				
								1200	1163	1005	974		7.87E-04				
								1500	1454	1215	1178		1.15E-03				
2	0.352	1305	40	30	5.0	5.12	3.0	0	0	350	342	6.0E-05	-1.10E-03	9.99E-07	3.53E-06	0.28	1.39E-06
								500	488	730	713		-7.21E-04				
								1000	976	1100	1074		-3.13E-04				
								1500	1464	1450	1415		1.57E-04				
								2000	1952	1820	1776		5.64E-04				
								2500	2440	2190	2138		9.71E-04				
2	0.411	7127	40	65	3.0	3.04	3.0	0	0	2150	2121	6.0E-05	-2.27E-03	3.87E-07	1.27E-06	0.30	5.55E-07
								2000	1973	3650	3601		-1.74E-03				
								4000	3946	4950	4883		-1.00E-03				
								6000	5919	6400	6314		-4.22E-04				
								8000	7893	7750	7646		2.64E-04				
								10000	9866	9150	9027		8.96E-04				
2	0.240	559	60	20	5.0	5.45	3.0	0	0	210	192	7.7E-05	-8.48E-04	1.97E-06	4.83E-06	0.41	3.33E-06
								200	183	355	325		-6.26E-04				
								400	367	482	442		-3.31E-04				
								600	550	605	555		-2.02E-05				
								800	733	730	669		2.83E-04				
								1000	917	855	784		5.85E-04				
2	0.316	2541	60	25	5.0	5.39	3.0	0	0	820	760	7.7E-05	-2.89E-03	1.38E-06	4.18E-06	0.33	2.06E-06
								800	742	1400	1298		-2.12E-03				
								1600	1483	1940	1799		-1.20E-03				
								2400	2225	2520	2336		-4.23E-04				
								3200	2967	3070	2846		4.59E-04				
								4000	3709	3600	3338		1.41E-03				

Table C.11: Detailed wetted wall column data – 2 m PZ

PZ	CO_2 Ldg	P^*_{CO2}	Temp	Pres	Gas_{Dry}	Gas	Liquid	$P_{CO2,in,dry}$	$P_{CO2,in,wet}$	$P_{CO2,out,dry}$	$P_{CO2,out,wet}$	$k^o_{l,prod}$	CO_2 Flux	K_G	k_g	K_G/k_g	k_g'
m	mol/mol_{alk}	Pa	C	psig	Std l/min	Std l/min	ml/s	Pa	Pa	Pa	Pa	m/s	$mol/s \cdot m^2$	$mol/s \cdot Pa \cdot m^2$	$mol/s \cdot Pa \cdot m^2$		$mol/s \cdot Pa \cdot m^2$
2	0.352	5593	60	30	5.0	5.35	3.0	0	0	1550	1450	7.6E-05	-4.86E-03	1.00E-06	3.69E-06	0.27	1.38E-06
								3500	3274	4100	3835		-1.88E-03				
								7000	6547	6800	6360		6.27E-04				
								10500	9821	9350	8745		3.60E-03				
								14000	13094	11850	11083		6.74E-03				
								17500	16368	14550	13609		9.24E-03				
2	0.411	25378	60	65	3.0	3.11	3.0	0	0	6200	5975	7.6E-05	-6.54E-03	2.97E-07	1.31E-06	0.23	3.84E-07
								10000	9637	13900	13396		-4.11E-03				
								20000	19274	21400	20624		-1.48E-03				
								30000	28912	29400	28333		6.33E-04				
								40000	38549	36700	35368		3.48E-03				
								50000	48186	44300	42693		6.01E-03				
2	0.239	2492	80	20	5.0	6.23	3.9	0	0	1050	842	9.9E-05	-4.24E-03	2.07E-06	5.45E-06	0.38	3.34E-06
								1500	1203	2000	1604		-2.02E-03				
								3000	2406	3050	2446		-2.02E-04				
								4500	3609	4100	3288		1.61E-03				
								6000	4812	5000	4010		4.04E-03				
								7500	6015	6000	4812		6.05E-03				
2	0.324	12260	80	40	5.0	5.72	4.1	0	0	3750	3279	1.0E-04	-9.60E-03	9.36E-07	3.21E-06	0.29	1.32E-06
								4000	3497	6825	5967		-7.23E-03				
								8000	6995	9650	8438		-4.22E-03				
								12000	10492	12600	11017		-1.54E-03				
								16000	13990	15450	13509		1.41E-03				
								20000	17487	18325	16023		4.29E-03				
2	0.239	9569	100	25	3.5	5.56	3.9	0	0	4800	3023	1.2E-04	-1.19E-02	1.55E-06	4.35E-06	0.36	2.40E-06
								5000	3149	8200	5164		-7.90E-03				
								10000	6297	11900	7494		-4.69E-03				
								15000	9446	15500	9761		-1.23E-03				
								20000	12595	18300	11524		4.20E-03				
								25000	15744	21600	13602		8.40E-03				
2	0.324	39286	100	60	4.0	4.98	4.1	0	0	14700	11807	1.3E-04	-2.20E-02	6.36E-07	2.10E-06	0.30	9.12E-07
								20000	16064	27800	22330		-1.17E-02				
								40000	32129	42500	34137		-3.75E-03				
								60000	48193	56500	45382		5.25E-03				
								80000	64258	71000	57029		1.35E-02				
								90000	72290	78500	63053		1.72E-02				

Table C.12: Detailed wetted wall column data – 5 m PZ

PZ	CO_2 Ldg	P^*_{CO2}	Temp	Pres	Gas_{Dry}	Gas	Liquid	$P_{CO2,in,dry}$	$P_{CO2,in,wet}$	$P_{CO2,out,dry}$	$P_{CO2,out,wet}$	$k^o_{l,prod}$	CO_2 Flux	K_G	k_g	K_G/k_g	k_g'
m	mol/mol_{alk}	Pa	C	psig	Std l/min	Std l/min	ml/s	Pa	Pa	Pa	Pa	m/s	$mol/s \cdot m^2$	$mol/s \cdot Pa \cdot m^2$	$mol/s \cdot Pa \cdot m^2$		$mol/s \cdot Pa \cdot m^2$
5	0.226	65	40	20	5.0	5.16	3.7	0	0	27	26	3.8E-05	-1.09E-04	2.24E-06	4.57E-06	0.49	4.39E-06
								35	34	49	47		-5.45E-05				
								70	68	69	66		6.05E-06				
								105	102	89	86		6.66E-05				
								140	136	110	106		1.23E-04				
								175	170	130	126		1.84E-04				
5	0.299	346	40	20	5.0	5.16	3.6	0	0	125	121	3.7E-05	-5.05E-04	1.65E-06	4.57E-06	0.36	2.57E-06
								300	291	320	310		-8.07E-05				
								600	581	510	494		3.63E-04				
								900	872	715	693		7.47E-04				
								1200	1163	925	896		1.11E-03				
								1500	1454	1135	1100		1.47E-03				
5	0.354	1120	40	30	5.0	5.12	3.6	0	0	345	337	3.6E-05	-1.08E-03	1.14E-06	3.53E-06	0.32	1.69E-06
								500	488	695	678		-6.11E-04				
								1000	976	1035	1010		-1.10E-04				
								1500	1464	1405	1371		2.98E-04				
								2000	1952	1740	1698		8.15E-04				
								2500	2440	2095	2045		1.27E-03				
5	0.402	4563	40	65	3.0	3.04	3.6	0	0	1700	1677	3.5E-05	-1.79E-03	4.88E-07	1.27E-06	0.38	7.93E-07
								2000	1973	2925	2886		-9.75E-04				
								4000	3946	4225	4168		-2.37E-04				
								6000	5919	5550	5475		4.74E-04				
								8000	7893	6800	6709		1.27E-03				
								10000	9866	7975	7868		2.14E-03				
5	0.226	385	60	20	5.0	5.45	3.7	0	0	167	153	4.9E-05	-6.74E-04	2.40E-06	4.83E-06	0.50	4.75E-06
								200	183	302	277		-4.12E-04				
								400	367	412	378		-4.84E-05				
								600	550	525	481		3.03E-04				
								800	733	635	582		6.66E-04				
								1000	917	757	694		9.81E-04				
5	0.299	1814	60	25	5.0	5.39	3.6	0	0	670	621	4.8E-05	-2.36E-03	1.61E-06	4.18E-06	0.39	2.62E-06
								800	742	1200	1113		-1.41E-03				
								1600	1483	1730	1604		-4.59E-04				
								2400	2225	2240	2077		5.64E-04				
								3200	2967	2790	2587		1.45E-03				
								4000	3709	3280	3041		2.54E-03				

Table C.13: Detailed wetted wall column data – 5 m PZ

PZ	CO_2 Ldg	P^*_{CO2}	Temp	Pres	Gas_{Dry}	Gas	Liquid	$P_{CO2,in,dry}$	$P_{CO2,in,wet}$	$P_{CO2,out,dry}$	$P_{CO2,out,wet}$	$k^o_{l,prod}$	CO_2 Flux	K_G	k_g	K_G/k_g	k_g'
m	mol/mol_{alk}	Pa	C	psig	Std l/min	Std l/min	ml/s	Pa	Pa	Pa	Pa	m/s	$mol/s \cdot m^2$	$mol/s \cdot Pa \cdot m^2$	$mol/s \cdot Pa \cdot m^2$		$mol/s \cdot Pa \cdot m^2$
5	0.354	5021	60	30	5.0	5.35	3.6	0	0	1525	1426	4.8E-05	-4.78E-03	1.21E-06	3.69E-06	0.33	1.80E-06
								3500	3274	4075	3811		-1.80E-03				
								7000	6547	6625	6196		1.17E-03				
								10500	9821	9025	8441		4.62E-03				
								14000	13094	11350	10616		8.30E-03				
								17500	16368	13750	12860		1.17E-02				
5	0.402	17233	60	65	3.0	3.11	3.4	0	0	5400	5204	4.6E-05	-5.69E-03	4.38E-07	1.31E-06	0.34	6.59E-07
								8000	7710	11350	10938		-3.53E-03				
								16000	15419	17150	16528		-1.21E-03				
								24000	23129	22400	21587		1.69E-03				
								32000	30839	27100	26117		5.17E-03				
								40000	38549	32400	31224		8.01E-03				
5	0.252	2192	80	20	5.0	6.23	4.1	0	0	1050	842	6.3E-05	-4.24E-03	2.52E-06	5.45E-06	0.46	4.67E-06
								1500	1203	2000	1604		-2.02E-03				
								3000	2406	2900	2326		4.04E-04				
								4500	3609	3825	3067		2.72E-03				
								6000	4812	4725	3789		5.15E-03				
								7500	6015	5600	4491		7.67E-03				
5	0.320	9699	80	40	5.0	5.72	3.9	0	0	3800	3323	6.1E-05	-9.73E-03	1.20E-06	3.21E-06	0.37	1.91E-06
								4000	3497	6100	5334		-5.38E-03				
								8000	6995	9100	7957		-2.82E-03				
								12000	10492	11900	10405		2.56E-04				
								16000	13990	14500	12678		3.84E-03				
								20000	17487	16800	14689		8.19E-03				
5	0.252	8888	100	25	4.0	6.35	3.9	0	0	5350	3369	8.1E-05	-1.51E-02	2.04E-06	4.87E-06	0.42	3.52E-06
								5000	3149	8200	5164		-9.03E-03				
								10000	6297	11400	7179		-3.95E-03				
								15000	9446	14500	9131		1.41E-03				
								20000	12595	18200	11461		5.08E-03				
								25000	15744	20900	13162		1.16E-02				
5	0.320	36960	100	60	4.0	4.98	3.9	0	0	15000	12048	8.0E-05	-2.25E-02	6.86E-07	2.10E-06	0.33	1.02E-06
								10000	8032	20200	16225		-1.53E-02				
								20000	16064	27500	22089		-1.12E-02				
								30000	24097	35200	28273		-7.80E-03				
								40000	32129	42200	33896		-3.30E-03				
								45000	36145	45200	36306		-3.00E-04				

Table C.14: Detailed wetted wall column data – 8 m PZ

PZ	CO_2 Ldg	P^*_{CO2}	Temp	Pres	Gas_{Dry}	Gas	Liquid	$P_{CO2,in,dry}$	$P_{CO2,in,wet}$	$P_{CO2,out,dry}$	$P_{CO2,out,wet}$	$k^o_{l,prod}$	CO_2 Flux	K_G	k_g	K_G/k_g	k_g'
m	mol/mol_{alk}	Pa	C	psig	Std l/min	Std l/min	ml/s	Pa	Pa	Pa	Pa	m/s	$mol/s \cdot m^2$	$mol/s \cdot Pa \cdot m^2$	$mol/s \cdot Pa \cdot m^2$		$mol/s \cdot Pa \cdot m^2$
8	0.235	68	40	20	5.0	5.16	4.0	0	0	27	26	2.3E-05	-1.07E-04	2.21E-06	4.57E-06	0.48	4.27E-06
								45	44	59	57		-5.45E-05				
								90	87	83	80		3.03E-05				
								135	131	109	106		1.05E-04				
								180	174	134	129		1.88E-04				
8	0.311	530	40	20	5.0	5.16	3.1	0	0	165	160	2.0E-05	-6.66E-04	1.38E-06	4.57E-06	0.30	1.98E-06
								300	291	365	354		-2.62E-04				
								600	581	575	557		1.01E-04				
								900	872	797	772		4.16E-04				
								1200	1163	1018	987		7.35E-04				
								1500	1454	1235	1197		1.07E-03				
8	0.340	1409	40	60	5.0	5.07	3.7	0	0	465	458	2.1E-05	-8.72E-04	7.39E-07	2.09E-06	0.35	1.14E-06
								500	493	800	789		-5.62E-04				
								1000	986	1140	1124		-2.62E-04				
								1500	1478	1465	1444		6.56E-05				
								2000	1971	1810	1784		3.56E-04				
								2400	2366	2100	2070		5.62E-04				
8	0.412	8153	40	70	3.0	3.04	3.7	0	0	2010	1985	2.1E-05	-1.99E-03	2.73E-07	1.19E-06	0.23	3.53E-07
								2000	1975	3625	3579		-1.61E-03				
								4500	4443	5400	5332		-8.93E-04				
								7000	6912	7300	7208		-2.98E-04				
								9500	9380	9225	9108		2.73E-04				
								11500	11355	10675	10540		8.18E-04				
8	0.235	430	60	20	5.0	5.45	3.6	0	0	190	174	3.0E-05	-7.67E-04	2.31E-06	4.83E-06	0.48	4.41E-06
								250	229	340	312		-3.63E-04				
								500	458	485	445		6.05E-05				
								750	687	640	587		4.44E-04				
								1000	917	790	724		8.48E-04				
								1150	1054	865	793		1.15E-03				
8	0.311	2407	60	25	5.0	5.39	3.1	0	0	780	723	2.8E-05	-2.75E-03	1.36E-06	4.18E-06	0.33	2.02E-06
								800	742	1320	1224		-1.83E-03				
								1600	1483	1930	1789		-1.16E-03				
								2400	2225	2470	2290		-2.47E-04				
								3200	2967	2990	2772		7.41E-04				
								4000	3709	3585	3324		1.46E-03				

Table C.15: Detailed wetted wall column data – 8 m PZ

PZ	CO_2 Ldg	P^*_{CO2}	Temp	Pres	Gas_{Dry}	Gas	Liquid	$P_{CO2,in,dry}$	$P_{CO2,in,wet}$	$P_{CO2,out,dry}$	$P_{CO2,out,wet}$	$k^o_{l,prod}$	CO_2 Flux	K_G	k_g	K_G/k_g	k_g'
m	mol/mol_{alk}	Pa	C	psig	Std l/min	Std l/min	ml/s	Pa	Pa	Pa	Pa	m/s	$mol/s \cdot m^2$	$mol/s \cdot Pa \cdot m^2$	$mol/s \cdot Pa \cdot m^2$		$mol/s \cdot Pa \cdot m^2$
8	0.340	7454	60	70	4.0	4.14	3.5	0	0	2700	2608	2.9E-05	-3.57E-03	5.94E-07	1.57E-06	0.38	9.57E-07
								2500	2415	4325	4177		-2.41E-03				
								5000	4829	5975	5771		-1.29E-03				
								7500	7244	7625	7365		-1.65E-04				
								10000	9659	9175	8862		1.09E-03				
								11000	10624	9825	9490		1.55E-03				
8	0.412	30783	60	70	3.0	3.11	3.7	0	0	7200	6954	2.9E-05	-7.14E-03	2.54E-07	1.23E-06	0.21	3.20E-07
								12000	11590	15800	15261		-3.77E-03				
								24000	23181	25500	24629		-1.49E-03				
								36000	34771	35900	34674		9.92E-05				
								48000	46361	44800	43271		3.17E-03				
								58000	56020	51700	49935		6.25E-03				
8	0.253	3255	80	20	5.0	6.23	4.0	0	0	1450	1163	4.0E-05	-5.85E-03	2.17E-06	5.45E-06	0.40	3.61E-06
								1500	1203	2400	1925		-3.63E-03				
								3000	2406	3275	2626		-1.11E-03				
								4500	3609	4400	3529		4.04E-04				
								6000	4812	5350	4290		2.62E-03				
								7500	6015	6275	5032		4.94E-03				
8	0.289	9406	80	40	5.0	5.72	4.0	0	0	3600	3148	4.0E-05	-9.22E-03	1.22E-06	3.21E-06	0.38	1.97E-06
								4000	3497	6300	5508		-5.89E-03				
								8000	6995	8950	7825		-2.43E-03				
								12000	10492	11700	10230		7.68E-04				
								16000	13990	14300	12503		4.35E-03				
								20000	17487	16700	14602		8.45E-03				
8	0.253	13605	100	30	3.5	5.21	4.0	0	0	7200	4832	5.4E-05	-1.58E-02	1.37E-06	3.66E-06	0.37	2.18E-06
								6000	4027	10700	7181		-1.03E-02				
								12000	8054	14800	9933		-6.14E-03				
								18000	12081	18400	12349		-8.77E-04				
								24000	16108	22900	15369		2.41E-03				
								30000	20135	26800	17987		7.02E-03				
8	0.289	32033	100	60	4.0	4.98	4.0	0	0	13800	11084	5.4E-05	-2.07E-02	7.63E-07	2.10E-06	0.36	1.20E-06
								15000	12048	22200	17832		-1.08E-02				
								30000	24097	33400	26828		-5.10E-03				
								45000	36145	44400	35663		9.00E-04				
								60000	48193	53400	42892		9.90E-03				
								75000	60242	62600	50282		1.86E-02				

Table C.16: Detailed wetted wall column data – 12 m PZ

PZ	CO_2 Ldg	P^*_{CO2}	Temp	Pres	Gas_{Dry}	Gas	Liquid	$P_{CO2,in,dry}$	$P_{CO2,in,wet}$	$P_{CO2,out,dry}$	$P_{CO2,out,wet}$	$k^o_{l,prod}$	CO_2 Flux	K_G	k_g	K_G/k_g	k_g'
m	mol/mol_{alk}	Pa	C	psig	Std l/min	Std l/min	ml/s	Pa	Pa	Pa	Pa	m/s	$mol/s \cdot m^2$	$mol/s \cdot Pa \cdot m^2$	$mol/s \cdot Pa \cdot m^2$		$mol/s \cdot Pa \cdot m^2$
12	0.231	331	60	20	5.0	5.45	3.9	0	0	140	128	1.8E-05	-5.65E-04	2.24E-06	4.83E-06	0.46	4.19E-06
								150	137	238	218		-3.55E-04				
								300	275	327	300		-1.09E-04				
								450	412	412	378		1.53E-04				
								600	550	506	464		3.79E-04				
								750	687	593	544		6.34E-04				
12	0.289	1865	60	25	5.0	5.39	3.8	0	0	550	510	1.8E-05	-1.94E-03	1.28E-06	4.18E-06	0.31	1.85E-06
								800	742	1150	1066		-1.23E-03				
								1600	1483	1760	1632		-5.64E-04				
								2400	2225	2290	2123		3.88E-04				
								3200	2967	2850	2642		1.23E-03				
								4000	3709	3420	3171		2.05E-03				
12	0.354	6791	60	30	5.0	5.35	3.8	0	0	1300	1216	1.7E-05	-4.07E-03	6.39E-07	3.69E-06	0.17	7.73E-07
								3000	2806	3750	3507		-2.35E-03				
								6000	5612	6100	5705		-3.13E-04				
								9000	8418	8700	8137		9.40E-04				
								12000	11224	11300	10569		2.19E-03				
								15000	14030	13600	12720		4.39E-03				
12	0.222	2115	80	30	5.0	5.91	3.9	0	0	1025	867	2.4E-05	-3.21E-03	2.07E-06	4.04E-06	0.51	4.24E-06
								1250	1058	1800	1523		-1.72E-03				
								2500	2116	2550	2158		-1.57E-04				
								3750	3173	3300	2793		1.41E-03				
								5000	4231	3925	3322		3.37E-03				
								6000	5077	4450	3766		4.86E-03				
12	0.290	9141	80	40	5.0	5.72	3.8	0	0	2900	2536	2.4E-05	-7.43E-03	1.01E-06	3.21E-06	0.32	1.48E-06
								4000	3497	5900	5159		-4.86E-03				
								8000	6995	8800	7694		-2.05E-03				
								12000	10492	11800	10317		5.12E-04				
								16000	13990	14400	12591		4.10E-03				
								20000	17487	17000	14864		7.68E-03				
12	0.222	7871	100	25	3.5	5.56	3.9	0	0	4800	3023	3.4E-05	-1.19E-02	2.02E-06	4.35E-06	0.47	3.78E-06
								5000	3149	8200	5164		-7.90E-03				
								10000	6297	11000	6927		-2.47E-03				
								15000	9446	14400	9068		1.48E-03				
								20000	12595	16700	10517		8.15E-03				
								25000	15744	19900	12532		1.26E-02				

Table C.17: Detailed wetted wall column data – 12 m PZ

PZ	CO_2 Ldg	P^*_{CO2}	Temp	Pres	Gas_{Dry}	Gas	Liquid	$P_{CO2,in,dry}$	$P_{CO2,in,wet}$	$P_{CO2,out,dry}$	$P_{CO2,out,wet}$	$k^o_{l,prod}$	CO_2 Flux	K_G	k_g	K_G/k_g	k_g'
m	mol/mol_{alk}	Pa	C	psig	Std l/min	Std l/min	ml/s	Pa	Pa	Pa	Pa	m/s	$mol/s \cdot m^2$	$mol/s \cdot Pa \cdot m^2$	$mol/s \cdot Pa \cdot m^2$		$mol/s \cdot Pa \cdot m^2$
12	0.290	33652	100	60	4.0	4.98	3.9	0	0	11800	9478	3.4E-05	-1.77E-02	5.95E-07	2.10E-06	0.28	8.30E-07
								15000	12048	21500	17269		-9.75E-03				
								30000	24097	33400	26828		-5.10E-03				
								45000	36145	44500	35743		7.50E-04				
								60000	48193	55500	44579		6.75E-03				
								75000	60242	65500	52611		1.42E-02				

Table C.18: Detailed wetted wall column data – 7 m MEA/2 m PZ

MEA	PZ	CO_2 Ldg	P^*_{CO2}	Temp	Pres	Gas_{Dry}	Gas	Liquid	$P_{CO2,in,dry}$	$P_{CO2,in,wet}$	$P_{CO2,out,dry}$	$P_{CO2,out,wet}$	$k^o_{l,prod}$	CO_2 Flux	K_G	k_g	K_G/k_g	k_g'
m	m	mol/mol_{alk}	Pa	C	psig	Std l/min	Std l/min	ml/s	Pa	Pa	Pa	Pa	m/s	$mol/s \cdot m^2$	$mol/s \cdot Pa \cdot m^2$	$mol/s \cdot Pa \cdot m^2$		$mol/s \cdot Pa \cdot m^2$
7	2	0.242	27	40	15	5.0	5.19	4.0	0	0	9	9	-	-4.39E-05	2.10E-06	5.37E-06	0.39	3.45E-06
									10	10	17	17		-3.40E-05				
									20	19	23	22		-1.18E-05				
									30	29	29	28		3.30E-06				
									40	39	36	34		2.12E-05				
									50	48	43	41		3.54E-05				
7	2	0.333	166	40	25	5.0	5.14	4.0	0	0	52	51	-	-1.83E-04	1.31E-06	3.98E-06	0.33	1.96E-06
									100	97	125	122		-8.82E-05				
									200	195	188	183		4.23E-05				
									300	292	260	253		1.41E-04				
									400	389	328	319		2.54E-04				
									500	487	403	392		3.42E-04				
7	2	0.416	1425	40	30	5.0	5.12	4.0	0	0	270	264	-	-8.46E-04	7.02E-07	3.53E-06	0.20	8.76E-07
									350	342	580	566		-7.21E-04				
									700	683	870	849		-5.33E-04				
									1050	1025	1120	1093		-2.19E-04				
									1400	1366	1410	1376		-3.13E-05				
									1750	1708	1690	1650		1.88E-04				
7	2	0.477	7418	40	60	5.0	5.07	3.9	0	0	1300	1281	-	-2.44E-03	3.58E-07	2.09E-06	0.17	4.32E-07
									4000	3943	4500	4435		-9.37E-04				
									8000	7885	8001	7886		-1.87E-06				
									12000	11828	11300	11138		1.31E-03				
									16000	15771	14550	14341		2.72E-03				
									20000	19713	17800	17545		4.12E-03				
7	2	0.242	178	60	20	5.0	5.45	4.1	0	0	77	71	-	-3.11E-04	2.19E-06	4.83E-06	0.45	4.00E-06
									85	78	129	118		-1.78E-04				
									170	156	176	161		-2.42E-05				
									255	234	232	213		9.28E-05				
									340	312	282	258		2.34E-04				
									425	390	336	308		3.59E-04				
7	2	0.333	1256	60	25	5.0	5.39	4.0	0	0	410	380	-	-1.45E-03	1.37E-06	4.18E-06	0.33	2.03E-06
									700	649	905	839		-7.23E-04				
									1050	974	1140	1057		-3.17E-04				
									1500	1391	1440	1335		2.12E-04				
									2000	1854	1810	1678		6.70E-04				
									2250	2086	1985	1840		9.35E-04				

Table C.19: Detailed wetted wall column data – 7 m MEA/2 m PZ

MEA	PZ	CO_2 Ldg	P^*_{CO2}	Temp	Pres	Gas_{Dry}	Gas	Liquid	$P_{CO2,in,dry}$	$P_{CO2,in,wet}$	$P_{CO2,out,dry}$	$P_{CO2,out,wet}$	$k^o_{l,prod}$	CO_2 Flux	K_G	k_g	K_G/k_g	k_g'
m	m	mol/mol_{alk}	Pa	C	psig	Std l/min	Std l/min	ml/s	Pa	Pa	Pa	Pa	m/s	$mol/s \cdot m^2$	$mol/s \cdot Pa \cdot m^2$	$mol/s \cdot Pa \cdot m^2$		$mol/s \cdot Pa \cdot m^2$
7	2	0.416	7122	60	30	5.0	5.35	4.0	0	0	1450	1356	-	-4.54E-03	7.28E-07	3.69E-06	0.20	9.08E-07
									2500	2338	3500	3274		-3.13E-03				
									5000	4677	5550	5191		-1.72E-03				
									7500	7015	7550	7062		-1.57E-04				
									10000	9353	9550	8932		1.41E-03				
									12500	11691	11500	10756		3.13E-03				
7	2	0.477	33704	60	70	5.0	5.18	4.0	0	0	8550	8258	-	-1.41E-02	3.13E-07	1.89E-06	0.17	3.75E-07
									15000	14488	18500	17868		-5.79E-03				
									30000	28976	30500	29459		-8.27E-04				
									45000	43464	43600	42111		2.31E-03				
									60000	57952	55500	53605		7.44E-03				
									75000	72439	68450	66113		1.08E-02				
7	2	0.242	1138	80	20	4.5	5.61	3.6	0	0	550	441	-	-2.00E-03	2.30E-06	4.98E-06	0.46	4.29E-06
									600	481	940	754		-1.24E-03				
									1200	962	1290	1034		-3.27E-04				
									1800	1443	1655	1327		5.27E-04				
									2400	1925	2010	1612		1.42E-03				
									3000	2406	2360	1893		2.32E-03				
7	2	0.333	6174	80	30	4.5	5.32	3.6	0	0	2400	2031	-	-6.77E-03	1.35E-06	3.69E-06	0.36	2.12E-06
									3500	2962	4800	4062		-3.67E-03				
									7000	5924	7100	6008		-2.82E-04				
									10500	8886	9400	7955		3.10E-03				
									14000	11847	11800	9986		6.20E-03				
									17500	14809	14100	11932		9.59E-03				
7	2	0.242	4340	100	20	3.5	6.07	3.6	0	0	3050	1758	-	-8.62E-03	2.54E-06	5.36E-06	0.47	4.83E-06
									5000	2882	6050	3487		-2.97E-03				
									10000	5764	8900	5130		3.11E-03				
									15000	8646	12100	6974		8.19E-03				
									19000	10951	14300	8242		1.33E-02				
									23000	13257	16750	9655		1.77E-02				
7	2	0.333	26571	100	40	4.0	5.47	3.6	0	0	10000	7313	-	-2.05E-02	8.79E-07	3.11E-06	0.28	1.23E-06
									13000	9507	19200	14040		-1.27E-02				
									26000	19013	28500	20841		-5.12E-03				
									39000	28520	38500	28154		1.02E-03				
									52000	38026	47500	34736		9.22E-03				
									65000	47533	57500	42048		1.54E-02				

Appendix D: Amine Concentration Effect on CO_2 Partial Pressure

This section explains mathematically why CO_2 partial pressure should not be a significant function of amine concentration for carbamate producing systems. Amine concentration should be important in determining the CO_2 partial pressure for bicarbonate producing systems. The difference is based on the stoichiometry of the reaction.

D.1 CARBAMATE FORMATION

Carbamate forming systems typically have the following stoichiometry:

$$2Am + CO_2 \leftrightarrow AmCOO^- + AmH^+ \tag{D.1}$$

The equilibrium constant for this equation can be written as Equation D.2. The equation can be solved for the partial pressure of CO_2 using Equation D.3.

$$K_{eq} = \frac{\left[AmCOO^-\right]\cdot\left[AmH^+\right]}{\left[Am\right]^2 \cdot P_{CO2}} \tag{D.2}$$

$$P_{CO2} = \frac{\left[AmCOO^-\right]\cdot\left[AmH^+\right]}{\left[Am\right]^2 \cdot K_{eq}} \tag{D.3}$$

If only carbamate is being formed, the following assumptions can be made:

$$\left[AmCOO^-\right] = \left[AmH^+\right] = Ldg \cdot \left[Am\right]_{Total} \tag{D.4}$$

$$\left[Am\right] = \left(1 - 2 \cdot Ldg\right) \cdot \left[Am\right]_{Total} \tag{D.5}$$

Substituting these values into Equation D.3 yields Equation D.6, which does not have a dependence on the amine concentration of the system.

$$P_{CO2} = \frac{\left(Ldg \cdot [Am]_{Total}\right) \cdot \left(Ldg \cdot [Am]_{Total}\right)}{\left((1 - 2 \cdot Ldg) \cdot [Am]_{Total}\right)^2 \cdot K_{eq}} = \frac{Ldg^2}{(1 - 2 \cdot Ldg)^2 \cdot K_{eq}} \quad \text{(D.6)}$$

D.2 BICARBONATE FORMATION

Bicarbonate forming systems typically have the following stoichiometry:

$$Am + CO_2 + H_2O \leftrightarrow HCO_3^- + AmH^+ \quad \text{(D.7)}$$

The equilibrium constant for this equation can be written as Equation D.8. The equation can be solved for the partial pressure of CO_2 using Equation D.9.

$$K_{eq} = \frac{[HCO_3^-] \cdot [AmH^+]}{[Am] \cdot P_{CO2} \cdot [H_2O]} \quad \text{(D.8)}$$

$$P_{CO2} = \frac{[HCO_3^-] \cdot [AmH^+]}{[Am] \cdot K_{eq} \cdot [H_2O]} \quad \text{(D.9)}$$

If only bicarbonate is being formed, the following assumption can be made:

$$[HCO_3^-] = [AmH^+] = Ldg \cdot [Am]_{Total} \quad \text{(D.10)}$$

$$[Am] = (1 - Ldg) \cdot [Am]_{Total} \quad \text{(D.11)}$$

Substituting these values into Equation D.9 yields Equation D.12, which does have a dependence on the amine concentration of the system.

$$P_{CO2} = \frac{\left(Ldg \cdot [Am]_{Total}\right) \cdot \left(Ldg \cdot [Am]_{Total}\right)}{\left((1 - Ldg) \cdot [Am]_{Total}\right) \cdot K_{eq} \cdot [H_2O]} = \frac{Ldg^2 [Am]_{Total}}{(1 - Ldg) \cdot K_{eq} \cdot [H_2O]} \quad \text{(D.12)}$$

Equation D.12 shows an expected result. For bicarbonate forming systems the CO_2 partial pressure will increase at constant loading with increases in amine concentration.

Appendix E: Piperazine Density and Viscosity Regressions

E.1 PIPERAZINE DENSITY

Piperazine density data were obtained by regressing 2–12 m PZ density measurements from Freeman at 20, 40, and 60˚C (Rochelle, Chen et al. 2009a).

The form of the piperazine molar volume equation is shown in Equation E.1, which uses the weight fractions of CO_2 and total PZ. The equation assumes the same thermal expansion behavior as water. Density can be obtained by dividing the molecular weight by the molar volume. Table E.1 reports the regressed constants A–D.

$$V_{PZso\ln} = V_{H2O} \ln\left(A \cdot \omega_{CO2} + B \cdot \omega_{PZ} + C \cdot \frac{\omega_{CO2}}{\omega_{PZ}} + D \right) \quad \text{(E.1)}$$

$$\rho_{PZso\ln} = \frac{MW_{PZso\ln}}{V_{PZso\ln}} \quad \text{(E.2)}$$

Table E.1: Regressed parameters for the PZ molar volume correlation

Parameter	Value
A	-0.059
B	4.47
C	-0.106
D	2.4

Figures E.1–E.4 show the fit of the correlation against the raw data at 2, 5, 8, and 12 m PZ.

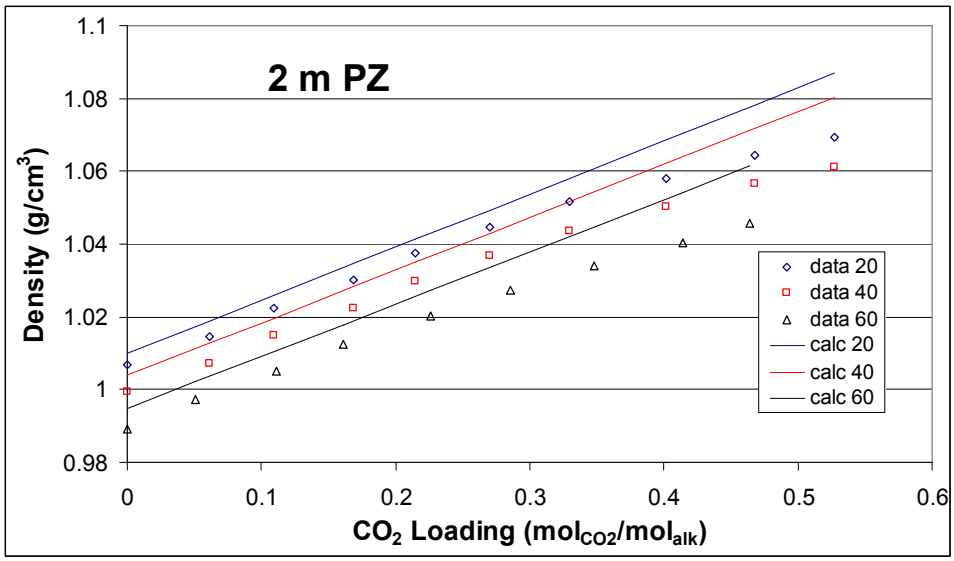

Figure E.1: 2 m PZ density at 20, 40, and 60˚C: points – data; lines – Equations E.1 and E.2

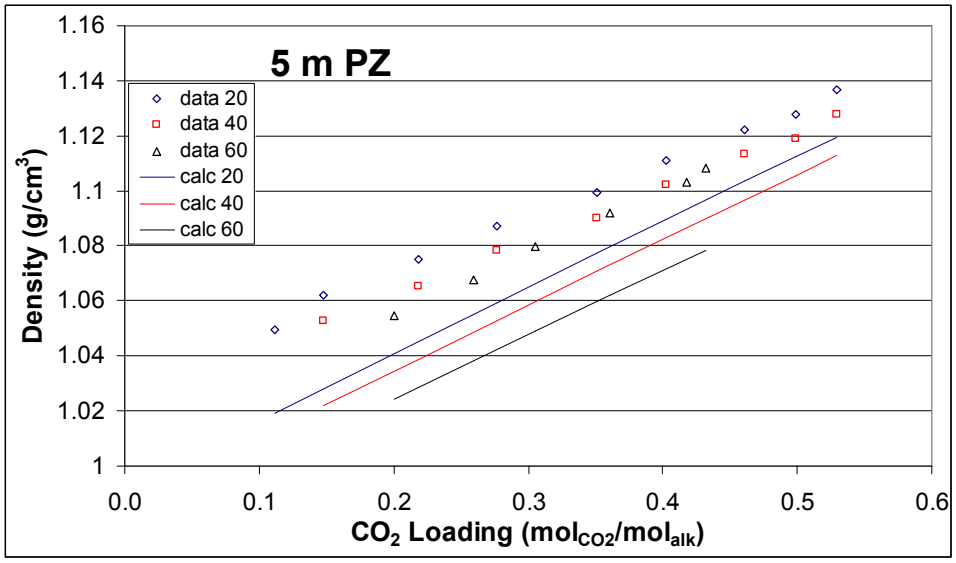

Figure E.2: 5 m PZ density at 20, 40, and 60˚C: points – data; lines – Equations E.1 and E.2

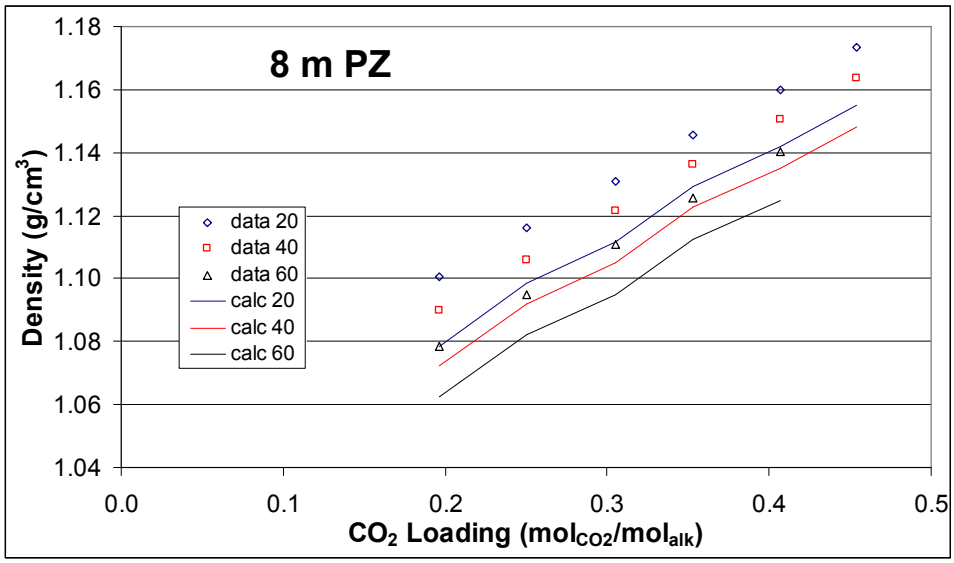

Figure E.3: 8 m PZ density at 20, 40, and 60˚C: points – data; lines – Equations E.1 and E.2

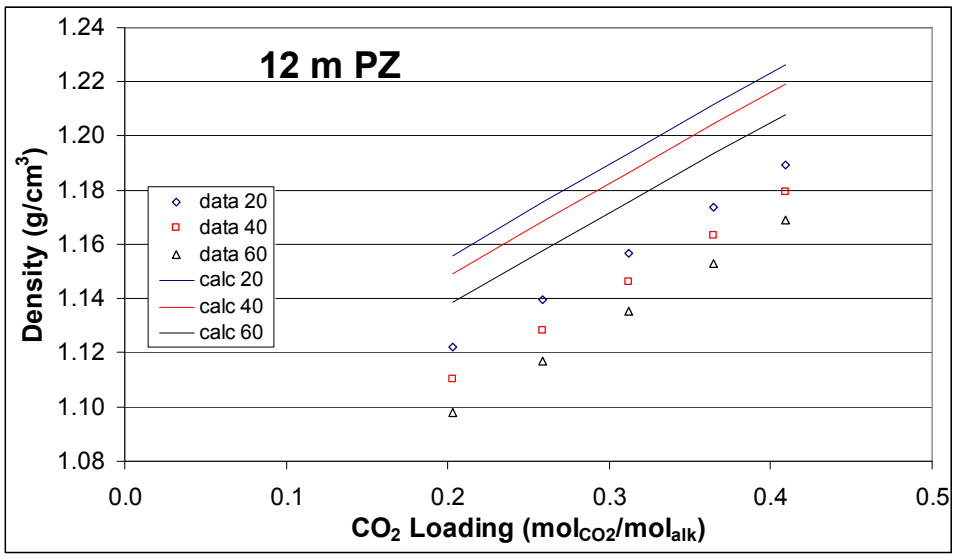

Figure E.4: 12 m PZ density at 20, 40, and 60˚C: points – data ; lines – Equations E.1 and E.2

The correlations shown in Figures E.1–E.4 do not accurately represent density data at each amine concentration. The density of piperazine solutions is overpredicted in

2 and 12 m PZ while it is underpredicted in 5 and 8 m PZ. The correlation averaged 1.5% error over the total data range: 2, 5, 7, 8, 9, 10, and 12 m PZ solutions.

Solution density is not an important parameter in these analyses. Density is required to calculate the liquid film mass transfer coefficient of the reactants and products. In many cases this term is negligible. When diffusion resistances become significant, density has a $1/6^{th}$ order dependence on $k^{o}_{l,prod}$ (Equation 3.16). Unlike viscosity, solution densities do not vary more than 20% over the total range of experimental conditions.

E.2 PIPERAZINE VISCOSITY

PZ solution viscosity values were obtained by regressing 5–12 m PZ viscosity measurements from Freeman at 25, 40, and 60˚C (Rochelle, Sexton et al. 2008a).

The form of the piperazine viscosity equation was based on the form Weiland (1998) used for MEA viscosity. Equation E.3 is linked to the viscosity of water and utilizes the wt% of piperazine on a CO_2-free basis. Temperatures are in Kelvin and loading is in mol_{CO2}/mol_{alk}. Table E.2 includes the regressed parameters. Figures E.5–E.7 show the fit of Equation E.3 to experimental data.

$$\eta = \eta_{H2O} \exp\left(\frac{\left[(a\Omega + b)T + (c\Omega + d)\right] \cdot \left[\alpha(e\Omega + fT + g) + 1\right]\Omega}{T^2}\right) \qquad \text{(E.3)}$$

Table E.2: Regressed parameters for the PZ viscosity equation

Parameter	a	b	c	d	e	f	g
Value	0.310	5.71	0.417	0.0267	-0.00752	-0.00574	2.51

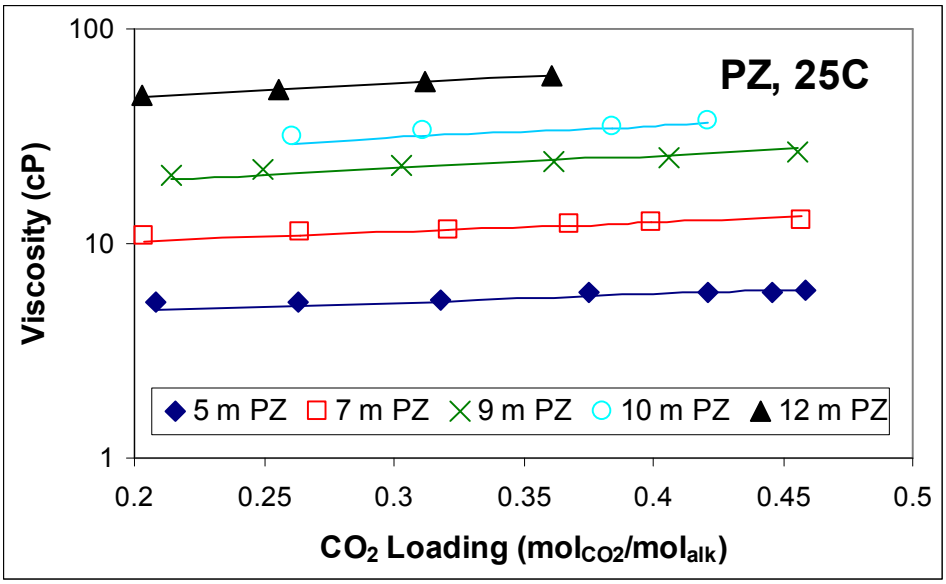

Figure E.5: 5–12 m PZ viscosity at 25˚C: points – data; lines – Equation E.3

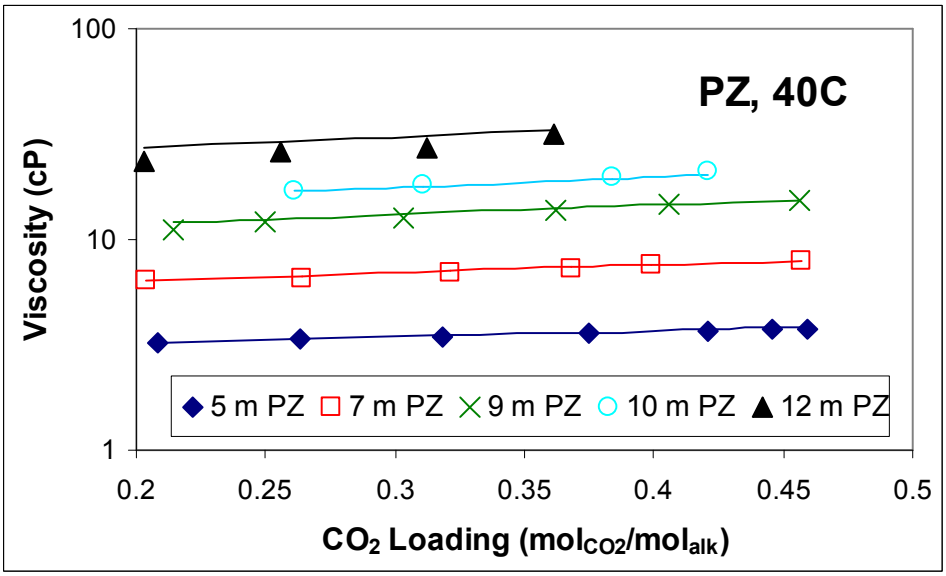

Figure E.6: 5–12 m PZ viscosity at 40˚C: points – data; lines – Equation E.3

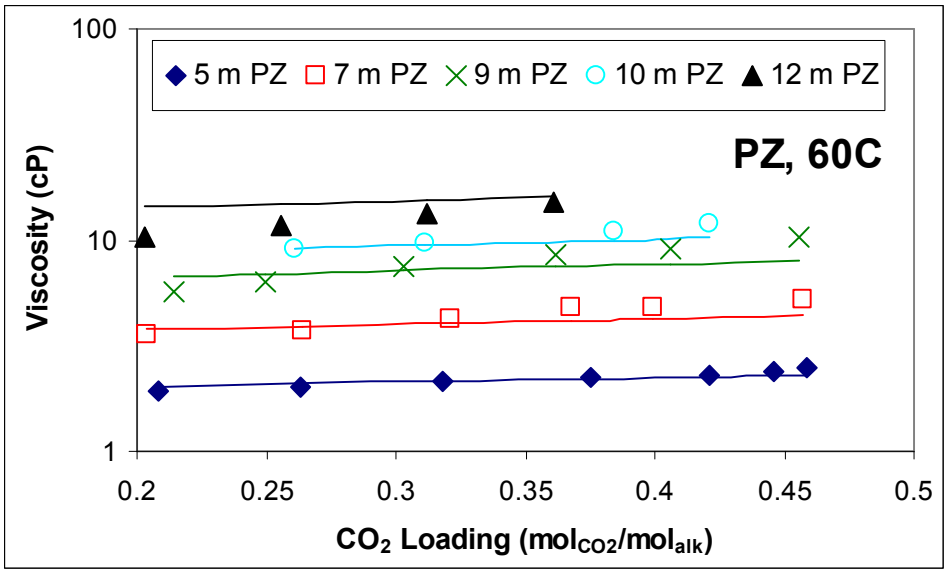

Figure E.7: 5–12 m PZ viscosity at 60˚C: points – data; lines – Equation E.3

Figures E.5–E.7 show good agreement between the viscosity correlation and the raw data. Viscosity was properly represented over the 5–12 m PZ, 25–60˚C range. Parts of the model required the extrapolation of Equation E.3 to 2 m PZ and up to 100˚C. The satisfactory fit with respect to changing temperature and PZ concentration in Figures E.5–E.7 suggests that the extrapolation to 2 m or 100˚C will not introduce significant error.

Unlike density, viscosity estimation is very important for amine solutions. Piperazine solution viscosities can change a factor of 10 with changes in amine concentration. These viscosity changes can drastically affect $k^{o}_{1,prod}$ as well as the diffusion coefficient of CO_2.

Appendix F: Calculated Spreadsheet Model Values

This section lists calculated values for the MEA and PZ spreadsheet models. Each parameter in the k_g' expressions is included in the following tables. Most of these data were generated to produce the figures presented in Chapter 5.

Table F.1: Calculated spreadsheet model results for 7 and 9 m MEA wetted wall column conditions

MEA	Temp	CO_2 Loading	$[MEA]_{free}$	γ_{CO2}	γ_{MEA}	$H_{CO2,soln}$	Density	Viscosity	D_{CO2}	$d(P_{CO2})d(ldg)$	[Alk]	Slope Equil	$k^{o}_{l,prod}$	k_l^o/slope	k_g''	Diffusion	Calc k_g'	Exp k_g'
m	C	mol_{CO2}/mol_{alk}	M			$Pa{\cdot}m^3/mol$	g/cm^3	cP	m^2/s	$Pa/(mol/mol_{alk})$	mol_{alk}/m^3	$Pa/(mol/m^3)$	m/s	$mol/s{\cdot}Pa{\cdot}m^2$	$mol/s{\cdot}Pa{\cdot}m^2$	Resistance	$mol/s{\cdot}Pa{\cdot}m^2$	$mol/s{\cdot}Pa{\cdot}m^2$
7	40	0.252	2.45	1.53	0.62	6317	1.06	2.00	1.2E-09	215	4916	0.04	4.61E-05	1.05E-03	2.90E-06	0%	2.89E-06	3.34E-06
		0.351	1.49	1.74	0.74	7199	1.08	2.18	1.1E-09	1516	4916	0.31	4.40E-05	1.43E-04	1.90E-06	1%	1.88E-06	1.40E-06
		0.432	0.72	1.94	0.85	8011	1.10	2.34	1.1E-09	9414	4916	1.92	4.23E-05	2.21E-05	9.82E-07	4%	9.40E-07	7.66E-07
		0.496	0.21	2.11	0.95	8717	1.11	2.48	1.0E-09	46265	4915	9.41	4.11E-05	4.36E-06	3.02E-07	6%	2.82E-07	3.47E-07
	60	0.252	2.42	1.42	0.47	8692	1.04	1.31	1.9E-09	1534	4849	0.32	5.94E-05	1.88E-04	3.20E-06	2%	3.14E-06	2.92E-06
		0.351	1.48	1.62	0.56	9906	1.06	1.43	1.8E-09	8925	4849	1.84	5.65E-05	3.07E-05	2.11E-06	6%	1.97E-06	1.70E-06
		0.432	0.74	1.81	0.64	11023	1.08	1.54	1.7E-09	47050	4848	9.70	5.43E-05	5.60E-06	1.12E-06	17%	9.32E-07	9.28E-07
		0.496	0.26	1.96	0.71	11995	1.09	1.64	1.6E-09	202553	4848	41.78	5.26E-05	1.26E-06	4.09E-07	25%	3.09E-07	3.76E-07
	80	0.271	2.21	1.37	0.37	11829	1.03	0.99	2.8E-09	11415	4787	2.38	6.73E-05	2.82E-05	3.20E-06	10%	2.87E-06	2.85E-06
		0.366	1.33	1.55	0.44	13409	1.05	1.08	2.6E-09	55364	4787	11.57	6.41E-05	5.55E-06	2.06E-06	27%	1.50E-06	1.87E-06
	100	0.271	2.18	1.29	0.30	15229	1.02	0.64	4.4E-09	50599	4719	10.72	8.65E-05	8.07E-06	3.60E-06	31%	2.49E-06	2.98E-06
		0.366	1.32	1.46	0.35	17264	1.04	0.71	4.1E-09	214665	4719	45.49	8.24E-05	1.81E-06	2.33E-06	56%	1.02E-06	1.40E-06
9	40	0.231	3.14	1.62	0.60	6674	1.06	2.58	1.0E-09	148	5831	0.03	4.03E-05	1.59E-03	3.19E-06	0%	3.19E-06	-
		0.324	2.07	1.87	0.71	7724	1.09	2.87	9.3E-10	863	5831	0.15	3.81E-05	2.57E-04	2.21E-06	1%	2.19E-06	1.86E-06
		0.382	1.41	2.05	0.78	8461	1.10	3.06	8.9E-10	2975	5830	0.51	3.67E-05	7.20E-05	1.55E-06	2%	1.52E-06	1.40E-06
		0.441	0.74	2.25	0.87	9283	1.12	3.28	8.5E-10	11683	5830	2.00	3.54E-05	1.77E-05	8.44E-07	5%	8.06E-07	8.36E-07
		0.496	0.22	2.45	0.95	10121	1.13	3.49	8.1E-10	46265	5829	7.94	3.43E-05	4.32E-06	2.53E-07	6%	2.39E-07	3.02E-07
	60	0.231	3.10	1.50	0.45	9184	1.05	1.64	1.6E-09	1096	5751	0.19	5.26E-05	2.76E-04	3.55E-06	1%	3.50E-06	3.80E-06
		0.324	2.05	1.74	0.53	10629	1.07	1.83	1.5E-09	5364	5750	0.93	4.96E-05	5.31E-05	2.46E-06	4%	2.35E-06	2.44E-06
		0.382	1.40	1.91	0.59	11643	1.09	1.97	1.4E-09	16461	5749	2.86	4.78E-05	1.67E-05	1.74E-06	9%	1.57E-06	1.47E-06
		0.441	0.77	2.09	0.65	12774	1.10	2.11	1.4E-09	57318	5749	9.97	4.60E-05	4.62E-06	9.78E-07	17%	8.07E-07	9.57E-07
		0.496	0.28	2.28	0.71	13926	1.12	2.25	1.3E-09	202553	5749	35.23	4.44E-05	1.26E-06	3.62E-07	22%	2.81E-07	3.24E-07
	80	0.265	2.68	1.49	0.37	12857	1.04	1.24	2.4E-09	10420	5675	1.84	6.25E-05	3.41E-05	3.39E-06	9%	3.08E-06	3.24E-06
		0.356	1.68	1.72	0.43	14833	1.07	1.39	2.2E-09	46313	5675	8.16	6.39E-05	7.82E-06	2.22E-06	22%	1.73E-06	1.75E-06
	100	0.265	2.64	1.40	0.29	16554	1.03	0.80	3.8E-09	46549	5593	8.32	7.93E-05	9.52E-06	3.84E-06	29%	2.74E-06	3.40E-06
		0.356	1.66	1.62	0.35	19098	1.05	0.89	3.5E-09	182248	5592	32.59	8.12E-05	2.49E-06	2.52E-06	50%	1.25E-06	1.33E-06

Table F.2: Calculated spreadsheet model results for 11 and 13 m MEA wetted wall column conditions

MEA	Temp	CO_2 Loading	$[MEA]_{free}$	γ_{CO2}	γ_{MEA}	$H_{CO2,soln}$	Density	Viscosity	D_{CO2}	$d(P_{CO2})d(ldg)$	[Alk]	Slope Equil	$k^{o}_{l,prod}$	k_l^o/slope	k_g''	Diffusion	Calc k_g'	Exp k_g'
m	C	mol_{CO2}/mol_{alk}	M			Pa·m³/mol	g/cm³	cP	m²/s	Pa/(mol/mol_{alk})	mol_{alk}/m^3	Pa/(mol/m³)	m/s	mol/s·Pa·m²	mol/s·Pa·m²	Resistance	mol/s·Pa·m²	mol/s·Pa·m²
11	40	0.261	3.17	1.83	0.63	7558	1.08	3.45	8.2E-10	254	6614	0.04	3.45E-05	9.00E-04	2.87E-06	0%	2.86E-06	3.36E-06
		0.353	1.97	2.16	0.74	8907	1.11	3.93	7.4E-10	1582	6613	0.24	3.22E-05	1.35E-04	1.84E-06	1%	1.81E-06	1.76E-06
		0.428	1.00	2.47	0.85	10183	1.13	4.36	6.9E-10	8560	6612	1.29	3.05E-05	2.35E-05	9.54E-07	4%	9.17E-07	7.14E-07
		0.461	0.59	2.62	0.90	10801	1.14	4.57	6.7E-10	19053	6612	2.88	2.97E-05	1.03E-05	5.67E-07	5%	5.38E-07	4.34E-07
	60	0.261	3.13	1.70	0.48	10400	1.07	2.15	1.4E-09	1780	6521	0.27	4.56E-05	1.67E-04	3.21E-06	2%	3.15E-06	3.35E-06
		0.353	1.96	2.01	0.56	12256	1.09	2.46	1.2E-09	9277	6520	1.42	4.24E-05	2.98E-05	2.07E-06	6%	1.93E-06	1.80E-06
		0.428	1.02	2.30	0.64	14012	1.11	2.75	1.1E-09	43134	6519	6.62	4.00E-05	6.05E-06	1.10E-06	15%	9.31E-07	8.71E-07
		0.461	0.63	2.43	0.67	14862	1.12	2.88	1.1E-09	89701	6519	13.76	3.90E-05	2.84E-06	6.88E-07	20%	5.54E-07	5.02E-07
	80	0.256	3.15	1.58	0.36	13679	1.05	1.53	2.0E-09	9104	6434	1.41	6.08E-05	4.30E-05	3.53E-06	8%	3.27E-06	4.35E-06
		0.359	1.86	1.90	0.44	16441	1.08	1.78	1.8E-09	48846	6433	7.59	5.61E-05	7.38E-06	2.16E-06	23%	1.67E-06	1.93E-06
	100	0.256	3.11	1.49	0.29	17612	1.03	0.96	3.3E-09	41139	6340	6.49	7.81E-05	1.20E-05	4.02E-06	25%	3.02E-06	3.72E-06
		0.359	1.85	1.80	0.35	21168	1.06	1.13	3.0E-09	191365	6339	30.19	7.33E-05	2.43E-06	2.47E-06	50%	1.22E-06	1.56E-06
13	40	0.252	3.63	1.92	0.62	7942	1.09	4.32	6.9E-10	215	7292	0.03	3.07E-05	1.04E-03	2.91E-06	0%	2.90E-06	3.08E-06
		0.372	1.89	2.44	0.77	10063	1.13	5.26	6.0E-10	2385	7290	0.33	2.63E-05	8.04E-05	1.55E-06	2%	1.52E-06	1.28E-06
		0.435	0.99	2.76	0.86	11394	1.15	5.84	5.6E-10	10114	7289	1.39	2.61E-05	1.88E-05	8.21E-07	4%	7.87E-07	6.96E-07
		0.502	0.18	3.15	0.96	13004	1.17	6.52	5.2E-10	54080	7288	7.42	2.46E-05	3.32E-06	1.51E-07	4%	1.45E-07	1.62E-07
	60	0.252	3.58	1.79	0.47	10928	1.07	2.64	1.2E-09	1534	7188	0.21	3.90E-05	1.83E-04	3.28E-06	2%	3.22E-06	2.98E-06
		0.372	1.89	2.27	0.58	13846	1.11	3.24	1.0E-09	13468	7187	1.87	3.50E-05	1.87E-05	1.76E-06	9%	1.61E-06	1.54E-06
		0.435	1.02	2.57	0.64	15678	1.13	3.60	9.3E-10	50236	7186	6.99	3.47E-05	4.96E-06	9.60E-07	16%	8.05E-07	7.56E-07
		0.502	0.27	2.93	0.72	17893	1.15	4.04	8.6E-10	233827	7185	32.54	3.19E-05	9.80E-07	2.55E-07	21%	2.02E-07	1.93E-07
	80	0.254	3.50	1.68	0.36	14561	1.06	1.86	1.8E-09	8837	7091	1.25	5.48E-05	4.40E-05	3.53E-06	7%	3.27E-06	4.21E-06
		0.355	2.11	2.06	0.43	17770	1.09	2.21	1.6E-09	45501	7089	6.42	5.00E-05	7.79E-06	2.15E-06	22%	1.69E-06	1.85E-06
	100	0.254	3.45	1.59	0.29	18747	1.04	1.15	2.9E-09	40035	6985	5.73	7.23E-05	1.26E-05	4.05E-06	24%	3.06E-06	3.66E-06
		0.355	2.10	1.94	0.34	22879	1.07	1.38	2.6E-09	179317	6984	25.68	6.58E-05	2.56E-06	2.50E-06	49%	1.27E-06	1.56E-06

Table F.3: Calculated spreadsheet model results for 7 and 13 m MEA at 20˚C (Figure 5.45)

MEA	Temp	CO_2 Loading	$[MEA]_{free}$	γ_{CO2}	γ_{MEA}	$H_{CO2,soln}$	Density	Viscosity	D_{CO2}	$d(P_{CO2})d(ldg)$	[Alk]	Slope Equil	$k^{o}_{l,prod}$	k_l^o/slope	k_g''	Diffusion	Calc k_g'
m	C	mol_{CO2}/mol_{alk}	M			$Pa \cdot m^3/mol$	g/cm^3	cP	m^2/s	$Pa/(mol/mol_{alk})$	mol_{alk}/m^3	$Pa/(mol/m^3)$	m/s	$mol/s \cdot Pa \cdot m^2$	$mol/s \cdot Pa \cdot m^2$	Resistance	$mol/s \cdot Pa \cdot m^2$
7	20	0.25	2.48	1.66	0.86	4383	1.07	3.57	6.8E-10	22	4960	0.00	3.28E-05	7.54E-03	2.55E-06	0%	2.55E-06
		0.3	1.99	1.77	0.94	4682	1.08	3.72	6.6E-10	62	4960	0.01	3.21E-05	2.56E-03	2.12E-06	0%	2.12E-06
		0.35	1.50	1.89	1.03	5002	1.09	3.88	6.4E-10	194	4960	0.04	3.15E-05	8.03E-04	1.66E-06	0%	1.66E-06
		0.4	1.01	2.02	1.12	5343	1.10	4.04	6.3E-10	657	4960	0.13	3.08E-05	2.32E-04	1.17E-06	0%	1.16E-06
		0.45	0.53	2.16	1.22	5708	1.11	4.20	6.1E-10	2408	4960	0.49	3.01E-05	6.20E-05	6.41E-07	1%	6.34E-07
		0.5	0.14	2.31	1.33	6097	1.12	4.38	5.9E-10	9581	4959	1.93	2.95E-05	1.53E-05	1.74E-07	1%	1.72E-07
		0.55	0.03	2.46	1.45	6513	1.13	4.56	5.7E-10	41401	4959	8.35	2.89E-05	3.46E-06	3.69E-08	1%	3.65E-08
		0.6	0.01	2.63	1.59	6958	1.14	4.74	5.6E-10	194358	4959	39.19	2.82E-05	7.20E-07	1.53E-08	2%	1.50E-08
13		0.25	3.69	2.08	0.86	5504	1.10	8.33	3.7E-10	22	7367	0.00	2.28E-05	7.76E-03	2.49E-06	0%	2.49E-06
		0.3	2.95	2.30	0.94	6074	1.11	9.01	3.5E-10	62	7366	0.01	2.18E-05	2.58E-03	2.01E-06	0%	2.01E-06
		0.35	2.22	2.54	1.03	6704	1.13	9.74	3.3E-10	194	7366	0.03	2.06E-05	7.80E-04	1.53E-06	0%	1.52E-06
		0.4	1.49	2.80	1.12	7399	1.15	10.53	3.1E-10	657	7365	0.09	2.01E-05	2.25E-04	1.03E-06	0%	1.03E-06
		0.45	0.76	3.09	1.22	8166	1.16	11.39	3.0E-10	2408	7364	0.33	1.78E-05	5.44E-05	5.33E-07	1%	5.27E-07
		0.5	0.12	3.41	1.33	9012	1.18	12.32	2.8E-10	9581	7364	1.30	1.63E-05	1.25E-05	8.71E-08	1%	8.65E-08
		0.55	0.02	3.76	1.45	9946	1.19	13.32	2.6E-10	41401	7363	5.62	1.64E-05	2.91E-06	1.22E-08	0%	1.22E-08
		0.6	0.01	4.15	1.59	10977	1.21	14.40	2.5E-10	194358	7362	26.40	1.57E-05	5.95E-07	5.62E-09	1%	5.57E-09

Table F.4: Calculated spreadsheet model results for 9 m MEA at 0.3 CO_2 loading (Figure 5.18)

MEA	Temp	CO_2 Loading	$[MEA]_{free}$	γ_{CO2}	γ_{MEA}	$H_{CO2,soln}$	Density	Viscosity	D_{CO2}	$d(P_{CO2})d(ldg)$	[Alk]	Slope Equil	$k^{o}_{l,prod}$	k_l^o/slope	k_g''	Diffusion	Calc k_g'
m	C	mol_{CO2}/mol_{alk}	M			$Pa \cdot m^3/mol$	g/cm^3	cP	m^2/s	$Pa/(mol/mol_{alk})$	mol_{alk}/m^3	$Pa/(mol/m^3)$	m/s	$mol/s \cdot Pa \cdot m^2$	$mol/s \cdot Pa \cdot m^2$	Resistance	$mol/s \cdot Pa \cdot m^2$
9	40	0.3	2.35	1.80	0.68	7439	1.08	2.79	9.3E-10	534	5831	0.09	3.86E-05	4.22E-04	2.45E-06	1%	2.44E-06
	50		2.34	1.74	0.58	8769	1.07	2.18	1.2E-09	1405	5798	0.24	4.46E-05	1.84E-04	2.60E-06	1%	2.56E-06
	60		2.32	1.68	0.51	10236	1.07	1.78	1.5E-09	3475	5750	0.60	5.03E-05	8.33E-05	2.73E-06	3%	2.64E-06
	70		2.31	1.62	0.45	11840	1.06	1.51	1.9E-09	8117	5713	1.42	5.57E-05	3.92E-05	2.86E-06	7%	2.67E-06
	80		2.29	1.57	0.39	13584	1.05	1.30	2.4E-09	17989	5675	3.17	6.11E-05	1.93E-05	2.99E-06	13%	2.59E-06
	90		2.28	1.53	0.35	15467	1.04	1.09	2.9E-09	37984	5635	6.74	6.80E-05	1.01E-05	3.12E-06	24%	2.38E-06
	100		2.26	1.48	0.31	17489	1.04	0.83	3.5E-09	76688	5593	13.71	7.93E-05	5.78E-06	3.24E-06	36%	2.07E-06

Table F.5: Calculated MEA spreadsheet model results for 60˚C, 0.4 CO_2 loading MEA solutions (Figure 5.19)

MEA	Temp	CO_2 Loading	$[MEA]_{free}$	γ_{CO2}	γ_{MEA}	$H_{CO2,soln}$	Density	Viscosity	D_{CO2}	$d(P_{CO2})d(ldg)$	[Alk]	Slope Equil	$k^{\circ}_{l,prod}$	k_l°/slope	k_g''	Diffusion	Calc k_g'
m	C	mol_{CO2}/mol_{alk}	M			$Pa{\cdot}m^3/mol$	g/cm^3	cP	m^2/s	$Pa/(mol/mol_{alk})$	mol_{alk}/m^3	$Pa/(mol/m^3)$	m/s	$mol/s{\cdot}Pa{\cdot}m^2$	$mol/s{\cdot}Pa{\cdot}m^2$	Resistance	$mol/s{\cdot}Pa{\cdot}m^2$
7	60	0.4	1.03	1.73	0.61	10567	1.07	1.50	1.7E-09	23809	4849	4.91	5.52E-05	1.12E-05	1.50E-06	12%	1.33E-06
8			1.12	1.84	0.61	11263	1.08	1.73	1.6E-09	23809	5316	4.48	4.86E-05	1.09E-05	1.51E-06	12%	1.32E-06
9			1.21	1.96	0.61	11977	1.09	2.01	1.4E-09	23809	5749	4.14	4.50E-05	1.09E-05	1.49E-06	12%	1.31E-06
10			1.29	2.07	0.61	12649	1.10	2.30	1.3E-09	23809	6148	3.87	4.19E-05	1.08E-05	1.48E-06	12%	1.30E-06
11			1.36	2.18	0.61	13329	1.11	2.64	1.2E-09	23809	6520	3.65	3.90E-05	1.07E-05	1.45E-06	12%	1.28E-06
12			1.43	2.29	0.61	13981	1.11	3.00	1.0E-09	23809	6864	3.47	3.83E-05	1.10E-05	1.42E-06	11%	1.26E-06
13			1.50	2.40	0.61	14633	1.12	3.40	9.6E-10	23809	7186	3.31	3.58E-05	1.08E-05	1.39E-06	11%	1.23E-06

Table F.6: Calculated spreadsheet model results for 7 and 9 m MEA at high CO_2 loading and temperature

MEA	Temp	CO_2 Loading	$[MEA]_{free}$	γ_{CO2}	γ_{MEA}	$H_{CO2,soln}$	Density	Viscosity	D_{CO2}	$d(P_{CO2})d(ldg)$	[Alk]	Slope Equil	$k^{\circ}_{l,prod}$	k_l°/slope	k_g''	Diffusion	Calc k_g'
m	C	mol_{CO2}/mol_{alk}	M			$Pa{\cdot}m^3/mol$	g/cm^3	cP	m^2/s	$Pa/(mol/mol_{alk})$	mol_{alk}/m^3	$Pa/(mol/m^3)$	m/s	$mol/s{\cdot}Pa{\cdot}m^2$	$mol/s{\cdot}Pa{\cdot}m^2$	Resistance	$mol/s{\cdot}Pa{\cdot}m^2$
7	80	0.45	0.59	1.73	0.51	14963	1.07	1.17	2.5E-09	279459	4786	58.39	6.46E-05	1.11E-06	9.74E-07	47%	5.18E-07
	100		0.67	1.63	0.41	19265	1.06	0.77	3.9E-09	952786	4718	201.95	8.29E-05	4.10E-07	1.25E-06	75%	3.09E-07
13	80		0.90	2.48	0.51	21411	1.12	2.61	1.4E-09	279459	7087	39.43	4.23E-05	1.07E-06	9.28E-07	46%	4.98E-07
	100		0.92	2.34	0.41	27566	1.10	1.62	2.3E-09	952786	6982	136.47	5.57E-05	4.08E-07	1.11E-06	73%	2.98E-07

Table F.7: Calculated spreadsheet model results for Hartono (2009) experimental conditions (Figure 5.43)

MEA	Temp	CO_2 Loading	$[MEA]_{free}$	γ_{CO2}	γ_{MEA}	$H_{CO2,soln}$	Density	Viscosity	D_{CO2}	k_g''	Exp k_g'
M	C	mol_{CO2}/mol_{alk}	M			$Pa{\cdot}m^3/mol$	g/cm^3	cP	m^2/s	$mol/s{\cdot}Pa{\cdot}m^2$	$mol/s{\cdot}Pa{\cdot}m^2$
0.5	40	0	0.5	0.972	0.326	4010	0.99	0.69	2.6E-09	5.71E-07	1.07E-06
1	40	0	1.0	0.985	0.326	4065	0.99	0.74	2.5E-09	1.10E-06	1.72E-06
2	40	0	2.0	1.013	0.326	4181	1.00	0.89	2.2E-09	2.04E-06	2.24E-06
3	40	0	3.0	1.041	0.326	4296	1.00	1.07	1.9E-09	2.83E-06	2.61E-06
4	40	0	4.0	1.070	0.326	4416	1.00	1.31	1.6E-09	3.45E-06	2.80E-06
5	40	0	5.0	1.100	0.326	4539	1.00	1.60	1.4E-09	3.96E-06	2.88E-06

Table F.8: Calculated pseudo first order spreadsheet model results for 5 M MEA at 40 and 60˚C (Figure 5.42)

MEA	Temp	CO_2 Loading	$[MEA]_{free}$	γ_{CO2}	γ_{MEA}	$H_{CO2,soln}$	Density	Viscosity	D_{CO2}	k_g"
M	C	mol_{CO2}/mol_{alk}	M			$Pa \cdot m^3/mol$	g/cm^3	cP	m^2/s	$mol/s \cdot Pa \cdot m^2$
5	40	0	4.92	1.10	0.40	4529	1.00	1.60	1.4E-09	4.77E-06
		0.05	4.43	1.17	0.44	4838	1.01	1.67	1.4E-09	4.46E-06
		0.1	3.93	1.25	0.48	5168	1.02	1.75	1.3E-09	4.12E-06
		0.15	3.44	1.34	0.52	5521	1.04	1.83	1.3E-09	3.74E-06
		0.2	2.95	1.43	0.57	5898	1.05	1.91	1.2E-09	3.34E-06
		0.25	2.47	1.53	0.62	6300	1.06	2.00	1.2E-09	2.89E-06
		0.3	1.98	1.63	0.68	6730	1.07	2.08	1.2E-09	2.41E-06
		0.35	1.50	1.74	0.74	7189	1.08	2.18	1.1E-09	1.90E-06
		0.4	1.02	1.86	0.81	7680	1.09	2.28	1.1E-09	1.34E-06
		0.45	0.56	1.99	0.88	8204	1.10	2.38	1.0E-09	7.65E-07
		0.5	0.19	2.12	0.96	8764	1.11	2.49	1.0E-09	2.69E-07
	60	0	4.85	1.02	0.30	6232	0.99	1.03	2.3E-09	5.28E-06
		0.05	4.37	1.09	0.33	6657	1.00	1.08	2.2E-09	4.93E-06
		0.1	3.88	1.16	0.36	7112	1.01	1.13	2.1E-09	4.55E-06
		0.15	3.40	1.24	0.39	7597	1.02	1.19	2.0E-09	4.14E-06
		0.2	2.92	1.33	0.43	8115	1.03	1.24	2.0E-09	3.68E-06
		0.25	2.44	1.42	0.47	8669	1.04	1.30	1.9E-09	3.20E-06
		0.3	1.96	1.52	0.51	9261	1.05	1.36	1.8E-09	2.67E-06
		0.35	1.49	1.62	0.55	9892	1.06	1.43	1.8E-09	2.10E-06
		0.4	1.03	1.73	0.61	10567	1.07	1.50	1.7E-09	1.50E-06
		0.45	0.59	1.85	0.66	11289	1.08	1.57	1.7E-09	8.92E-07
		0.5	0.24	1.98	0.72	12059	1.10	1.64	1.6E-09	3.74E-07

Table F.9: Calculated pseudo first order spreadsheet model results for 7 M MEA at 40 and 60˚C (Figure 5.42)

MEA	Temp	CO_2 Loading	$[MEA]_{free}$	γ_{CO2}	γ_{MEA}	$H_{CO2,soln}$	Density	Viscosity	D_{CO2}	k_g"
M	C	mol_{CO2}/mol_{alk}	M			$Pa \cdot m^3/mol$	g/cm^3	cP	m^2/s	$mol/s \cdot Pa \cdot m^2$
7	40	0	6.97	1.16	0.40	4786	1.01	2.60	9.8E-10	5.52E-06
		0.05	6.27	1.27	0.44	5257	1.02	2.81	9.3E-10	5.03E-06
		0.1	5.57	1.40	0.48	5774	1.04	3.03	8.8E-10	4.53E-06
		0.15	4.88	1.54	0.52	6342	1.05	3.27	8.3E-10	4.01E-06
		0.2	4.18	1.69	0.57	6965	1.07	3.53	7.9E-10	3.49E-06
		0.25	3.49	1.85	0.62	7651	1.08	3.81	7.5E-10	2.95E-06
		0.3	2.80	2.04	0.68	8403	1.10	4.11	7.1E-10	2.39E-06
		0.35	2.11	2.24	0.74	9230	1.11	4.43	6.7E-10	1.83E-06
		0.4	1.43	2.46	0.81	10138	1.13	4.78	6.3E-10	1.25E-06
		0.45	0.75	2.70	0.88	11135	1.14	5.16	6.0E-10	6.69E-07
		0.5	0.19	2.96	0.96	12230	1.16	5.57	5.7E-10	1.74E-07
	60	0	6.87	1.08	0.30	6585	0.99	1.59	1.7E-09	6.23E-06
		0.05	6.18	1.18	0.33	7233	1.01	1.72	1.6E-09	5.67E-06
		0.1	5.50	1.30	0.36	7945	1.02	1.86	1.5E-09	5.10E-06
		0.15	4.81	1.43	0.39	8726	1.04	2.01	1.4E-09	4.52E-06
		0.2	4.13	1.57	0.43	9585	1.05	2.17	1.3E-09	3.92E-06
		0.25	3.45	1.72	0.47	10527	1.07	2.35	1.2E-09	3.32E-06
		0.3	2.77	1.89	0.51	11563	1.08	2.54	1.2E-09	2.70E-06
		0.35	2.10	2.08	0.55	12700	1.10	2.75	1.1E-09	2.07E-06
		0.4	1.43	2.28	0.61	13950	1.11	2.98	1.1E-09	1.43E-06
		0.45	0.79	2.51	0.66	15322	1.13	3.22	1.0E-09	7.97E-07
		0.5	0.27	2.76	0.72	16829	1.14	3.49	9.4E-10	2.80E-07

Table F.10: Calculated spreadsheet model results for 2, 5, 8, and 12 m PZ wetted wall column conditions

PZ	Temp	CO_2 Loading	$[PZ]_{free}$	$[PZCOO^-]$	γ_{CO2}	γ_{PZ}	γ_{PZCOO}	$H_{CO2,soln}$	Density	Viscosity	D_{CO2}	$d(P_{CO2})d(ldg)$	[Alk]	Slope Equil	$k^o_{l,prod}$	$k_l{}^o$/slope	k_g''	Diffusion	Calc k_g'	Exp k_g'
m	C	mol_{CO2}/mol_{alk}	M	M				Pa·m³/mol	g/cm³	cP	m²/s	Pa/(mol/mol_{alk})	mol_{alk}/m^3	Pa/(mol/m³)	m/s	mol/s·Pa·m²	mol/s·Pa·m²	Resistance	mol/s·Pa·m²	mol/s·Pa·m²
2	40	0.24	0.48	0.32	1.38	0.057	0.038	5698	1.04	1.11	1.9E-09	2255	3421	0.66	6.14E-05	9.32E-05	3.38E-06	4%	3.26E-06	3.32E-06
		0.316	0.21	0.32	1.52	0.057	0.038	6264	1.05	1.13	1.8E-09	13581	3419	3.97	6.07E-05	1.53E-05	1.87E-06	11%	1.67E-06	2.04E-06
		0.352	0.13	0.27	1.59	0.057	0.038	6551	1.05	1.14	1.8E-09	32203	3419	9.42	6.04E-05	6.41E-06	1.32E-06	17%	1.09E-06	1.39E-06
		0.411	0.05	0.15	1.71	0.057	0.038	7050	1.06	1.16	1.8E-09	134954	3418	39.49	5.98E-05	1.51E-06	5.96E-07	28%	4.28E-07	5.55E-07
	60	0.24	0.55	0.22	1.28	0.080	0.038	7841	1.03	0.76	2.9E-09	11494	3390	3.39	7.72E-05	2.28E-05	5.88E-06	21%	4.67E-06	3.33E-06
		0.316	0.28	0.21	1.41	0.080	0.038	8619	1.04	0.77	2.8E-09	57257	3388	16.90	7.65E-05	4.53E-06	3.16E-06	41%	1.86E-06	2.06E-06
		0.352	0.19	0.17	1.48	0.080	0.038	9014	1.05	0.78	2.8E-09	124088	3388	36.63	7.62E-05	2.08E-06	2.17E-06	51%	1.06E-06	1.38E-06
		0.411	0.08	0.10	1.59	0.080	0.038	9701	1.05	0.79	2.8E-09	448729	3387	132.50	7.56E-05	5.71E-07	9.57E-07	63%	3.58E-07	3.84E-07
	80	0.239	0.58	0.14	1.20	0.106	0.038	10393	1.02	0.59	4.0E-09	47213	3350	14.09	9.90E-05	7.02E-06	9.58E-06	58%	4.05E-06	3.34E-06
		0.324	0.29	0.13	1.34	0.106	0.038	11553	1.03	0.60	4.0E-09	236248	3349	70.54	1.00E-04	1.42E-06	4.72E-06	77%	1.09E-06	1.32E-06
	100	0.239	0.59	0.09	1.14	0.138	0.038	13381	1.00	0.40	6.3E-09	167679	3304	50.75	1.25E-04	2.46E-06	1.57E-05	86%	2.13E-06	2.40E-06
		0.324	0.30	0.08	1.26	0.138	0.038	14875	1.01	0.40	6.2E-09	710204	3303	215.04	1.27E-04	5.89E-07	7.74E-06	93%	5.47E-07	9.12E-07
5	40	0.226	0.84	0.95	2.00	0.075	0.038	8246	1.04	3.19	8.6E-10	1627	6801	0.24	3.76E-05	1.57E-04	4.70E-06	3%	4.56E-06	4.39E-06
		0.299	0.30	0.95	2.43	0.075	0.038	10006	1.06	3.36	8.3E-10	9060	6774	1.34	3.66E-05	2.74E-05	2.39E-06	8%	2.20E-06	2.57E-06
		0.354	0.15	0.71	2.81	0.075	0.038	11576	1.07	3.49	8.1E-10	33794	6753	5.00	3.58E-05	7.16E-06	1.39E-06	16%	1.16E-06	1.69E-06
		0.402	0.08	0.45	3.19	0.075	0.038	13145	1.08	3.61	7.9E-10	108302	6735	16.08	3.52E-05	2.19E-06	7.74E-07	26%	5.72E-07	7.93E-07
	60	0.226	0.98	0.72	1.86	0.104	0.038	11347	1.03	2.00	1.4E-09	8585	6739	1.27	4.95E-05	3.88E-05	8.47E-06	18%	6.96E-06	4.75E-06
		0.299	0.47	0.69	2.26	0.104	0.038	13768	1.05	2.08	1.4E-09	39852	6712	5.94	4.85E-05	8.17E-06	4.31E-06	35%	2.82E-06	2.62E-06
		0.354	0.26	0.51	2.61	0.104	0.038	15928	1.06	2.14	1.4E-09	129567	6692	19.36	4.78E-05	2.47E-06	2.42E-06	49%	1.22E-06	1.80E-06
		0.402	0.14	0.32	2.96	0.104	0.038	18088	1.07	2.19	1.3E-09	368302	6674	55.18	4.62E-05	8.37E-07	1.29E-06	61%	5.08E-07	6.59E-07
	80	0.238	0.99	0.52	1.80	0.139	0.038	15546	1.02	1.44	2.1E-09	46339	6657	6.96	6.28E-05	9.02E-06	1.31E-05	59%	5.34E-06	4.67E-06
		0.321	0.48	0.44	2.24	0.139	0.038	19369	1.04	1.48	2.1E-09	223023	6626	33.66	6.08E-05	1.81E-06	6.12E-06	77%	1.39E-06	1.91E-06
	100	0.238	1.04	0.36	1.70	0.179	0.038	20015	1.01	0.91	3.5E-09	164900	6565	25.12	8.08E-05	3.22E-06	2.24E-05	87%	2.81E-06	3.52E-06
		0.321	0.52	0.31	2.12	0.179	0.038	24938	1.03	0.92	3.4E-09	674404	6535	103.20	8.02E-05	7.77E-07	1.03E-05	93%	7.22E-07	1.02E-06
8	40	0.231	0.89	1.55	2.66	0.090	0.038	10988	1.09	8.80	4.2E-10	1828	9396	0.19	2.29E-05	1.17E-04	3.94E-06	3%	3.81E-06	4.27E-06
		0.305	0.20	1.48	3.48	0.090	0.038	14369	1.11	9.46	4.0E-10	10449	9325	1.12	2.03E-05	1.81E-05	1.68E-06	9%	1.54E-06	1.98E-06
		0.36	0.11	1.04	4.25	0.090	0.038	17540	1.13	9.98	3.8E-10	39058	9273	4.21	2.10E-05	4.98E-06	9.76E-07	16%	8.16E-07	1.14E-06
		0.404	0.07	0.67	4.99	0.090	0.038	20573	1.14	10.42	3.7E-10	113723	9232	12.32	2.05E-05	1.66E-06	5.86E-07	26%	4.34E-07	3.53E-07
	60	0.231	1.07	1.24	2.48	0.125	0.038	15119	1.08	5.08	7.3E-10	9527	9310	1.02	3.03E-05	2.96E-05	7.28E-06	20%	5.85E-06	4.41E-06
		0.305	0.37	1.14	3.24	0.125	0.038	19772	1.10	5.33	7.0E-10	45280	9240	4.90	2.83E-05	5.77E-06	2.98E-06	34%	1.97E-06	2.02E-06
		0.36	0.21	0.80	3.95	0.125	0.038	24135	1.12	5.53	6.8E-10	147523	9189	16.05	2.89E-05	1.80E-06	1.69E-06	48%	8.72E-07	9.57E-07
		0.404	0.14	0.51	4.64	0.125	0.038	28309	1.13	5.69	6.7E-10	384810	9148	42.06	2.90E-05	6.90E-07	1.01E-06	59%	4.11E-07	3.20E-07
	80	0.253	0.95	0.96	2.51	0.167	0.038	21732	1.07	3.40	1.1E-09	61358	9182	6.68	3.99E-05	5.97E-06	1.00E-05	63%	3.74E-06	3.61E-06
		0.289	0.60	0.91	2.87	0.167	0.038	24761	1.08	3.45	1.1E-09	121062	9148	13.23	3.96E-05	2.99E-06	6.35E-06	68%	2.03E-06	1.97E-06
	100	0.253	0.95	0.77	2.37	0.216	0.038	27979	1.06	1.99	2.0E-09	212018	9055	23.41	5.43E-05	2.32E-06	1.66E-05	88%	2.03E-06	2.18E-06
		0.289	0.57	0.74	2.71	0.216	0.038	31880	1.07	2.00	2.0E-09	389806	9022	43.21	5.42E-05	1.25E-06	9.86E-06	89%	1.11E-06	1.20E-06
12	60	0.231	1.07	1.88	3.20	0.148	0.038	19528	1.15	14.37	3.4E-10	9527	12099	0.79	1.82E-05	2.31E-05	5.56E-06	19%	4.48E-06	4.19E-06
		0.289	0.21	1.71	4.16	0.148	0.038	25407	1.17	14.98	3.3E-10	32230	11985	2.69	1.78E-05	6.60E-06	1.88E-06	22%	1.46E-06	1.85E-06
		0.354	0.09	1.08	5.59	0.148	0.038	34122	1.19	15.69	3.2E-10	129567	11861	10.92	1.73E-05	1.59E-06	9.04E-07	36%	5.76E-07	7.73E-07
	80	0.222	1.34	1.49	2.88	0.198	0.038	24880	1.13	8.75	5.8E-10	34402	11976	2.87	2.43E-05	8.44E-06	1.10E-05	57%	4.78E-06	4.24E-06
		0.29	0.23	1.41	3.92	0.198	0.038	33872	1.15	8.94	5.7E-10	123384	11845	10.42	2.40E-05	2.30E-06	2.74E-06	54%	1.25E-06	1.48E-06
	100	0.222	1.34	1.31	2.72	0.256	0.038	32032	1.12	4.79	1.0E-09	126320	11811	10.70	3.42E-05	3.20E-06	1.89E-05	86%	2.73E-06	3.78E-06
		0.29	0.21	1.30	3.70	0.256	0.038	43610	1.14	4.78	1.0E-09	396502	11681	33.94	3.42E-05	1.01E-06	3.97E-06	80%	8.04E-07	8.30E-07

Table F.11: Calculated spreadsheet model results for 8 m PZ at 20˚C (Figure 5.46)

PZ	Temp	CO_2 Loading	$[PZ]_{free}$	[PZCOO$^-$]	γ_{CO2}	γ_{PZ}	γ_{PZCOO}	$H_{CO2,soln}$	Density	Viscosity	D_{CO2}	$d(P_{CO2})d(ldg)$	[Alk]	Slope Equil	$k^o_{l,prod}$	k_l^o/slope	k_g''	Diffusion	Calc k_g'
m	C	mol_{CO2}/mol_{alk}	M	M				$Pa{\cdot}m^3/mol$	g/cm^3	cP	m^2/s	$Pa/(mol/mol_{alk})$	mol_{alk}/m^3	$Pa/(mol/m^3)$	m/s	$mol/s{\cdot}Pa{\cdot}m^2$	$mol/s{\cdot}Pa{\cdot}m^2$	Resistance	$mol/s{\cdot}Pa{\cdot}m^2$
8	20	0.2	0.49	1.48	2.58	0.062	0.038	6832	1.08	17.31	2.2E-10	123	9481	0.01	1.40E-05	1.08E-03	1.71E-06	0%	1.71E-06
		0.25	0.49	1.84	3.10	0.062	0.038	8190	1.10	18.51	2.1E-10	454	9432	0.05	1.35E-05	2.80E-04	1.75E-06	1%	1.74E-06
		0.3	0.12	1.71	3.71	0.062	0.038	9817	1.11	19.79	2.0E-10	1704	9384	0.18	1.30E-05	7.16E-05	1.09E-06	1%	1.07E-06
		0.35	0.06	1.28	4.45	0.062	0.038	11768	1.13	21.15	1.9E-10	6498	9337	0.70	1.26E-05	1.80E-05	6.97E-07	4%	6.71E-07
		0.4	0.04	0.82	5.34	0.062	0.038	14106	1.14	22.62	1.8E-10	25182	9290	2.71	1.21E-05	4.47E-06	4.02E-07	8%	3.69E-07
		0.45	0.02	0.37	6.40	0.062	0.038	16910	1.16	24.18	1.7E-10	99156	9243	10.73	1.17E-05	1.09E-06	1.64E-07	13%	1.43E-07
		0.5	0.00	0.03	7.67	0.062	0.038	20270	1.17	25.86	1.6E-10	396737	9198	43.14	1.13E-05	2.62E-07	1.19E-08	4%	1.14E-08

Table F.12: Calculated spreadsheet model results for 5 m MEA at 0.3 CO_2 loading (Figure 5.35)

PZ	Temp	CO_2 Loading	$[PZ]_{free}$	[PZCOO$^-$]	γ_{CO2}	γ_{PZ}	γ_{PZCOO}	$H_{CO2,soln}$	Density	Viscosity	D_{CO2}	$d(P_{CO2})d(ldg)$	[Alk]	Slope Equil	$k^o_{l,prod}$	k_l^o/slope	k_g''	Diffusion	Calc k_g'
m	C	mol_{CO2}/mol_{alk}	M	M				$Pa{\cdot}m^3/mol$	g/cm^3	cP	m^2/s	$Pa/(mol/mol_{alk})$	mol_{alk}/m^3	$Pa/(mol/m^3)$	m/s	$mol/s{\cdot}Pa{\cdot}m^2$	$mol/s{\cdot}Pa{\cdot}m^2$	Resistance	$mol/s{\cdot}Pa{\cdot}m^2$
5	40	0.3	0.30	0.95	2.43	0.075	0.038	10034	1.06	3.36	8.2E-10	9278	6773	1.37	3.42E-05	2.50E-05	2.36E-06	9%	2.16E-06
	50		0.39	0.82	2.34	0.089	0.038	11828	1.05	2.59	1.1E-09	19916	6745	2.95	3.99E-05	1.35E-05	3.15E-06	19%	2.55E-06
	60		0.47	0.69	2.26	0.104	0.038	13807	1.05	2.08	1.4E-09	40709	6713	6.06	4.94E-05	8.15E-06	4.27E-06	34%	2.80E-06
	70		0.54	0.57	2.19	0.120	0.038	15971	1.04	1.74	1.7E-09	79563	6675	11.92	5.61E-05	4.71E-06	5.78E-06	55%	2.59E-06
	80		0.59	0.48	2.12	0.139	0.038	18323	1.04	1.47	2.1E-09	149246	6634	22.50	6.10E-05	2.71E-06	7.62E-06	74%	2.00E-06
	90		0.61	0.40	2.06	0.158	0.038	20864	1.03	1.22	2.6E-09	269584	6589	40.91	6.96E-05	1.70E-06	9.78E-06	85%	1.45E-06
	100		0.63	0.33	2.00	0.179	0.038	23591	1.02	0.92	3.2E-09	470294	6541	71.89	7.88E-05	1.10E-06	1.23E-05	92%	1.01E-06

Table F.13: Calculated spreadsheet model 60˚C, 0.4 CO_2 loading PZ solutions (Figure 5.36)

PZ	Temp	CO_2 Loading	$[PZ]_{free}$	[PZCOO$^-$]	γ_{CO2}	γ_{PZ}	γ_{PZCOO}	$H_{CO2,soln}$	Density	Viscosity	D_{CO2}	$d(P_{CO2})d(ldg)$	[Alk]	Slope Equil	$k^o_{l,prod}$	k_l^o/slope	k_g''	Diffusion	Calc k_g'
m	C	mol_{CO2}/mol_{alk}	M	M				$Pa{\cdot}m^3/mol$	g/cm^3	cP	m^2/s	$Pa/(mol/mol_{alk})$	mol_{alk}/m^3	$Pa/(mol/m^3)$	m/s	$mol/s{\cdot}Pa{\cdot}m^2$	$mol/s{\cdot}Pa{\cdot}m^2$	Resistance	$mol/s{\cdot}Pa{\cdot}m^2$
2	60	0.4	0.09	0.12	1.57	0.080	0.038	9568	1.05	0.79	2.7E-09	352510	3387	104.07	8.09E-05	7.78E-07	1.15E-06	60%	4.63E-07
3			0.12	0.19	1.99	0.088	0.038	12156	1.05	1.10	2.2E-09	352510	4620	76.30	6.78E-05	8.88E-07	1.34E-06	60%	5.34E-07
4			0.14	0.26	2.45	0.096	0.038	14977	1.06	1.56	1.7E-09	352510	5702	61.82	5.65E-05	9.14E-07	1.39E-06	60%	5.52E-07
5			0.15	0.34	2.95	0.104	0.038	17996	1.07	2.19	1.3E-09	352510	6676	52.80	4.72E-05	8.93E-07	1.36E-06	60%	5.39E-07
6			0.15	0.41	3.47	0.111	0.038	21176	1.09	3.05	1.0E-09	352510	7566	46.59	3.96E-05	8.50E-07	1.28E-06	60%	5.11E-07
7			0.15	0.48	4.01	0.118	0.038	24487	1.11	4.20	8.2E-10	352510	8388	42.03	3.35E-05	7.96E-07	1.18E-06	60%	4.75E-07
8			0.15	0.54	4.57	0.125	0.038	27898	1.13	5.68	6.6E-10	352510	9153	38.51	2.79E-05	7.26E-07	1.06E-06	59%	4.31E-07
9			0.14	0.60	5.14	0.131	0.038	31385	1.15	7.56	5.4E-10	352510	9869	35.72	2.55E-05	7.13E-07	9.48E-07	57%	4.07E-07
10			0.13	0.65	5.72	0.137	0.038	34926	1.17	9.91	4.4E-10	352510	10542	33.44	2.17E-05	6.48E-07	8.37E-07	56%	3.65E-07
11			0.12	0.70	6.31	0.143	0.038	38499	1.19	12.79	3.7E-10	352510	11176	31.54	1.89E-05	6.01E-07	7.34E-07	55%	3.30E-07
12			0.10	0.74	6.89	0.148	0.038	42090	1.21	16.26	3.1E-10	352510	11777	29.93	1.67E-05	5.57E-07	6.40E-07	53%	2.98E-07

Table F.14: Calculated spreadsheet model results for 1.8 m PZ at 40˚C (Figure 5.44)

PZ	Temp	CO_2 Loading	$[PZ]_{free}$	$[PZCOO^-]$	γ_{CO2}	γ_{PZ}	γ_{PZCOO}	$H_{CO2,soln}$	Density	Viscosity	D_{CO2}	$d(P_{CO2})d(ldg)$	[Alk]	Slope Equil	$k^o_{l,prod}$	k_l^o/slope	k_g''	Diffusion	Calc k_g'
m	C	mol_{CO2}/mol_{alk}	M	M				$Pa{\cdot}m^3/mol$	g/cm^3	cP	m^2/s	$Pa/(mol/mol_{alk})$	mol_{alk}/m^3	$Pa/(mol/m^3)$	m/s	$mol/s{\cdot}Pa{\cdot}m^2$	$mol/s{\cdot}Pa{\cdot}m^2$	Resistance	$mol/s{\cdot}Pa{\cdot}m^2$
1.8	40	0	1.57	0.00	1.02	0.056	0.038	4202	1.01	0.97	2.0E-09	10	3147	0.00	7.32E-05	2.32E-02	9.48E-06	0%	9.48E-06
		0.1	1.12	0.09	1.14	0.056	0.038	4704	1.02	1.00	2.0E-09	91	3146	0.03	7.23E-05	2.50E-03	6.61E-06	0%	6.59E-06
		0.2	0.63	0.23	1.28	0.056	0.038	5266	1.04	1.03	1.9E-09	890	3145	0.28	7.14E-05	2.52E-04	4.05E-06	2%	3.98E-06
		0.3	0.25	0.29	1.43	0.056	0.038	5895	1.05	1.05	1.9E-09	9278	3145	2.95	7.05E-05	2.39E-05	2.02E-06	8%	1.86E-06
		0.4	0.06	0.15	1.60	0.056	0.038	6600	1.06	1.08	1.9E-09	103141	3145	32.80	6.97E-05	2.12E-06	6.74E-07	24%	5.12E-07

Table F.15: Calculated spreadsheet model results for 1.2 M PZ (Figure 5.44)

PZ	Temp	CO_2 Loading	$[PZ]_{free}$	$[PZCOO^-]$	γ_{CO2}	γ_{PZ}	γ_{PZCOO}	$H_{CO2,soln}$	Density	Viscosity	D_{CO2}	$d(P_{CO2})d(ldg)$	[Alk]	Slope Equil	$k^o_{l,prod}$	k_l^o/slope	k_g''	Diffusion	Calc k_g'
M	C	mol_{CO2}/mol_{alk}	M	M				$Pa{\cdot}m^3/mol$	g/cm^3	cP	m^2/s	$Pa/(mol/mol_{alk})$	mol_{alk}/m^3	$Pa/(mol/m^3)$	m/s	$mol/s{\cdot}Pa{\cdot}m^2$	$mol/s{\cdot}Pa{\cdot}m^2$	Resistance	$mol/s{\cdot}Pa{\cdot}m^2$
1.2	25	0.0063	1.2	0.00	1.07	0.041	0.038	3188	1.03	1.23	1.5E-09	2	2476	0.00	6.34E-05	8.90E-02	4.47E-06	0%	4.47E-06
	60	0.0066	1.2	0.00	0.94	0.074	0.038	5734	1.02	0.60	3.3E-09	104	2442	0.04	9.71E-05	2.27E-03	1.30E-05	1%	1.29E-05

Table F.16: Calculated spreadsheet model results for 8 m PZ at high CO_2 loading and temperature

PZ	Temp	CO_2 Loading	$[PZ]_{free}$	$[PZCOO^-]$	γ_{CO2}	γ_{PZ}	γ_{PZCOO}	$H_{CO2,soln}$	Density	Viscosity	D_{CO2}	$d(P_{CO2})d(ldg)$	[Alk]	Slope Equil	$k^o_{l,prod}$	k_l^o/slope	k_g''	Diffusion	Calc k_g'
m	C	mol_{CO2}/mol_{alk}	M	M				$Pa{\cdot}m^3/mol$	g/cm^3	cP	m^2/s	$Pa/(mol/mol_{alk})$	mol_{alk}/m^3	$Pa/(mol/m^3)$	m/s	$mol/s{\cdot}Pa{\cdot}m^2$	$mol/s{\cdot}Pa{\cdot}m^2$	Resistance	$mol/s{\cdot}Pa{\cdot}m^2$
2	80	0.375	0.17	0.11	1.42	0.106	0.038	12309	1.11	0.60	4.0E-09	634610	3576	177.47	8.97E-05	5.05E-07	2.82E-06	85%	4.28E-07
	100		0.18	0.07	1.34	0.138	0.038	15848	1.09	0.40	6.2E-09	1725967	3526	489.48	1.14E-04	2.32E-07	4.67E-06	95%	2.21E-07
8	80		0.28	0.55	3.91	0.166	0.038	33817	1.18	3.56	1.1E-09	634610	9690	65.49	3.51E-05	5.35E-07	2.67E-06	83%	4.46E-07
	100		0.27	0.42	3.69	0.216	0.038	43540	1.17	2.02	1.9E-09	1725967	9555	180.63	4.85E-05	2.68E-07	4.06E-06	94%	2.52E-07

References

Aboudheir, A., P. Tontiwachwuthikul, et al. (2003). "Kinetics of the reactive absorption of carbon dioxide in high CO2-loaded, concentrated aqueous monoethanolamine solutions." Chemical Engineering Science **58**: 5195–5210.

Al-Juaied, M. (2004). Carbon Dioxide Removal from Natural Gas by Membranes in the Presence of Heavy Hydrocarbons and by Aqueous Diglycolamine/Morpholine. Chemical Engineering, The University of Texas at Austin. **PhD:** 398.

Al-Juaied, M. and G. T. Rochelle (2006). "Absorption of CO2 in Aqueous Blends of Diglycolamine and Morpholine." Chemical Engineering Science **61**(12): 3830–3837.

Alper, E. (1990). "Reaction Mechanism and Kinetics of Aqueous Solutions of 2-Amino-2-methyl-1-propanol and Carbon Dioxide." Ind. Eng. Chem. Res. **29**: 1725–1728.

Alvarez-Fuster, C., N. Midoux, et al. (1980). "Chemical Kinetics of the Reaction fo Carbon Dioxide with Amines in the Pseudo m-nth Order Conditions in Aqueous and Organic Solutions." Chem. Engr. Sci. **35**(8): 1717–1723.

Astarita, G. (1961). "Carbon Dioxide Absorption in Aqueous Monoethanolamine Solutions." Chem. Engr. Sci. **16**: 202–207.

Barnola, J. M., D. Raynaud, et al. (2003). "Historical CO2 record from the Vostok ice core." In Trends: A Compendium of Data on Global Change. Carbon Dioxide Information Analysis Center, Oak Ridge National Laboratory, U.S. Department of Energy, Oak Ridge, Tenn., U.S.A.

Barth, D., C. Tondre, et al. (1986). "Stopped-Flow Investigations of the Reaction Kinetics of Carbon Dioxide with Some Primary and Secondary Alkanolamines in Aqueous Solutions." Int. J. Chem. Kinetics **18**: 445–457.

Bishnoi, S. and G. T. Rochelle (2000). "Absorption of Carbon Dioxide into Aqueous Piperazine: Reaction Kinetics, Mass Transfer and Solubility." Chem. Engr. Sci. **55**: 5531–5543.

Bishnoi, S. and G. T. Rochelle (2002a). "Absorption of Carbon Dioxide into Aqueous Piperazine/Methyldiethanolamine." AIChE Journal **48**(12): 2788–2799.

Bishnoi, S. and G. T. Rochelle (2002b). "Thermodyanamics of Piperazine/Methyldiethanolamine/Water/Carbon Dioxide." Ind. Eng. Chem. Res. **41**: 604–612.

Blauwhoff, P. M. M., G. F. Versteeg, et al. (1983). "A Study on the Reaction Between CO2 and Alkanolamines in Aqueous Solutions." Chem. Engr. Sci. **38**(9): 1411–1429.

Bronsted, J. N. (1928). "Acid and basic catalysis." Chemical Reviews **5**: 231–338.

Browning, G. J. and R. H. Weiland (1994). "Physical Solubility of Carbon Dioxide in Aqueous Alkanolamine via Nitrous Oxide Analogy." Journal of Chemical and Engineering Data **39**: 817–822.

Caplow, M. (1968). "Kinetics of carbamate formation and breakdown." Journal of the American Chemical Society **90**(24): 6795–6803.

Clarke, J. K. A. (1964). "Kinetic of Absorption of Carbon Dioxide in Monoethanolamine Solutions at Short Contact Times." Ind. and CE Fundamentals **3**(3): 239–245.
Crooks, J. E. and J. P. Donnellan (1989). "Kinetics and Mechanism of the Reaction Between Carbon Dioxide and Amines in Aqueous Solution." J. Chem. Soc. Perkin Trans. II: 331–333.
Cullinane, J. T. (2005). Thermodynamics and Kinetics of aqueous piperazine with potassium carbonate for carbon dioxide absorption. Chemical Engineering. Austin, TX, The University of Texas at Austin**:** 295.
Cullinane, J. T. and G. T. Rochelle (2006). "Kinetics of Carbon Dioxide Absorption into Aqueous Potassium Carbonate and Piperazine." Industrial & Engineering Chemistry Research **45**(8): 2531–2545.
Cussler, E. L. (1997). Diffusion: Mass Transfer in Fluid Systems, Cambridge University Press.
Danckwerts, P. V. (1970). Gas-Liquid Reactions, McGraw-Hill, Inc.
Danckwerts, P. V. (1979). "The reaction of CO2 with ethanolamines." Chemical Engineering Science **34**(4): 443–446.
Danckwerts, P. V. and M. M. Sharma (1966). "Absorption of Carbon Dioxide into Solutions of Alkalis and Amines (with Some Notes on Hydrogen Sulphide and Carbonyl Sulphide)." Chem. Engr.: CE244–CE280.
Dang, H. (2000). CO2 absorption rate and solubility in monoethanolamine/piperazine/water. Chemical Engineering. Austin, TX, The University of Texas at Austin. **M.S.E.:** 129.
Dang, H. and G. T. Rochelle (2003). "CO2 Absorption Rate and Solubility in Monoethanolamine/Piperazine/Water " Separation Science and Technology **38**(2): 337–357.
Davis, J. D. (2009). Thermal Degradation of Aqueous Amines Used for Carbon Dioxide Capture. Chemical Engineering. Austin, TX, The University of Texas at Austin. **PhD:** 278.
Derks, P. W. J., T. Kleingeld, et al. (2006). "Kinetics of Absorption of Carbon Dioxide in Aqueous Piperazine Solution." Chem. Engr. Sci. **61**(20): 6837–6854.
DIPPR (1979). Vapor Pressures and Critical Points of Liquids XIV: Aliphatic Oxygen-Nitrogen Compounds. Item 79030. London, Engineering Sciences Data.
Donaldson, T. L. and Y. N. Nguyen (1980). "Carbon Dioxide Reaction Kinetics and Transport in Aqueous Amine Membranes." Ind. Eng. Chem. Fundam. **19**: 260–266.
EIA. (2008a). "International Energy Annual 2006." Retrieved May 7, 2009, from http://www.eia.doe.gov/iea/carbon.html.
EIA. (2008b). "U.S. Coal Supply and Demand: 2008 Review." Retrieved August 6, 2009, from http://www.eia.doe.gov/cneaf/coal/page/special/consumption.html.
Emmert, R. E. and R. L. Pigford (1962). "Gas Absorption Accompanied by Chemical Reaction: A Study of the Absorption of Carbon Dioxide in Aqueous Solutions of Monoethanolamine." AlChE Journal **8**(2): 171–175.

Ermatchkov, V., A. Perez-Salado Kamps, et al. (2006b). "Solubility of Carbon Dioxide in Aqueous Solutions of N-Methyldiethanolaine in the Low Gas Loading Region." Ind. Eng. Chem. Res. **45**: 6081–6091.

Ermatchkov, V., A. Perez-Salado Kamps, et al. (2006a). "Solubility of Carbon Dioxide in Aqueous Solutions of Piperazine in the Low Gas Loading Region." Journal of Chemical and Engineering Data **51**(5): 1788–1796.

Hamborg, E. S., P. W. J. Derks, et al. (2008). "Diffusion Coefficients of N2O in Aqueous Piperazine Solutions Using the Taylor Dispersion Technique from (293 to 333) K and (0.3 to 1.4) mol.dm-3." J. Chem. Eng. Data **53**: 1462–1466.

Hartono, A. (2009). Characterization of diethylenetriamine (DETA) as absorbent for CO2. Chemical Engineering. Trondheim, Norway, Norwegian University of Science and Technology. **Ph.D.:** 243.

Hikita, H., S. Asai, et al. (1977). "The Kinetics of Reaction of Carbon Dioxide with Monoethanolamine, Diethanolamine and Triethanolamine by a Rapid Mixing Method." Chem. Engr. **13**: 7–12.

Hilliard, M. (2008). A Predictive Thermodynamic Model for an Aqueous Blend of Potassium Carbonate, Piperazine, and Monoethanolamine for Carbon Dioxide Capture from Flue Gas. Chemical Engineering. Austin, TX, The University of Texas at Austin. **Ph.D.:** 1025.

Hobler, T. (1966). Mass Transfer and Absorbers, Pergamon Press.

IPCC (2007). Climate Change 2007 - The Physical Science Basis. IPCC Fourth Assessment Report, Intergovernmental Panel on Climate Change.

Jamal, A., A. Meisen, et al. (2006). "Kinetics of Carbon Dioxide Absorption and Desorption in Aqueous Alkanolamine Solutions Using a Novel Hemispherical Contactor - I. Experimental Apparatus and Mathematical Modeling." Chem. Engr. Sci. **61**: 6571–6589.

Jensen, M. B., E. Jorgensen, et al. (1954). "Reactions Between Carbon Dioxide and Amino Alcohols." Acta Chem. Scand. **8**(7): 1137–1140.

Jou, F.-Y., A. E. Mather, et al. (1995). "The Solubility of CO2 in a 30 Mass Percent Monoethanolamine Solution." The Canadian Journal of Chemical Engineering **73**(1): 140–147.

Keeling, C. D. and T. P. Whorf (2005). "Atmospheric CO2 records from sites in the SIO air sampling network." In Trends: A Compendium of Data on Global Change. Carbon Dioxide Information Analysis Center, Oak Ridge National Laboratory, U.S. Department of Energy, Oak Ridge, Tenn., U.S.A.

Kiehl, J. T. and K. E. Trenberth (1997). "Earth's Annual Global Mean Energy Budget." Bulletin of the American Meterological Society **78**(2): 197–208.

Laddha, S. S. and P. V. Danckwerts (1981a). "Reaction of CO2 with Ethanolamines: Kinetics from Gas Absorption." Chem. Engr. Sci. **36**: 479–482.

Laddha, S. S., J. M. Diaz, et al. (1981b). "The N2O Analogy: the Solubilities of CO2 and N2O in Aqueous Solutions of Organic Compounds." Chemical Engineering Science **36**: 229–230.

Leder, F. (1971). "The Absorption of CO2 into Chemically Reactive Solutions at High Temperature." Chem. Engr. Sci. **26**: 1381–1390.

Littel, R. J., G. F. Versteeg, et al. (1992). "Kinetics of CO2 with Primary and Secondarty Amines in Aqueous Solutions - II. Influence of Temperature on Zwitterion Formation and Deprotonation Rates." Chem. Engr. Sci. **47**(8): 2037–2045.

Mshewa, M. M. (1995). Carbon Dioxide Desorption/Absorption with Aqueous Mixtures of Methyldiethanolamine and Diethanolamine at 40 to 120C. Chemical Engineering. Austin, TX, The University of Texas at Austin. **Ph.D.**

NCDC. (2009). "Global Surface Temperature Anomalies." Retrieved May 6, 2009, from http://www.ncdc.noaa.gov/oa/climate/research/anomalies/index.php#anomalies.

Neftel, A., H. Friedli, et al. (1994). "Historical CO2 record from the Siple Station ice core." In Trends: A Compendium of Data on Global Change. Carbon Dioxide Information Analysis Center, Oak Ridge National Laboratory, U.S. Department of Energy, Oak Ridge, Tenn., U.S.A.

Okoye, C. I. (2005). Carbon Dioxide Solubility and Absorption Rate in Monoethanolamine/Piperazine/H2O. Chemical Engineering. Austin, TX, The University of Texas at Austin. **M.S.E.:** 57.

Pacheco, M. A. (1998). Mass Transfer, Kinetics and Rate-Based Modeling of Reactive Absorption. Chemical Engineering. Austin, TX, The University of Texas at Austin. **Ph.D.:** 291.

Pacheco, M. A., S. Kaganoi, et al. (2000). "CO2 absorption into aqueous mixtures of diglycolamine and methyldiethanolamine." Chemical Engineering Science **55**: 5125–5140.

Penny, D. and T. Ritter (1983). "Kinetic Study of Reaction Between Carbon Dioxide and Primary Amines." J. Chem. Soc. Faraday Trans. **79**: 2103–2109.

Pigford, R. L. (1941). Counter-Diffusion in a Wetted Wall Column. Degree of Doctor of Philosophy in Chemistry. Urbana, The University of Illinois**:** 107.

Rao, A. B. and E. S. Rubin (2002). "A Technical, Economic, and Environmental Assessment of Amine-Based CO2 Capture Technology for Power Plant Greenhouse Gas Control." Environmental Science and Technology **36**(20): 4467–4475.

Rochelle, G. T., S. Bishnoi, et al. (2001). Research Needs for CO2 Caputre from Flue Gas by Aqueous Absorption/Stripping, The University of Texas at Austin**:** 156. U.S. Department of Energy - No. DE-AF26-99FT01029.

Rochelle, G. T., X. Chen, et al. (2009a). "CO2 Capture by Aqueous Absorption - 1st Quarterly Progress Reports 2009." from http://www.che.utexas.edu/rochelle_group/Pubs/Rochelle_Q1_Report_2009.pdf.

Rochelle, G. T., X. Chen, et al. (2009b). "CO2 Capture by Aqueous Absorption - 2nd Quarterly Progress Reports 2009." from http://www.che.utexas.edu/rochelle_group/Pubs/Rochelle_Q2_Report_2009.pdf.

Rochelle, G. T., R. Dugas, et al. (2008). "CO2 Capture by Aqueous Absorption - 2nd Quarterly Progress Reports 2008." from http://www.che.utexas.edu/rochelle_group/Pubs/2nd_quarterly_report_2008.pdf.

Rochelle, G. T., A. Sexton, et al. (2008a). "CO2 Capture by Aqueous Absorption - 3rd Quarterly Progress Reports 2008." from

http://www.che.utexas.edu/rochelle_group/Pubs/Rochelle_Research_Report_Q3_2008.pdf.
Rochelle, G. T., A. Sexton, et al. (2008b). CO2 capture by aqueous absorption, 4th quarterly progress reports 2007. Luminant Carbon Management Program, The University of Texas at Austin**:** 58-62.
Rochelle, G. T., A. Sexton, et al. (2009). "CO2 Capture by Aqueous Absorption - 4th Quarterly Progress Reports 2008." from http://www.che.utexas.edu/rochelle_group/Pubs/Rochelle Research Report Q4 2008.pdf.
Rubin, E. S., A. B. Rao, et al. (2004). Comparative Assessment of Fossil Fuel Power Plants with CO2 Capture and Storage. 7th International Conference on Greenhouse Gas Control Technologies, Vancouver, Canada.
Sada, E., H. Kumazawa, et al. (1976a). "Simultaneous Absorption of Carbon Dioxide and Hydrogen Sulphide into Aqueous Monoethanolamine Solutions." Chem. Engr. Sci. **31**: 839-841.
Sada, E., H. Kumazawa, et al. (1985). "Chemical Kinetics of the Reaction of Carbon Dioxide with Ethanolamine in Non-aqueous Solvents." AlChE Journal **31**(8): 1297–1303.
Samanta, A. and S. S. Bandyopadhyay (2007). "Kinetics and Modeling of Carbon Dioxide Absorption into Aqueous Solutions of Piperazine." Chem. Engr. Sci. **62**(24): 7312–7319.
Satori, G. and D. W. Savage (1983). "Sterically Hindered Amines for CO2 Removal from Gases." Ind. Eng. Chem. Fundam.(22): 239–249.
Sharma, M. M. (1965). "Kinetics of Reactions of Carbonyl Sulphide and Carbon Dioxide with Amines and Catalysis by Bronsted Bases of the Hydrolysis of COS." Trans. Faraday Soc. **61**: 681–688.
Shim, J.-G., J.-H. Kim, et al. (2009). "DFT Calculations on the Role of Base in the Reaction between CO2 and Monoethanolamine." Ind. Eng. Chem. Res. **48**: 2172–2178.
Smith, M. J., T. H. Flowers, et al. (2002). "Method for the measurement of the diffusion coefficient of benzalkonium chloride." Water Research **36**: 1423–1428.
Snijder, E. D., M. J. M. te Riele, et al. (1993). "Diffusion Coefficients of Several Aqueous Alkanolamine Solutions." J. Chem. Eng. Data **38**(3): 475–480.
Sun, W.-C., C.-B. Yong, et al. (2005). "Kinetics of the Absorption of Carbon Dioxide into Mixed Aqueous Solutions of 2-amino-2methyl-1-propanol and Piperazine." Chem. Engr. Sci. **60**(2): 503–516.
Tomcej, R. A. and F. D. Otto (1989). "Absorption of Carbon Dioxide and Nitrous Oxide into Aqueous Solutions of Methyldiethanolamine." AIChE Journal **35**(5): 861–864.
Versteeg, G. F., L. A. J. Van Dijck, et al. (1996). "On the Kinetics Between CO2 and Alkanolamines Both in Aqueous and Non-aqueous Solutions. An Overview." Chem. Engr. Comm **144**: 113–158.

Versteeg, G. F. and W. P. M. Van Swaaij (1988). "Solubility and diffusivity of acid gases (carbon dioxide, nitrous oxide) in aqueous alkanolamine solutions." Journal of Chemical and Engineering Data **33**(1): 29–34.

Vivian, J. E. and D. W. Peaceman (1956). "Liquid-Side Resistance in Gas Absorption." AIChE Journal **2**: 437–443.

Watson, J. R. and J. V. Sengers (1986). "Improved International Formullations for the Viscosity and Thermal Conductivity of Water Substance." J. Phys. Chem. Ref. Data **15**: 1291.

Weiland, R. H., J. C. Dingman, et al. (1998). "Density and Viscosity of Some Partially Carbonated Aqueous Alkanolamine Solutions and Their Blends." Journal of Chemical and Engineering Data **43**(3): 378–382.

Xu, S., F. D. Otto, et al. (1991). "Physical Properties of Aqueous AMP Solutions." Journal of Chemical and Engineering Data **36**(1): 71–75.

Zaytsev, I. D. and G. G. Asayev (1992). Properties of Aqueous Solutions of Electrolytes, CRC Press Inc.

Vita

Ross Dugas was born on June 9, 1981 in Houma, Louisiana to Scott Dugas and Kathy Theriot Dugas. After graduating from Vandebilt Catholic High School in Houma, Louisiana in May 1999, he enrolled at The University of Louisiana at Lafayette. In May 2003, he graduated magna cum laude with a Bachelor of Science in chemical engineering. In August 2003, he enrolled at The University of Texas at Austin and joined the research group of Dr. Gary T. Rochelle. Ross completed a Master of Science degree in May 2006.

Ross has accepted full-time employment with Dow Chemical in Freeport, Texas.

Permanent address: 111 Leighton Loop

Houma, Louisiana 70360

This dissertation was typed by the author.